Exploring Redox Chemistry, Conformational Dynamics and Diradical Properties of Expanded Porphyrinoids

A Thesis

Submitted in Partial Fulfillment of the

Requirements for the Degree of

Doctor of Philosophy

By

Madan D Ambhore

ID: 20143325

Indian Institute of Science Education and Research (IISER), Pune

2019

Dedicated to my Parents.

Mrs. Late. Gangabai and Mr. Digambarrao Ambhore

Dr. V. G. Anand
Professor

Certificate

Certified that the work described in this thesis entitled "*Exploring Redox Chemistry Conformational Dynamics and Diradical Properties of Expanded Porphyrinoids*" submitted by *Mr. Madan D Ambhore* was carried out by the candidate, under my supervision. The work presented here or any part of it has not been included in any other thesis submitted previously for the award of any degree or diploma from any other university or institution.

Date: 30th December, 2019

Dr. V. G. Anand

Research Supervisor

Declaration

I declare that this written submission represents my ideas in my own words and wherever other's ideas have been included; I have adequately cited and referenced the original sources. I also declare that I have adhered to all principles of academic honesty and integrity and have not misrepresented or fabricated or falsified any idea/data/fact/source in this submission. I understand that violation of the above will result in disciplinary actions by the Institute and can also evoke penal action from the sources, which have thus not been properly cited or from whom appropriate permission has not been taken when needed.

Date: 30ᵗʰ December 2019   **Madan D Ambhore**

ID: 20143325

Acknowledgements

Contents

III.B.1   Additive Induced Conformational Polymorphism and Diradical Chemistry in Expanded Isophlorins

III.B.2   38π aromatic expanded isophlorins at the crossroads of diradical chemistry

IV.B   Synthesis and Characterization of Phenylene Bridged Isophlorin Dimer

Synopsis

The thesis entitled as "**E**xploring Redox Chemistry, **C**onformational Dynamics and **D**iradical Properties of **E**xpanded Porphyrinoids" investigates different properties of expanded porphyrinoids. Expanded porphyrinoids are the "Macrocycles that contain pyrrole/thiophene/furan, or other heterocyclic subunits linked either directly or through one or more spacer atoms in such a manner that the internal ring pathway contains a minimum of seventeen atoms". In order to understand concept of aromaticity for expanded porphyrinoids, this thesis describes simple, efficient and straight-forward methods for synthesis of planar expanded porphyrinoids. The detailed spectroscopic evidences including UV-Vis absorption spectroscopy, Nuclear magnetic resonance (NMR) spectroscopy etc. have been employed to propose solution state structure. Solid state geometries and conformational dynamics is further proved by using single crystal X-ray diffraction studies. Redox and Magnetic properties of these macrocycles was established using Cyclic Voltammetry (CV), Electron paramagnetic resonance spectroscopy (VT-EPR), and Super Conducting Quantum Interface Devise (SQUID) measurement, wherever possible. Apart from syntheses and structural characterization, electronic and redox properties of these macrocycles have been described with suitable support from quantum mechanical calculations. This thesis is comprised into four chapters. A detailed overview on the concept of aromaticity/antiaromaticity of porphyrin and its expanded derivatives, the structure induced loss of aromaticity and synthetic methods to overcome structure induced loss of aromaticity, along with conformational flexibility and importance of these macrocycles for stabilizing stable organic diradical species are highlighted in the first chapter.

Second chapter provides a brief introduction to expanded derivatives of porphyrin such as hexaphyrin and octaphyrin. They have attracted wide attention due to the apparent role of pyrrole to switch nitrogen between imine and amine which is crucial to access multiple redox states in a given expanded porphyrinoid by proton coupled electron transfer reactions. In principle a hexaphyrin can be reduced to a 30π electrons macrocycle and an octaphyrin can accommodate 40π electrons. However, only stand-alone synthesis of such species is known and found to be stable with specific substituents. In contrast to the conventional reversible two-electron redox process, wide range and reversible four and six-electron redox process in the expanded porphyrins has been

demonstrated in this chapter. A core-modified hexaphyrin has been isolated and characterized comprehensively in three different oxidation states that bear 26π, 28π and 30π electrons. Suitable redox agents could interchange all these states. Particularly, the reduction of 28π macrocycle by 30π electrons was accomplished for the first time by employing Zn/NH_4Cl as the reducing agent. Exploring a similar strategy, an octaphyrin was isolated and comprehensively characterized in its 34π, 36π, 38π and 40π electrons states. The subtle multi-step two-electron redox transformations are accompanied by flexible structural landscape as established by spectroscopic and X-ray diffraction techniques. A higher number of multi-redox states 26π, 28π, 30π for hexaphyrin and 34π, 36π, 38π and 40π for octaphyrin has been proved upon substituting pyrrole for thiophene.
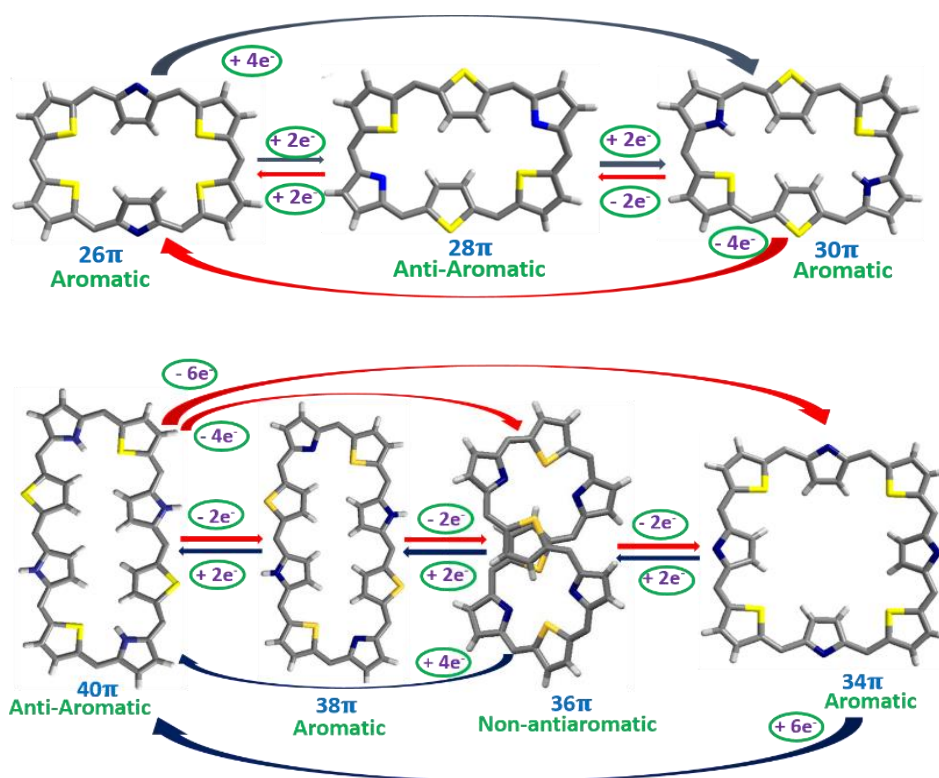
The third chapter describes the synthesis, characterization and flexible structural features for three different structural variants of 38π aromatic expanded isophlorins. These octaphyrins have eight heterocyclic rings connected by six meso carbons and a α-α connection either by bithiophene or biselenophene to complete the macrocyclic framework.

NICS= - 15.27 ppm   NICS = - 18.23 ppm   NICS= - 14.68 ppm
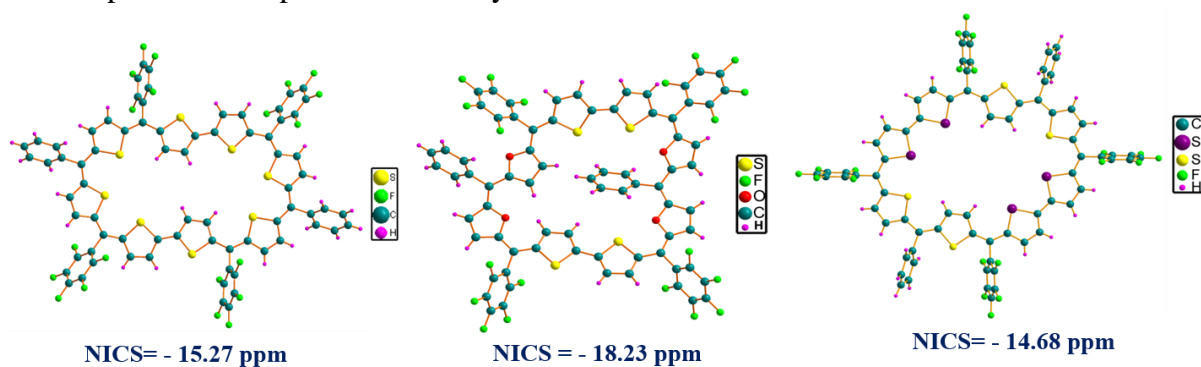
A highlight of this chapter is the structural transformation of a 38π octathiophene expanded isophlorin in the presence of topologically similar other macrocycles. This rare phenomenon is known as additive induced conformational polymorphism. Even though expanded porphyrinoids are known to alter their geometry between planar and non-planar topologies, this is the first example of inter-conversion between two different planar structures for the same macrocycle. Such structural modifications are perhaps impossible through a rational synthetic design. However, polymorphism offers a plausible route for such post-synthetic structural engineering and can unlock many unexpected molecular structures of these fascinating π-conjugated macrocycles.

38π
Aromatic
NICS= -15.27

28π
Antiaromatic
NICS= 19.00
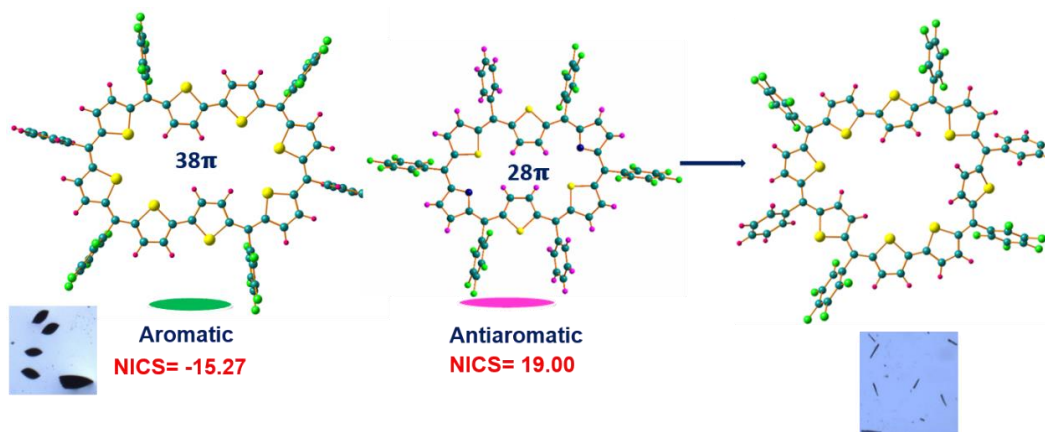
Apart from their dynamic structural variations, these molecules have been found to be in close equilibrium between closed-shell and open shell diradical species. Computational and

experimental studies revealed that the pro-aromaticity of thiophenes as the driving force for existence of diradical nature. It was implied that aromaticity gaining of consecutive non-aromatic thiophene rings and the net energy minimization that eventually surpasses the total energy required to break the double bond is responsible for the formation of diradicals. Diradical property of these macrocycles was proven experimentally through NMR and EPR spectroscopy. These experimental results were adequately supported by DFT calculations.
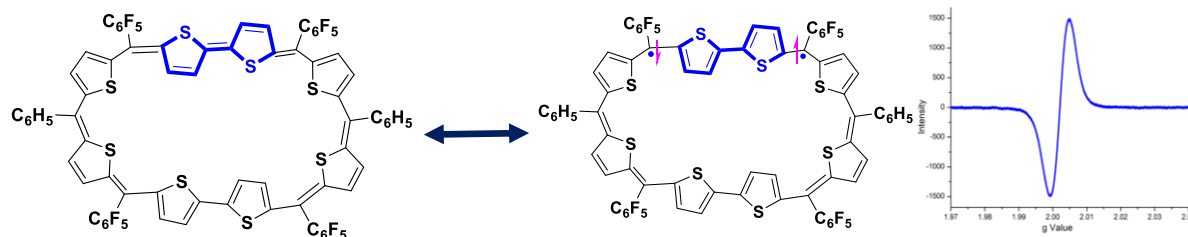
Fourth chapter is divided into two parts, A and B. Part-A describes the studies related to the role of benzene aromaticity upon its incorporation into anti-aromatic framework. Compared to quinoidal oligothiophene, the quinoidal oligo-paraphenylene is supposed to exhibit pronounced diradical character, due to the larger aromatic resonance energy in the benzene ring than that of thiophene ring. This was studied by the synthesis and structural characterization of benzene and biphenyl appended and benzene bridged isophlorins. Dication of benzene appended isophlorin showed appreciable diradical character, which was studied using variable temperature ^{1}H NMR, EPR and SQUID measurement. This was further supported by DFT studies.
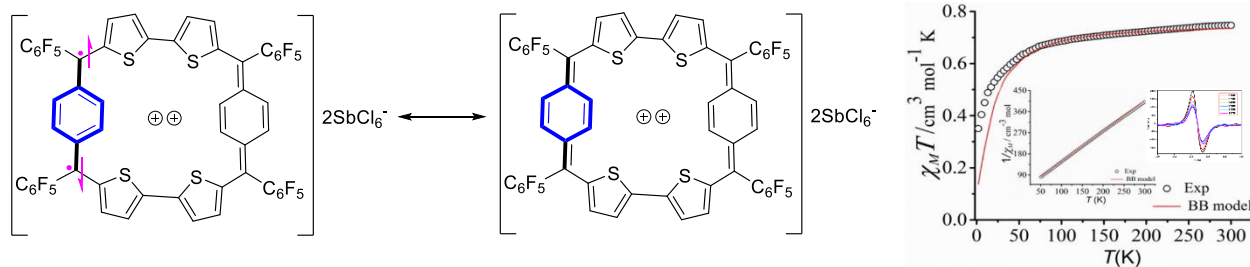
An attempt to synthesize the benzene bridged isophlorin dimer, resulted in benzene covalently engulfed by a macrocyclic framework. Such a structure is possible due to the two different condensation routes between the precursors. A subtle difference in the electronic absorption, NMR spectrum and additional support from computational studies confirmed the formation of an octaphyrin with eight furans. Its dication displayed a resolved NMR spectrum, signifying closed shell electronic ground state neglecting the possibility for formation of diradicals.
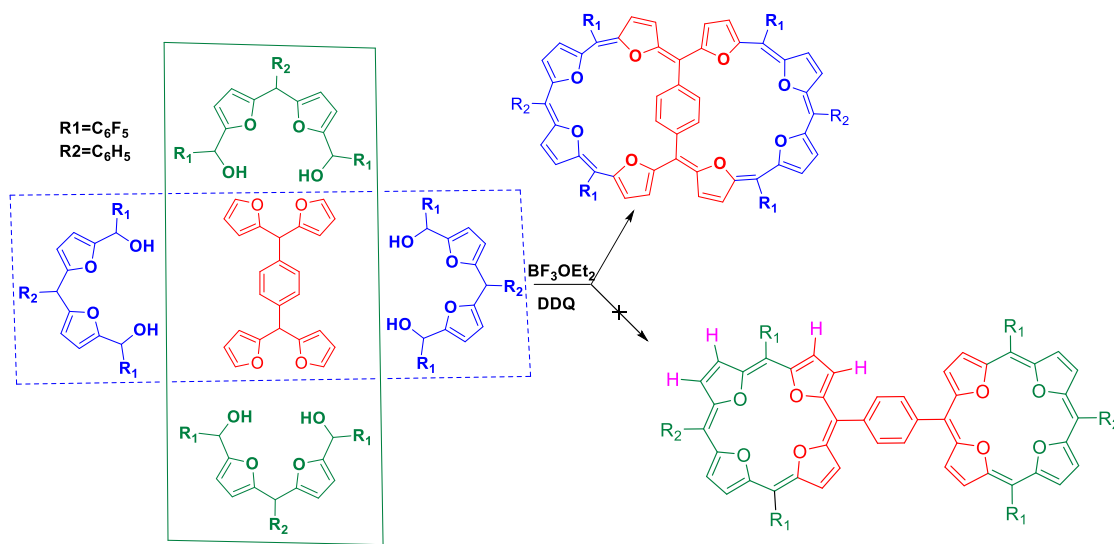
In summary, this thesis describes the synthesis of expanded porphyrinoids that are capable of multiple reversible redox reactions. All the redox processes are one-step two-electron reactions that switch the macrocycles between aromatic and anti-aromatic states. In between these states, there exists the unconventional radical species, which are supposed to be highly reactive and hence could not be isolated. For the first time, this thesis has proved reversible redox for the expanded derivatives of porphyrin and isophlorin. In addition, the serendipitous observation of polymorphism for expanded isophlorin is a highlight of this thesis. Structural dynamics of expanded porphyrinoids has been well documented, but a different topology for the same macrocycle has not been identified. In fact, additive induced polymorphism appears to be an attractive methodology to stabilize different polymorphs of an expanded porphyrinoid. Identification of suitable additives can open up mine of unusual structures and their associated properties related to π conjugation.

List of Publications

1) Wide range redox states of expanded Porphyrinoids, M. D. Ambhore, A. Basavarajappa and V. G. Anand *Chem. Commun.,* **2019**, 55, 6763—6766.

2) Isophlorinoids: The antiaromatic congener of Porphyrinoids B. K. Reddy, A Basavarajappa, M. D Ambhore, V. G. Anand, *Chem. Rev.* **2017,** 1*17* (4), 3420-3444.

3) Non planar core-modified dibenzi-expanded Isophlorins, R. Gaur, M. D. Ambhore and V. G. Anand, *J. Porphyrins Phthalocyanines.* **2019** 23, 1-5

Chapter 1

I.1 Introduction:

Porphyrin is an 18π aromatic aza-annulene comprising of regularly arranged four pyrrole and four methine carbons. Its main conjugation path contains 18π electrons and obeys Huckel's rule for aromaticity. By virtue of its macrocyclic π conjugation, this naturally occurring pigment absorbs visible light in the region between 400 to 600 nm.[1] Besides its rich metalation chemistry and interesting electronic behavior, porphyrin has attracted wide interest in various applications ranging from material science to medicine. In recent years, a variety of modifications on the porphyrin has been attempted to synthesize unnatural structural analogs of porphyrin such as n-confused porphyrin [2],isophlorin[3], core-modified[4] porphyrin, ring contracted[5,] and ring expanded porphyrins[7-10].

Among them, isophlorin is a non-natural anti-aromatic macrocycle. In 1960, Woodward hypothesized this macrocycle as a probable unstable intermediate during the synthesis of chlorophyll.[3] Pyrrole and aldehyde covalently assemble into unconjugated tetrapyrrole porphyrinogen, **I.1**, under acidic conditions. Further oxidation of porphyrinogen to porphyrin, **I.3** is suspected to be a two-step process (figure-1). At first, the porphyrinogen undergoes four-electron oxidation to the transient isophlorin, **I.2**, which subsequently undergoes two-electron oxidation to yield the porphyrin, **I.3**.
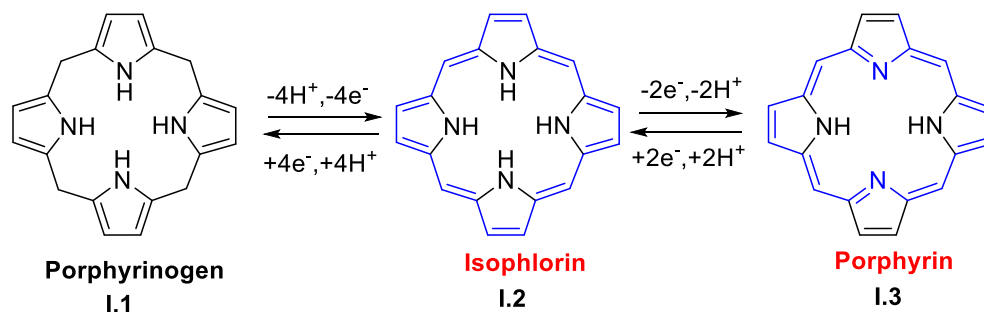
Figure-1: Schematic representation for porphyrin isophlorin interconversion.

Isophlorin **I.2** and porphyrin **I.3** differ in chemical composition by only two hydrogens but there is a clear difference in the conjugated pathway of between these two cyclic π systems. Porphyrin can be considered as heteroannulene due to the involvement of two nitrogen atoms into the sp^2

framework leading to planar macrocycle with 18π electrons along its conjugated pathway. Porphyrin suites as a perfect example to obey Huckle's rule for aromaticity [11]. In contrast, isophlorin's effective delocalization of π electron flows through the periphery by avoiding the nitrogen atoms in the effective delocalization of the sp^2 framework. It accounts for 20π electrons and fits into antiaromatic 4nπ systems, [12] which is supposed to be the main reason for its unstable nature. The presence of four hydrogens in the center of the macrocycle generates sufficient repulsive forces to deviate the macrocycle from planarity. In an attempt to overcome the steric hindrance, Vogel and co-workers pioneered the synthesis of macrocycles derived from thiophene/furan/selenophene by replacing all the pyrrole rings of a porphyrin.[4a-f] These molecules resemble the cyclic structure of porphyrin and are expected to stabilize a 20π electrons conjugated system in their neutral state. However, they undergo quick two-electron oxidation to form an 18π porphyrin dication by electron transfer reaction [4b, 4c].

The tetraoxaisophlorin **I.5** was isolated as black crystals, which were unstable at ambient temperature and could be stored at -78°C. Upon addition of $HClO_4$, it underwent facile two-electron oxidation to yield the corresponding aromatic dication, **I.4** (figure-2). An attempt to reduce dication **I.4** to the neutral tetraoxaisophlorin by potassium metal yielded the highly reduced 22π dianionic isophlorin **I.6.** [4e] The *meso* protons were found to resonate at -0.3 ppm in its ^{1}H NMR spectrum suggesting a strong diatropic ring current effect expected of aromatic macrocycles.
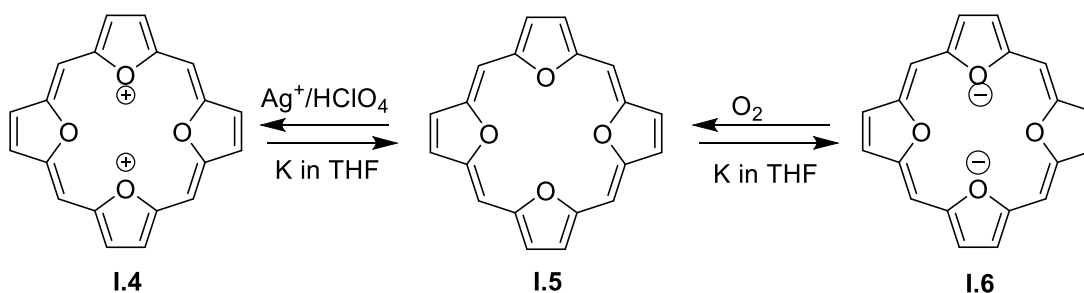
Figure-2: Redox chemistry of 20π isophlorin.

Conversion of 18π dicationic macrocycle to the dianionic 22π state, can be envisaged as four electron reduction through a neutral 20π isophlorin intermediate. Such multiple electron transfer associated with the stabilization of various electronic states was suggestive of the pro-metallic behavior of isophlorinoids. This interesting phenomenon could be much more explored with expanded porphyrinoids.

The first expanded porphyrin can be traced back to R. B. Woodward's serendipitous discovery of sapphyrin,[13] as a pentapyrrolic macrocycle (figure-3). In 1990, Sessler and coworkers report on Sapphyrin **I.7**[14] demonstrated the potential of expanded porphyrins in the field of anion recognition, aromaticity, photodynamic therapy (PDT), and as contrast agents for magnetic resonance imaging(MRI).[15-17] The same group also identified "Turcasarin" as a decapyrrolic non-planar macrocycle with a"figure-of-eight" conformation for an expanded porphyrin.[18]

I.7
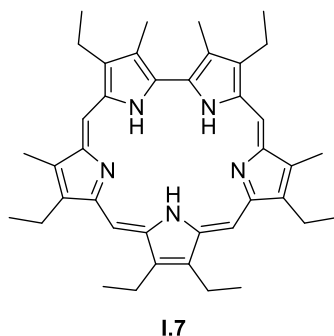
Figure-3: Sapphyrin an example for expanded porphyrin.

To generalize the structural aspects of porphyrin in its expanded derivatives, Sessler and Seidel defined expanded porphyrins as "macrocycles that contain pyrrole/thiophene/furan, or other heterocyclic subunits linked either directly or through one or more spacer atoms in such a manner that the internal ring pathway contains a minimum of 17 atoms.[19] Osuka and co-workers serendipitously discovered a series of meso pentaflurophenyl substituted expanded porphyrins (figure-4), during the synthesis of tetrakis(pentaflurophenyl) porphyrin.[22,21,22]

Porphyrin
I.8

N-fused [22]penttaphyrin
I.9
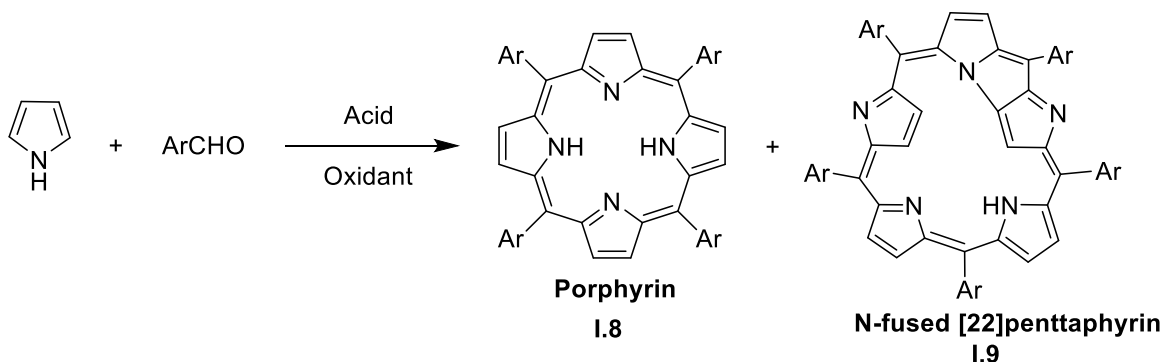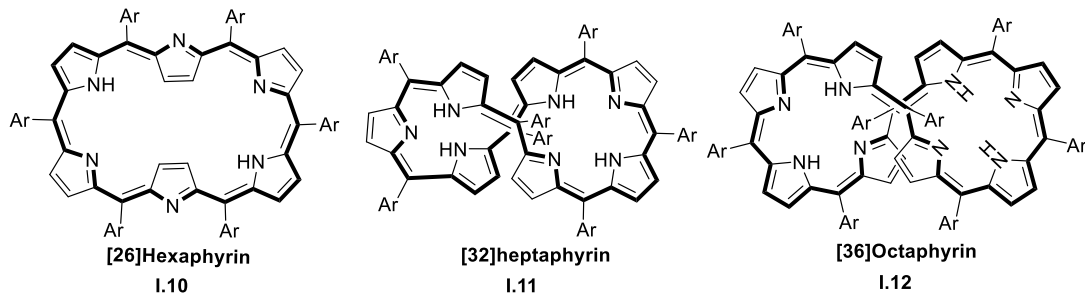
Figure-4: One pot synthesis of *meso*-aryl substituted porphyrin and expanded porphyrinoids.

Higher membered macrocycles isolated from this reaction included pentaphyrin (**I.9)**, hexaphyrin (**I.10**), heptaphyrin (**I.11**), octaphyrin (**I.12**), nonaphyrin, decaphyrin, and even higher analogs. With increasing number of heterocyclic rings in comparison to porphyrin, the larger macrocycles exhibited conformational flexibility. Therefore, they prefer to exist in the twisted conformation, which ultimately results in structure induced loss of aromaticity/antiaromaticity.

I.2 Structure induced loss of aromaticity/antiaromaticty in expanded porphyrinoids:

A twisted octapyrrole **I.17** was reported by Vogel and co-workers [23] during their attempt to synthesize a structural isomer of porphyrin, **I.15** (scheme-1). Unexpectedly they observed the formation of a macrocycle consisting of eight pyrrole rings rather than the expected tetrapyrrole macrocycle. Under typical MacDonald type condensation conditions, a bipyrrole dialdehyde **I.13** was condensed with a dipyrrylethane dicarboxylic acid **I.14** catalyzed by perchloric acid.
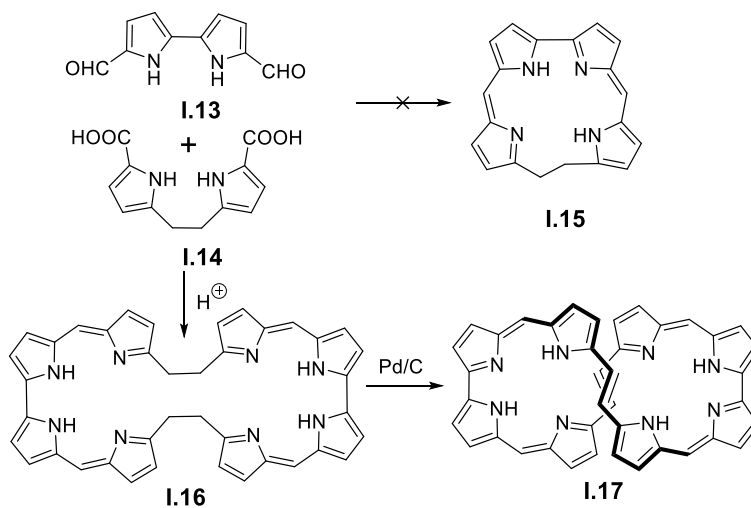
Scheme-1: Synthesis of the octapyrrolic macrocycle **I.17**. The 3, 4-diethyl substituents of the pyrrole rings are omitted for clarity.

13

Predominantly **I.16** was observed as a partially oxidized product. Subsequently thermal dehydrogenation of **I.16** in the presence of 10% Palladium on carbon (Pd/C) yielded the completely conjugated octaphyrin **I.17**. The octaphyrin formed tetrakis(hydroperchlorate) or tetrakis(hydrochloride) when treated with perchloric acid and 10% hydrochloric acid, respectively. ^{1}H NMR of the octaphyrin **I.17** did not exhibit any significant paratropic ring current effects as expected of a 36π anti-aromatic macrocycle. Single crystal X-ray diffraction analysis of the dichloride and the perchlorate salts revealed the non-planar structure of **I.17**. It was observed that the dichloride salt resulted from the deprotonation and the perchlorate salt due to the tetraprotonation of the macrocycle. In either case, the macrocycle adopted a twisted structure resembling the figure-of-eight topology. To explore the structural features of octaphyrin, they studied the role of *meso* carbons on the topology of the macrocycle.[23a, 23b] Therefore they reacted bipyrrole dialdehyde **I.18** with dipyrromethane dicarboxylic acid **I.19** under similar reaction conditions employed for the synthesis of **I.21** (scheme-2).
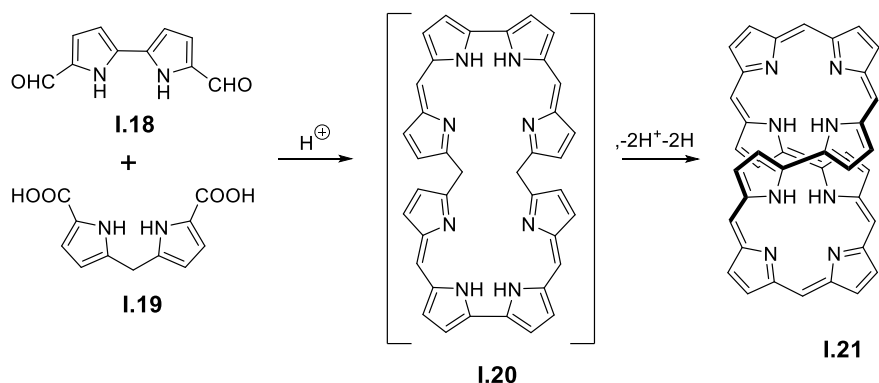
Scheme 2. Synthesis of the octapyrrolic macrocycle **13**. 3, 4-diethy1 substituents of the pyrrole rings are omitted for clarity.

Formation of 34π octaphyrin **I.21** was observed, and which favored over the tetrapyrrolic corrole. As **I.21** formally accounts for 34π electrons, it was expected to show diatropic ring current effect in the ^{1}H NMR spectrum for aromatic macrocycle. However, similar to the case of 36π octaphyrin, **I.21** did not reveal significant diatropic ring current effects, which was suggestive of its non-planar structure and later confirmed from single-crystal X-ray diffraction analysis.

Later, Shinokubo and co-worker reported the synthesis of a 32π octaphyrin by metal-assisted coupling reaction of functionalized metal-dipyrrinato complex **I.22**.[24,25] In an earlier attempt, they

synthesized antiaromatic nor-corrole **I.25** in 90% yields by the reductive homocoupling of α,α'-dibromodipyrrin nickel(II) complex **I.22** in the presence of Ni(0) and triphenylphosphine (scheme-3).
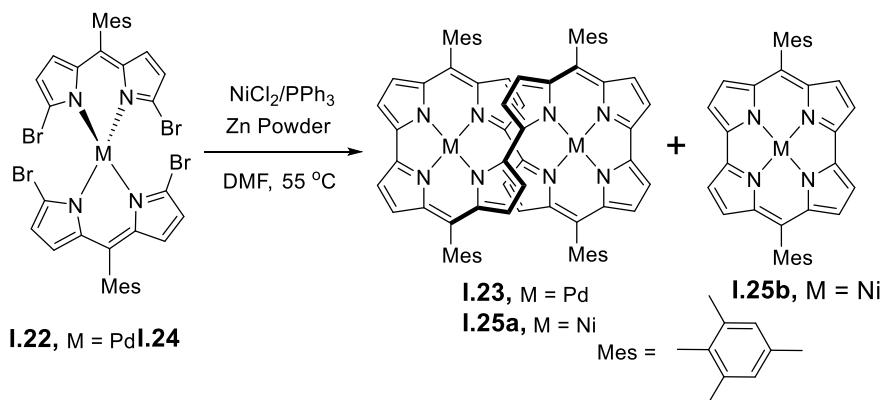
Scheme-3: Metal-templated intramolecular and intermolecular homocoupling of α,α'-dibromodipyrrin metal(II)complex to octaphyrin **21** and norcorrole.

Their studies revealed the ratio of the product formed was very much dependent on the nickel complex employed in the cyclization reaction. A similar reductive homocoupling reaction with an α,α'-dibromodipyrrin palladium(II) complex, **I.24**, yielded 32π octaphyrin, **I.23**, exclusively in 35% yields.[24,25]. The single-crystal X-ray diffraction analysis revealed a figure of eight geometry with two palladium metal ions ligated by the macrocycle, **I.23**. ^{1}H NMR characterization revealed weak paratropic ring current effects, as expected from the non-planar structure of the macrocycle. The estimated NICS value for **I.23** also supported non-planar topology due to structure induced loss of antiaromaticity.

Chandrashekar and co-workers have explored an area of expanded porphyrins, by replacing pyrrole rings of macrocycle with other heterocycles, typically thiophene, in the octaphyrin framework. In their attempts to synthesize core modified octaphyrin, dithiatetrapyrrane, **I.26**, was reacted with aryl aldehyde under acid-catalyzed conditions followed by oxidation with chloranil to yield a 34π octaphyrin, **I.27** (scheme-4).[26]
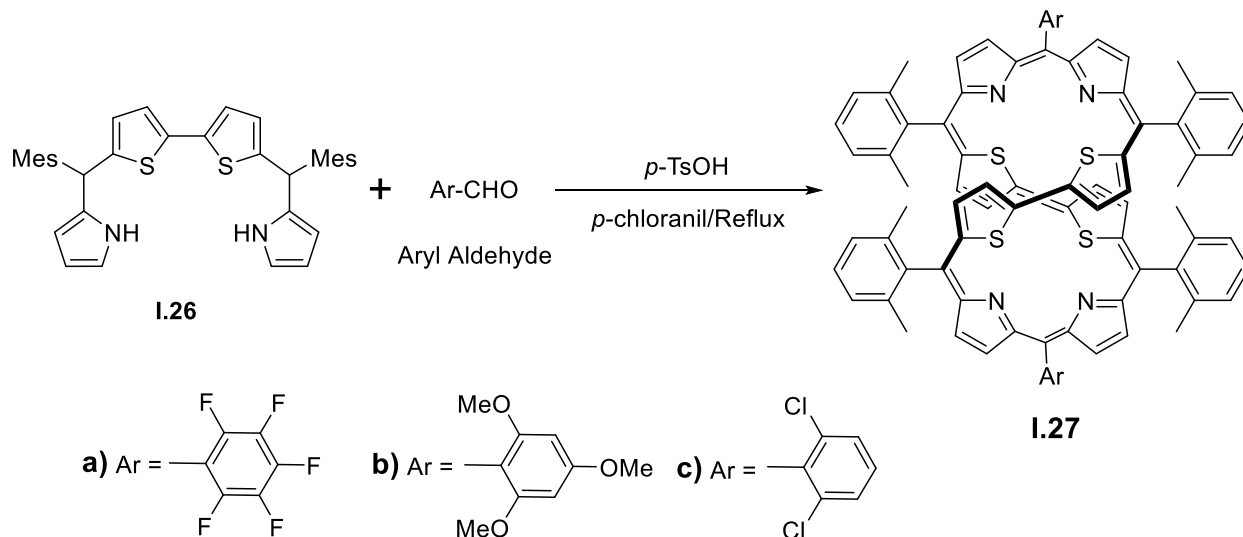
Scheme-4: Synthesis of core-modified octaphyrins.

Spectroscopic characterization and single-crystal X-ray diffraction analysis confirmed a twisted configuration for the 34π octaphyrin **I.27**. It could not sustain a flat topology even though the adjacent thiophene units were oriented in an anti-parallel arrangement. It was inferred that the additional *meso* carbons increase the volume of the macrocyclic core, which is suitable enough for the crisscrossed bithiophene units leading to a corrole like pockets. Latos and co-workers reported two core modified octaphyrins[27], containing four pyrroles and four thiophene units with eight meso positions, obtained by the reaction of pyrrole and thiophene diol under acidic condition. (scheme-5)
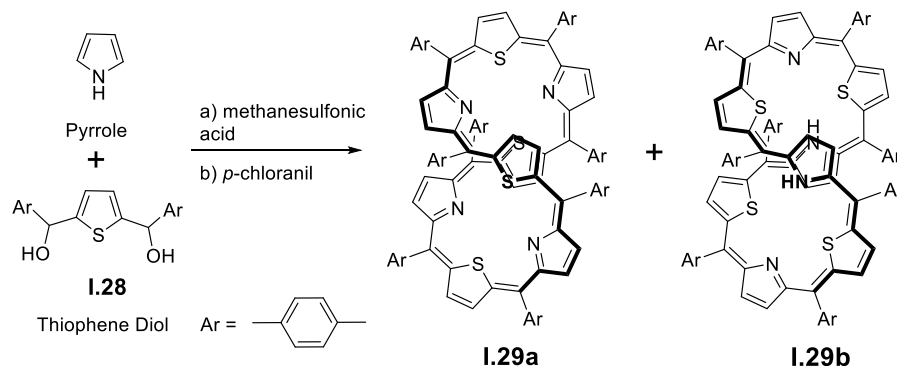
Scheme-5: Synthesis of 36π and 38π core-modified tetrathiaoctaphyrins.

Two different tetrathiaoctaphyrins, **I.29a-b**, with a difference of two mass units, were isolated from this reaction. Macrocycle **I29.a** corresponded to 36π octaphyrin, while the **I.29b** accounted for a 38π macrocycle. Only two protons made the difference between the two macrocycles but made a significant impact on their electronic properties. At the same time, they were also found to be inter-convertible between themselves through a reversible two-electron redox process. The 36π octaphyrin, **I.29a**, was quantitatively dihydrogenated to the 38π octaphyrin, **I.29b**, with reducing agents such as sodium borohydride or sodium hyposulfite. In an opposite reaction, the tetrathiaoctaphyrin **I.29b** was quantitatively dehydrogenated to 36π octaphyrin, **I.29a**, upon oxidation by *p*-chloranil. Such inter-convertible systems represent typical examples of proton-coupled electron transfer reactions in organic molecules. From detailed NMR analyses and computational calculations, it was concluded that both **I.29a** and **I.29b** adopted a figure-of-eight configuration rather than a planar structure. The ^{1}H NMR spectrum did not reveal significant diatropic ring current effects for **I.29b**, while only marginal paratropic ring current effects were reported for **I.29a**. Regardless of similar structure characteristics, variable temperature NMR spectroscopy revealed fluxional behavior for **I.29a**. The macrocycle could exist in two different conformations with a twisted topology. Based on the probable reaction mechanism for the transformation, the inter-conversion energy was estimated to be 63.6 ± 3.0 kJmol^{-1}.

Anand and co-workers synthesized an octaphyrin[28] with four thiophene and four furan rings (scheme-6). Since both the heterocyclic rings bear divalent chalcogen atoms, such macrocycles are devoid of amine imine conversion. **I.30** accounts for 40π electrons and expected to show antiaromatic characteristics.
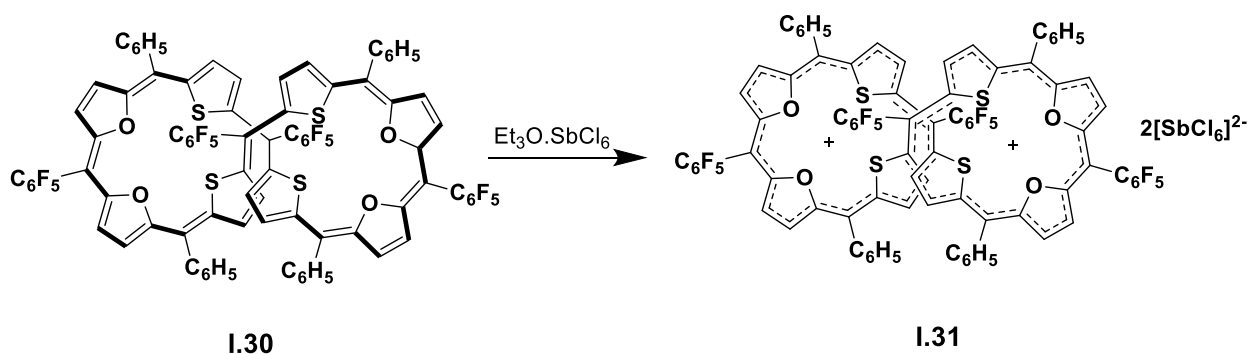
Scheme-6: Two electron oxidation of 40π isophlorin.

^{1}H NMR studies did not reveal significant paratropic chemical shifts, and signals were observed in the region 5.0 to 9.0 ppm. This observation parallels the structural characteristics of the non-planar nature of the macrocycle. Single crystal X-ray diffraction analysis revealed a figure of eight conformations in agreement with NMR. The estimated NICS value of 3.5 ppm for the **I.30,** was suggestive of the non-antiaromatic characteristics for the macrocycle. **I.30** can be oxidized to 38π dicationic octaphyrin **I.31** using Meerwein salt. A marked absence in diatropic ring current was in support of the observed non-planar topology as determined from single-crystal X-ray analysis. Both the **I.30** and **I.31** undergo structure-induced loss of planarity due to its flexible nature and therefore correspond to non-antiaromatic and non-aromatic octaphyrin, respectively.

Ring inversion induces planarity to the macrocycle:

Numerous efforts from many research groups for the synthesis of planar octaphyrin went futile, due to structure induced loss of planarity. Invariably several reports on octaphyrin usually reported ring inversion of one or two heterocyclic units in the macrocycle. It was implied that the ring inversion of the heterocyclic unit has an important role in obtaining planar octaphyrin. Chandrashekar and co-workers [29, 30] reported the synthesis of a planar 34π octaphyrin, **I.33**, containing four thiophenes and four pyrrole heterocyclic units. The macrocycle was synthesized through an acid-catalyzed oxidative coupling reaction of a modified tetrapyrrane, **I.32**, derived by the condensation of bithiophene diol and pyrrole (scheme-7).
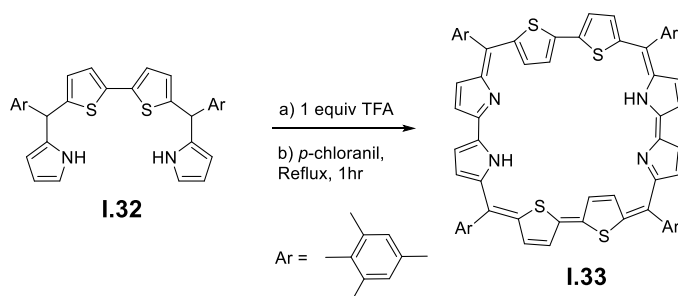
Scheme-7: 32π core-modified octaphyrin the example for planar octaphyrin.

I.33 was characterized as an aromatic macrocycle based on proton NMR spectroscopy. The upfield signal at δ -2.21 ppm for the NH protons supplemented the aromatic feature expected of a 34π octaphyrin **I.33**. Single crystal X-ray diffraction analysis confirmed the planar structure of the macrocycle and also revealed the ring inversion of two thiophene rings. In the proton NMR

spectrum, the protons of the inverted thiophene ring resonated as two doublets at δ -5.38 and 5.83 ppm arising from diatropic ring current effects. Even though such ring inversions are common in meso aryl expanded porphyrins, this was the first report of an octaphyrin with inverted heterocyclic units.

Later in 2009, Reddy et al. [31] reported a planar antiaromatic octaphyrin with eight furan units. Synthesis of this macrocycle was achieved by a simple one-pot reaction between furan and pentaflorobenzaldehyde catalyzed by boron trifluoride diethyl etherate. The 30π hexa furan **I.34** also formed along with 40π octafuran **I.35**. In the ^{1}H NMR spectrum, **I.35** showed only two singlets centered at δ 9.40 and 5.85 ppm, which strongly suggest the planar topology of the molecule. Its molecular structure determined from X-ray diffraction studies appeared to be an extended version of the 30π macrocycle, **I.34**. Ring inversions of the alternate furan rings further justified the crucial role of ring flipping in large porphyrinoids/isophlorinoids in adopting planar conformation.
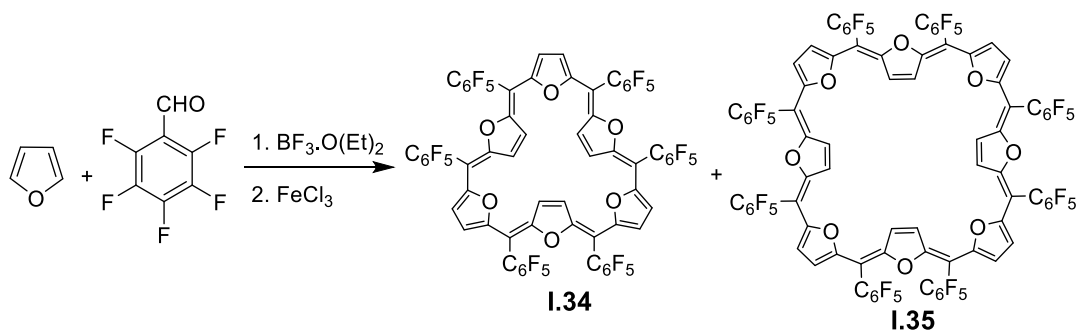
Scheme-8: One-pot synthesis of 40π octafuran.

Osuka, Kim, and co-workers [32] discovered the conditions under which a twisted 36π octaphyrin, **I.36**, is transformed into a planar antiaromatic macrocycle. In their experiments, they observed the addition of a strong base such as TBAF lead to the unfolding of the macrocycle in a two-step process. After the addition of 40 equivalents of TBAF, the proton NMR analysis revealed diatropic ring current effects in support of an aromatic Mobius 36π system, **[I.36]**. (scheme-9)

Ar = C$_6$F$_5$

I.36
Twisted Octaphyrin

-H$^+$ / +H$^+$

+2H$^+$ / -2H$^+$

-H$^+$ / +H$^+$

[I.36]$^-$
Mobius Aromatic Octaphyrin
Monoanionic species

[I.36]$^{2-}$
Planar Octaphyrin
Dianionic species
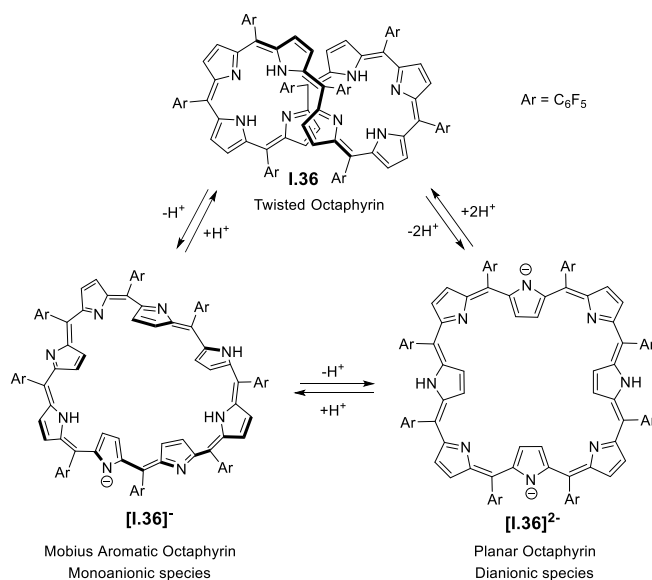
Scheme-9: Deprotonation induced conformational dynamics for octaphyrin.

Crystallization of the product obtained upon adding a huge excess of TBAF (~ 7000 equiv.) lead to the identification of a planar 36π octaphyrin, [**I.36**]$^{2-}$. Two tetrabutyl-ammonium cations, one each above and below the plane of the macrocycle, were observed in the single-crystal X-ray diffraction analysis confirming the dianionic feature of the macrocycle. Even though proton NMR analysis could not be observed for the dianionic species, the estimated chemical shift value of +22.6 ppm from NICS calculations indicated a strong antiaromatic character for the planar ocatphyrin dianion. The chemical shift value estimated from NICS calculations for the monoanionic species was found to be -11.9 ppm and supported the observed proton NMR spectrum. These observations highlight the unexplored aspect of 36π octaphyrin's ability to switch between twisted and planar conformation in response to an external stimuli. The authors ascribe this transfiguration to the loss of intramolecular weak hydrogen bonding between the imine pyrroles and the amine pyrroles, which is supposed to be responsible for strengthening the figure-of-eight configuration. In another report, Chandrashekar and co-workers[33] showed the unfolding of octaphyrin from a figure of eight to a planar topology upon protonation by TFA. (scheme-10)
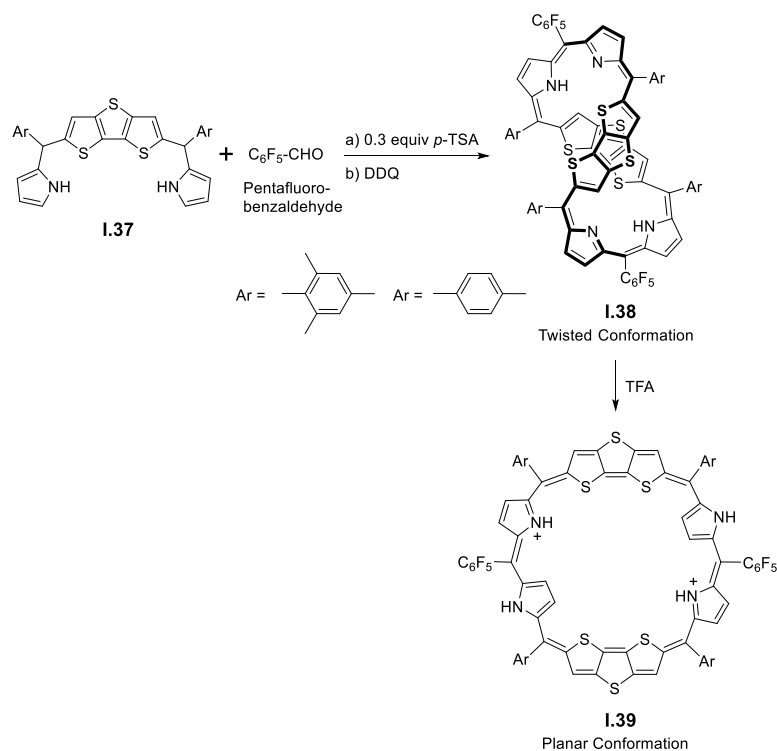
Scheme-10: Twisted to the planar conversion of doubly fused-octaphyrin upon protonation.

A 36π tetrathiaoctaphyrin was synthesized by employing the tetrapyrrane derivative of a fused-dithienothiophene (DTT), **I.37**. Under acidic conditions, **I.37** was condensed with pentafluorobenzaldehyde followed by oxidation with DDQ to yield the 36π octaphyrin, **I.38,** and adopted a figure-of-eight conformation. The spectroscopic characterization did not support any ring current effects expected of the 4nπ antiaromatic molecule. However, at 178K, two NH signals corresponding to two protons were identified at δ 18.70 and -0.10 ppm upon the addition of the TFA. The single-crystal X-ray diffraction analysis of this protonated species, **I.39**, revealed a planar structure with two ring inverted pyrrole rings. Two trifluoroacetate ions, one each above and below the plane of the macrocycle, established its diprotonated state. Recently, Latos and co-workers[34] described protonation triggered ring inversion in an expanded porphyrin (scheme-11) incorporated with α-α pyridine into the framework of rubyrin. Single-crystal x-ray diffraction analysis revealed a close-to-planar geometry for the macrocycle in solid-state except for the slight tilt of α, β-pyridine, concerning the plane of the molecule defined by four meso carbon atoms. Further, co-planar adjacent pyrrole and pyridine rings were involved in (pyrrole)NH-N(pyridine) hydrogen bond.
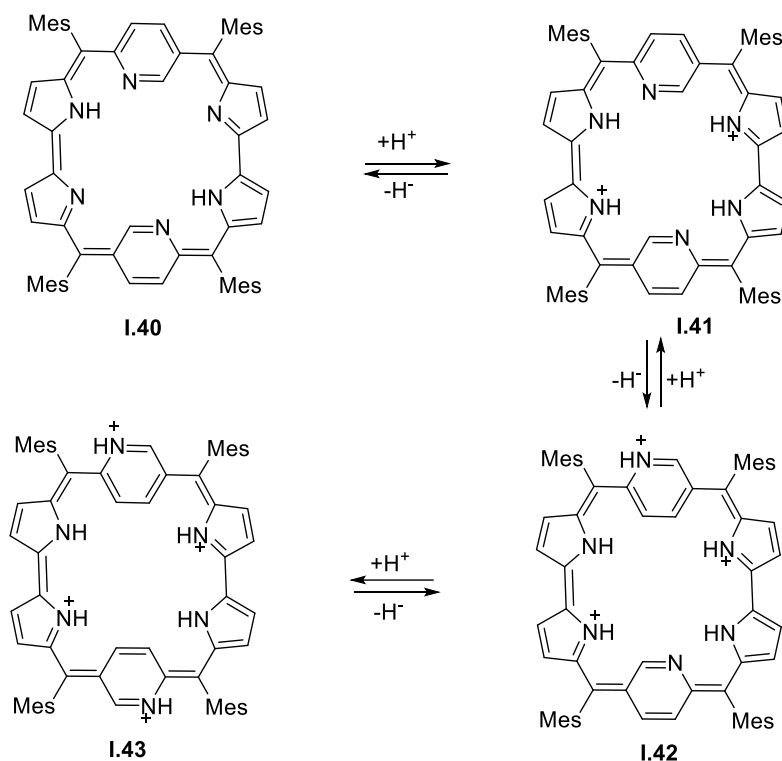
Scheme-11: Protonation induces ring inversions.

Protonation of **I.40** varied with the different protic acids. With a tetracationic species, **I.43**, was generated with methane sulfonic acid **I.43**, (scheme-11) while protonation with TFA resulted in tricationc species **I.42** and a dication was the sole product in the presence dichloro acetic acid (DCA). Molecular structure of monocationic species **I.41** and **I.43** was confirmed by X-ray diffraction analysis. The macrocycle **I.43** is nearly planar except for the slight tilt of α, β-pyridine moiety. Ring inversion of both the pyridine ring was confirmed by X-ray diffraction analysis.

Apart from topological switching, few expanded porphyrins are known to undergo redox switching between aromatic to antiaromatic state and vice versa using a suitable oxidizing and reducing agent. Sessler and co-workers reported a reversible proton-coupled redox switching of 24π antiaromatic macrocycle [35] **I.44** to the aromatic 26π macrocycle **I.46** via 25π unstable radical cation **I.45**. (scheme-12)
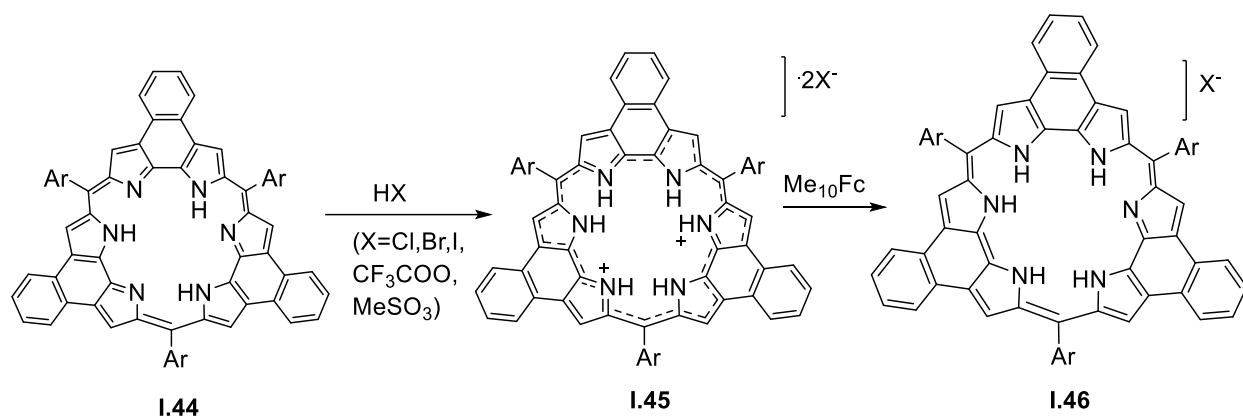
Scheme-12: Reversible Redox switching of 24π antiaromatic macrocycles.

The same group studied multiple redox switching in an annulated core modified octaphyrin [36] **I.47** (scheme-13), whose synthesis was achieved through naphtobipyrrole and dithieno thiophene diole under BF₃.OEt₂ catalyzed reaction. Further oxidation with 2,3-dichloro-4,5-dicyano-benzoquinone (DDQ), initial purification, and subsequent addition of MnO₂ lead to the isolation of macrocycle in 15% yields.
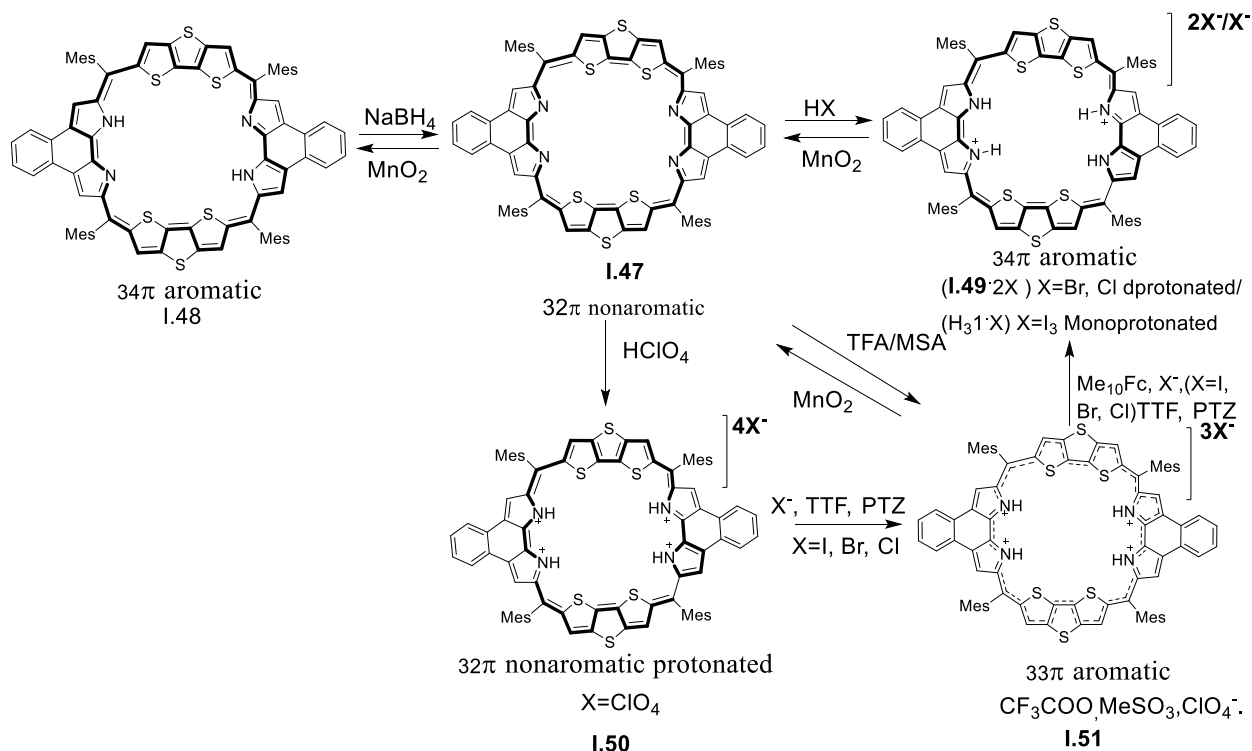
Scheme-13: Multiple redox switching in annulated core-modified rosarin.

Studies of reversible redox switching of non-aromatic annulated rosarian **I.47** by HX revealed a two-electron reduction to 34π aromatic dicationic macrocycle, **I.49**. It could be oxidized back to **I.47** by treatment with MnO_2. In another process, **I.47** was reduced to a neutral 34π macrocycle **I.48** by $NaBH_4$ and oxidized back to **I.47** by MnO_2. In contrast, the addition of $HClO_4$ lead to the formation of non-aromatic tetra cationic macrocycle **I.50**, which undergoes a one-electron reduction to 34π dicationic macrocycle **I.49** via 33π radical cation intermediate **I.51**. This 33π radical intermediate cation **I.51** could be oxidized to 32π non-aromatic **I.47** using MnO_2. In a separate process, **I.47** was reduced to 33π **I.51** intermediate using TFA/MSA. Single crystal X-ray revealed a nearly planar structure for **I.43** and other cationic species. Osuka and co-workers reported interconversion of hexaphyrin [37] between aromatic 26π **I.52** and anti-aromatic 28π **I.53** states by employing suitable oxidizing and reducing agents (scheme-14). Pyrrole containing macrocycles have the added the advantage of amine-imine conversion of pyrrole nitrogen, such that they can easily switch between aromaticity by proton-coupled electron transfer reaction.
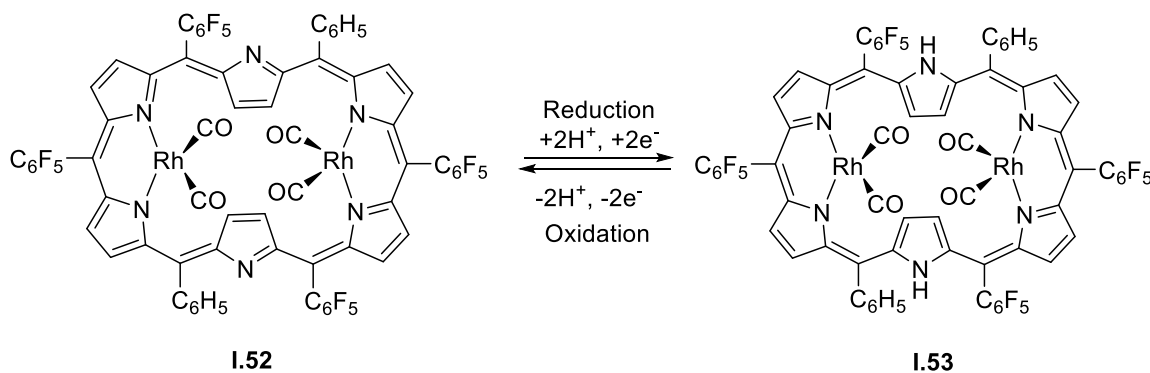
Scheme-14: PCET in dimetallated hexaphyrin.

Apart from these proton-coupled redox reactions, the flexible nature of expanded porphyrin enables them to switch between the aromatic and antiaromatic state with the same number of proton and π electrons. Temperature-dependent conformational changes observed for hexaphyrins **I.54** with different meso substitutions (figure-5) were reported by Osuka and coworkers.[38] Hexaphyrins exist in equilibrium among several rapidly interconverting Möbius conformations in solution at room temperature. Upon decreasing temperature to $-100°C$ in THF, these rapid interconversions among Möbius conformers are frozen, allowing the detection of a single hexaphyrin species **I.53** suggestive of its energetically most stable state only at lower temperatures.

But in solid-state, it adopts either planar **I.54** or Möbius-twisted conformations **I.55**, depending upon the *meso*-aryl substituents and crystallization conditions used. This implies a narrow energy gap between these two conformers, which can be affected by a variety of parameters such as solvent polarity, hydrogen bonding ability, which can affect crystal packing in the solid-state.

I.54   **I.55**
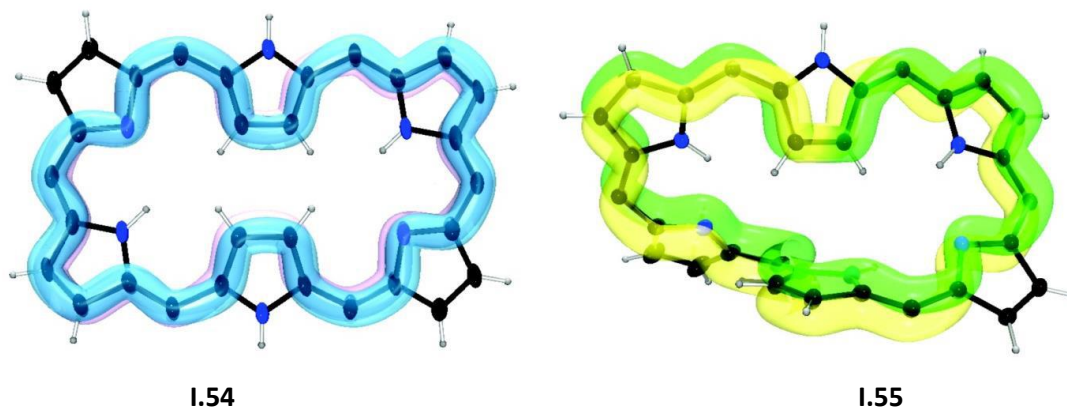
Figure-5: Solvent dependent conformational dynamics for hexaphyrin.

Similarly, Latos-Grażyński[39] and co-workers reported solvent and temperature-dependent conformational changes between Hückel antiaromatic and Mobius aromatic conformations of *p*-benzi[28]hexaphyrin, in which two rotating phenylene rings acts as "topology selector." The macrocycle is folded into the figure-eight structure, and depending upon the orientation of phenylene rings, the macrocycle adopts a unique conformation (figure-6). In contrast to the 4nπ annulenoid corresponding to Mobius aromaticity in **I.57**, **I.58** existed as twisted Huckel's antiaromatic and **I.56** adopted Huckels planar antiaromaticity in the solution state. All these forms were identified for a single oxidation state of the macrocycle.
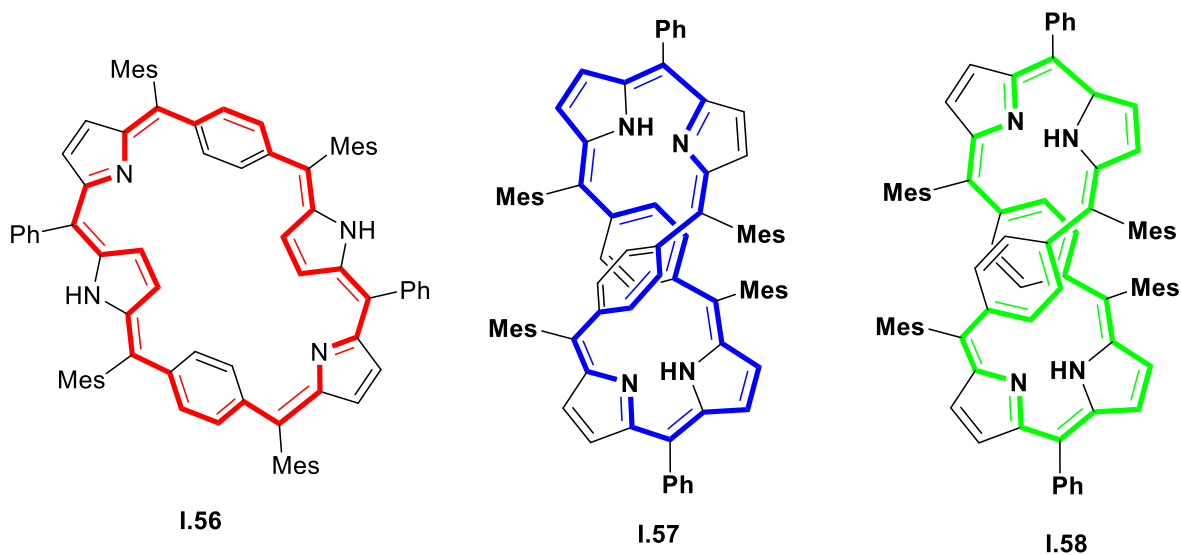
Figure-6: Hückel antiaromatic and Mobius aromatic conformations of *p*-benzi[28]hexaphyrin.

In general, expanded porphyrins are flexible and can be expected to exist as structural polymorphs in the solid-state. One of the methods that can be employed to develop various polymorphs of an expanded porphyrin is by adding a structurally similar additive to the macrocycle during the crystallization process. Such additive induced polymorphism is an important area of research, currently in crystallography. Controlling polymorphism is one of the most difficult challenges for pharmaceutical industries. Presently, additive induced polymorphism is known for small organic molecules only. In 2004, Gautam Desiraju and co-workers[40] reported additive induced polymorphism of trinitrobenzene **I.59** (it is crystalline solid with centrosymmetric space group Pbca) which is known as explosive for more than 100 years, and structurally similar to trisindane **I.60**. Mixing 1:1 and 2:1 ratio of trinitrobenzene and triindane was expected to yield a molecular complex by the co-crystallization technique (figure-7). Instead, a new polymorph of TNB(trinitrobenzene) **I.61** crystalized in non-centrosymmetric orthorhombic space group Pca21, Z=2

Orthorhombic Pbca   Orthorhombic Pca21
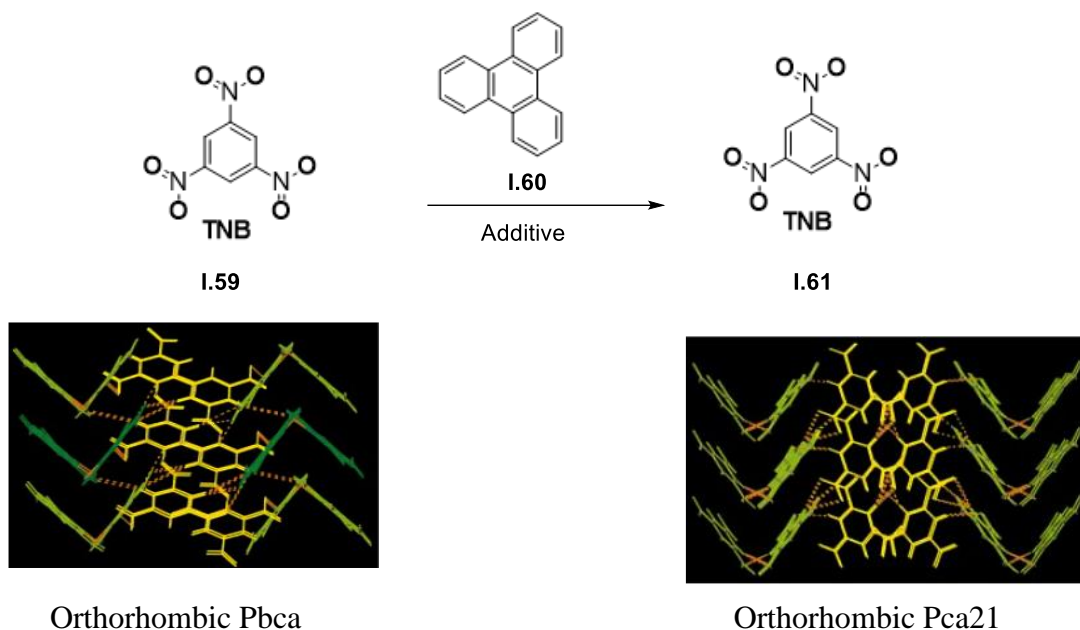
Figure-7: Additive induced polymorphism of TNB.

Similarly, in 2015, Z.K Nagi[41] reported additive induced polymorphism of ortho-amino benzoic acid **I.64** by using benzoic acid **I.65** as additive. The space group of *o*-amino benzoic acid **I.64** changed from orthorhombic to monoclinic **I.66** (figure-8)

Orthorhombic   Monoclinic
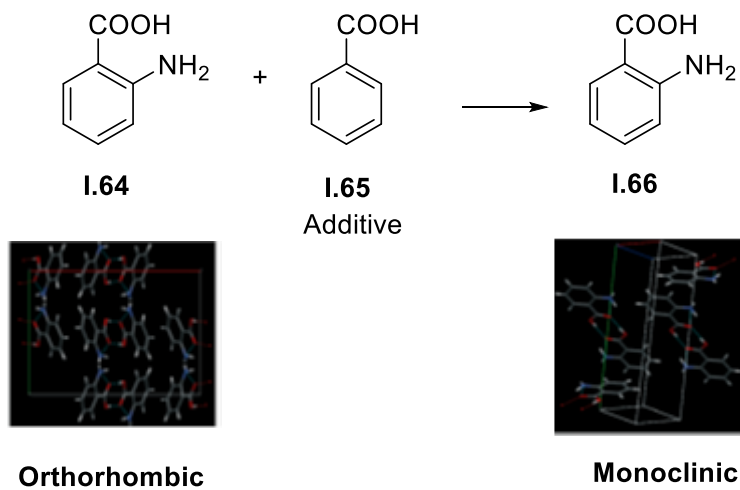
Figure-8: Additive induced polymorphism of Orthoamino benzoin acid.

Recent studies have revealed that expanded porphyrins provide an excellent platform for stabilizing organic radicals.[42] The remarkable stability of porphyrinoid radicals is mainly due to effective spin delocalization attributed to their unique structural and electronic flexibilities. These radicals generally exhibit unique properties such as NIR absorption bands, magnetic properties,

and small redox gaps.[42]. Owing to their chemical stability and unique properties, porphyrinoid-based radicals are promising candidates for applications in organic electronics. Jishan Wu and coworkers have reported bithiophene, and cyclopenta[2,1-b:3,4-b']bithiophene-bridged expanded porphycenes (figure-9) such as **I.67** and **I.68**. [43]
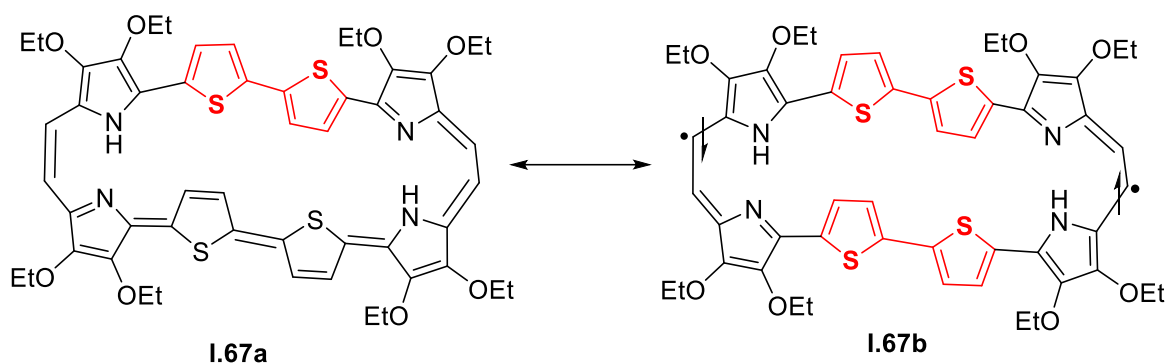
Figure-9: Illustrative example for the diradical generation in core-modified porphycene.

In **I.67a,** one quinoidal bithiophene unit must be drawn in its closed-shell resonance form, implying that $(y_0 = 0.63)$. The spin density of the singlet ground state was evenly distributed over the whole π framework. Even though the crystal structure of **I.68** could not be established, yet it also accounted for a moderate diradical character $(y_0 = 0.68)$ and tetraradical character $(y_1 = 0.18)$. Thus they were regarded as open-shell tetraradicaloid with an evenly distributed spin density over the whole conjugation framework (figure-10).
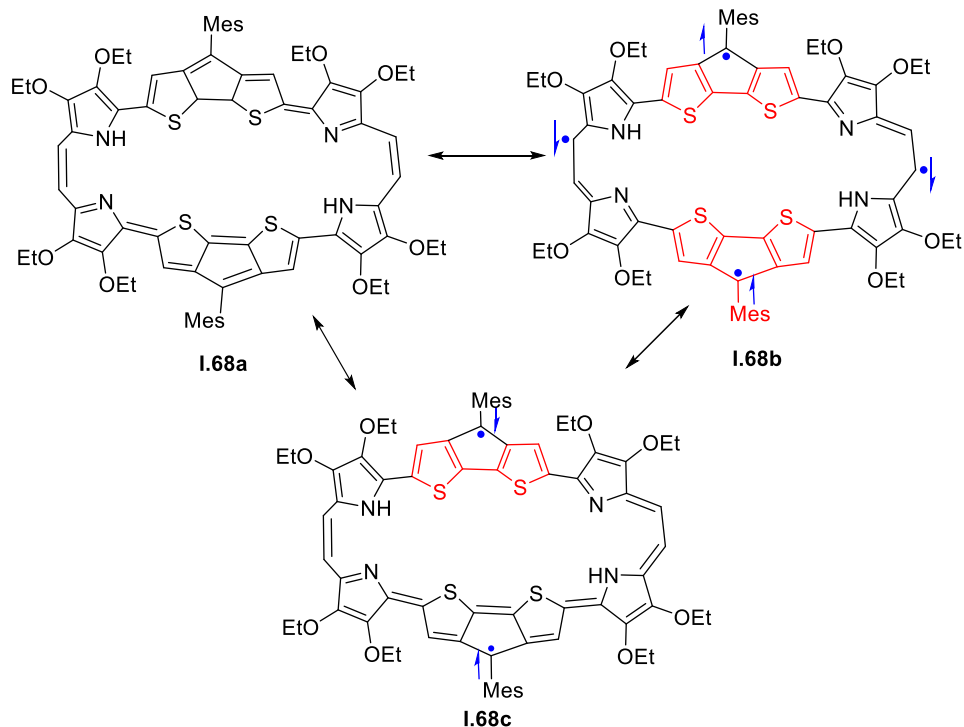
Figure-10: Illustrative example for the diradical and tetraradical generation in core-modified porphycene.

Compared to quinoidal oligothiophene, quinoidaloligoparaphenele is expected to show a larger diradical character due to large aromatic resonance energy of benzene ring than thiophene ring[44] leading to high reactivity. Such reactive species can be stabilized by incorporating a proaromatic unit such as p-quinodimethane (p-QDM)[44] into expanded porphyrin/isophlorin π conjugation framework. Similar to the quinoidal oligothiophene, the fundamental driving force to the diradical resonance form is recovery of the aromaticity of non- aromatic quinoidal rings (figure-11).
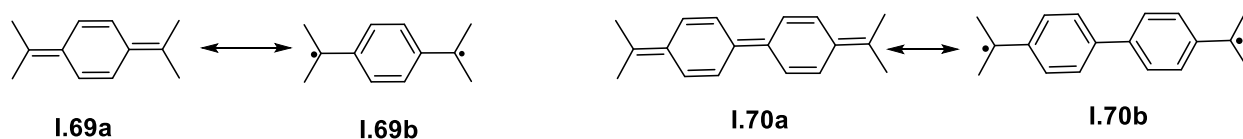
Figure-11: Thieles and Tschischibabin hydrocarbon.

Osuka and co-workers[45] synthesized a near planar octapyrrole, **I.73,** with benzene ring as a spacer at the center of the macrocycle. The predesigned tetrapyrrole precursor 1,4-(bis)dipyrromethane benzene, **I.71**, was condensed with a dipyrromethane carbinol, **I.72**, under acidic conditions followed by oxidation with *p*-chloranil (scheme-15).
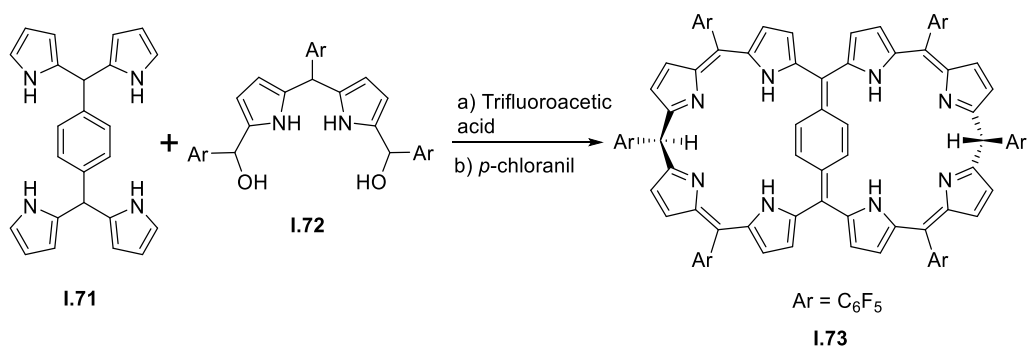
Scheme-15: Synthesis of *p*-quinodimethane-bridged core modified octaphyrin.

This reaction yielded macrocycles with two different orientations leading to the formation of the octapyrrole with a phenylene ring at the center of the macrocycle in less than 1% yields. However, the expected porphyrin dimer was obtained in 2% yields. Single-crystal X-ray diffraction analysis revealed that octapyrrole **I.73** adopted a nearly planar structure. Proton NMR studies revealed incomplete oxidation of the macrocycle with two sp^3 meso carbons similar to calix pyrroles. More interestingly, the central benzene ring was characterized as a *p*-quinodimethane. Here, the benzene ring lost its aromaticity and adopted the quinoidal structure due to the effective π conjugation of octapyrrole.

Aim of this thesis

Due to the presence of extended π conjugated network and interesting redox chemistry, expanded porphyrinoids can be utilized as promising candidates in organic electronics, non-linear optics, and energy storage devices. After studying vast literature on this field, it is found that expanded derivatives of porphyrins undergo structure induced loss of aromaticity, and there are very fewer methodologies available for obtaining planar expanded porphyrinoids. Therefore, in this thesis, it was decided to develop simple and efficient methodologies for the generation of these macrocycles. Porphyrinoids can display multiple redox states, owing to pyrrole's reversible switch between imine and amine nitrogen by proton-coupled electron transfer reactions. Porphyrin can exist in three different redox states, such as 20π isophlorin [3], 18π porphyrin [3,] and 16π porphyrin [3b]. These different electronic states for porphyrin have not been achieved to date for a single molecular entity. Chen et al. isolated 20π isophlorin by substituting electron-withdrawing substituents at the β-position of pyrrole. Whereas Yamamoto. et al. obtained a 16π antiaromatic porphyrin by substituting bulky tertiary butyl group on all the β-positions of porphyrin. Expanded derivatives of porphyrin such as hexaphyrin and octaphyrin contain more number of imine type nitrogen than that of porphyrin. Therefore, they are expected to adopt a wide range of redox states with huge variation in the structural landscape due to repulsion between the hydrogen at the center of macrocycles or due to steric effects in the ionic states.

Heterocyclic ring inversions are generally observed for planar macrocycles. Two thiophene rings in the bithiophene prefer to orient opposite to each other into its solid-state structure. Therefore, it was decided to study the effects of the oligomeric bithiophene unit on to octaphyrin framework. A characteristic feature of these fluxional macrocycles is to adopt multiple conformations. Inter-conversion between two or more structures may be directly correlated to their respective thermodynamic stability. Various solution state structural conformers are analogous to polymorphs when isolated in the solid-state due to their distinct physical properties. Spectroscopic techniques in the solution state can estimate the kinetics of structural transformations, whilst freezing the different conformations into solid-state is a tedious endeavor. Identifying the right conditions to arrest the apparent and the unperceived conformers is a task limited only by imagination, as justified by polymorphism. Expanded congeners of porphyrin and isophlorin belong to that class of flexible macrocycles with a high potential to exhibit polymorphism. Vivid

and diverse topological manifestations of these π-conjugated macrocycles are attributed to the synthetic protocols that have continuously engineered for more than a decade. Many of these molecules are known to be fluxional as they can exhibit more than one conformation with variation in the condition of crystallization, solvents, temperature, or by co-crystallization with suitable additives. Linear quinoidal oligothiophenes are known to exist in the diradical state by the recovery of aromaticity into its benzenoid form. The introduction of this oligomeric unit could be the platform for obtaining macrocyclic diradicals. Benzene is more aromatic than then thiophene and incorporation of a pro-aromatic unit such as p-quinodimethane (p-QDM) into expanded porphyrin/isophlorin π conjugation framework may lead to the formation of the stable compound with distinctive diradical character. Similarly, benzene can be utilized as a spacer to connect two antiaromatic isophlorin. Isophlorins are known to behave as pseudo metals, and therefore it may lead to interesting redox chemistry, with suitable oxidizing and reducing agent agents. This thesis aims to explore the multiple redox states, the resulting structural transformtions and the associated electronic properties of porphyrinoids. Adequate quantum mechanical calculations will also be employed for a theoretical interpretation of the experimental results.

Chapter 2: A wide-range of redox states in expanded Porphyrinoids

II.1 Introduction:

Based on the number of π electrons, Huckle's empirical rule distinguishes planar conjugated molecules as aromatic and anti-aromatic systems. In principle, an aromatic (or anti-aromatic) system can be reduced or oxidized to $4n\pi$ (or to $(4n+2)\pi$) species through a two-electron redox process. The isophlorin-porphyrin, **II.2**-**II.3**, couple[3] represents a redox driven inter-convertible 20π and 18π states. Ideally, the two-electron reduction of a porphyrin should yield a 20π isophlorin, **II.2**,[46] while the corresponding oxidation of porphyrin should result in 16π anti-aromatic macrocycle, **II.4**.[47] However, the structural intricacies associated with the stability of $4n\pi$ species **II.4** and **II.2** do not promote the reversible four-electron redox in a unique porphyrin (scheme-II.1).
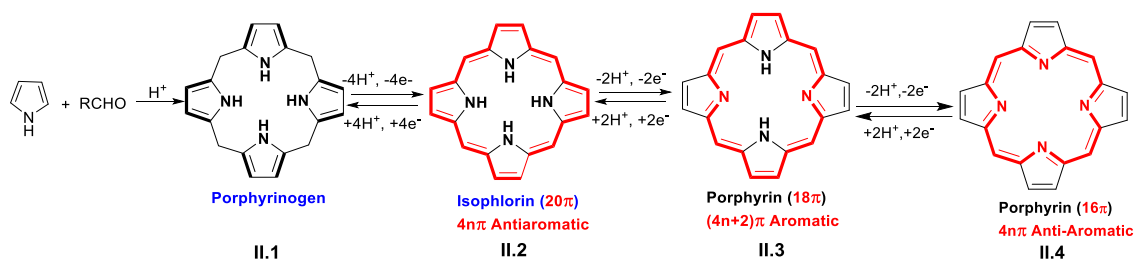
Scheme-II.1: Expected redox chemistry for porphyrin.

Therefore several structural modifications, such as substituting electron-withdrawing group (scheme-II.2) and bulky tertiary butyl group (scheme-II.3), are made on the periphery of the tetrapyrrolic macrocycle to achieve 20π[46] and 16π[47] macrocycles as stable $4n\pi$ systems respectively.
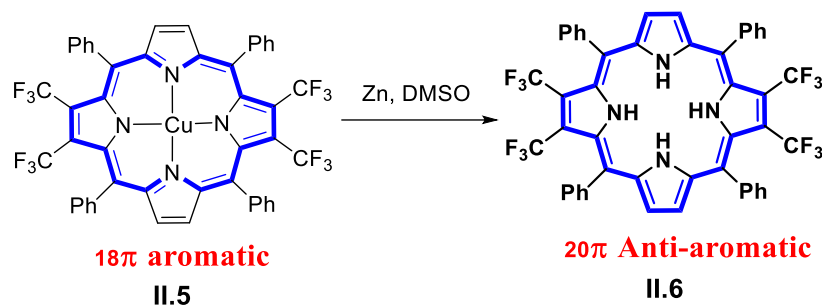
Scheme-II.2: Synthesis of 20π isophlorin **II.6** with electron-withdrawing substituents.
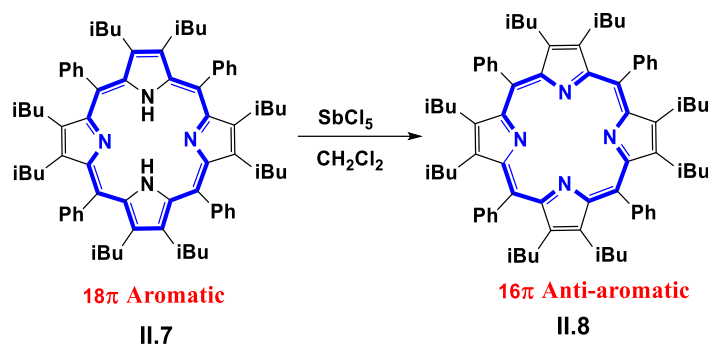
Scheme-II.3: Synthesis of 16π porphyrin **II.8** with bulky substitutions.

Macrocycles containing pyrrole/thiophene/furan, or other heterocyclic subunits linked either directly or through one or more spacer atoms in such a manner that the internal ring pathway contains a minimum of 17 atoms are called as expanded porphyrins.[21] Amongst the expanded porphyrins, hexaphyrin is the simplest of the macrocycles, originally introduced by Cavaleiro et al. as a 26π aromatic macrocycle, which can be reduced to 28π hexaphyrin using tosyl hydrazine (TsNHNH₂).[48] Later, Osuka and co-workers synthesized hexaphyrin through a one-pot reaction between pentaflorobenzaldehyde and pyrrole, and established a similar redox dependent inter convertibility. Simple redox reagents such as NaBH₄ and DDQ were employed as reducing and oxidizing agents respectively to interconvert 26π aromatic and 28π anti-aromatic states of the macrocycle.[49] Extending the process by two more electrons, it can be envisaged that a 26π hexaphyrin with four imine nitrogens can accept four protons and four electrons to be reduced to 30π aromatic state. Achieving a highly reduced state in the single molecular framework is found to be challenging without suitable substituents on the heterocyclic units. Osuka and co-workers attempted the synthesis of a 30π isophlorin by the two-electron reduction of 28π hexaphyrin by substituting the ethylsulfanyl group to the periphery of the macrocycle.[50] They observed that the

34

ethylsulfanyl groups were critical to the reduction of 28π hexaphyrin to the 30π expanded isophlorin. However, it was found to be unstable and succumbs to oxidation over a period of time in the presence of atmospheric oxygen, which further supports the unstable nature of highly reduced hexapyrrole hexaphyrin with 30π electrons. Later, Anand et. al. successfully synthesized highly stable 30π expanded isophlorins, by replacing all the pyrrole units of hexaypyrrole hexaphyrin with other heterocycles such as thiophene/furan/selenophene.[51] The obtained 30π expanded isophlorin with chalcogens such as O/S/Se prevented the proton-coupled electron transfer (PCET) observed in pyrrole containing hexaphyrins. Replacing two thiophene units of a 30π isophlorin could generate 28π core modified porphyrin, which could also exhibit unobserved but the expected PCET between 28π core modified expanded porphyrin and 30π expanded isophlorin (scheme-II.4).
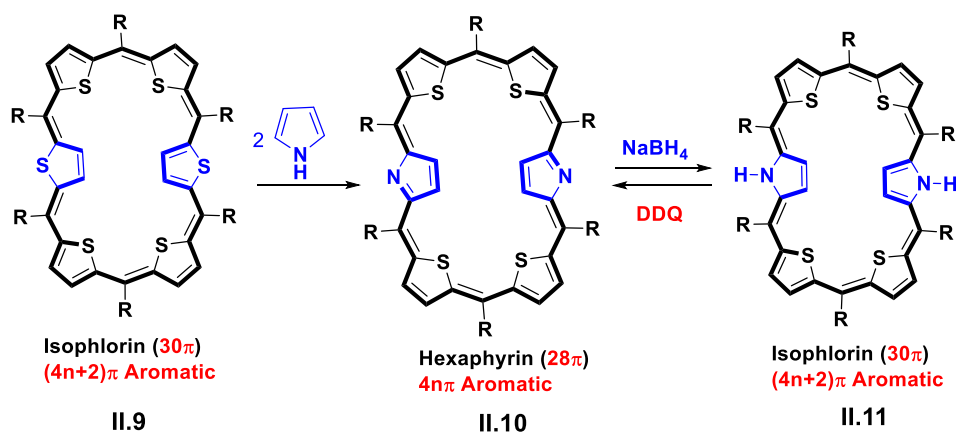
Scheme-II.4: Synthetic strategy for 28π (**II.10**) and 30π (**II.11**) hexaphyrins.

II.2 Synthesis and charecterization of core-modified hexaphyrin II.10.

Synthesis of core-modified hexaphyrin II.10

Hexaphyrin, **II.10**, was synthesized by an acid-mediated condensation of dithiapyrane dicarbinol, **II.12**, with pyrrole in inert conditions and followed by oxidation open to air (scheme-II.5). The expected product was purified from silica-gel column chromatography as an orange-colored band in 12% yields.
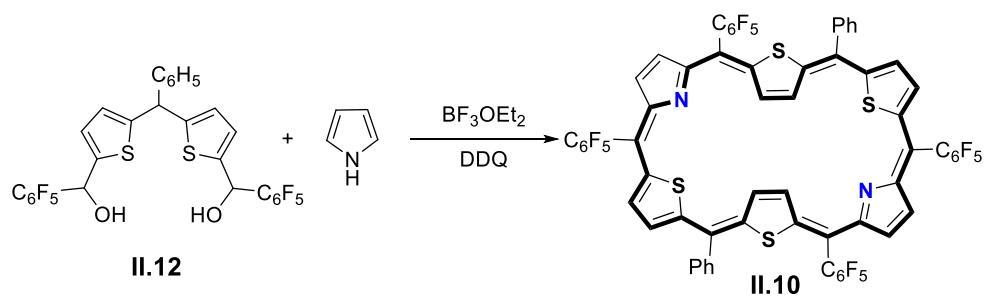
Scheme-II.5: Synthesis of core modified hexaphyrin **II.10**.
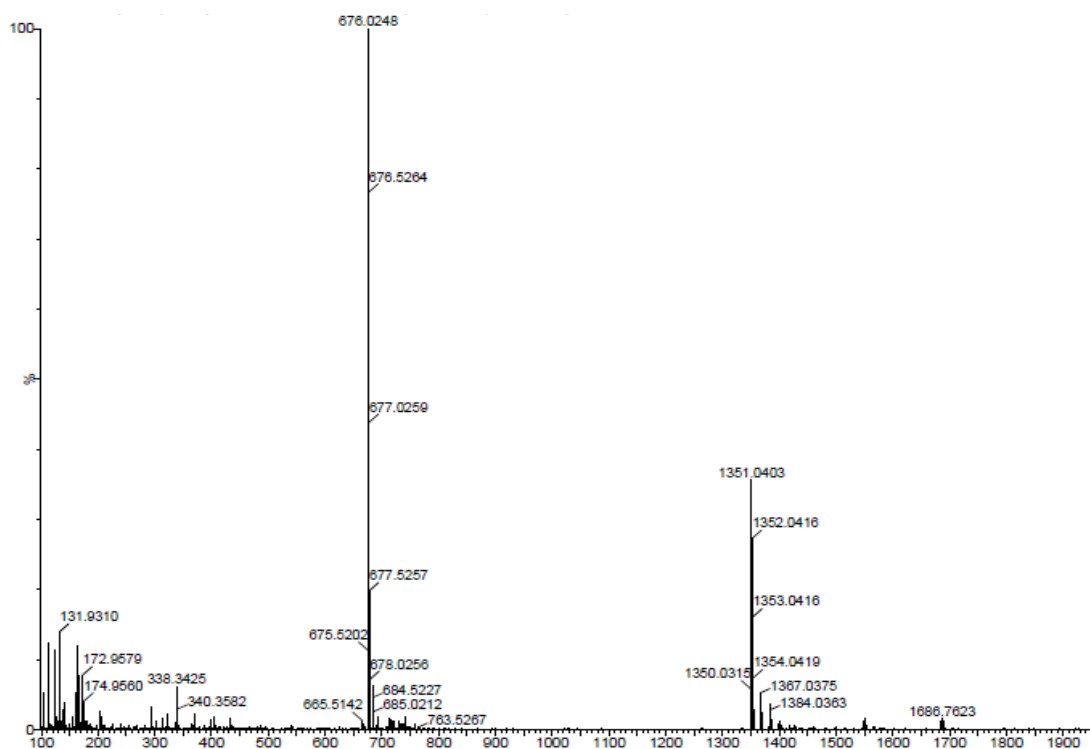
Figure II.1: High-resolution mass spectrum of **II.10**.

Structural Characterization of core modified hexaphyrin:

The hexaphyrin **II.10** was analyzed through high-resolution mass spectrometry (figure-II.1), UV-Vis, NMR Spectroscopy, X-ray crystallography, and cyclic volumetric studies.

Electronic absorption studies

The UV-Vis absorption spectrum of 28π hexaphyrin, **II.10**, was recorded in distilled dichloromethane, which displayed high energy absorption at 471nm (13000), followed by shoulder peak at 551nm (8000) (figure-II.2).
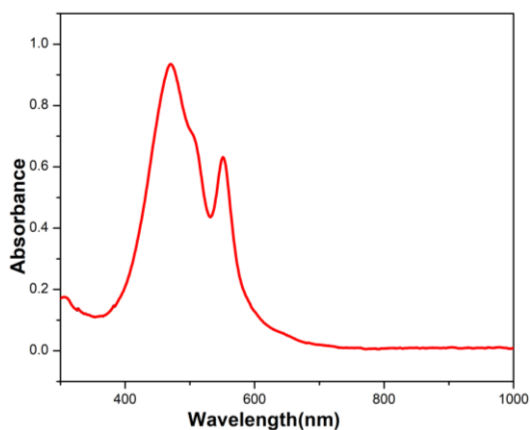
Figure II.2: UV-Vis Absorption spectrum of (10^{-5}M) **II.10** in CH_2Cl_2.

NMR characterization

The ^{1}H NMR spectrum of **II.10** recorded at 298K exhibited paratropic ring current effect expected of a 4nπ anti-aromatic system arising from 28π electrons conjugated pathway. Two doublets with the integration of two protons each were observed at δ 16.82 and 15.62 ppm. Another four doublets, corresponding to two protons each, were observed between δ 4.83 to 4.53 ppm (figure-II.3). As expanded porphyrins are known to exhibit ring inverted structures, the chemical shift of the protons are differentiated by the orientation of the heterocyclic rings in the macrocycle. Downfield and upfield chemical shift for the protons antiaromatic systems are known to be the reverse of diatropic ring current effects observed in aromatic systems. Hence, in the case of ring inversion, the protons at the center of the macrocycle will experience a down-field shift in comparison to the high field shift for the protons on the periphery of the macrocycle. Therefore, the low field doublets can be attributed to the protons of ring inverted heterocycles. ^{1}H-^{1}H COSY spectrum of **11.10** recorded in chloroform-*d* displayed three sets of correlations for doublets at δ (i) 16.82 and 15.66, (ii) 5.16 and 4.83, (iii) 4.70 and 4.53 ppm (figure-II.4). The observed sets of doublets confirmed the coupling of adjacent β protons of the heterocyclic rings. Symmetry of the macrocycle varies significantly if thiophene or pyrrole rings are inverted. Inversion of diagonally opposite thiophene rings would render the macrocycle less symmetrical in comparison to the pyrrole ring inversion. Observation of six doublets in the ^{1}H NMR spectrum of **11.10** suggested a lower symmetry of the macrocycle owing to ring inverted thiophene units.

37
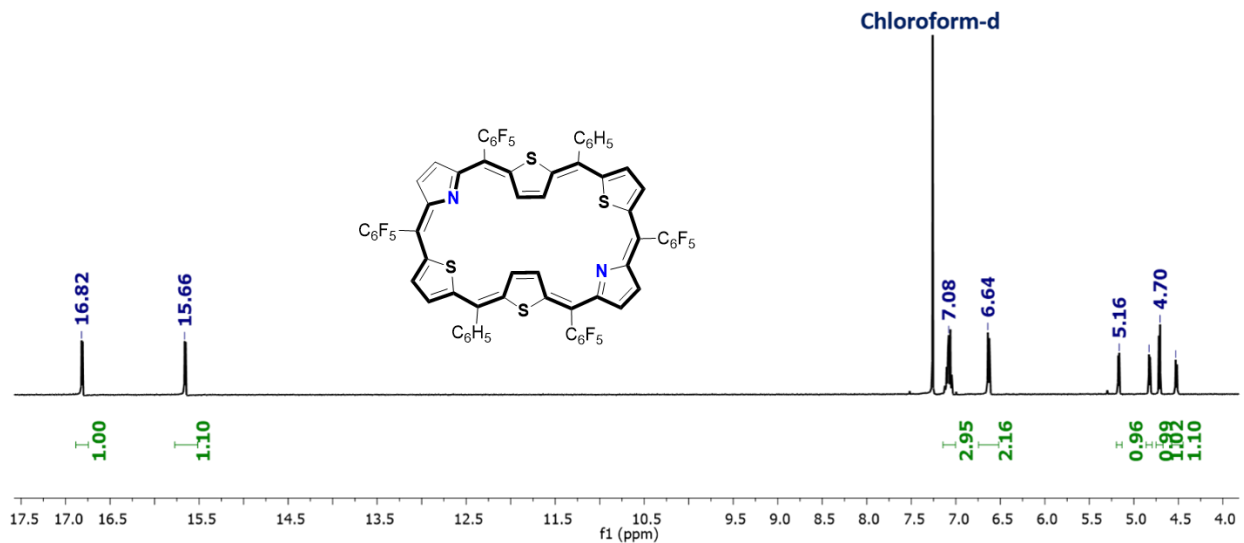
Figure II.3: ^{1}H NMR of **II.10** in chloroform-*d* at 298K.
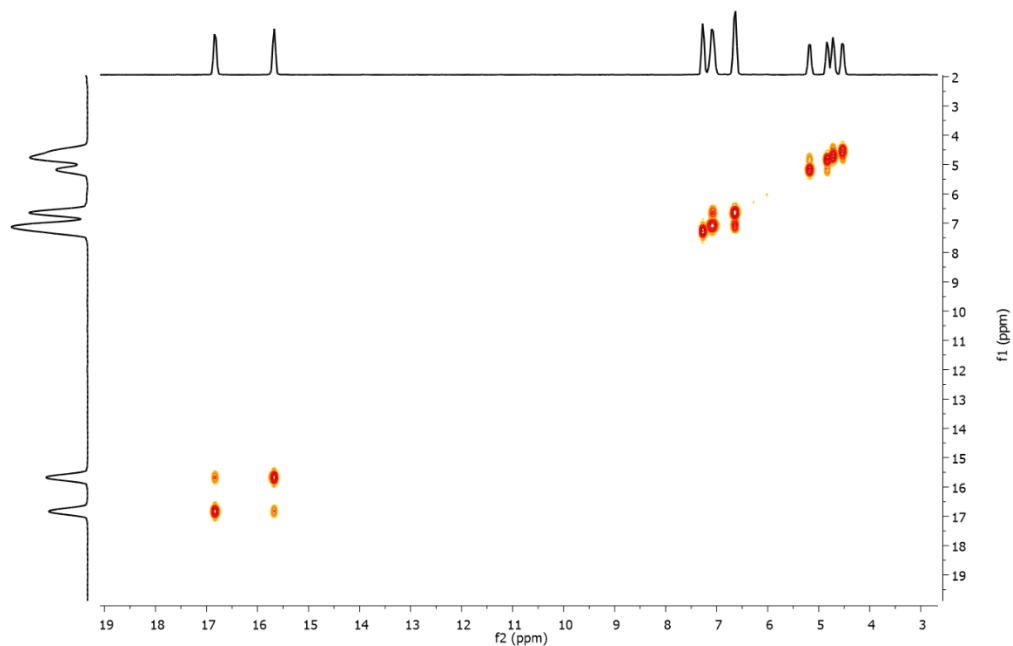
Figure II.4: ^{1}H-^{1}H COSY spectrum of **II.10** in Chloroform-*d* at 298K.

Single crystal X-ray diffraction analysis of core-modified hexaphyrin II.10:

The structural characteristics of **II.10** in solid-state were confirmed by its molecular structure obtained by single-crystal X-ray diffraction analysis of good quality crystal grown in chloroform/hexane by using vapor diffusion method.
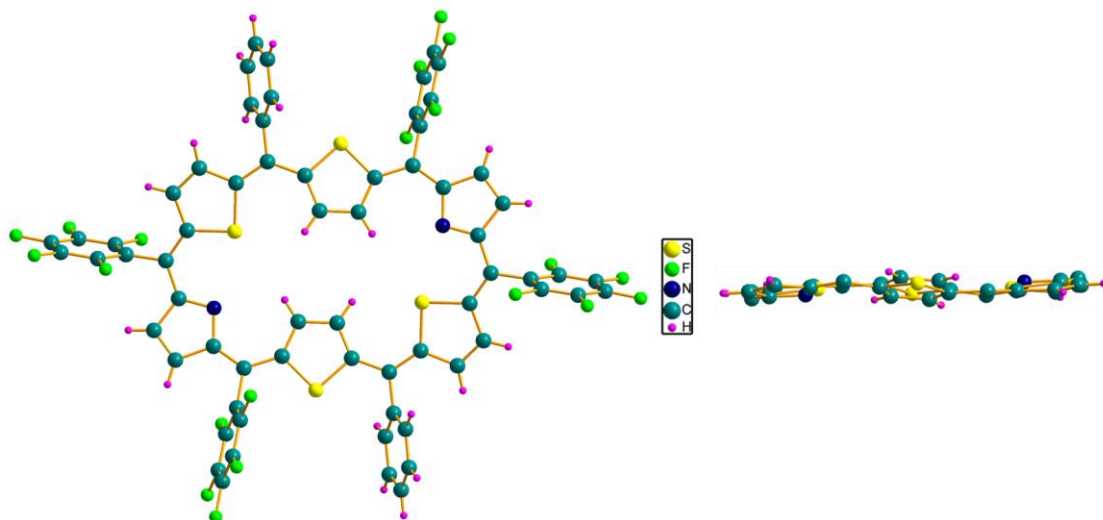
Figure II.5: Top view (left) and side view (right) of molecular structure for **II.10**. Phenyl rings are omitted from side view for clarity.

The molecule crystallized in triclinic space group with inversion of two diametrically opposite thiophene rings and remaining four heterocyclic units (pyrrole and thiophene) are pointing towards the center of macrocycle. All the phenyl and pentaflurophenyl rings are found to be near-orthogonal to the mean macrocyclic plane. This structure further validated the observed paratropic ring current effects observed in its ^{1}H NMR spectrum.

Cyclic voltammetry studies
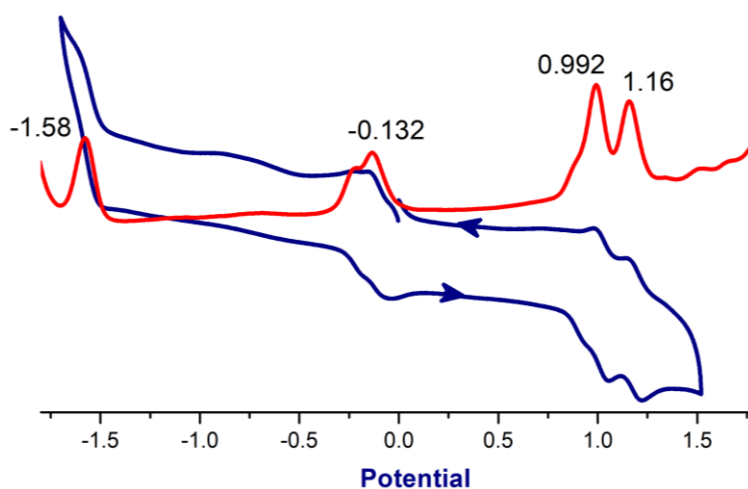
Figure II.6: Cyclic voltammogram (blue) and Differential pulse voltammetry (red) of **II.10** in dichloromethane   containing 0.1M tetrabutylammonium perchlorate as the supporting electrolyte recorded at 50 mVs^{-1}.

Preliminary cyclic voltammetric studies for **II.10** exhibited two reduction waves at -1.58V and -0.13V and two oxidation waves at 0.99V and 1.16V respectively (Figure-II.6), Therefore suitable redox reagents could be employed to reduce this 28π antiaromatic system to the 30π aromatic state or oxidized to the 26π aromatic dication. Inspired from the electrochemical behavior, the chemical synthesis of reduced 30π and oxidized 26π aromatic species of **II.10**, was attempted under different chemical redox condition.

II.3 Synthesis and characterization of II.13

Synthesis and electronic absorption studies of II.13

Meerwein's salt $[Et_3O]^+[SbCl_6]^-$ [52] is known to be an effective one-electron oxidant of π-conjugated molecules and a classic redox reagent for aromaticity switching by electron transfer reaction.[12,13] Anticipating two-electron ring oxidation, **II.10** was treated with $[SbCl_6]^-[Et_3O]^+$ in dichloromethane (scheme-II.6). Addition of Meerwein salt to **II.10** induced an immediate color change, from orange to green with redshift in its absorption spectrum from 471 nm (13000) to 676 nm (32000) followed by low energy absorption bands at 893 nm (2500) and 990 nm (2100) (Figure-II.7).
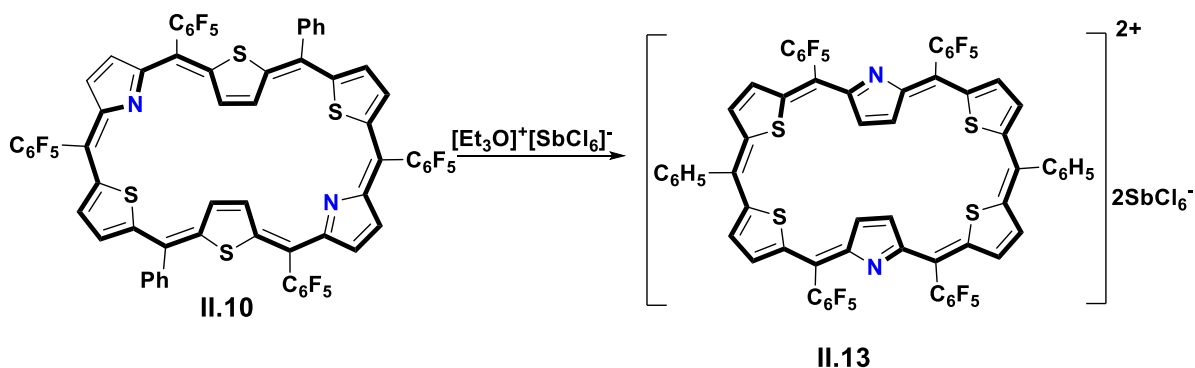
Scheme-II.6: Two electron oxidation of **II.10** to **II.13**.
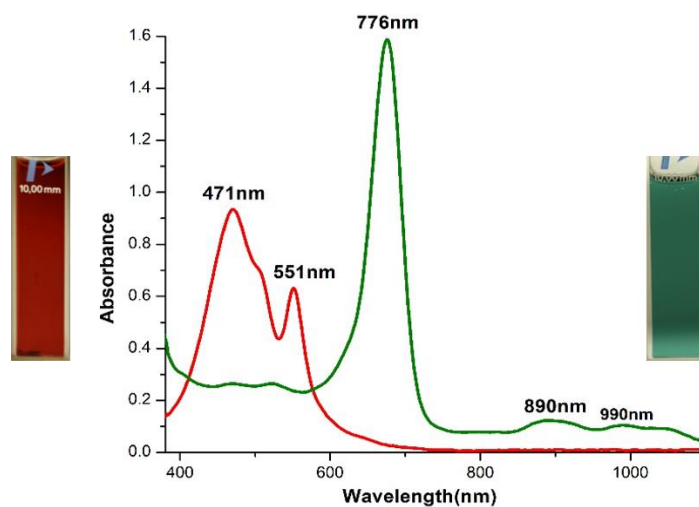
Figure II.7: Absorption changes observed for (10^{-5}M) **II.10** (red) upon oxidation to **II.13** (green) in dichloromethane.
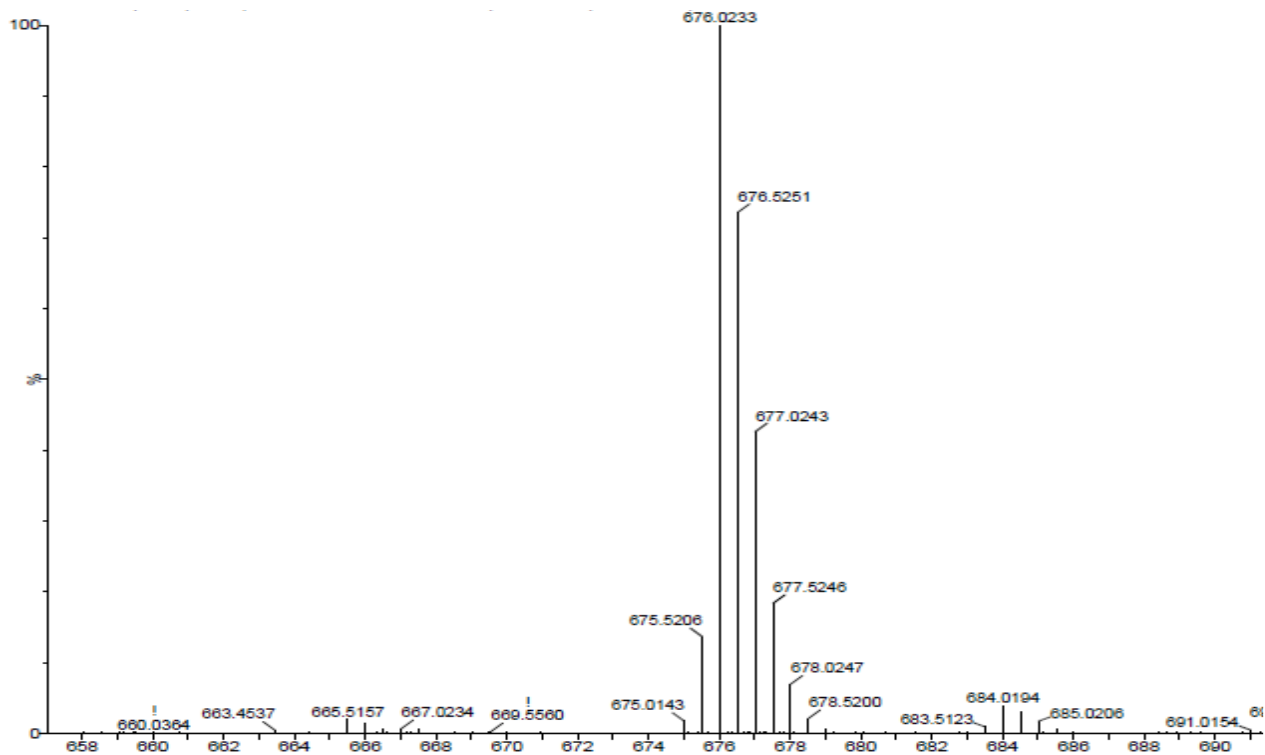
Figure II.8: High resolution mass spectrum (HRMS) of **II.13**.

Structural characterization of II.13:

¹H NMR Studies of II.13

The ¹H NMR spectrum of the oxidized species, **II.13**, recorded in dichloromethane-d_2 displayed well-resolved signals at 233K negating the possibility of radical species. Four doublets, corresponding to two protons, each resonated at δ 8.96, 8.75, 8.57, and 8.43 ppm. A singlet corresponding to four protons was observed at δ -0.14 ppm. Observation of downfield and upfield shifts for the oxidized species further supported the ring oxidation of antiaromatic **II.10** to the aromatic dication, **II.13**. Reduced number of signals also implied redox induced conformational change without unsettling the planar topology. In comparison to the **II.10**, a higher symmetry for the aromatic macrocycle was envisaged by the outward flipping of inverted thiophene and the inward flip of the pyrrole β-carbons. Protons of the ring inverted pyrrole are exposed to the diatropic ring current effect of 26π aromatic macrocycle, **II.13**, and hence resonated as an upfield singlet. HRMS spectrum of **II.13** displayed a mass m/2 peak with an isotopic abundance of 0.5, characteristic of dicationic species.
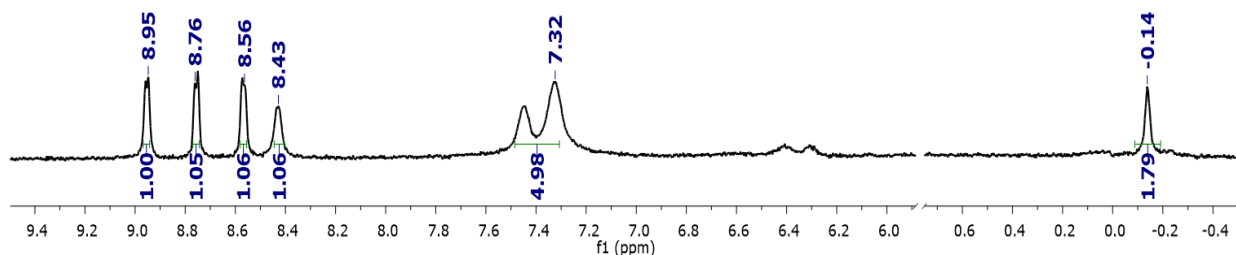
Figure II.9: ¹H NMR spectrum of **II.13** at 233K in CD₂Cl₂. (Signals observed in the range between 1-5.5 ppm correspond to ethyl chloride and diethyl ether from Meerwein salt).

Single crystal X-ray diffraction analysis of II.13
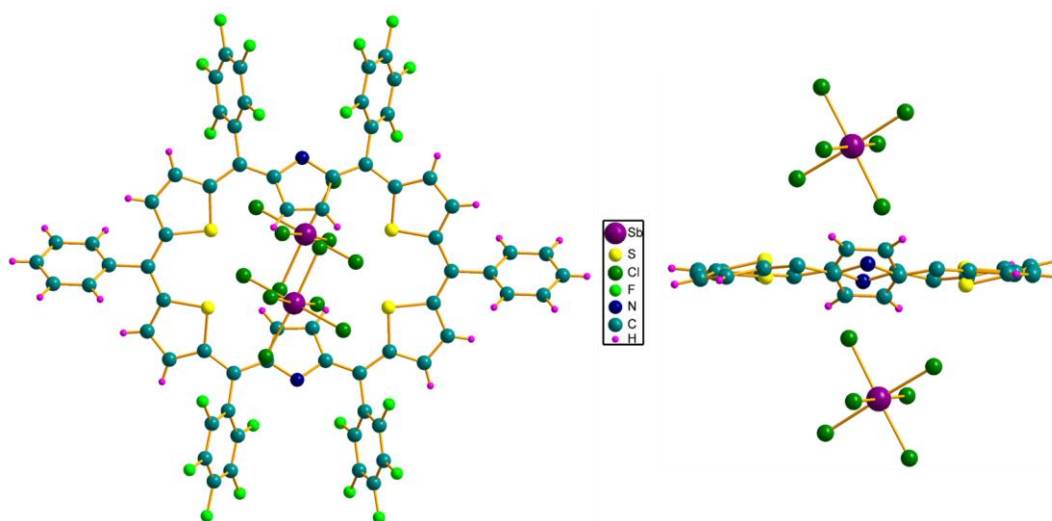
Figure II.10: Molecular structure [(left) Top view, (right) Side view] of **II.13**. Phenyl rings are omitted from side view for clarity.

Molecular structure of **II.13** determined from single-crystal X-ray diffraction confirmed ring inverted pyrroles with a near-planar topology of the macrocycle (Figure **II.10**). In support of the observed 1H NMR spectrum for the oxidized species, both the pyrrole rings were inverted and hence the b-protons were exposed to the diatropic ring current of the aromatic macrocycle. The presence of two antimony hexachloride $[SbCl_6]^-$ anions located one above and below the plane of the macrocycle, justified the two-electron ring oxidation of the antiaromatic 28π hexaphyrin

II.4 Synthesis and Characterization of II.11

Synthesis and electronic absorption studies of II.11

Electrochemical measurement displayed signature two-electron reduction of **II.10.** Osuka and co-workers established $NaBH_4$ as a proton-coupled electron transfer reagent to reduce 26π hexaphyrin to 28π.[49] However the attempted reduction of **II.10** using an excess of $NaBH_4$ went futile. As observed with antiaromatic macrocycles,[53,54] it was expected that two-electron reduction of dication, **II.13**, will yield the corresponding neutral macrocycle, **II.10**. However, reduction of **II.13** with metallic Zn (scheme- II.7) yielded a new unstable blue colored species which immediately converted to **II.10**. A possible reason for the appearance of a temporary blue color could be envisaged for the over reduction of **II.13** by four electrons to the dianionic state. To confirm this hypothesis, NH_4Cl was added as a proton source to quench the dianionic state of the macrocycle

resulting in a significant blue-shifted band as identified through electronic absorption spectrum (figure-II.11). It displayed a vivid pink-colored solution with an even more intense absorption at 552 nm (36000) followed by low energy bands at 683 nm (3600) and 742 nm (1500) for **II.11**. The newly formed 30π macrocycle **II.11** can be oxidized by two electron to 28π macrocycle, **II.10**, upon treating with MnO_2, whereas it can be oxidized by four electrons to **II.13** by employing Meerwein salt (scheme-II.8).

Scheme-II.7: Reduction of **II.13** and **II.10** to **II.11** by Zn/NH₄Cl.
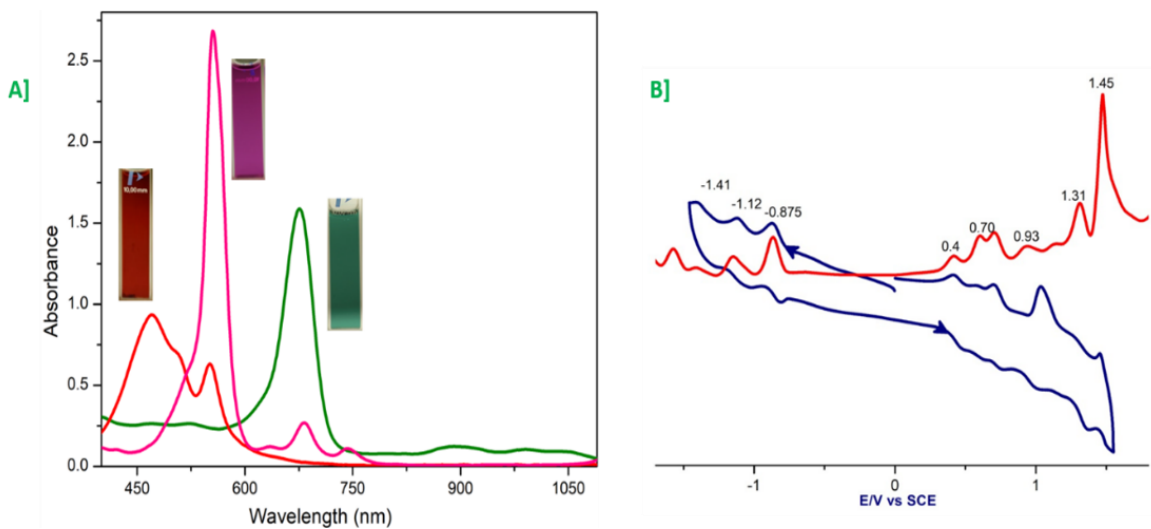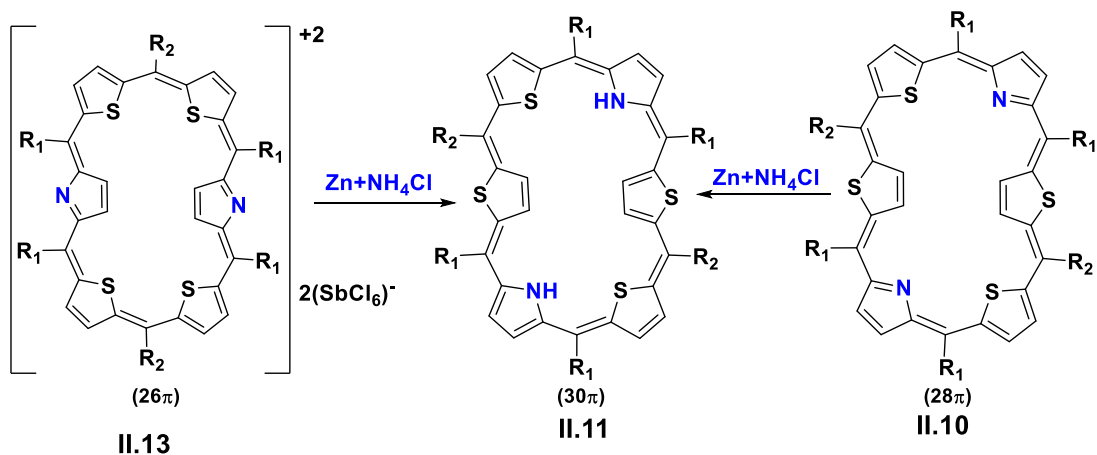
Figure II.11: A] Absorption changes observed in the solution of **II.11**(pink) upon oxidation by MnO₂ to **II.10** (orange) and **II.13** (green) upon the addition of Meerwein salt. B] Cyclic (blue) and differential pulse (red) Voltamogram of **II.11** in dichloromethane containing 0.1M tetrabutylammonium perchlorate as the supporting electrolyte recorded at scan rate of 50 mV s⁻¹.

Structural characterization of II.11:

HRMS and ^{1}H NMR studies

A high-resolution mass spectrum of **II.11** displayed m/z value of 1352.0455. It corresponded to two units more than the observed value for **II.10**, signifying the addition of two protons. The ^{1}H NMR spectrum of this species displayed four doublets, corresponding to two protons each, in the downfield region between δ 8.25 and 9.15 ppm. Two more doublets corresponding to two protons each were detected at δ -1.40 and -1.60 ppm (figure-II.12A). In addition to these two shielded signals, a broad singlet observed at δ -2.0 ppm, corresponding to two protons, was found to diminish upon the addition of D_2O (figure-II.12B). These signals asserted significant ring current effects for this macrocycle. In addition, deuterium exchange studies justified the presence of NH protons of the pyrrole rings resulting from the reduction by Zn/NH_4Cl. An important observation was the flipping of pyrrole ring upon reduction of **II.10** to **II.11**. Since the two-electron reduction of **II.13** by Zn/NH_4Cl did not yield **II.10**, the NMR data strongly advocated the formation of 30π isophlorin species, **II.11**, with two NH's in the center of the macrocycle. Further support for the expanded isophlorin **II.11** was observed by the three sets of correlation for β-protons of three heterocyclic rings at δ (i) 9.0 and 8.94, (ii) 8.36 and 8.25, (iii) -1.40 and -1.60 ppm (figure II.13).
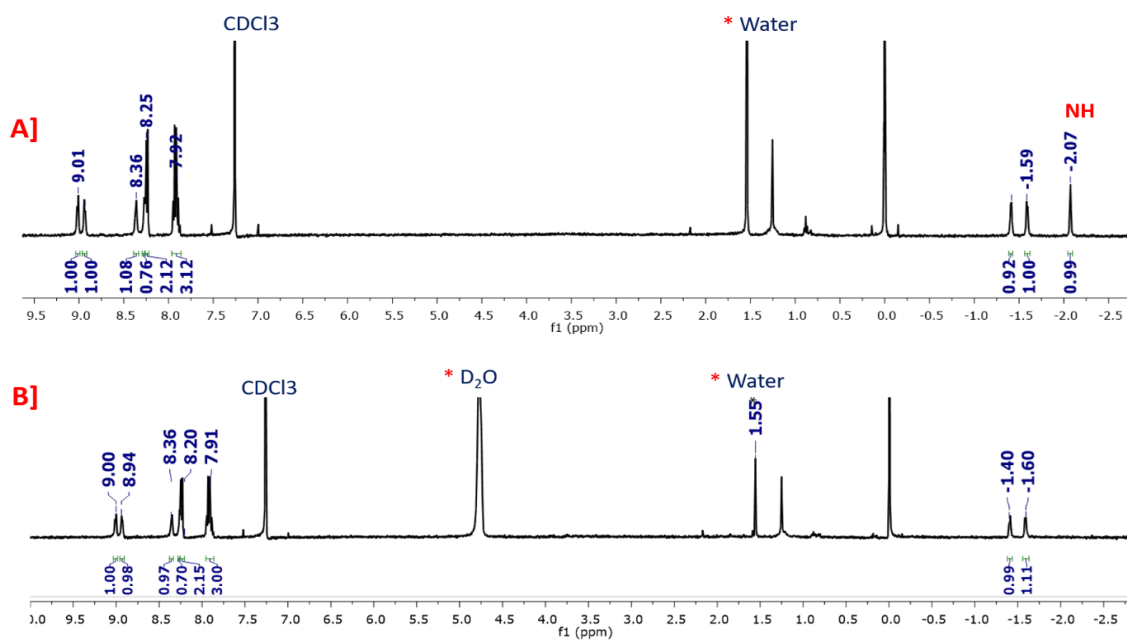
Figure II.12: A] ^{1}H NMR spectrum of **II.11** at 298K in CDCl₃. B] ^{1}H NMR spectrum of **II.11** at 298K in CDCl₃ upon the addition of D_2O.
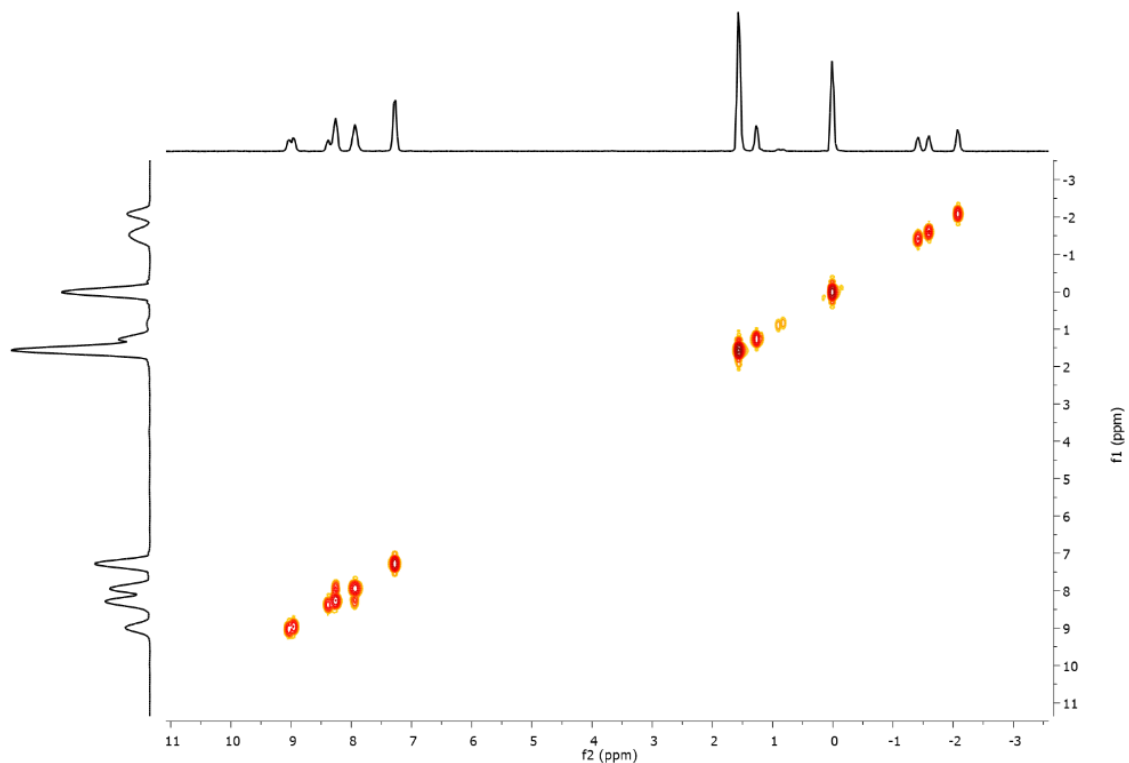
Figure II.13: ^1H-^1H COSY Spectrum of **II.11.**

Single crystal X-ray diffraction analysis of II.11
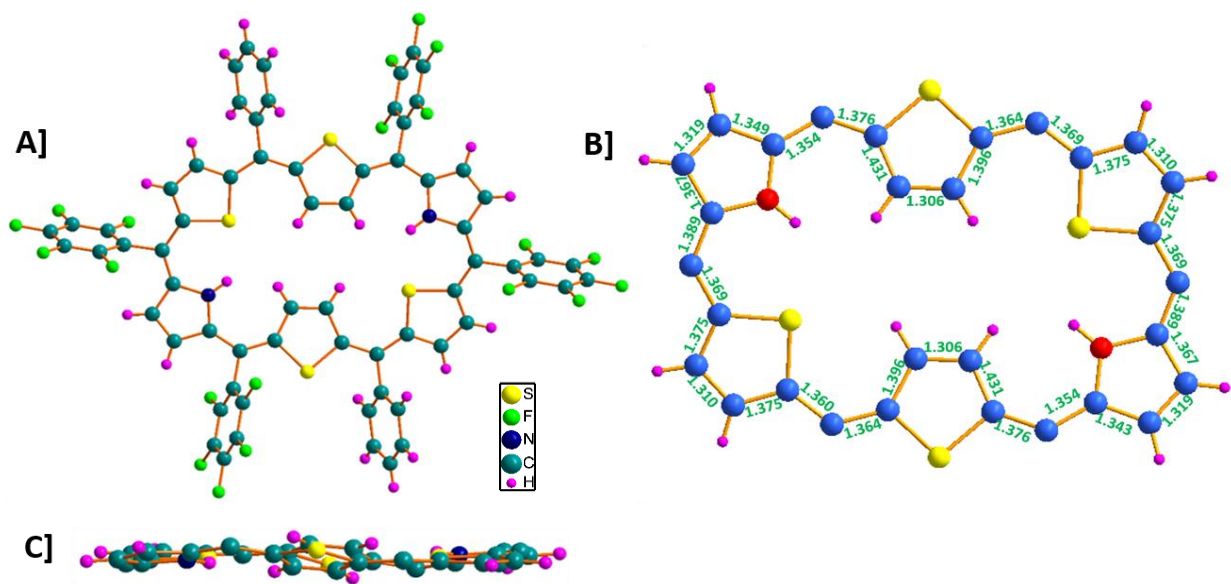
Figure II.14: Top view **A]** Top view, **C]** side view and **B]** Bond length equalization study from of molecular structure of **II.11**. Meso-phenyl rings are omitted for clarity from side view.

Further justification for the molecular structure of **II.11** was established through single crystal X-ray diffraction analysis (figure-II.14). Good quality single crystals of **II.11** grown in CHCl$_3$/Hexane. It revealed that **II.11** sustained its structural similarity to **II.10**. Bond length equalization in **II.11** undoubtedly demonstrated the aromatic nature of macrocycle, which was further supported by the estimated NICS[55] value of -14.26 ppm and clockwise orientation of arrows in the ACID[56] plot.
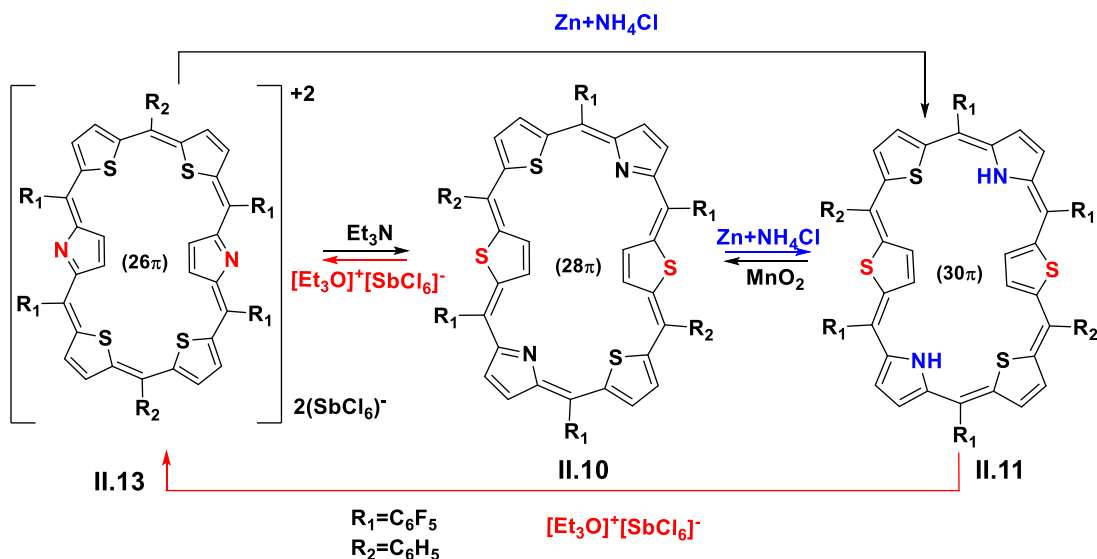
Scheme-II.8: Successive and alternate redox switching between hexaphyrins.

For the first time, a hexaphyrin macrocycle was found to exhibit three different oxidation states based on reversible redox reaction. Regular reducing agents could switch the macrocycle between 28π and 26π electrons states. It required a much stronger reducing agent such Zn/NH$_4$Cl to induce proton coupled electron transfer to reduce the 28π expanded porphyrin to the 30π expanded isophlorin.

Exploring Multiple Redox States for Core-Modified Octaphyrin

Zn and NH_4Cl couple turned out to be a very efficient reducing agent to access a highly reduced state of core-modified hexaphyrin. Employing Zn dust with aqueous NH_4Cl for the reduction of either **II.13** and **II.10** to **II.11** concurs with the stoichiometric ratio expected of two- and four-electron ring reductions to the 30π core-modified isophlorin (equations: 1-3) respectively.

26π (**II.13**) + Zn $\rightarrow 28 \pi$ (**II.10**) + $ZnCl_2$ + $2SbCl_5$ (1)

28π (**II.10**) + Zn + $2NH_4Cl \rightarrow 30 \pi$ (**II.11**) + $ZnCl_2$ + $2NH_3\uparrow$ (2)

26π (**II.13**) +2Zn+$2NH_4Cl \rightarrow 30 \pi$ (**II.11**) +$2SbCl_5$+$4ZnCl_2$ + $2NH_3\uparrow$ (3)
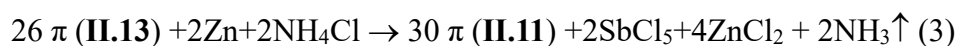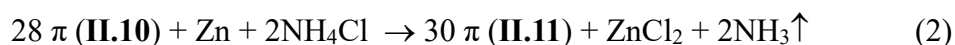
Stoichiometry described for the reduction of macrocycles could not be possible using reducing agent such as $NaBH_4$. PCET assisted inter-conversion for non-planar octaphyrins **II.15** and **II.16** was established by Latos and co-workers.[27] However, two more additional redox states, **II.14** (34π) and **II.17** (40π), can also be foreseen for octaphyrin **II.15** using reagents which were employed to establish three redox states of core-modified hexaphyrin. Hence, four different redox states for core-modified octaphyrin **II.15** can be hypothesized through reversible redox processes (scheme-II.9).
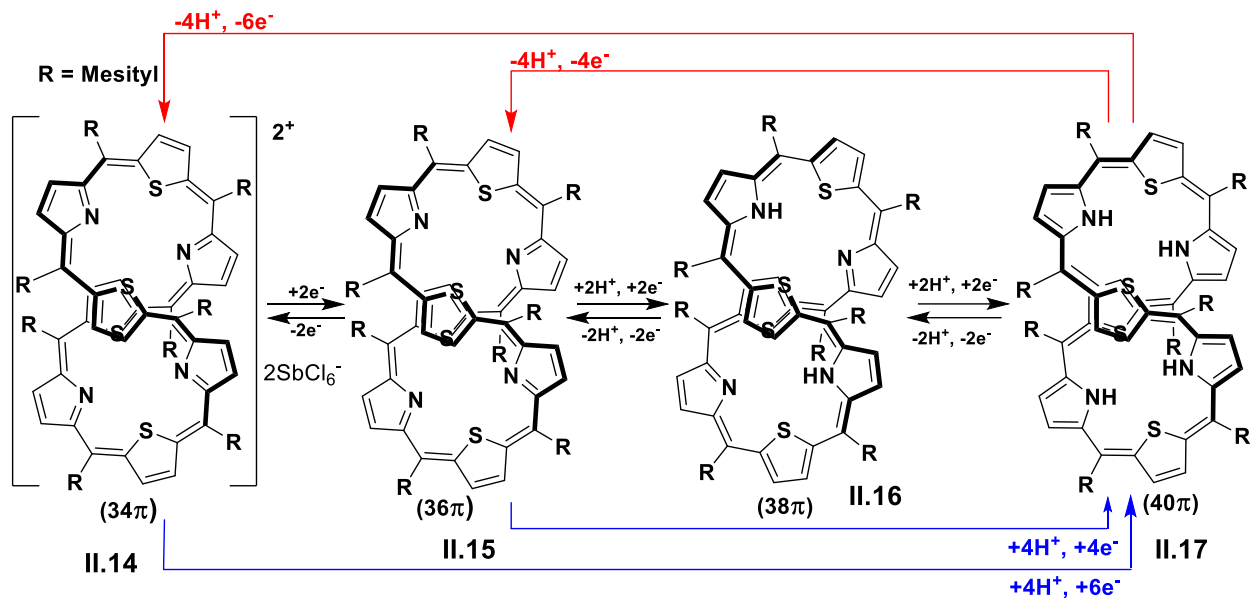
Scheme-II.9: Possible redox states for core-modified octaphyrin **II.15.**

II.5 Synthesis structural characterization tetrathiaoctaphyrin II.15:

Synthesis and electronic absorption studies of II.15

II.15 was synthesized by a reported procedure [27]. Employing a similar acid mediated condensation between thiophene-2,5-diylbis(mesitylmethanol) and pyrrole (scheme-11.10) yielded the desired macrocycle in 2% yields as a marine green colored band in dichloromethane/hexane on basic alumina column.
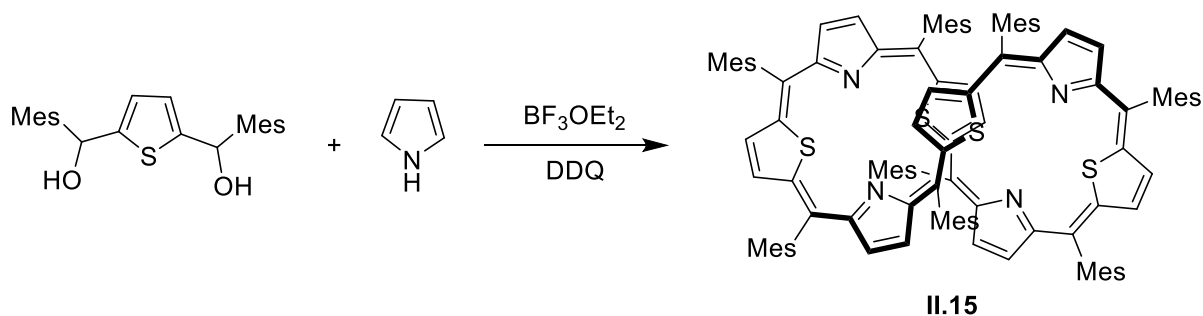
Scheme-II.10: Synthesis of tetrathiaoctaphyrin **II.15**

Structural characterization of II.15:
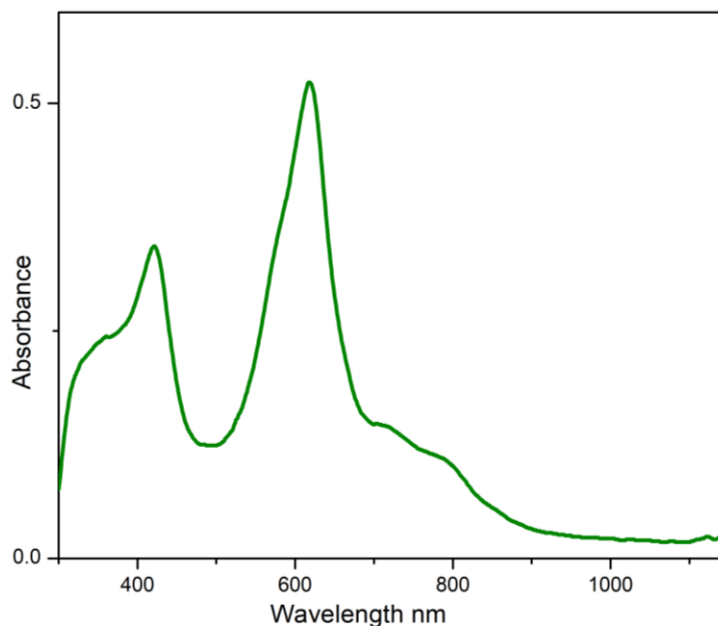
Figure II.13: UV-Vis Absorption spectrum of (10^{-6}M) **II.15** in CH_2Cl_2.

High-resolution mass spectrum displayed mass (m/z=1633.7279) corresponding to that of **II.15**. UV-Vis absorption spectrum recorded in dichloromethane showed absorption maxima at 617 nm (ε=9000), which was in agreement with reported value (figure-II.13).

^{1}H NMR Studies of II.15

The ^{1}H NMR spectrum displayed signals between δ 10.04 to 5.82 ppm (figure-II.14). As this molecule accounts for 36π electrons, it is expected to display a paratropic ring current effect for the $4n\pi$ system. Yet, no such shift was observed in its ^{1}H NMR spectrum due to the non-planar nature of the macrocycle. **II.15** is expected to retain the figure of eight geometry irrespective of meso-substituents. In tune with this expectation, the observed correlation of protons in the ^{1}H-^{1}H COSY spectrum (figure-II.15) further justified the figure of eight geometry.
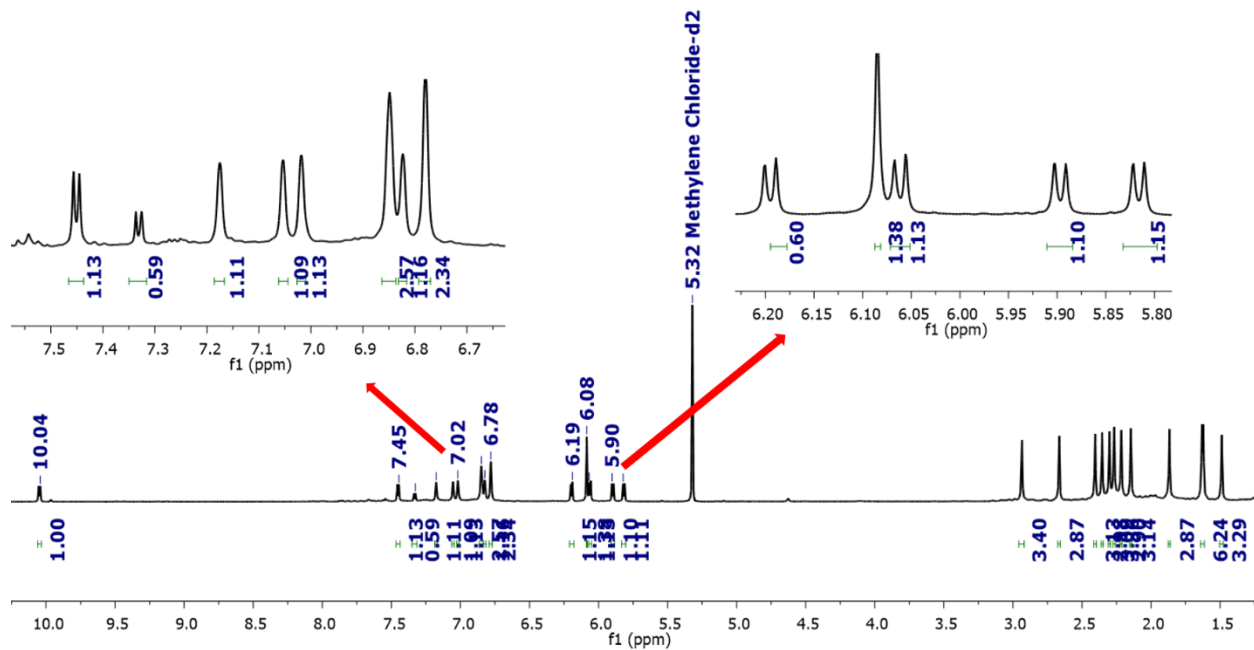
Figure II.14: ^{1}H NMR spectrum of **II.15** recorded at 213K in CD_2Cl_2.
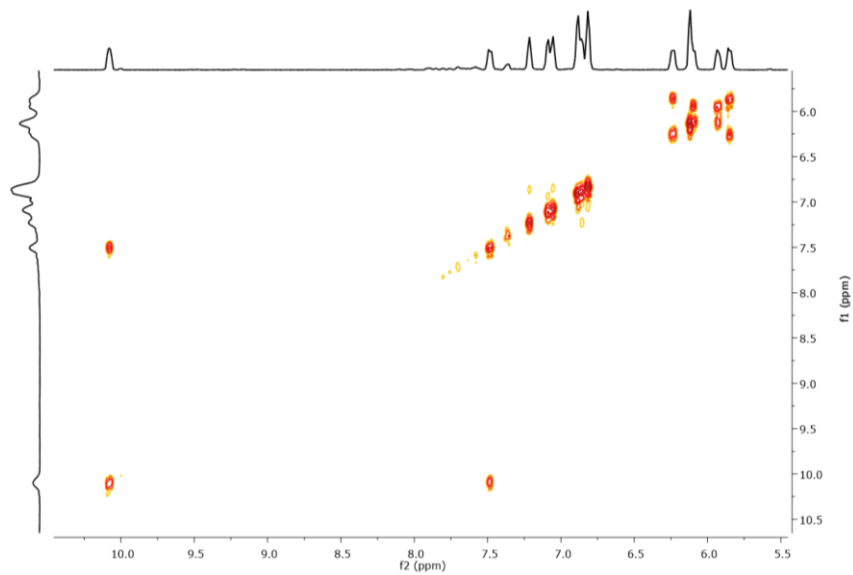
Figure II.15: Partial ^{1}H-^{1}H COSY spectrum of **II.15** recorded in CD_2Cl_2 at 213K.

Single crystal X-ray diffraction studies of II.15
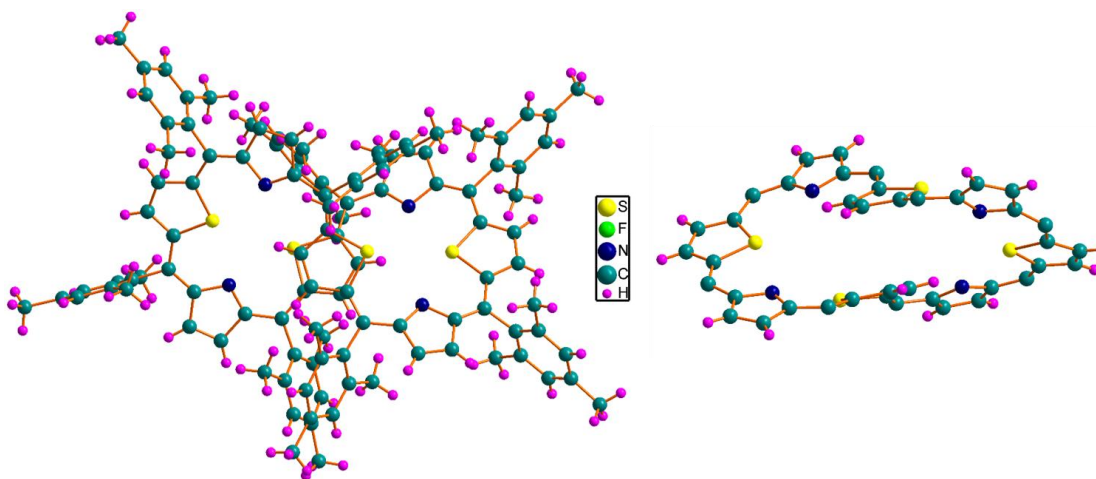
Figure II.16: Top view (left) and side view (left) of **II.15**. Meso-substituents are omitted from side view for clarity.

Good quality crystals were grown from DCM/hexane solvent system. The molecular structure of **II.15** determined by single-crystal X-ray diffraction analysis (figure-II.16) revealed a figure of eight geometry. Solid-state geometry of tetrathiaoctaphyrins was not explored with previously reported toluyl substituted macrocycle.[27] Two of the thiophene rings occupied the central position of twist, while the remaining heterocyclic units were found pointing towards the center of the macrocycle.

Cyclic voltammetry studies

Cyclic voltammetric studies for **II.15** performed in dichloromethane displayed four reversible reduction waves at -1.19V, -0.89V, -0.64V, and -0.47V and two oxidation waves centered at 0.67V and 0.94V. This signified that the 36π macrocycle, **II.15**, could be reduced by four electrons to 40π macrocycle and it could as well be oxidized by two electrons to a 34π system employing appropriate redox reagent.
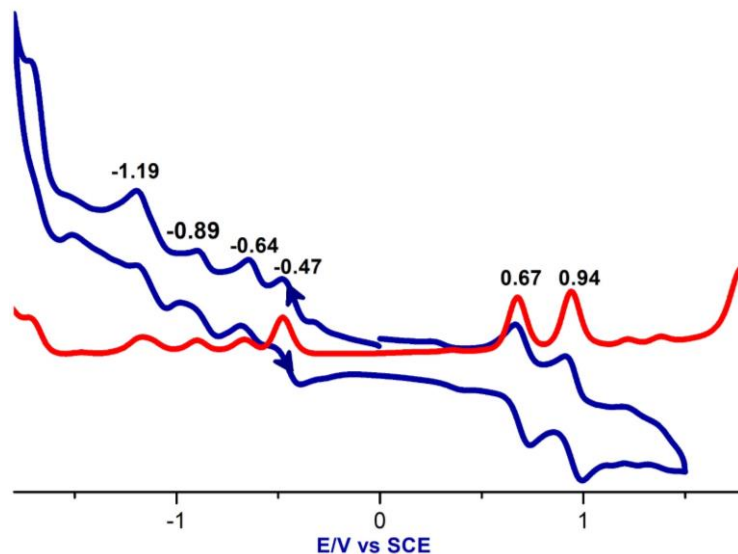
Figure II.17: Cyclic (Blue) and Differential pulse (red) voltammograms of **II.15** in dichloromethane containing 0.1M tetrabutyl ammonium perchlorate as the supporting electrolyte recorded at 50 mVs^{-1}.

II.6 Synthesis and Structural characterization of II.16:

Synthesis and electronic study of II.16

Two electron redox behavior of **II.15** between 36π and 38π was already shown by Latos and co-worker using NaBH$_4$. A similar method was explored to access the 38π macrocycle **II.16**. UV-Vis absorption spectrum showed a red shift in the absorption of **II.16** from 617 nm to 708 (15000), followed by characteristic low energy transitions at 916 nm (1300), 1040 nm (1600), 429 nm (6300), 510 nm (2400) for **II.16** (scheme-II.18)**.**
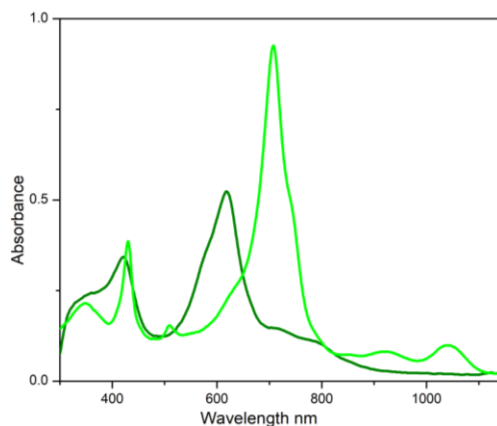
Figure II.18: Absorption changes observed in the solution of (10^{-5}M) **II.15** upon addition of NaBH$_4$ to **II.16** in CH$_2$Cl$_2$**.**

53

^{1}H NMR Studies of II.16

^{1}H NMR spectrum of **II.16** recorded in dichloromethane-d_2, was well resolved at low temperature (figure-II.20B). It suggested the possible fluxional property of the macrocycle at higher temerpatures (figure-II.20A). However it did not display signals corresponding to the reported figure of eight geometry. Rather it revealed diatropic ring current effect for 38π aromatic macrocycle. Four signals were observed in the downfield region at δ 9.69, 9.65, 8.52, 8.49 ppm with corresponding to two protons each and four up field signals at δ -2.55, -2.89, -3.17 and δ - 3.35 ppm for protons of the heterocyclic rings. In additions to these signals, it also displayed a broad signal at δ 11.24 ppm which diminished upon the addition of D$_2$O. Observation of this unexpected spectrum suggested a planar structure with ring inversion of two pyrrole and thiophene rings respectively. Correlation in the ^{1}H-^{1}H COSY spectrum (figure-II.22) further supported a planar structure for **II.16**. Observed NMR pattern suggested untwisting the figure of eight geometry into a planar form for **II.16** (figure 11.19). Therefore replacement of toluyl substituents with a bulky mesityl group changes the geometry of **II.16** and converts the non-aromatic state to an aromatic state.
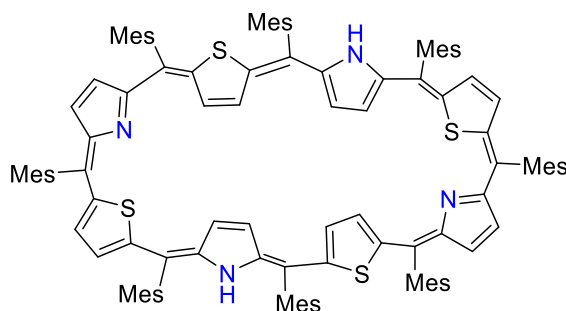
Figure II.19: Expected geometry for **II.16** based on NMR studies.
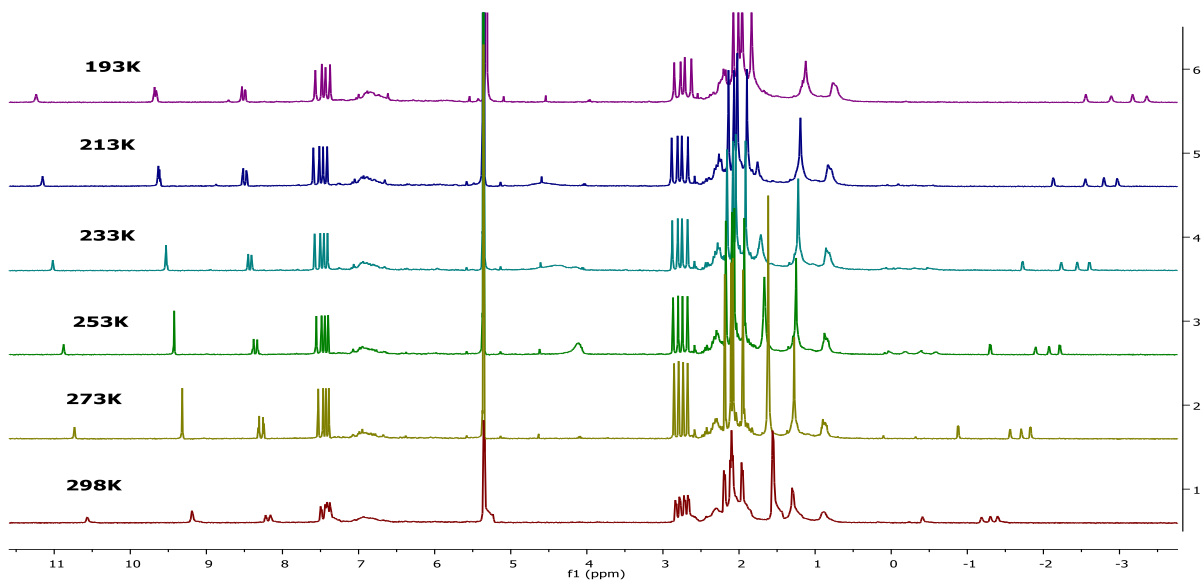
Figure II.20A: Variable temperature ^{1}H NMR spectra of **II.16** recorded in CD$_2$Cl$_2$.
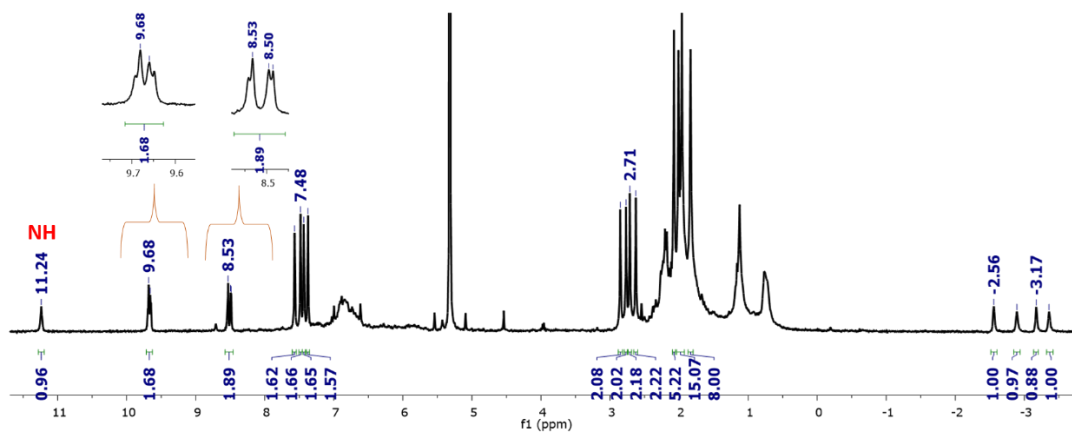
Figure II.20B: ^{1}H NMR spectrum of **II.16** at recorded in CD$_2$Cl$_2$ at 193K.
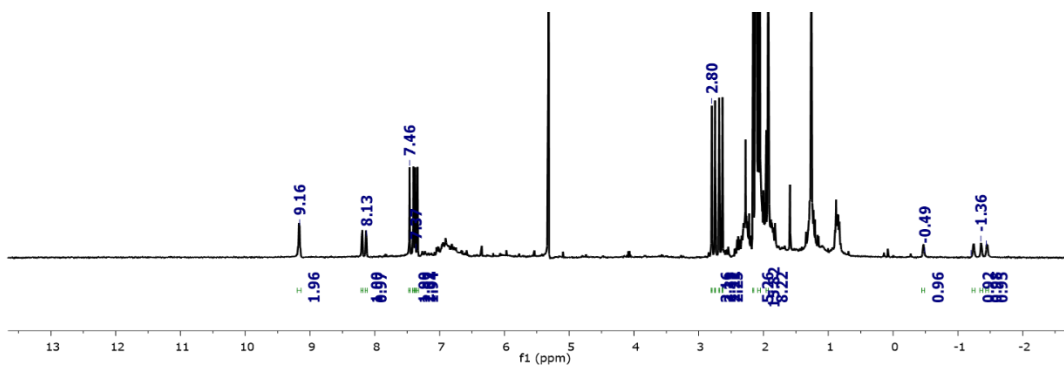
Figure II.21: ^{1}H NMR spectrum of **II.16** upon addition of D_2O at 298K.
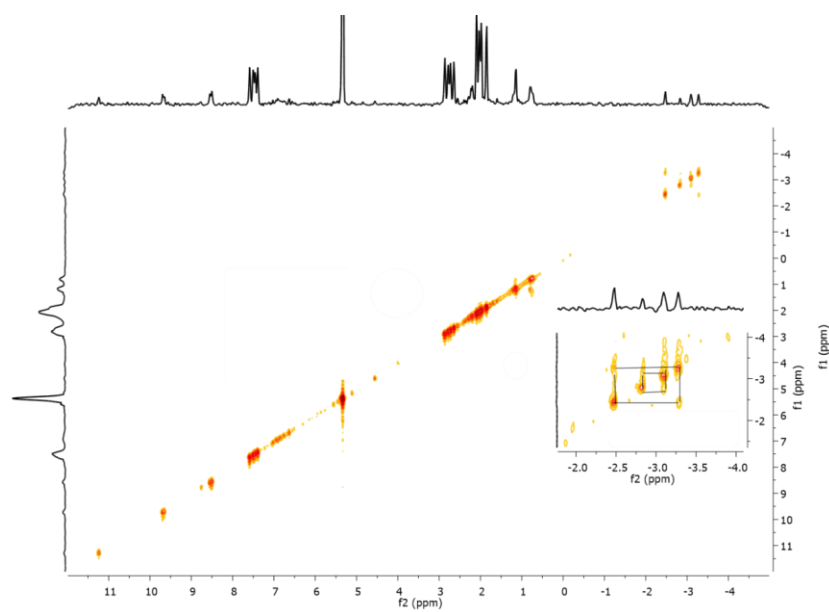
Figure II.22: ^{1}H-^{1}H COSY spectra of **II.16** in CD_2Cl_2 at 193K.

II.7 Synthesis and structural characterization of II.14

Synthesis and electronic properties of II.14

Apart from the redox states described above, two more additional redox states, **II.14** (34π) and **II.17** (40π), can be foreseen for octaphyrin **II.15**. The green-colored 36π octaphyrin, **II.15**, was oxidized quantitatively (scheme-II.11) with Meerwein salt to yield a blue colored solution identified as **II.14**. The dicationic state of the macrocycle was further confirmed from the observed *m*/2 value (818.3687) in mass spectrometry (figure-II-23A). Its electronic absorption spectrum displayed an intense red-shifted band at 767 nm (38000) followed by near-IR bands at 1110 nm (2700) and 1291 nm (3300) (figure-II.23B).
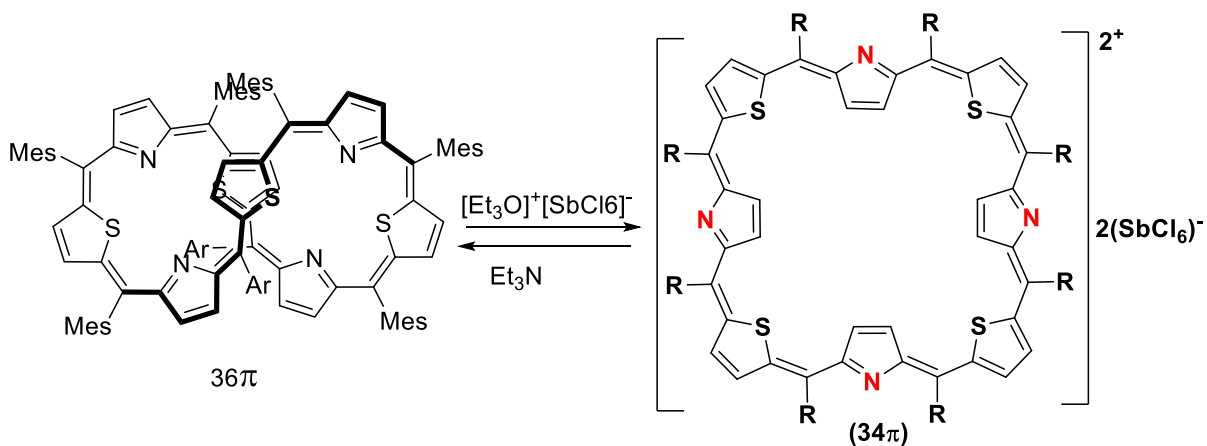
Scheme-II.11: Synthesis of tetrathiaoctaphyrin **II.14**

57
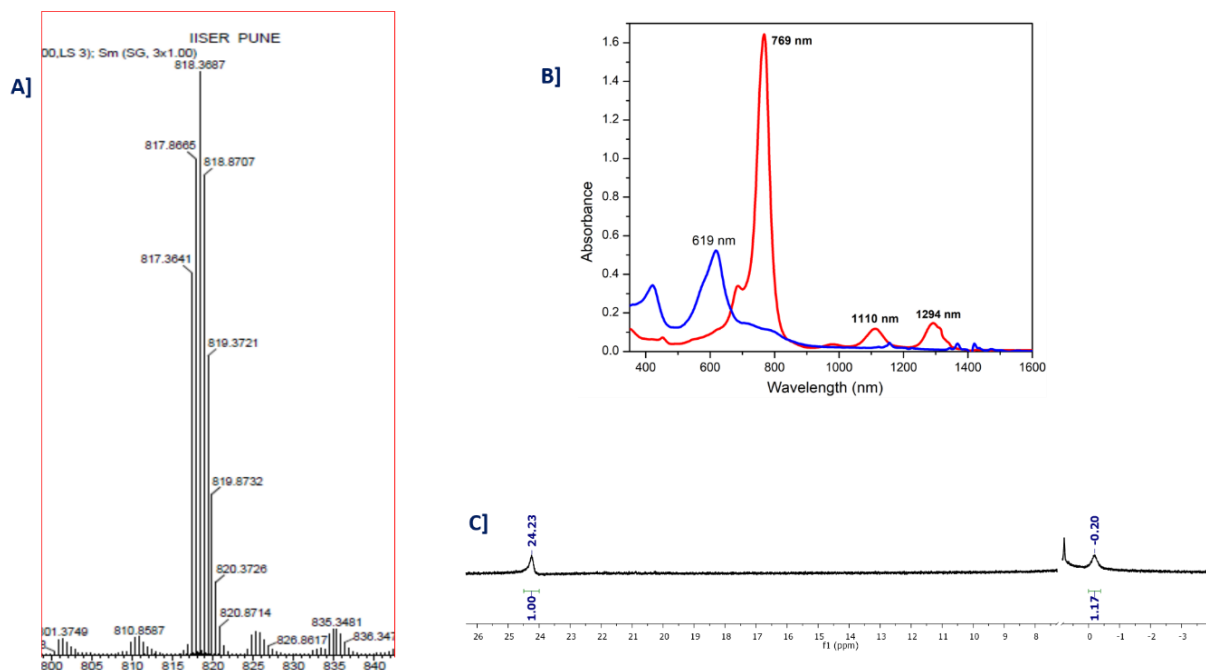
Figure II.23: A] HRMS spectrum of **II.14**, **B]** Absorption changes observed to the solution of **II.15** upon addition of Meerwein salt and **C]** ^{1}H NMR spectrum of **II.14** in CD$_2$Cl$_2$ (^{1}H NMR spectrum of **II.14** recorded at 213K in CD$_2$Cl$_2$ (Signal observed in the range between 1 to 6 ppm corresponds to ethyl chloride and diethyl ether from Meerwein salt).

^{1}H NMR study of II.14

 By two-electron ring oxidation, **II.14** accounts for 34π electrons and hence expected to typify diatropic ring current effects in its ^{1}H NMR spectrum. Unfortunately, **II.14** encountered poor solubility in common organic solvents. In its proton NMR spectrum recorded at 223K in CD$_2$Cl$_2$, two broad singlets corresponding to an equal number of protons were observed at δ 24.23 and 0.20 ppm (figure-II.23C). The upfield signal is attributed to the β C-H protons of the inverted pyrrole rings, and the downfield signal corresponds to thiophene protons. Accordingly, the estimated NICS value of -14.33 ppm bestowed further support to the aromatic character of the dicationic species.

Single crystal X-ray diffraction studies of II.14

The oxidized species was crystallized in acetonitrile, and the structure determined from single-crystal X-ray diffraction studies revealed an unpredicted planar conformation (figures-II.24). Two [SbCl$_6$]$^-$ anions were found to be associated with the macrocycle in support of two-electron ring oxidation of **II.15**. In the planar structure of **II.14,** all the pyrrole rings were found to be inverted, such that the nitrogen's are replaced by the respective β-protons in the macrocyclic core.

Figure II.24: Top view (left) and side view (right) of molecular structure of **II.14**. Meso-substituents are omitted from a side view for clarity.

II.8 Synthesis and structural characterization of II.17

Synthesis and electronic absorption studies of II.17
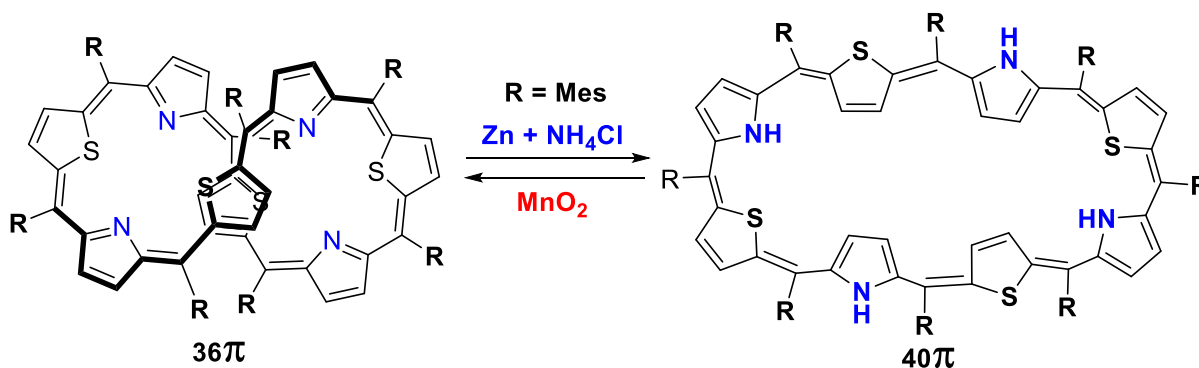
Scheme-II.12: Synthesis of tetrathiaoctaphyrin **II.17**

Following the protocol as described in equations 1-3, an attempt to reduce the dication **II.14** with zinc dust and aqueous ammonium chloride (scheme-II.12) resulted in a pink colored solution that deviated completely from electronic characteristics of **II.15** and **II.16**. It displayed a relatively blue-shifted absorption at 553 nm (18000) with a high energy shoulder at 516 nm (9000) (figure-II 25A). Low energy absorptions followed these two bands at 707 nm (5000) and 1050 nm (570).
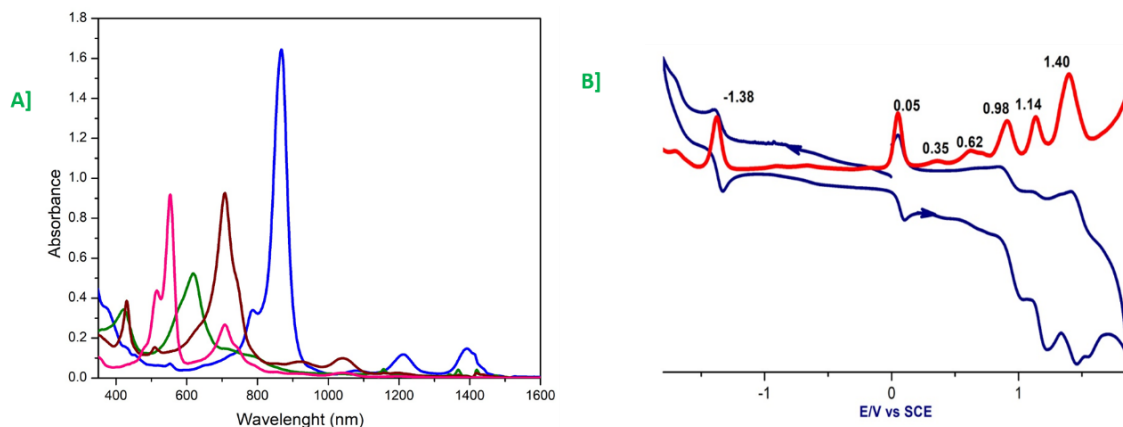
Figure II.25: A] Absorption changes observed to the solution of **III.15** (green line) to **II.17** (pink line) upon adding Zn/NH$_4$Cl, **II.17** changes to **II.15** (green line) upon adding MnO$_2$ and to **II.14** (blue line) by adding Meerwein salt. **B]** Cyclic (blue line) and differential pulse (red line) Voltammograms of **II.17** in dichloromethane containing 0.1M tetrabutyl ammonium perchlorate as the supporting electrolyte recorded at a scan rate of 50 mV s^{-1}.

^{1}H NMR studies of II.17

In tandem with the conformational spectacle, a phenomenal six-electron reduction of **II.14** to core-modified 40π expanded isophlorin, **II.17**, was discerned through spectroscopic analyses. This induced reduction in symmetry was further vindicated by a well-resolved ^{1}H NMR spectrum of **II.17** recorded in d_8-toluene at 253K (figure-II.27). Five signals corresponding to two protons each were observed both in the low field and high field region of the NMR spectrum. Being a planar 40π system, **II.17** is expected to display paratropic ring current and differentiate the protons of the inverted thiophene and pyrrole rings. Hence, the upfield signals at δ 0.01, -1.45, -1.74, and -1.94 ppm correspond to the protons of non-inverted pyrrole and thiophene rings. An equal number of such signals at δ 9.73, 9.45, 9.33, and 5.94 ppm are assigned to the protons of inverted

thiophene/pyrrole rings. Their diminishing intensity upon the addition of D₂O (figure-II.28) identified the two different NH's at δ 0.35 and 10.88 ppm.
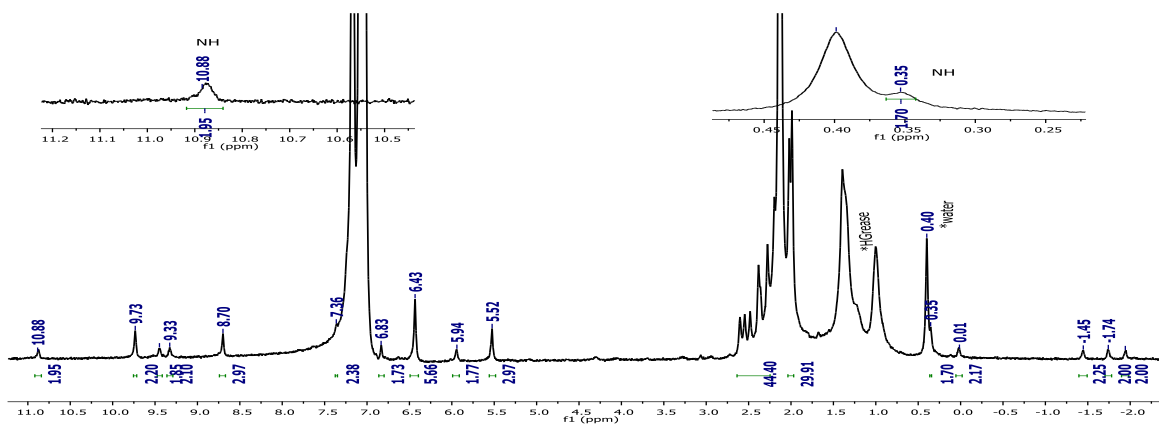
Figure II.27: ¹H NMR spectrum of **II.17** at 253K recorded in toluene-*d₈.*
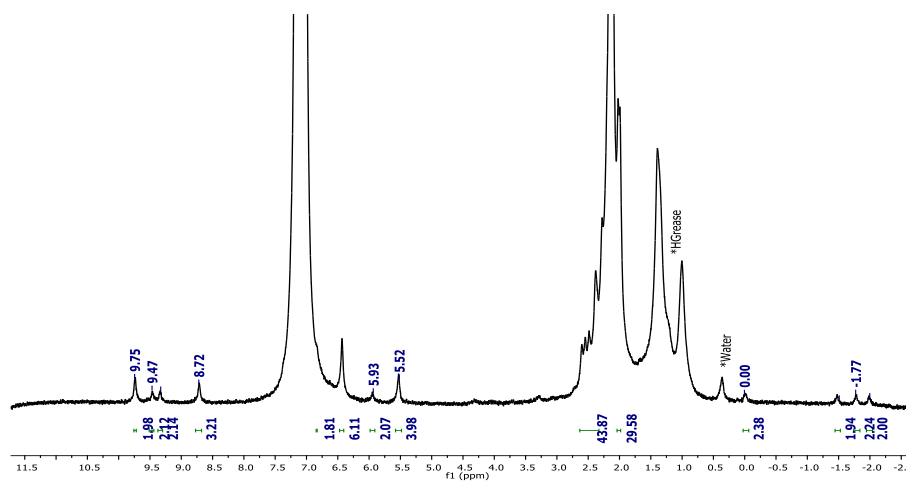
Figure II.28: ¹H NMR spectrum of **II.17** upon addition of D₂O at 253K in toluene-*d₈.*

¹H-¹H COSY revealed four sets of co-relation (figure-II.29); two co-relations in the downfield region, and the other two co-relations observed in the up filed region, which strongly support ¹H NMR observation.
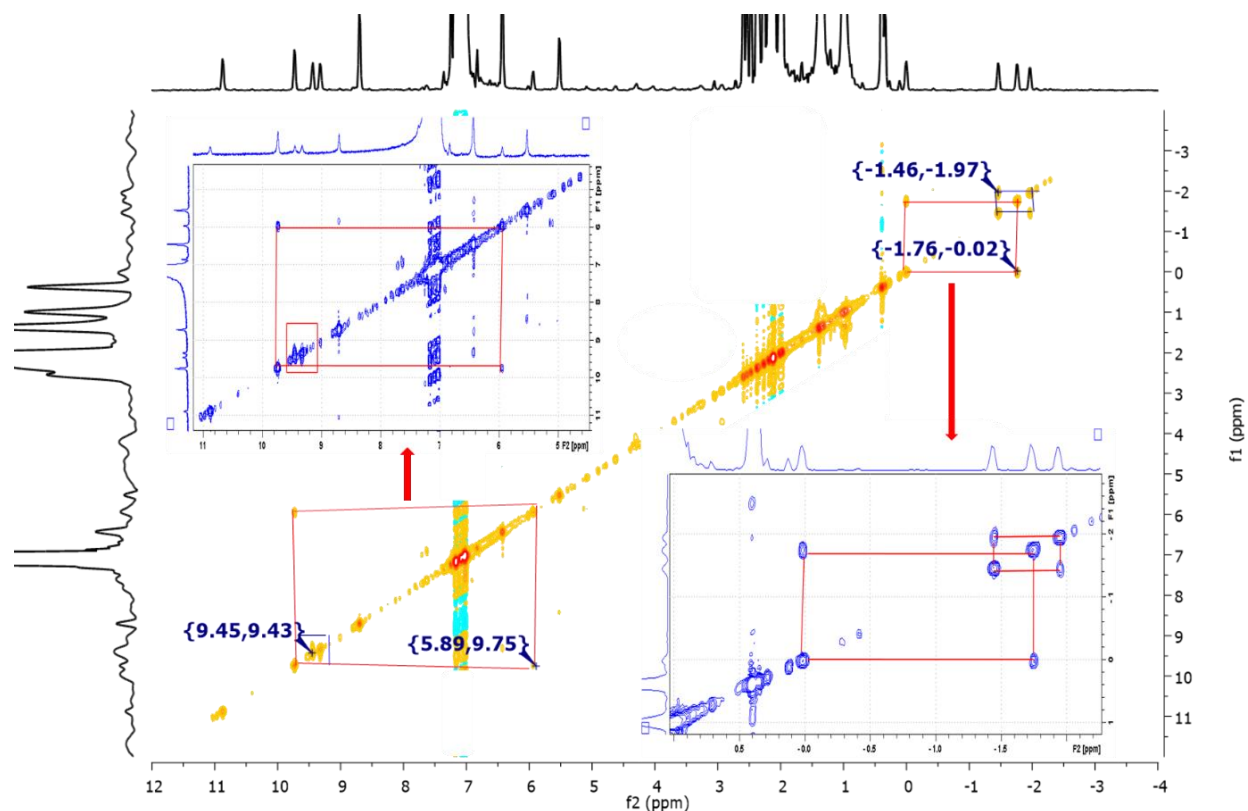
Figure II.29: ^{1}H-^{1}H COSY spectrum of **II.17** at 253K in toluene-d_8.

The estimated NICS values of +9.87 ppm authenticated the justification for antiaromatic characteristics of **II.17**. Apart from the reversible six-electron redox, even four-electron reversible redox between **II.15** and **II.17** could be established by employing MnO_2/ (Zn+NH$_4$Cl) couple. Following the observed redox process, the cyclic voltammogram of 36π octaphyrin, **II.15**, (figure-II.17) exhibited two oxidations corresponding to the dicationic **II.14,** and four reductions consistent with the identification of 40π octaphyrin, Cyclic voltammogram of **II.17** displayed six oxidation waves (figure-II.25) suggesting the formation of 34π aromatic dicationic species **II.14**.

Single crystal X-ray diffraction studies of II.17

Molecular structure of **II.17** was determined from single-crystal X-ray diffraction on crystals grown from chloroform/hexane revealed a refashioned planar topology from a square to a rectangular geometry for an octaphyrin (figure-II.26). This topological alteration was accompanied by an unusual ring inversion of the heterocyclic units. Unlike in **II.14**, two pairs of adjacent pyrrole and thiophene rings, placed opposite to each other, were found to be inverted in **II.17**. Even through conformational reversibility between twisted and planar conformations has been observed in very few porphyrinoids.[32], [49], [53],[57] , octaphyrin **II.17**, **II.16** and **II.14** represents a rare interconversion between three different plane topologies for the same porphyrinoid (scheme-II.13).
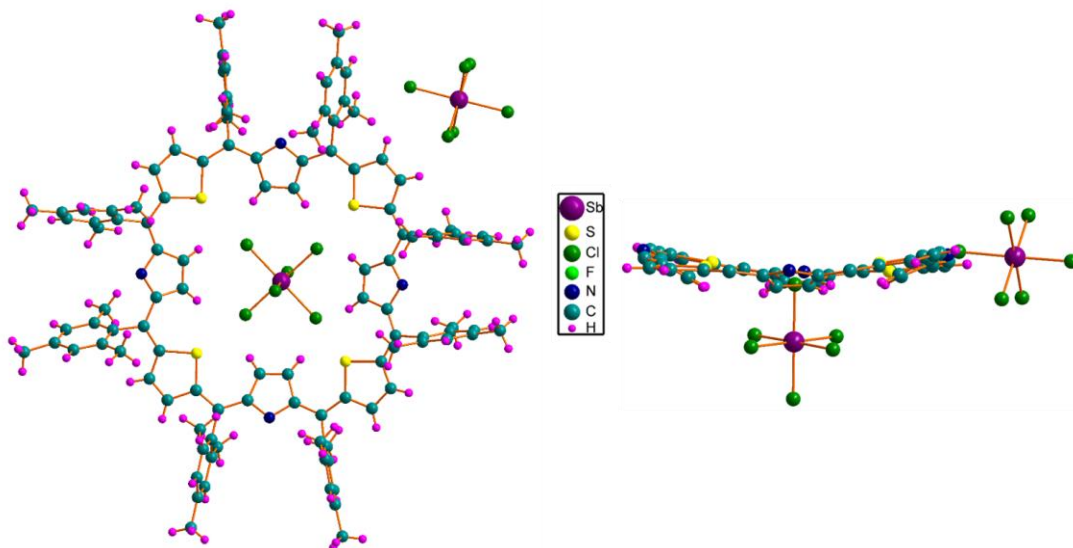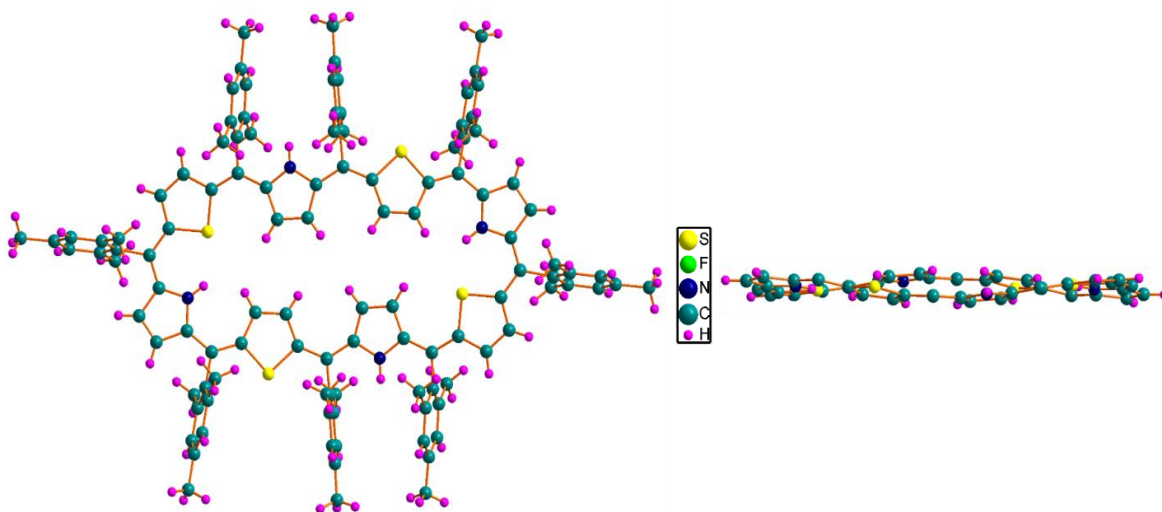

Figure II.26: Top view (left) and side view (right) for the molecular structure of **II.17**. Meso-substituents are omitted in the side view for clarity.

II.9 Redox chemistry of octaphyrins
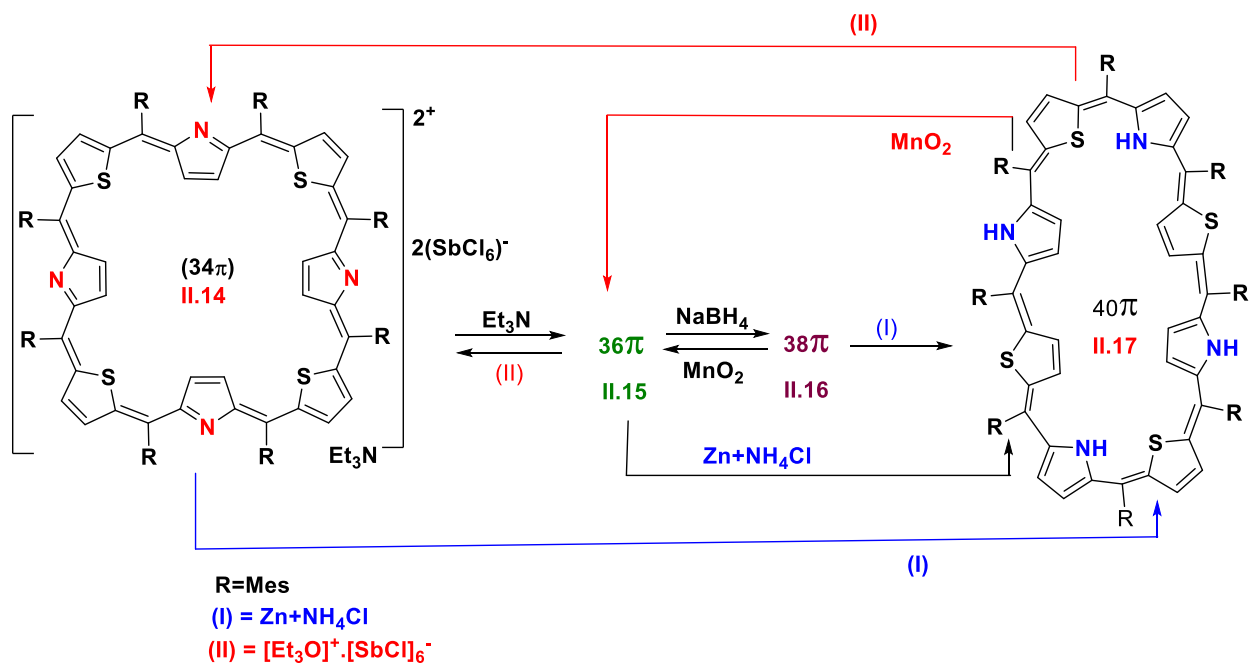
Scheme-II.13: Successive and alternate redox switching of tetrathiaoctaphyrin with conformational flexibility

II.10 Quantum mechanical calculations:

Nucleus Independent Chemical Shift (NICS)

The measure of aromaticity and anti-aromaticity of **II.10, II.11, II.13, II.14,** and **II.17** estimated through quantum mechanical calculation were performed with the help of the Gaussian09 rev D program. [58] The necessary calculations were carried out by employing Density Functional Theory (DFT) with Becke's three-parameter hybrid exchange functional (B3LYP) 631G (d, p) basis set for all the atoms in the molecules that were subjected to these calculations. The molecular structure obtained from single-crystal X-ray diffraction analysis was employed to obtain the optimized geometry structure. Recently, Schleyer et al. introduced the use of the negative of the calculated magnetic shielding at the center, which is referred as "Nucleus independent chemical shift" (NICS) as a simple magnetic criterion to measure aromaticity/anti-aromaticity (or non-aromaticity) in cyclic conjugated systems when the species is placed in the magnetic field. The negative NICS indicates aromatic and positive NICS represents anti-aromatic characteristics (table-II.1).

Macrocycle	NICS(0)ppm	AICD	λ max (nm)	Huckel aromaticity
II.13	-12.25	Clockwise	676	Aromatic
II.10	19.00	Anti-clockwise	471	Anti-Aromatic
II.11	-14.26	Clockwise	552	Aromatic
II.14	-14.33	Clockwise	769	Aromatic
II.17	9.87	Anti-clockwise	553	Anti-Aromatic

Table II.1: Estimated NICS values for macrocycles **II.13** to **II.17**.

TD-DFT calculation and redox properties

Understanding of redox switching was further supported by TD-DFT calculation performed with the B3LYP/631G (d, p) level of theory. Theoretical vertical excitation energy calculated from optimized geometry supported the experimentally observed values from UV-Vis absorption spectroscopy for **II.13**, **II.10**, **II.11**, (figure-II.30) **II.15,** and **II.17** (figure-II.31).
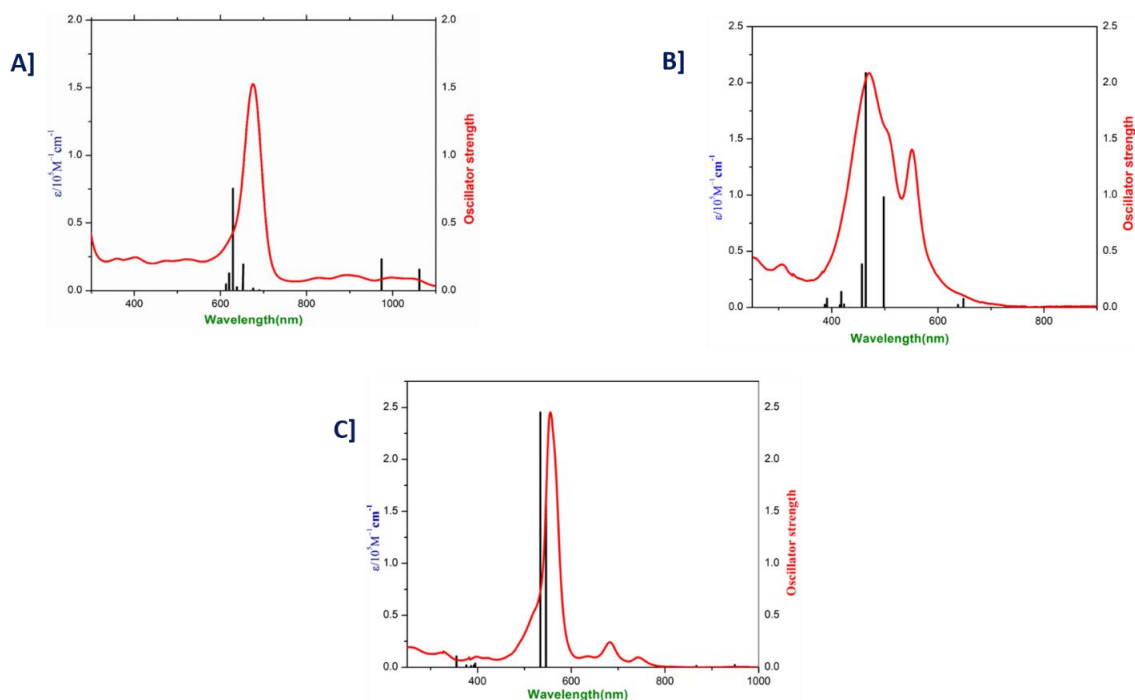
Figure II.30: The steady-state absorption spectra (red line) of A] **II.13**, B] **II.10,** and C] **II.11** recorded in CH_2Cl_2 along with the theoretical vertical excitation energies(Black bar) obtained from TD-DFT calculations carried out at the B3LYP/6-31G(d, p) level.
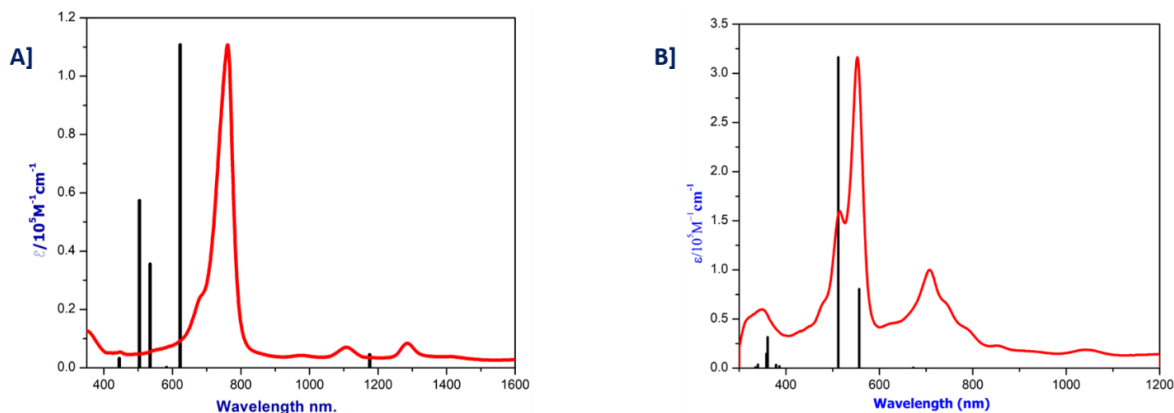
Figure II.31: The steady-state absorption spectra (red line) of A] **II.14** and B] **II.17** recorded in CH_2Cl_2 along with the theoretical vertical excitation energies(Black bar) obtained from TD-DFT calculations carried out at the B3LYP/6-31G(d, p) level.

Anisotropy of induced current density (ACID)

Another criterion to determine the ring current effects in the aromatic and anti-aromatic system is by calculating the Anisotropy of Induced-Current Density (ACID). It was used to visualize ring current induced by the delocalized π electrons. The magnitude, as well as direction of the ring current, can be directly represented by the ACID plots when the external magnetic field is applied orthogonal to the mean macrocyclic plane. It displays current density plots that were obtained by the continuous applying set of gauge transformation (CGST) method to calculate the current densities, and the obtained results were plotted using POVRAY 3.7 software for windows. In the ACID plot, the clockwise ring current represents aromatic molecule, and anti-aromatic ring currents are representative of the anti-aromatic nature of given molecules (figures-II.32 and II.33). Also, it is a useful tool to determine the path of delocalized π electrons in a cyclic conjugated system using an arrow.
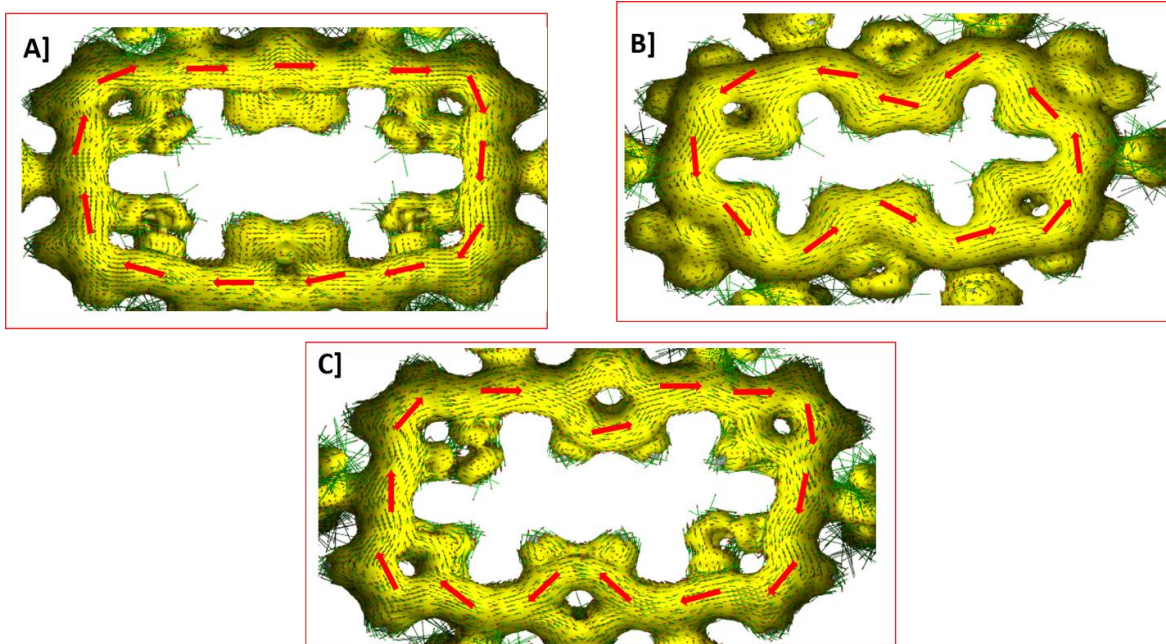
Figure II.32: ACID plot for **II13** (A), **II.10** (B) and **II.11** (C). At iso value 0.02, external magnetic field is applied orthogonal to the macrocycle plane.
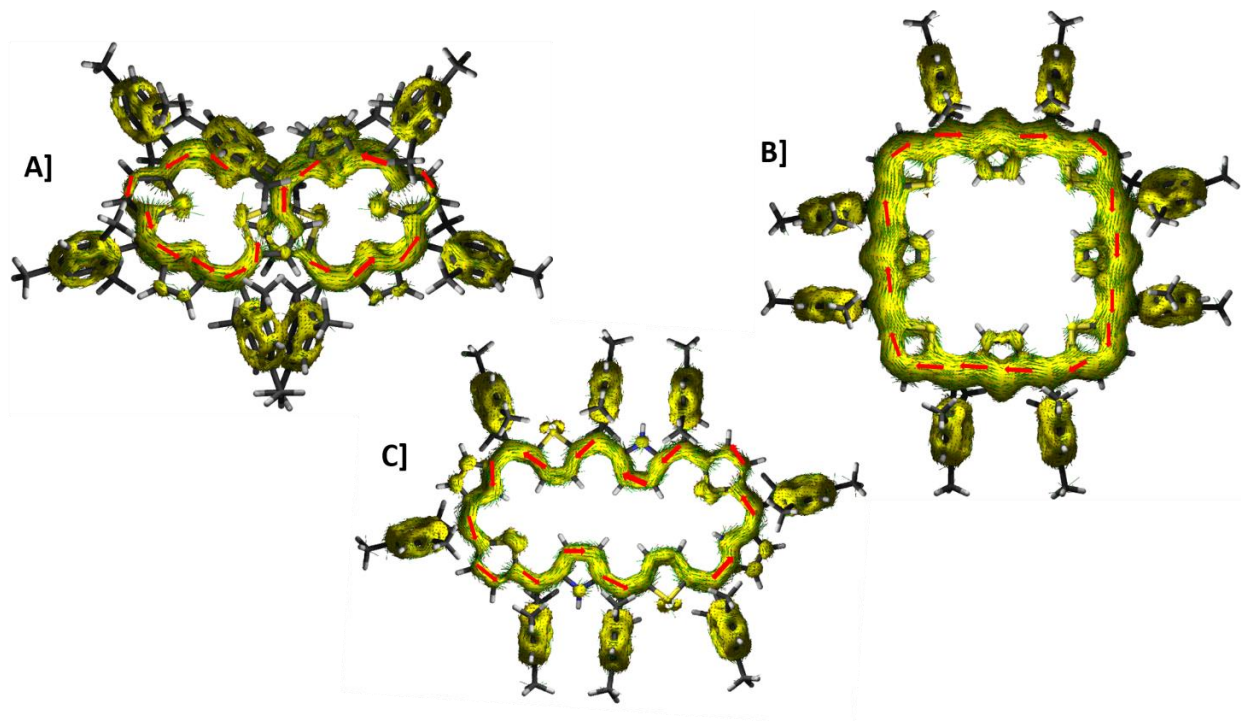
Figure II.33: AICD plot for **II.15** (A), **II.14** (B) and **II.17** (C). At iso value 0.04 external magnetic field is applied orthogonal to the macrocycle plane.

Conclusions

This chapter demonstrates a wide range and reversible four-electron and six-electron redox process for two different expanded porphyrins, respectively. It is in stark contrast to the conventional reversible two-electron redox process observed in expanded porphyrinoids. The subtle multi-step two-electron redox transformations are accompanied by the flexible structural landscape as established by spectroscopic and X-ray diffraction techniques. The paradigm shift in the redox properties can be attributed to the easing of a rigid 18π porphyrin structure to an elastic framework in its expanded derivatives. A higher number of multi-redox states can be anticipated upon reinstating pyrrole for thiophenes in expanded porphyrinoids. Three different redox states for hexaphyrin with two different geometries and four different redox states for octaphyrin with three different structures were isolated and characterized both in solution and solid states. The electrochemical and quantum mechanical study buttress the obtained results. Perhaps, a rare and facile reduction by metallic zinc signifies pro-metallic characteristics of these organic molecules. By breaching the widespread conception of a thermodynamic barrier between $4n\pi$ and $(4n+2)\pi$ states, the reversible redox reactions kindles robust performance of these π systems for applications in organic electronics.

Experimental Section

Column chromatography was performed on basic alumina and silica in glass columns. ^{1}H-NMR spectra were recorded on a Bruker 400 MHz spectrometer. Chemical shifts were reported as the delta scale in ppm relative to $CHCl_3$ (7.28) or CD_2Cl_2 ($\delta = 5.51$). Electronic spectra were recorded on a Perkin-Elmer λ- 35 UV-Vis spectro-photometer and Shimadzu UV3600 UV/Vis/NIR spectrophotometer in an optical quartz cuvette (10 mm path length). High-Resolution Mass spectrum (HRMS) was obtained using WATERS G2 Synapt Mass Spectrometer. Single-crystal diffraction analysis data were collected at 100K with a BRUKER KAPPA APEX II CCD Duo diffractometer (operated at 1500 W power: 50 kV, 30 mA) using graphite monochromatic Mo Kα radiation ($\lambda = 0.71073$ Å). In the case of disordered solvent molecules, the contributions to the scattering arising from the disordered solvents in the crystal were removed by the use of the utility SQUEEZE in the PLATON software package. More information on crystal structures can also be obtained from the Cambridge Crystallographic Data Centre (CCDC) with deposition number 1897560(**II.13**), 1897561(**II.10**), 1897874(**II.11**), 1897562(**II.14**), 1897563(**II.17**),

1912149(**II.15**). Cyclic voltammetry (CV) and Differential pulse voltammetry (DPV) measurements were carried out on a BAS electrochemical system using a conventional three-electrode cell in dry CH_2Cl_2 containing tetrabutylammonium perchlorate as the supporting electrolyte. Measurements were carried out under an Argon atmosphere. A glassy carbon (working electrode), a platinum wire (counter electrode), and a saturated calomel (reference electrode) were used. The final results were calibrated with the ferrocene/ferrocenium couple. Quantum mechanical calculations were performed with the Gaussian09 rev D program suite using a High-Performance Computing Cluster facility of IISER PUNE. All calculations were carried out by Density functional theory (DFT) with Becke's three-parameter hybrid exchange functional and the Lee-Yang-Parr correlation functional (B3LYP) and 6-31G(d, p) basis set for all the atoms were employed in the calculations. The molecular structures obtained from single-crystal analysis were used to obtain the geometry optimized structures. To simulate the steady-state absorption spectra, the time-dependent TD-DFT calculations were employed on the optimized structures. Molecular orbital contributions were determined using GaussSum 2.2.Program package. The global ring centers for the NICS (0) values were designated at the non-weighted mean centers of the macrocycles. The NICS (0) value was obtained with gauge independent atomic orbital (GIAO) method based on the optimized geometries.

Materials:

Dichloromethane (CH_2Cl_2) was dried by refluxing and distillation over P_2O_5. Commercially available pyrrole and thiophene were freshly distilled before use. Other reagents and solvents were of commercial reagent grade and were used without further purification.

Synthesis of II.10: A flame-dried 500-mL two neck round-bottomed flask was charged with ((phenylmethylene)bis(thiophene-5,2-diyl))bis((perfluorophenyl)methanol (0.37mmol), **II.12**[5], and pyrrole (0.37mmol), in 200 mL of anhydrous dichloromethane under nitrogen atmosphere and degassed with nitrogen for further ten minutes. $BF_3.OEt_2$ (0.37mmol) was added under dark using a syringe, and the resulting solution was stirred for one hour under an inert atmosphere. After adding DDQ (1.16 mmol), the reaction mixture was opened to air and stirred for one more hour. A few drops of triethylamine were added and passed through a short pad of basic alumina. This mixture was concentrated and further purified by basic alumina column chromatography using CH_2Cl_2/Hexane as eluent. **II.10** obtained in 12% yield as an orange-colored band.

HR-MS (ESI-TOF): m/z=1351.0403 (found), Calculated for ($C_{66}H_{22}F_{20}N_2S_4$); (1350.0346+H).

UV-Vis (CH$_2$Cl$_2$): λ_{max} nm (ε, Lmol^{-1}cm^{-1}): 471 (13000). 551 (8000).

^{1}H NMR (400 MHz, CDCl$_3$, 298K) δ: 16.82 (d, J=4.4 Hz, 2H), 15.66 (d, J=4.4 Hz, 2H), 7.08 (m, 6H), 6.64 (m, 4H), 5.16 (d, J=4.8 Hz, 2H), 4.83 (d, J=4.8 Hz, 2H), 4.70 (d, J=6 Hz, 2H), 4.53 (d, J=6 Hz, 2H).

Selected Crystal data: C$_{66}$ H$_{22}$ F$_{20}$ N$_2$ S$_4$ (M_r = 1351.10), triclinic, space group *P -1*, *a* = 6.2671(13), *b* =12.536(3), *c* =18.175(4) Å, α = 77.166(5), β = 89.244(6), γ = 77.342(6), *V* = 1357.5(5) Å, *Z* = 1, *T* =100(2) K, D$_{calcd}$ = 1.653cm^{-3}, R$_1$ = 0.0507 (I>2sigma (I)), R_w (all data) = 0.1584(6715), GOF = 0.889.

Synthesis of II.13: The dication **II.13**, was synthesized by the addition of triethyl oxonium hexachloridoantimonate (10 mg) to a solution of **II.10** (2.5 mg) in dry dichloromethane and the resulting solution was stirred for ten minutes under nitrogen atmosphere. Evaporation of the solution gave a green colored compound.

HRMS: m/z = 676.0233(found) calculated for (C$_{66}$H$_{22}$F$_{20}$N$_2$S$_4$)$^{+2}$ (675.0173+H).

^{1}H NMR (400 MHz, CDCl$_3$, 298K) δ: 8.96 (d, J=4.4 Hz 2H), 8.75 (d, J=4.8 Hz, 2H), 8.57 (d, J=4 Hz, 2H), 8.43 (br s, 2H), 7.45 (br s, 4H), 7.33 (br s, 6H), -0.14 (br s, 4H).

UV-Vis (CH$_2$Cl$_2$): λ_{max} nm (ε, Lmol^{-1}cm^{-1}): 676 (32000), 893 (2500), 990 (2100).

Crystal data C$_{66}$H$_{22}$F$_{20}$N$_2$S$_4$, 2(Cl$_6$, Sb), (M_r = 4164.0(9)), monoclinic, space group *P 21/c*, *a* = 11.5683(14), *b* = 16.3145(19), *c* = 22.437(3) Å, α = 90, β = 100.478(2), γ = 90; *V* = 4164.0(9) Å3, *Z* = 2, *T* = 100(2) K , D$_{calcd}$ = 1.611g cm^{-3}, R$_1$ = 0.0547 (I>2sigma(I)), R_w (all data) = 0.1551(10334), GOF = 1.050.

Synthesis of II.11: To a solution of **II.13** or **II.10** (2 mg) in dichloromethane, zinc dust was added in excess, followed by the addition of aqueous NH$_4$Cl, the reaction was stirred for 5 minutes. The solution was filtered through Whatman filter paper to remove excess zinc powder. The resulting solution was extracted with DCM (20 mL x 2) and dried over anhydrous Na$_2$SO$_4$. The solvent was evaporated under reduced pressure to obtain **II.11** quantitatively.

HRMS: (ESI-TOF): m/z =1352.0455 (found), (Calculated For: C$_{66}$H$_{24}$F$_{20}$N$_2$S$_4$. 1352.0503).

UV-Vis (CH$_2$Cl$_2$): λ_{max} nm (ε, Lmol^{-1}cm^{-1}): 552 (36000), 683(3600), 742 (1500).

¹H NMR: (400 MHz, CDCl₃, 253K) δ: 9.0 (d, J=4.8 Hz, 2H), 8.94 (d, J=4 Hz, 2H), 8.36 (br s, 2H), 8.25 (br s, 2H), 8.23 (m, 4H), 7.91 (m, 6H), -1.40 (d, J=4.4 2H), -1.60 (d, J=4.4 Hz, 2H), -2.07 (s, 2H, Exchangeable with D₂O).

Selected Crystal data $C_{66}H_{24}F_{20}N_2S_4$, (M_r = 1353.11), triclinic, space group *-1, a = 6.102(7), b = 12.262(14), c = 17.76(2)* Å, α = 77.22(3), *β = 89.22(3)*, γ = 78.68(3); *V* = 1270(3) Å3, *Z* = 1, *T* = 100(2) K , D_{calcd} = 1.769g cm⁻³, R₁ = 0.0920(1257) R_w (all data) = 0.3114(5954), GOF = 0.837.

Synthesis of II.15 and II.16: A reported procedure synthesized them.[31]

II.15: HRMS: (ESI-TOF): *m/z* =1633.7279 (found), (Calculated For: $C_{112}H_{104}N_4S_4$. 1632.7144 + H).

UV-Vis (CH₂Cl₂): λ_{max} nm (ε, Lmol⁻¹cm⁻¹): 419 (9000), 622(5000), 742.

¹H NMR: (400 MHz, CD2Cl₂, 213K) δ: 10.04 (d, J=4.4 Hz, 2H), 7.45 (d, J=4.4 Hz, 2H), 7.33 (d, J=4Hz, 2H), 7.18 (br s, 2H), 7.05 (br s, 2H), 7.02(br s, 2H), 6.85 (br s, 4H), 6.82 (br s, 2H), 6.78(br s, 4H), 6.19 (d, J=4.8 Hz, 2H), 6.08 (br s, 2H), 6.07(d, J=4.4 Hz, 2H), 5.90(d, J=4.8 Hz, 2H), 5.82(d, J=4.8 Hz, 2H), 2.93(br s, 6H),2.66(br s, 6H), 2.40(br s, 6H), 2.35(br s, 6H), 2.30(br s, 6H), 2.26(br s, 6H), 2.21(br s, 6H), 2.14(br s, 6H), 1.86(br s, 6H), 1.63 (br s, 6H), 1.62(br s, 6H), 1.48(br s, 6H).

Selected Crystal data $C_{112}H_{104}N_4S_4$, (M_r = 1634.24), monoclinic, space group *C 2/c, a = 50.346(15), b = 16.533(5), c = 29.033(8)* Å, α = 90, *β = 112.241(9)*, γ = 90; *V* = 22368(11) Å3, *Z* = 8, *T* = 100(2) K , D_{calcd} = 0.971g cm⁻³, R₁ = 0.0692(13419) R_w (all data) = 0.2017(20809), GOF = 1.105.

II.16: HRMS: (ESI-TOF): *m/z* =1634.7246 (found), (Calculated For: $C_{112}H_{106}N_4S_4$. 1634.7300).

UV-Vis (CH₂Cl₂): λ_{max} nm (ε, Lmol⁻¹cm⁻¹): 708 (15000), 916(1300), 1040(1600), 429(6300), 510(2400).

¹H NMR: (400 MHz, CD2Cl₂, 193K) 11.24(br s, 2H, exchangeable with D₂O), 9.69(d, J=4.4 Hz, 2H), 9.65(d, J=4 Hz, 2H), 8.52 (d, J=3.6 Hz, 2H), 8.49(d, J=4 Hz, 2H), 7.56(br s, 4H), 7.48(br s, 4H), 7.43(br s 4H), 7.37(br s, 4H), 2.85(br s, 4H), 2.76(br s, 4H), 2.71(br s, 4H), 2.62(br s, 4H), 2.07(br s, 11H), 2.08-1.95(br s, 30H), 1.86(br s, 16H), -2.55(br s, 2H), -2.89(br s, 2H), -3.17(br s, 2H), -3.35(br s, 2H).

Synthesis of II.14: The dication **II.14** was synthesized by the addition of triethyl oxonium hexachloridoantimonate (20 mg) to a solution of **II.15** or **II.16** (2 mg) in dry dichloromethane and the resulting solution was stirred for 10 minutes under nitrogen atmosphere. Evaporation of the solution gave light blue colored compound which was further washed with diethyl ether and hexane to remove ethyl chloride produced in the course of the reaction.

HRMS: m/z = 818.3687(found) calculated for $(C_{112}H_{104}N_4S_4)^{+2}$ (816.3572+2H).

UV-Vis (CH$_2$Cl$_2$): λ_{max} nm (ε, Lmol^{-1}cm^{-1}): 767 nm (38000), 1110 (2700), 1291 (3300).

^{1}H NMR (400 MHz, CD$_2$Cl$_2$, 213K) δ: 24.23 (br s, 8H), 0.20 (br s, 8H).

Crystal data: C$_{112}$ H$_{103}$ N4 S$_4$, 2(Cl$_6$ Sb) [+ solvent], M_r = 2303.16, monoclinic, space group P $21/n$, a = 23.877(5), b = 21.397(5), c = 24.554(6) Å, α = 90, β = 108.515(4), γ = 90; V = 11894(5) Å3, Z = 4, T = 100(2) K , D$_{calcd}$ = 1.286g cm^{-3}, R$_1$ = 0.1469(8208), R_w (all data) = 0.4181(22134), GOF = 1.077.

Synthesis of II.17: To a solution of **II.14, II.15,** or **II.16** (2 mg) in dichloromethane, zinc dust was added in excess, followed by the addition of aqueous NH$_4$Cl, the reaction was stirred for 5 minutes. The solution was filtered through Whatman filter paper to remove excess zinc powder. The resulting solution was extracted with DCM (20 mL X 2) and dried over anhydrous Na$_2$SO$_4$. The solvent was evaporated under reduced pressure to obtain **II.17** quantitatively.

HRMS Data: (ESI-TOF): m/z =1637.7415 (found), Calcd. For: C$_{112}$H$_{108}$N$_4$S$_4$; (1636.7457+H).

UV-Vis (CH$_2$Cl$_2$): λ_{max} nm (ε, Lmol^{-1}cm^{-1}): 553 (18000), 516(9000) 707 (5000), 1050(570).

^{1}H NMR (400 MHz, CD$_2$Cl$_2$, 253K) δ: 10.88 (s, 2H exchangeable with D$_2$O), 9.73 (br s, 2H), 9.45 (br s, 2H), 9.32 (br s, 2H), 8.70 (s, 2H,), 6.83 (s, 2H), 6.43(s, 6H), 5.94 (br s, 2H), 5.52 (s, 3H), 2.2 to 2.5 (multiple signals, 74H), 0.35 (br s, 2H exchangeable with D$_2$O), 0.01 (br s, 2H), -1.45 (br s, 2H), -1.74 (br s, 2H), -1.94 (br s, 2H).

Selected Crystal data: C$_{112}$ H$_{108}$ N$_4$ S$_4$, 4(C H Cl$_3$) (Mr = 2115.74), monoclinic, space group P 21/n, a = 18.330(12), b = 14.715(9), c = 19.877(12), Å, α = 90, β = 96.404(14), γ = 90, 5328(6)Å^3,

$Z = 2$, $T = 100$ K, ρcalcd = 1.319 g/cm³, R_{int} (all data) = 0.0762, R_1 (all data) = 0.1586, R_w (all data) = 0.2273, GOF = 1.075.
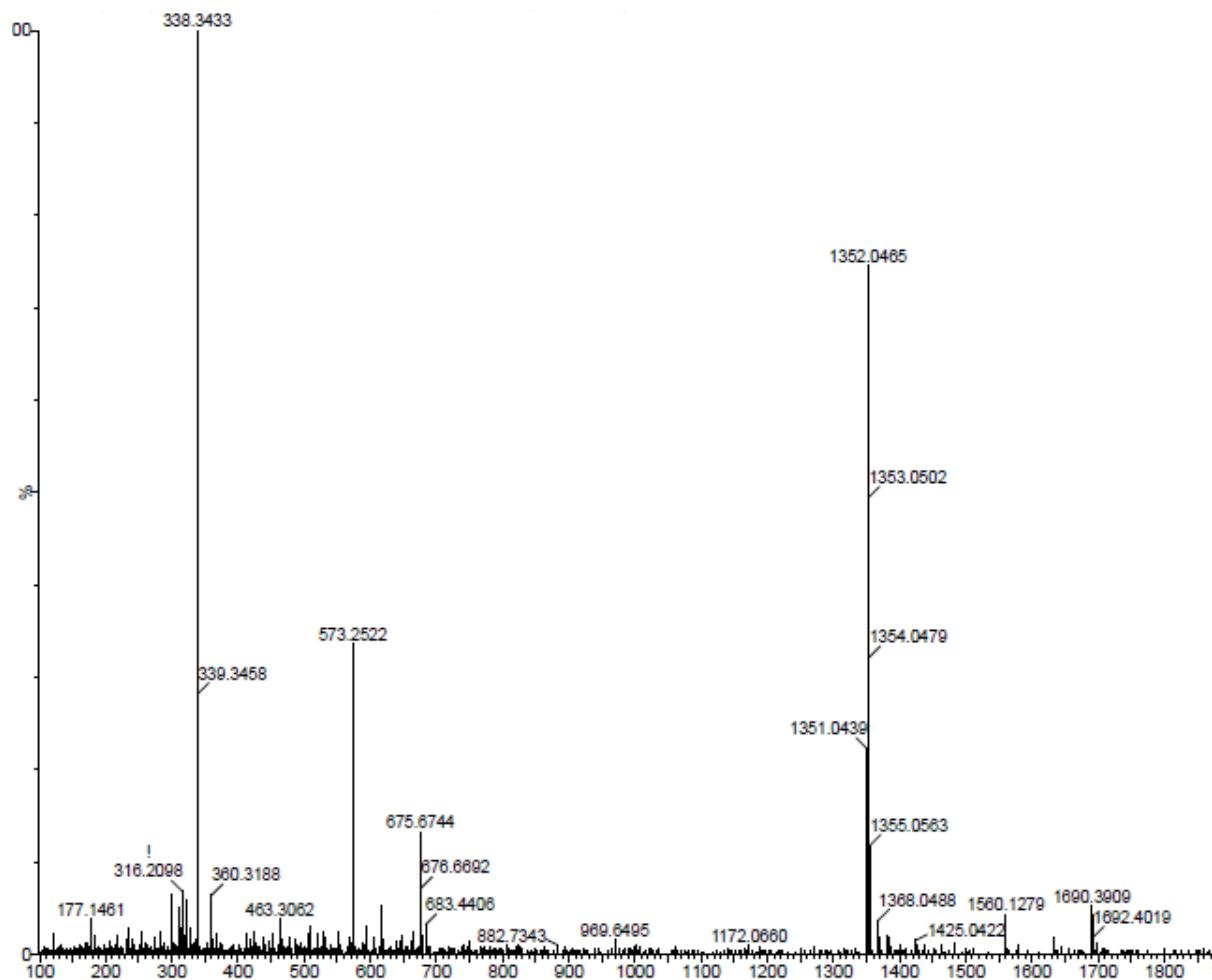
Figure II.34: HRMS spectrum of **II.11**
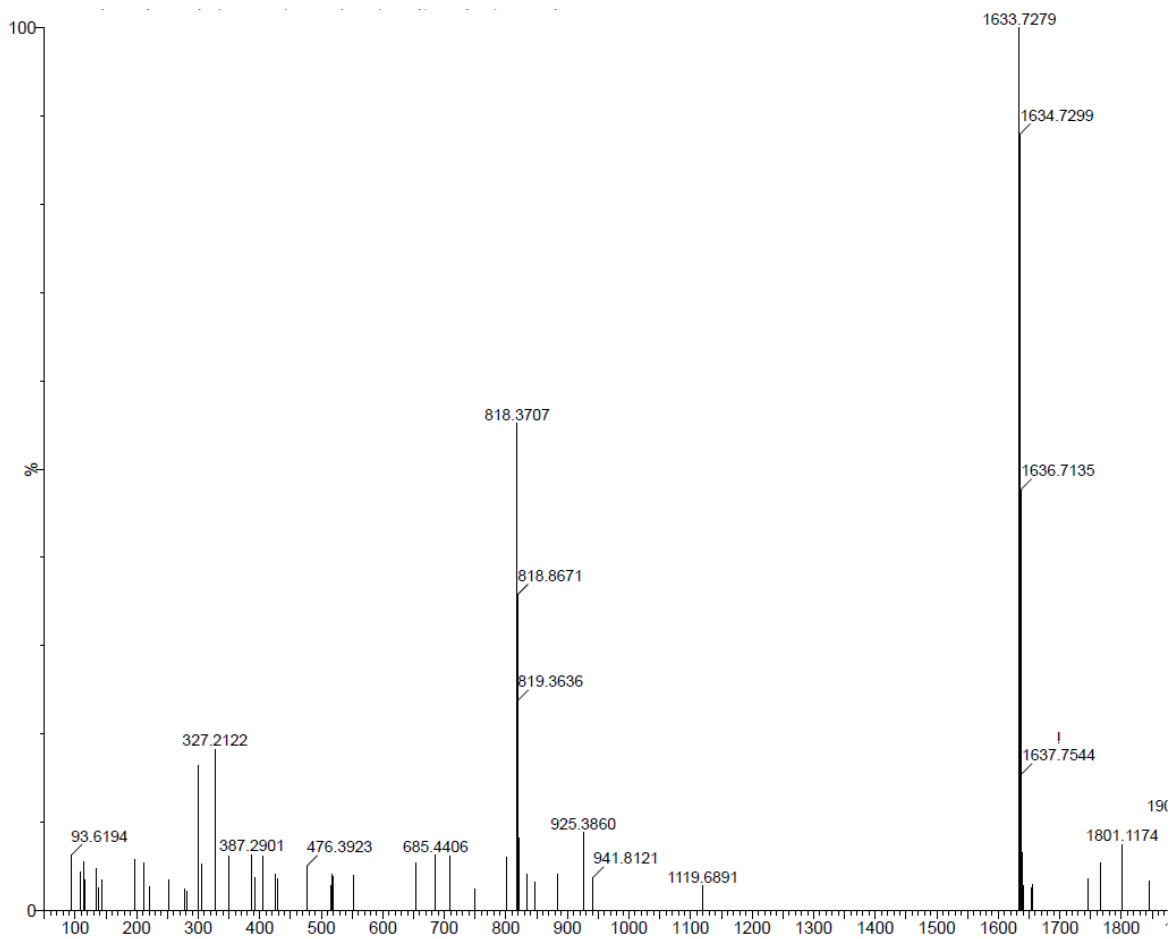
Figure II.35: HRMS spectrum of **II.15**
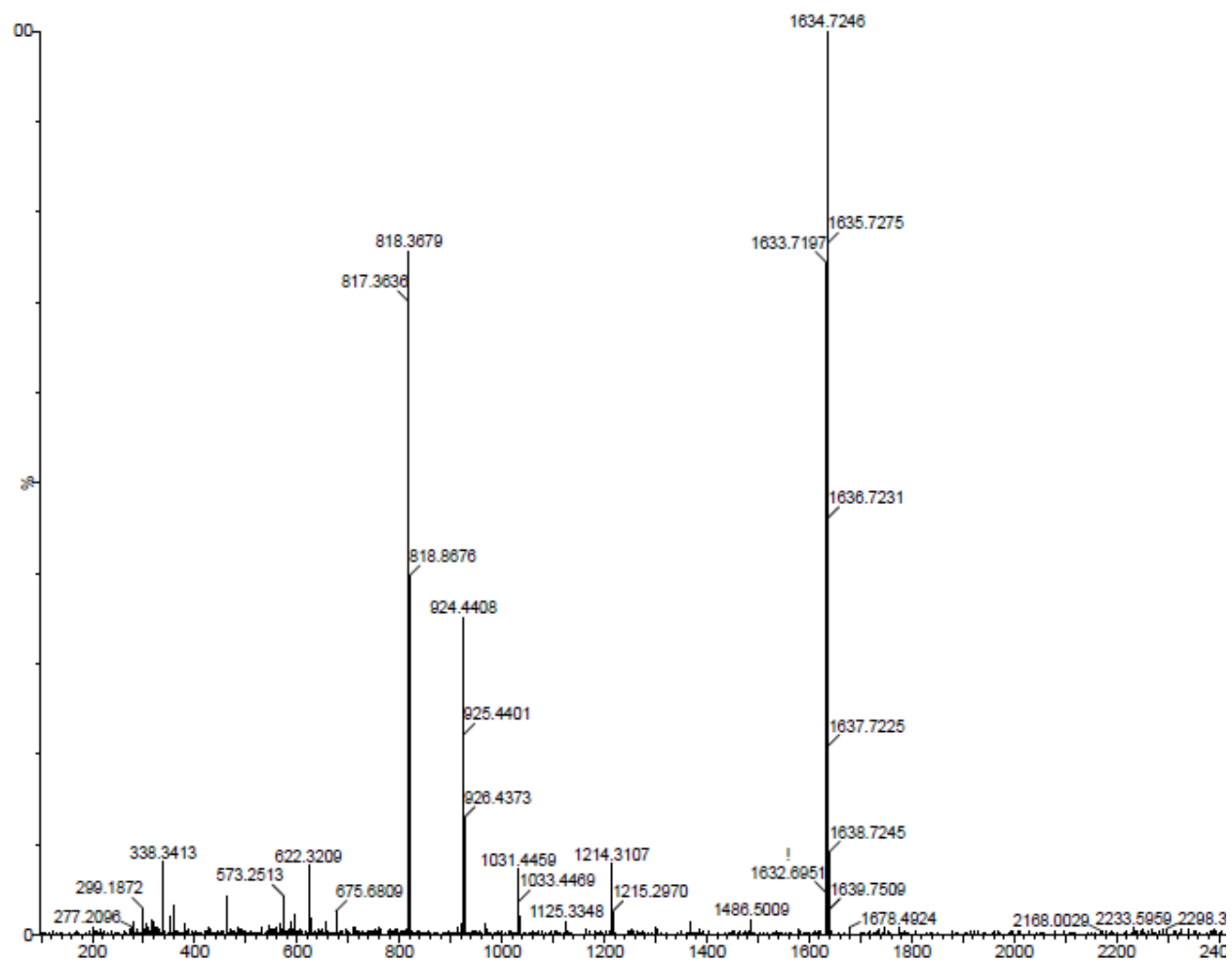
Figure II.36: HRMS spectrum of **II.16**
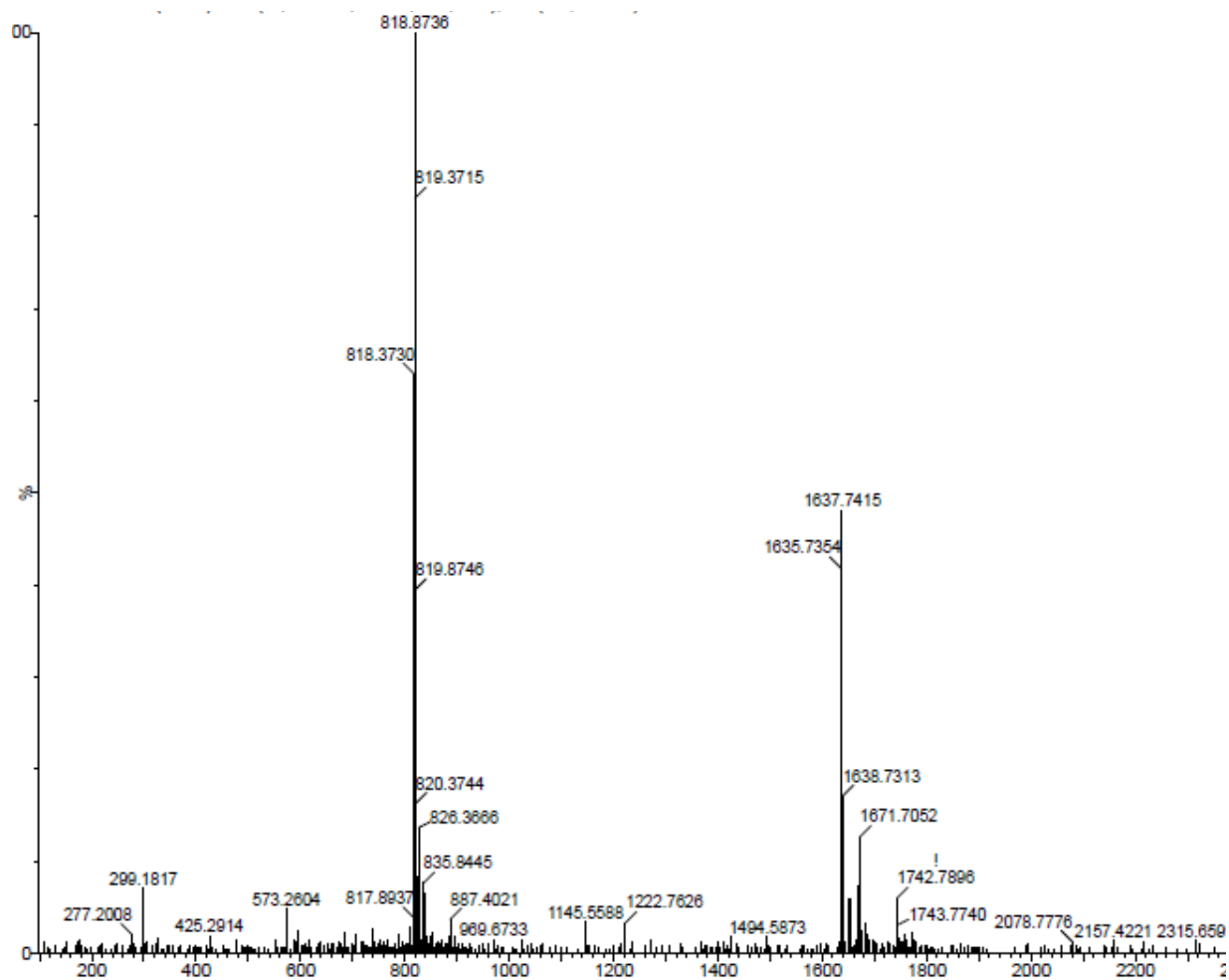
Figure II.37: HRMS spectrum of **II.17**

Chapter-3

38π Aromatic Expanded Isophlorins and Additive Induced Polymorphism

Part-A

Synthesis and Characterization of Structurally Variant 38π Expanded Isophlorins

III.A] Introduction:

Aromaticity is the fundamental concept in the chemistry which is unambiguously used to predict possible properties of cyclic conjugated molecules. An accepted rule is Huckel's empirical formula of $(4n+2)\pi$ electrons along the cyclic conjugated pathway. The property of aromatic molecules to sustain the ring current effect in the presence of external magnetic field, results in large anisotropic diamagnetic susceptibility that can be identified by NMR spectroscopy. The annulenes (C_nH_n) with a conjugation circuit of $[4n+2]\pi$ electrons is known to be aromatic in nature.[59] Breslow extended this concept and coined the rule for antiaromaticity, which proposed that annulenes with $[4n]\pi$ electrons are antiaromatic with opposite ring current effect and with reduced stability with respect to aromatic systems.[12] Porphyrin,**III.1**, being a $[4n+2]\pi$ electrons macrocycle is a structural analog of planar [18] annulenes (figure-1).[23] It exhibits diatropic ring current effects in its NMR

spectrum resulting in upfield shift for the inner NH protons and downfield shift of β-CH protons of the pyrrole rings.
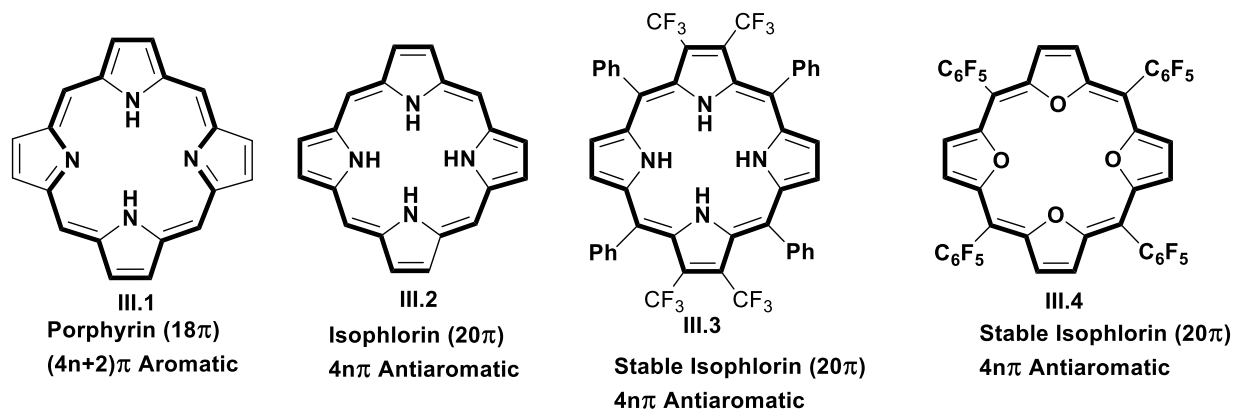
Figure-III.1: 18π porphyrin, 20π isophlorin and 20π core modified isophlorin.

Isophlorin, **III.2**, is an antiaromatic structural congener of porphyrin in which the ring current flows through the periphery of macrocycle and accounts for 20π electrons. Therefore, it is known to typify [4n]π electrons rule.[3] Isophlorin's inherent instability is attributed to the rapid conversion of amine nitrogen to imine under ambient conditions. However, a relatively stable 20π isophlorin, under inert conditions, has been isolated by substituting electron-withdrawing groups at the β position of two pyrroles in the isophlorin **III.3**.[46] Alternatively, core modification and meso pentafluro phenyl substitution resulted in the formation of an air stable isophlorin **III.4**.[60] Varying the extent of π-conjugated network of isophlorin by incorporation of small aromatic heterocycles such as furan, thiophene, selenophene, significantly altered its electronic properties. These new class of macrocycles are termed as expanded isophlorins. [55] and satisfy Huckel's [4n+2]π electrons rule. Design and synthesis of such expanded cyclic aromatic assemblies are attractive targets for tuning optical and electronic properties for possible applications in organic electronics, non-linear optics, and energy storage devices. Synthesis of such expanded six membered 30π isophlorins (figure-III.2) was achieved by Anand et. al, **III.5** to **III.8** [31,51] These molecules show typical structural diversity depending on nature of heterocyclic unit used. Osuka and co-workers reported another example for a 30π aromatic hexapyrrolic expanded isophlorin, **III.9**, in the neutral state with diethylsulfanyl groups on the β positions of the pyrrole rings, which was found to be highly unstable at ambient temperature.[50]
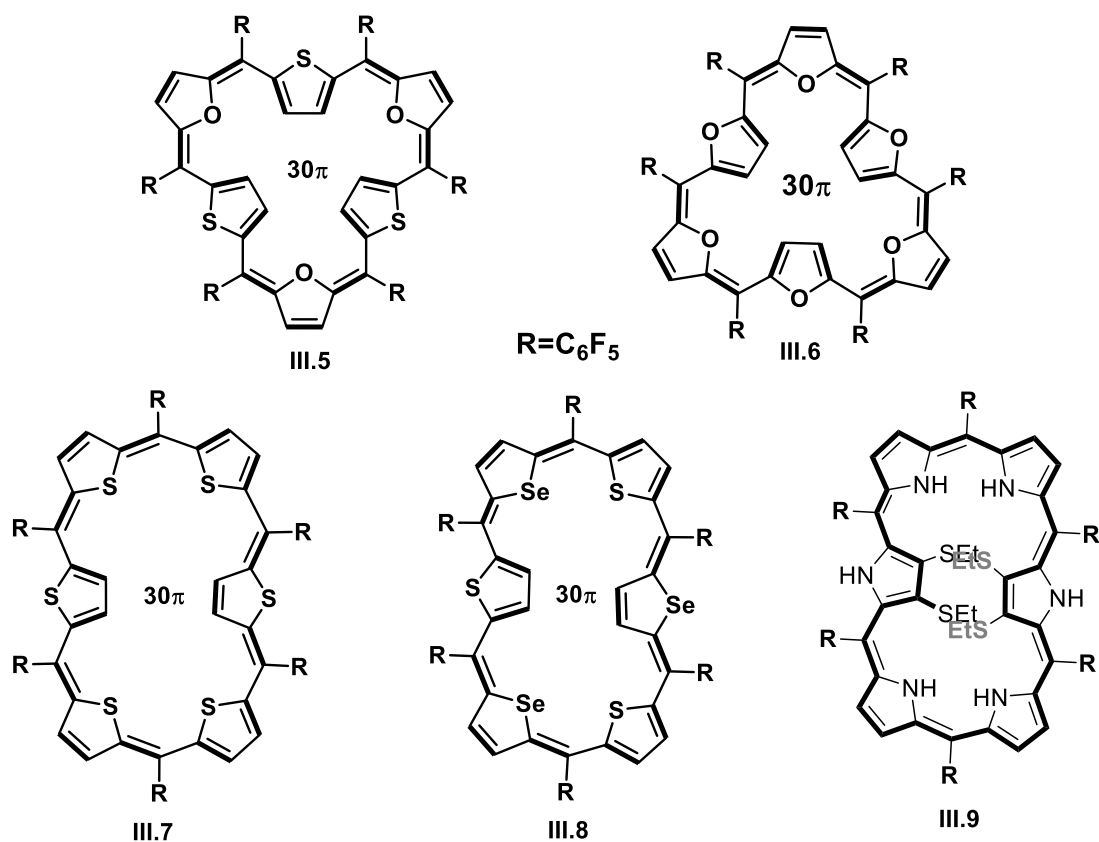
Figure-III.2: Examples for structurally variants of 30π isophlorins.

Expanded aromatic isophlorins with eight heterocyclic rings, can show interesting optoelectronics and structural properties. Synthesis of such aromatic expanded isophlorins with eight heterocycles are not very common, due to their inherent flexibility and structure induced loss of aromaticity. As discussed in the first chapter, heterocyclic ring inversions are crucial role for macrocyclic planarity. Therefore, to overcome the challenge of flexibility, attempts were made to employ a rigid precursor such as bithiophene and biselenophene for the synthesis of eight membered aromatic isophlorins. Solid state structure of bithiophene revels, both the thiophene rings in bithiophene point opposite to each other, this heterocyclic ring inversion can be beneficial to induce the planarity into the macrocycle. [57]

III.A.1 Synthesis and characterization of 38π Isophlorins III.12

Synthesis

The synthesis of the desired macrocycles was attempted by using easily made precursors. Acid mediated condensation between dithienyl dicarbinol III.10 and bithiophene **III.11** was performed in dry dichloromethane, followed by oxidation with DDQ to open air (scheme-III.1). MALDI-TOF/TOF mass spectrometric analysis (figure-III.3) of the reaction mixture displayed an m/z of 1550.8337, which confirmed the formation expected macrocycle. The macrocycle of interest, **III.12**, was isolated as a dark purple colored band in 28% yields by passing the reaction mixture through basic alumina column.
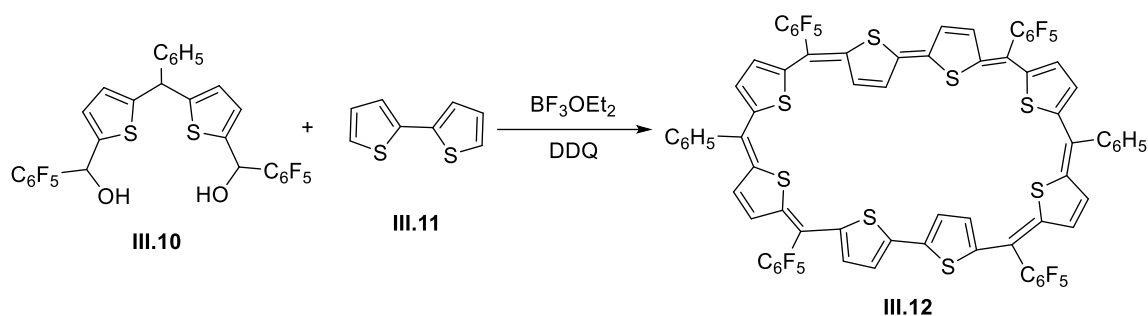
Scheme-III.1: Synthesis of 38π aromatic isophlorin **III.12**.
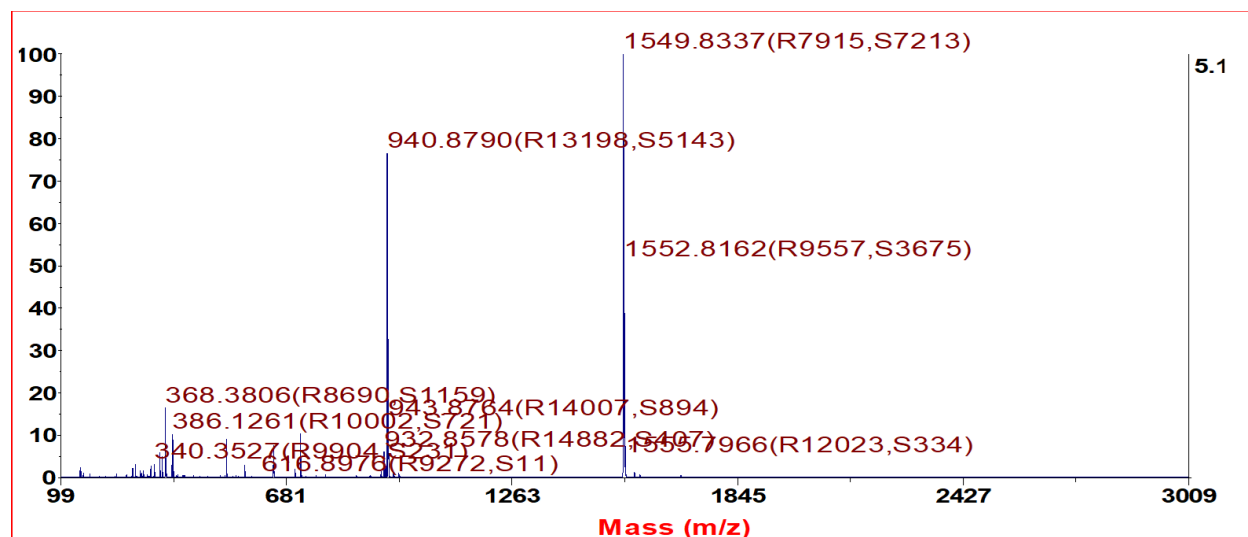
Figure-III.3: MALDI-TOF/TOF mass spectrum of the reaction mixture.

HRMS, ^{1}H NMR and electronic absorption studies:

The high-resolution mass spectrometric analysis of **III.12** displayed m/z at 1449.9481 corresponding to the exact mass of 1549.9462. Due to an intense color, it was found to absorb in the visible part of the electromagnetic spectrum with an absorption maxima at 580 nm (130000), followed by low energy transitions at 709 (20000) and 759 (20000) nm (figure-III.4).
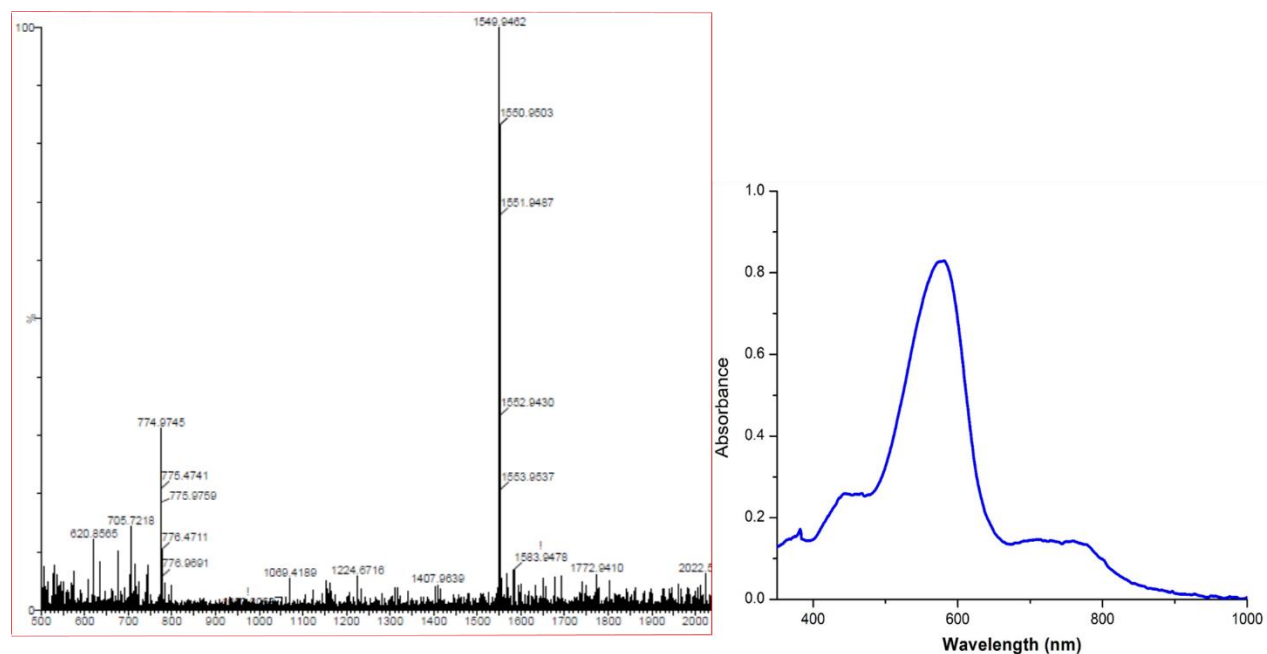
Figure-III.4: HRMS spectrum (left) and UV-Vis absorption spectrum (right) of [10^{-6}M] **III.12** recorded in CH_2Cl_2.

Further analysis by ^{1}H NMR spectroscopy displayed only two signals at δ 7.5 and 7.2 ppm, signifying **III.12** could be highly fluxional, at room temperature (figure-III.5).
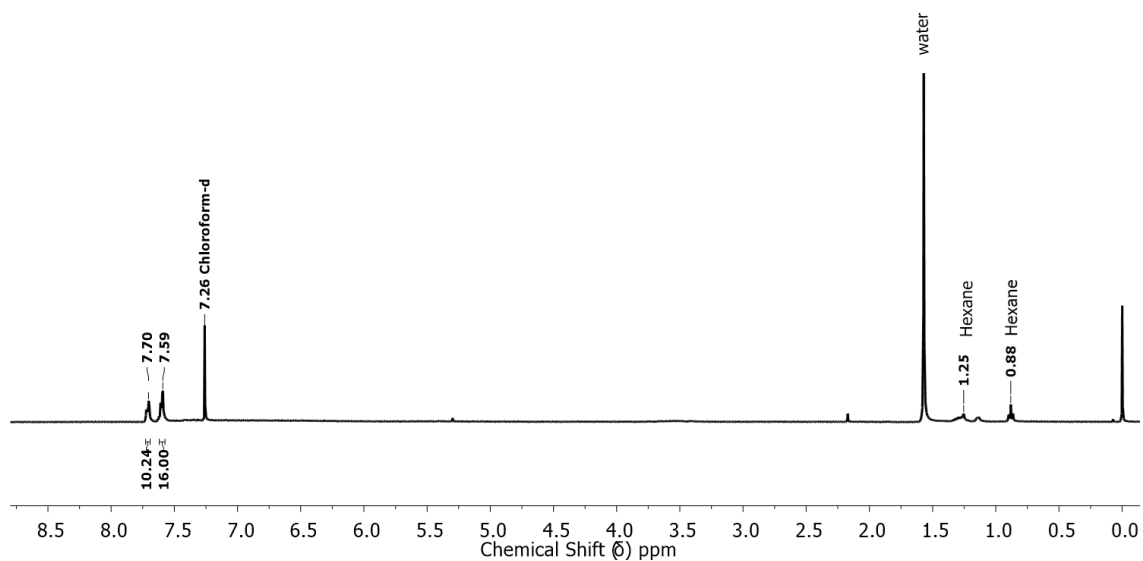
Figure-III.5: ^{1}H NMR Spectrum of **III.12** at 298K in CDCl$_3$.

Variable temperature NMR spectroscopy (figure-III.6) was employed to arrest the suspected fluxional characteristics of **III.12**. Upon lowering the temperature, a well-resolved spectrum was observed at 253K in CDCl$_3$ (figure-III.7). Overall, it displayed six doublets corresponding to two-protons each at δ 8.34 7.57, 7.39, 7.36, 6.53 and 6.20 ppm. A lone broad singlet observed at δ 5.08 ppm corresponded to four protons. Protons of the phenyl rings resonated at δ 7.76 and 7.65, ppm. The observed NMR pattern with a reduced number of signals in the ^{1}H NMR spectrum could be inferred for a symmetric topology. However, the observed chemical shift values of **III.12** did not justify ring current effects expected of an aromatic 38π expanded isophlorin. The observation of doublets supported ortho coupling of protons on the heterocyclic rings. This was further confirmed by ^{1}H-^{1}H COSY spectrum recorded at 253K (figure-III.8), which showed three correlations for the six β protons of thiophene rings, at (i) 8.33 and 7.38, (ii) 7.57 and7.39, (iii) 6.52 and 6.22. The observation of a broad singlet at a relatively higher field suggested a different environment for the four protons in comparison to the other doublets. As the thiophene units are anti-parallel in a bithiophene unit, it could be envisaged that two thiophene units adopt ring-inverted structures with respect to the macrocycle.
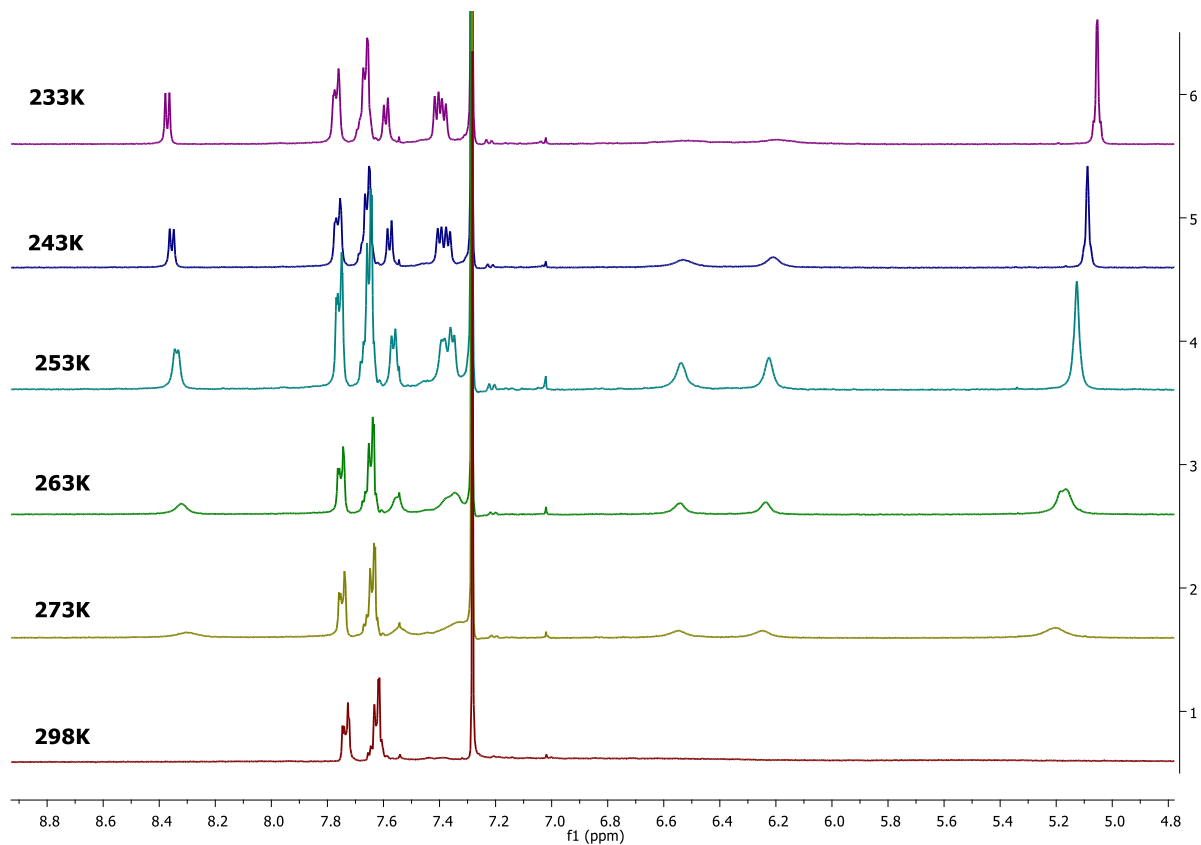
Figure-III.6: Variable temperature ^{1}H NMR Spectrum of **III.12** in Chloroform-*d*.
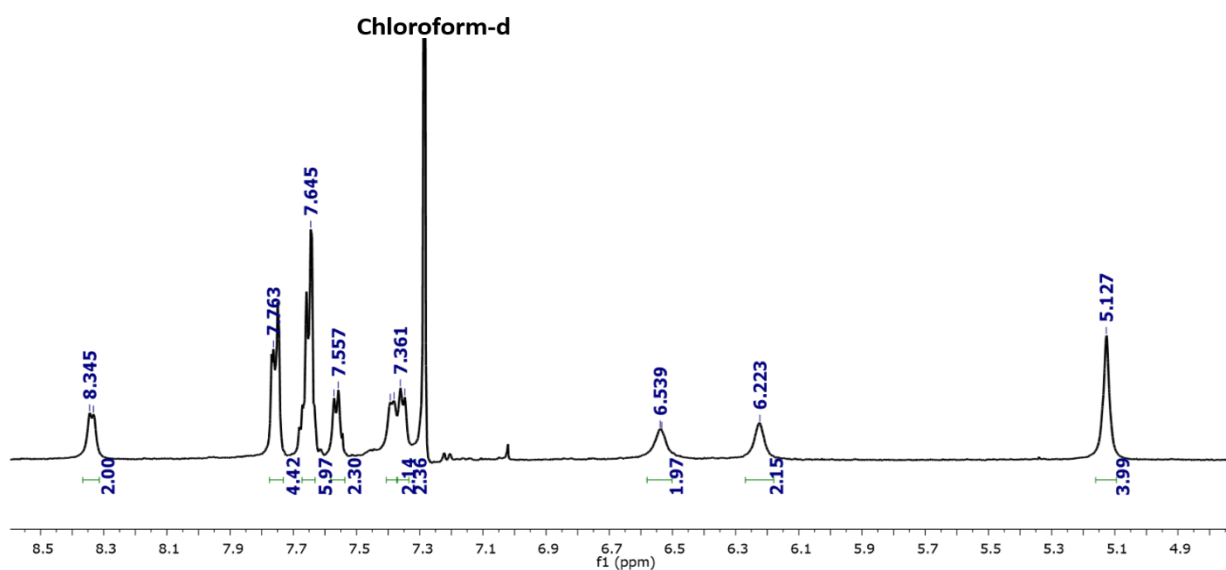
Figure-III.7: Partial ^{1}H NMR spectrum of **III.12** recorded at 253K in Chloroform-*d*.
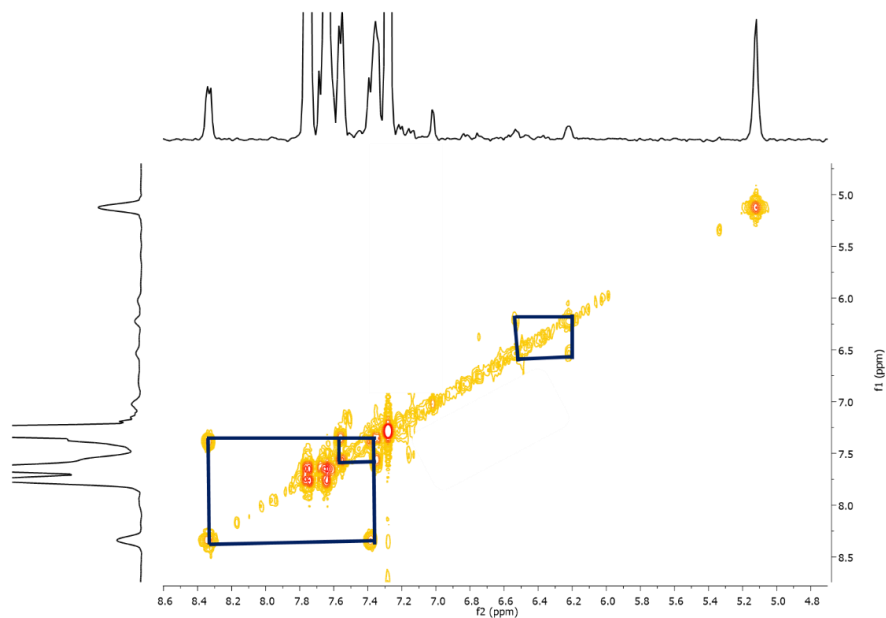
Figure-III.8: ^{1}H-^{1}H COSY spectrum of **III.12** recorded at 253K Chloroform-*d*.

Single crystal X-ray diffraction analysis:

Absolute confirmation of the molecular structure for **III.12** was elucidated by a single-crystal X-ray diffraction analysis. Good quality single crystals were grown by the vapor diffusion method from solution of **III.12** in CHCl$_3$ and methanol vapor. The macrocycle crystalized in triclinic space group **P-1** and revealed an unexpected planar geometry (figure-III.9). However, as expected, inversion of diametrically opposite thiophene units was observed in the macrocycle.
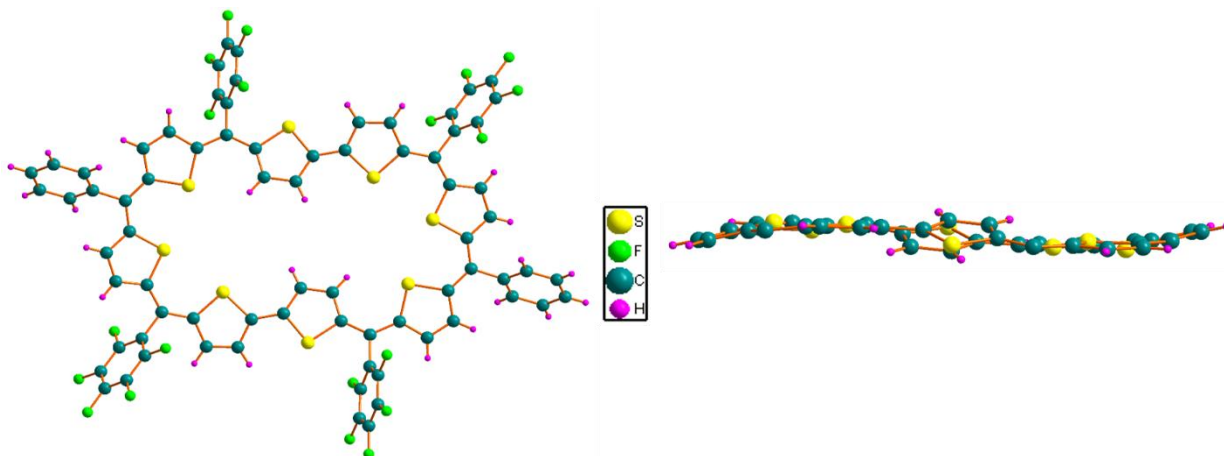
Figure-III.9: A] molecular structure **III.12** lateral view, B] side view (Meso-substituents from side view and packing diagrams are omitted for clarity).
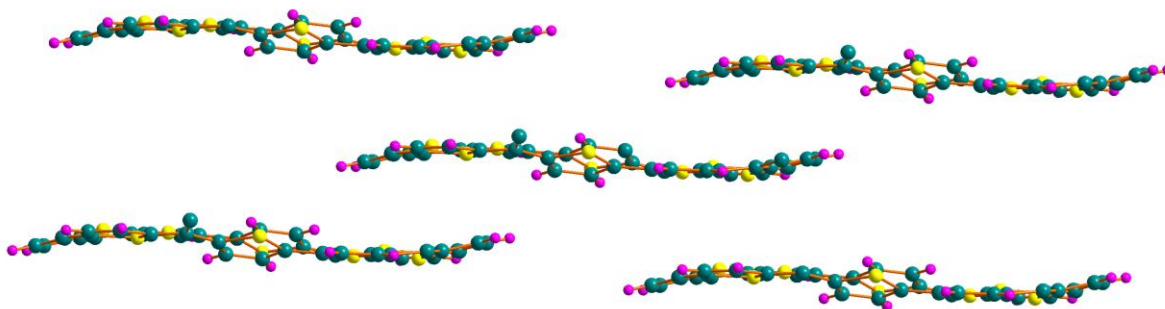
Figure-III.10: π-stacking observed in the crystal lattice of **III.12**. Phenyl groups and solvents are omitted for clarity.

Unlike the octafuran macrocycle, **I.35**, molecule acquires a rectangular planar geometry and displayed weak π-π stacking interaction with an inter-planar distance of 4.20Å. (Figure-III.10). Encouraged by the observation of a planar 38π tetraoctathiophene, it was anticipated that similar macrocycles could be synthesized by replacing dithienyl methane with analogous bis-heterocycles. As furan and thiophene have similar structural and electronic properties, difuryl methane was employed to synthesize a 38π macrocycle similar to **III.12**,

III.A.2 (a) Synthesis and characterization of III.14A

Anticipating a structural analog of **III.12**, reaction between difuryl dicarbinol **III.13** and bithiophene **III.11** were performed (scheme-III.2) under similar reaction condition as described in scheme-III.1. Formation of the desired macrocycle **III.14A** was identified from the MALDI-TOF/TOF mass spectrum of the reaction mixture. It was purified from the reaction mixture through basic alumina column chromatography in 16% yields.
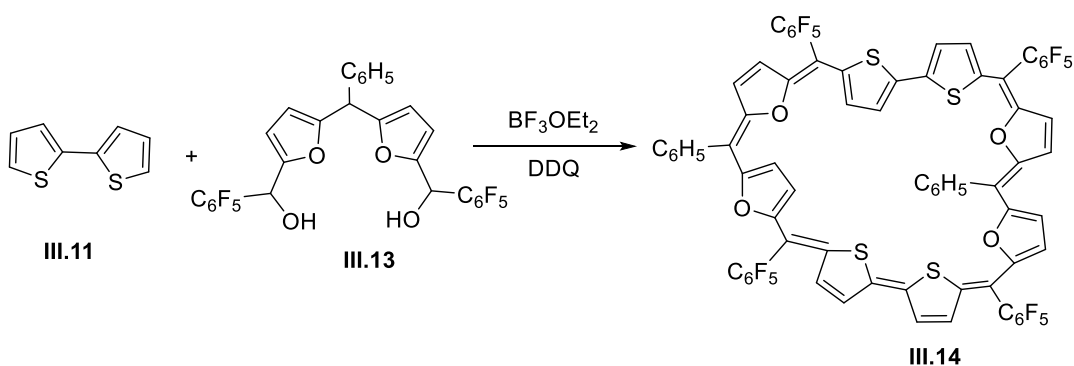
Scheme-III.2 Synthesis of 38π aromatic isophlorin **III.14A**.

86

Structural characterization:

HRMS and electronic absorption studies

High-resolution mass spectrometric (HRMS) analysis of **III.14A** displayed an m/z value of 1486.0381, corresponding to the expected macrocycle (figure-III.11A). Due to an intense colored solution, it was found to absorb at 580 nm (130000) in the visible part of the electromagnetic spectrum. (Figure-III.11B).
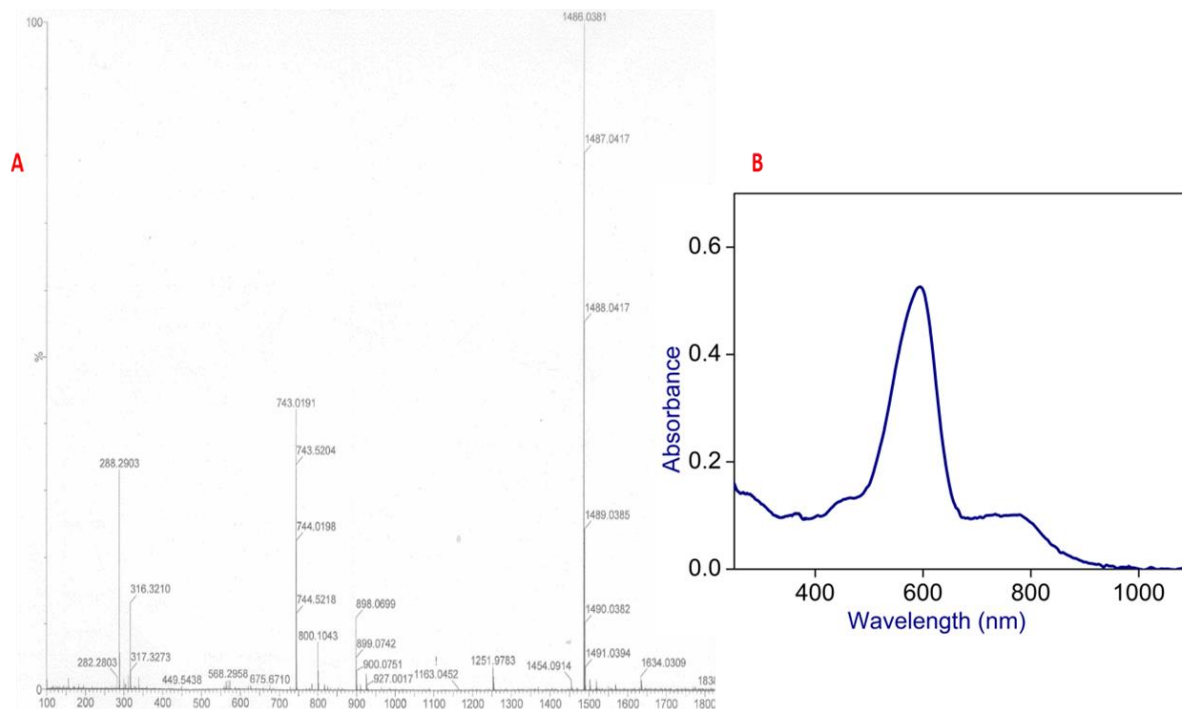
Figure-III.11: A] HRMS spectrum of **III.12** B] UV-Vis Absorption spectrum of [10^{-5}]. **III.14** recorded in CH_2Cl_2.

NMR studies:

The ^{1}H-NMR spectrum of **III.14A** recorded in acetone-d_6, displayed only four signals between δ 9.0 to 7.0 ppm. Two signals around δ 5.0 ppm, observed at room temperature was completely different from that of ^{1}H NMR of **III.12**. This unresolved spectrum at room temperature implied fluxional characteristics of the macrocycle and could not be inferred for any possible structure. Therefore variable temperature ^{1}H NMR spectra (figure-III.12) were recorded to arrest this suspected fluxionality. It was found that upon decreasing temperature, a well-resolved spectrum was observed at 193K and displayed signals in the region ranging from δ 10.0 to 3.0 ppm (figure-III.13). Overall eighteen signals were observed at 193K leading to the inference that macrocycle

adopted a highly unsymmetrical structure. Nine signals corresponding to equal number of protons were observed at δ 9.45, 9.34, 9.24, 9.06, 8.61, 8.49, 8.4, 8.25, 8.19, 8.13 ppm and two other signals for five protons at δ 7.98, 7.69 ppm. In contrast, another set of signals for five protons was observed at δ 5.34, 5.03 ppm as well as four signals corresponding to one proton each was found at δ 4.34, 4.15, 3.87, and 3.37 ppm.
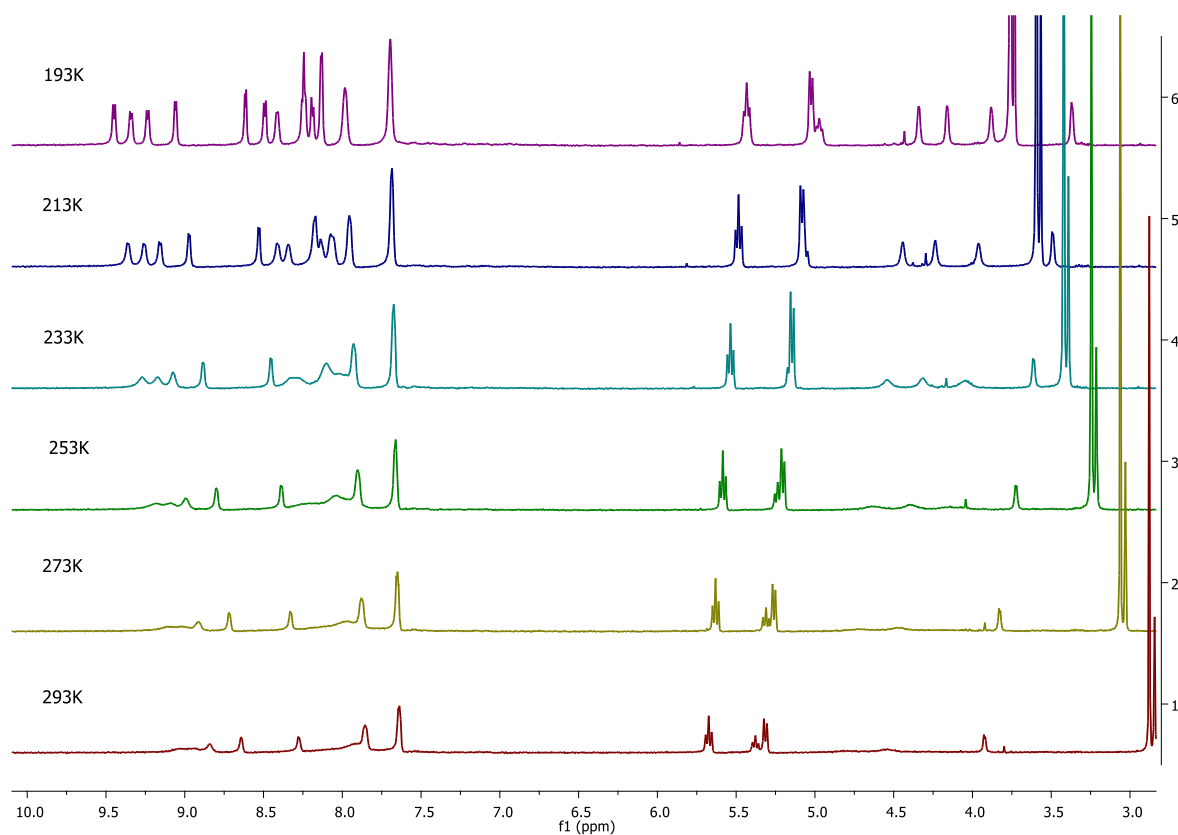
Figure-III.12: Variable temperature ^{1}H NMR Spectrum of **III.14** in Acetone-d_6.
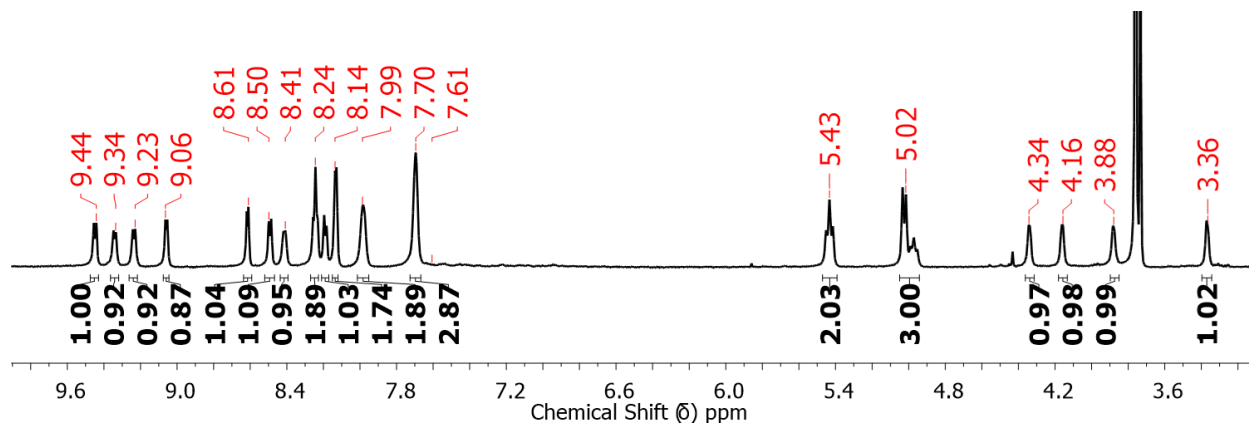
Figure-III.13: ^{1}H NMR Spectrum of **III.14** at 193K in Acetone-d_6.

The observed ^{1}H NMR spectrum was further supported by ^{1}H-^{1}H COSY spectrum (figure-III.14), which displayed six correlations in the downfield region at δ (i) 9.43 and 8.47, (ii) 9.32 and 8.42, (iii) 9.23 and 8.24, (iv) 9.04 and 8.24, (v) 8.59 and 8.22, (vi) 7.96 and 7.70. These correlations could be attributed to β-protons of the heterocyclic rings. Similarly, two correlations for inverted heterocyclic rings were observed at (viii) 4.34 and 3.42, (ix) 4.15 and 3.87 ppm. A third correlation was observed for the high field signals at (vii) 5.41 and 5.02 ppm.
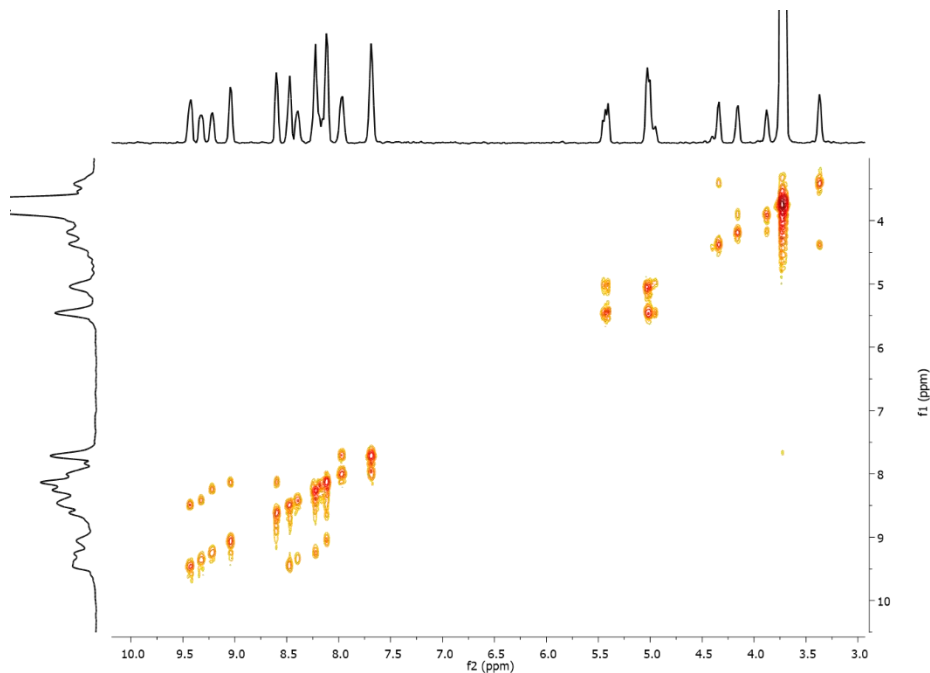
Figure-III.14: partial ^{1}H-^{1}H COSY spectrum of **III.14A** at 193K in Acetone-*d₆*.

These observations from NMR spectroscopy suggested unsymmetrical ring inverted structure and deviated significantly from the octathiophene macrocycle **III.12**. However, it was not possible to identify the protons of thiophene, furan and phenyl rings from ^{1}H NMR analysis. Hence, multiple attempts were made to obtain good quality single crystals to determine the absolute structure of the macrocycle.

Single crystal X-ray diffraction analysis:

Figure-III.15: A] Top view (left) and side view (right) of the molecular structure of. **III.14A** (Meso-substituents are omitted for clarity in the side view).

Single crystal X-ray diffraction analysis of good quality crystal grown from $CHCl_3$/MeOH revealed a triclinic system with a P-1 space group. It was found to adopt a near planar geometry (figure-III.15). In support of the ^{1}H NMR analysis the structure was highly unsymmetrical due to multiple ring inversions due to thiophene, furan and a phenyl ring. In one of the two bithiophene units, the thiophenes adopted a rare parallel orientation and the other retained the regular anti parallel orientation. Similarly, one of the difuryl units was found to adopt a parallel orientation of the heterocyclic rings and the other unit displayed a ring-inverted structure. The phenyl ring substituted on one of the normal difuryl units was found to be inverted leading to exposure of the phenyl protons to the diatropic ring current of the macrocycle. This structure was found to resonate with the observed asymmetrical nature of its ^{1}H NMR spectrum. Particularly, the chemical shift of one of the phenyl ring signals around 5 δ ppm and four signals for β protons at up filed region signified presence of diatropic ring current effect. Therefore the up field signals correspond to the protons of the inverted furan and thiophene rings that are exposed to the diatropic ring current of 38π aromatic system. The estimated NICS value of -18.23 ppm is in complete agreement with the observed experimental results. Aromatic ring current was further supported by the close wise orientation of arrows in the ACID plot.

III.A.2 (b) Synthesis and characterization of III.14B

In an attempt to synthesize structural analog of **III.12** with furan derivative, substitution of bithiophene dicarbinol with bifuryl dicarbinol resulted in to a unique structure for **III.14A**, with one of the *meso* phenyl ring is inverted in to the macrocyclic plane. To understand effect of bithiophene on to the planarity of macrocycles, it was decided to replace bithiophene from **III.12** with other heterocycles such as bifuran or biselenophene.
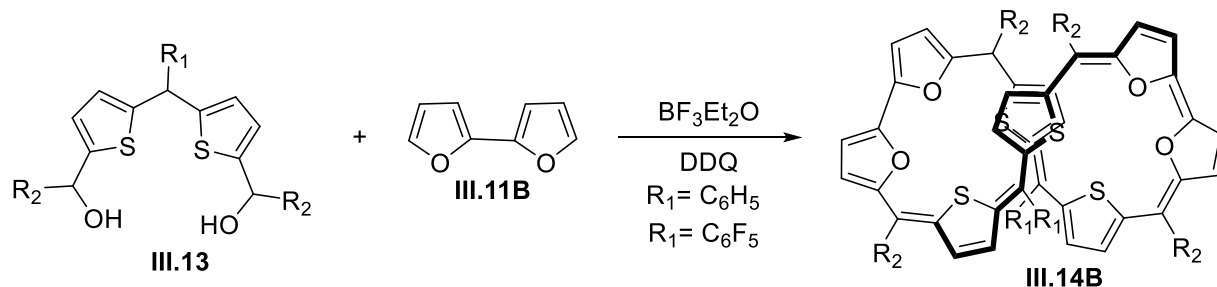
Scheme-III.3 Synthesis of 38π non-aromatic isophlorin **III.14B**.

Synthesis of desired macrocycle was achieved by acid mediated condensation between bifuran and bithiophene dicarbinol. MALDI-TOF/TOF mass spectrometric analysis of reaction mixture confirms formation of expected macrocycle. Purification through basic alumina column gives green colored band in 2% yield. Isolated macrocycle showed sharp absorption with absorption maxima of 737nm (84000) along with low energy shoulder band at 509 (3700) and 371nm (5100) (figure-III.16). Which is very different from **III.14A**, suggest different conformation for **III.14B**.
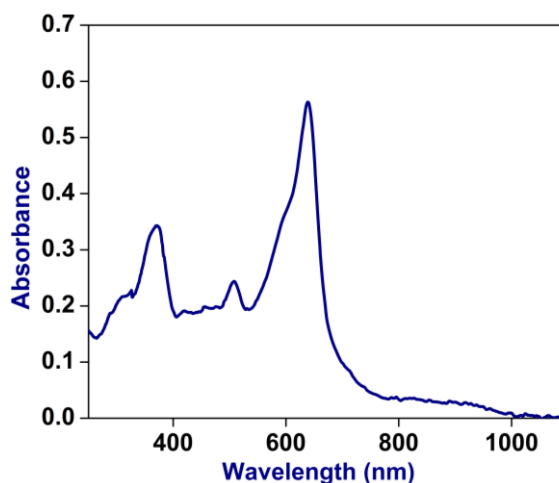
Figure-III.16: Absorption spectrum of [10^{-5}]. **III.14B** recorded in CH_2Cl_2.

¹H NMR Studies: The ¹H-NMR spectrum of **III.14B** was recorded in acetone-d_6, at room temperature, it displayed multiple signals, which does not infer to any possible structure. Therefore, variable temperature ¹H-NMR spectra were recorded and a well resolved spectrum was observed at 233K (figure-III.17). It displayed eight doublet between 7.73 to 5.51 δppm with integration of two protons each. Observed resonance in the region of δ 7.73 to 5.51 ppm suggest absence of diatropic ring current for aromatic macrocycle. ¹H-¹H COSY spectrum was recorded at 233K (figure-III.18). Four correlations were observed for the protons at (i) 7.75 and 7.23, (ii) 7.71 and 6.83, (iii) 7.35 and 6.49, (iv) 5.83 and 5.53 δppm. The observed sets of doublets confirmed the coupling of adjacent β protons of the heterocyclic rings
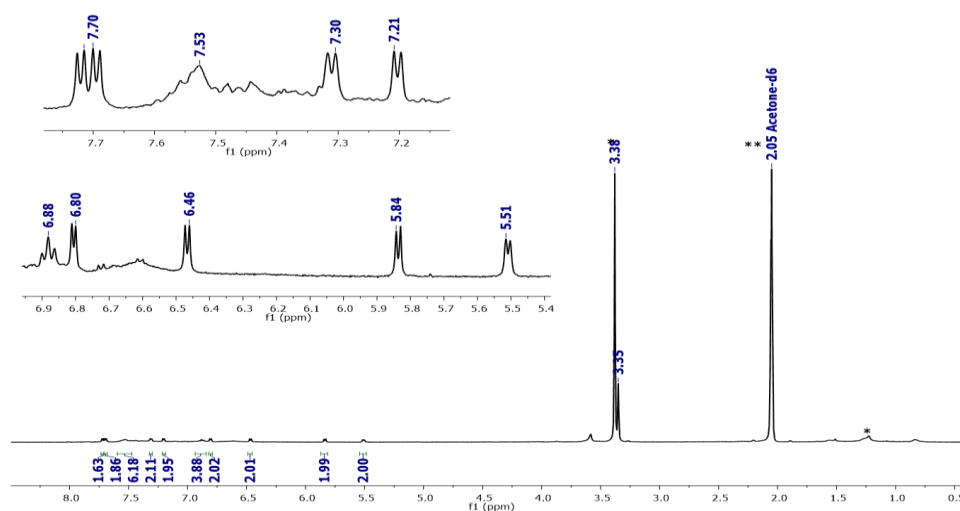
Figure-III.17: ¹H NMR Spectrum of **III.14B** at 233K in Acetone-d_6.
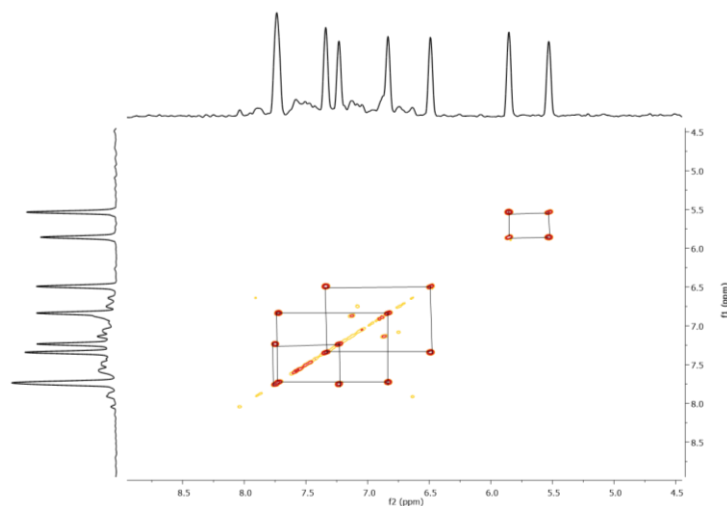
Figure-III.18: ¹H-¹H COSY Spectrum of **III.14B** at 233K in Acetone-d_6.

Single crystal X-ray diffraction analysis: Molecular structure of **III.14B** was determined by single crystal X-ray analysis. The good quality crystal was obtained after multiple attempts by slow evaporation of chloroform/hexane. The obtained structure reveled figure of eight geometry with monoclinic C2/c space group (figure-III.19). This is remarkable in the context of an octa thiophene, **III.12**, and the furan derivative **III.14A**, which displayed planar conformation with the inversion of heterocyclic rings. However, the molecular structure of **III.14B** sans any such inversions of heterocyclic rings lead to the twisting of the macrocycle. It can be expected that the molecular twist can happen on a segment with either of the heterocyclic rings. Yet, it was observed that the figure-of-eight conformation was achieved by the crossing of the dithienyl methane units at the center of the macrocycle. The two bifuran units were positioned on opposite ends of the structure leading to two corrole-like pockets. All the heterocyclic units have a uniform orientation such that the heteroatoms are directed towards the center of macrocycle.
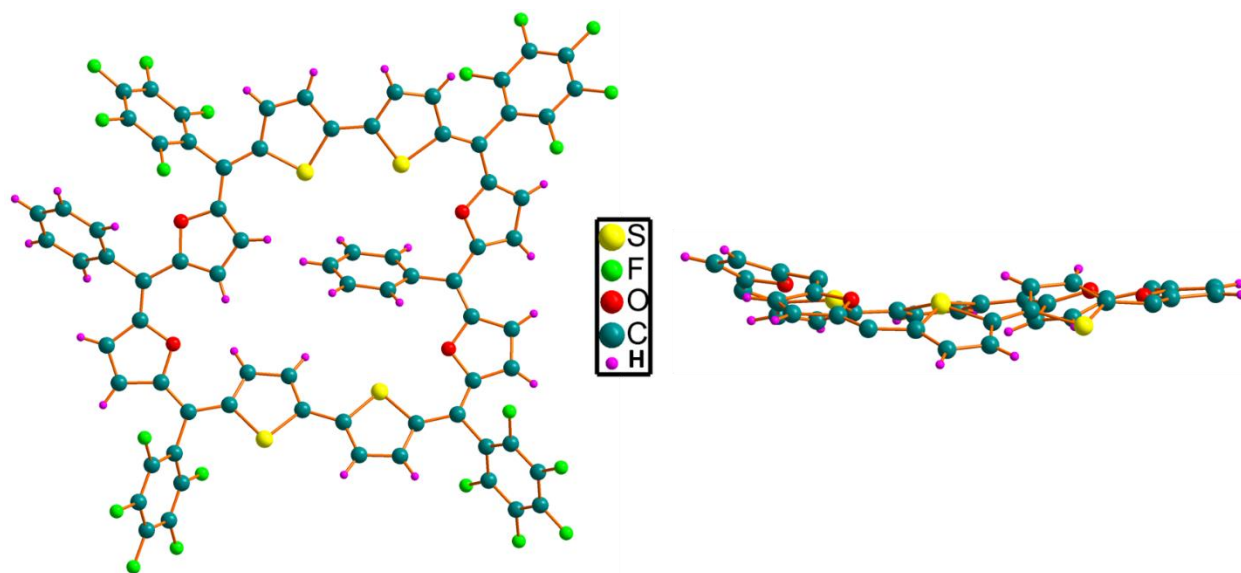

Figure-III.19: A] Top view (left) and B] side view (right) of the molecular structure of. **III.14B** (Meso-substituents are omitted for clarity in the side view).

III.A.3 Synthesis and characterization of III.16

Based on the structural modification upon substituting thiophene by furans, an attempt was made to replace the bithiophenes with biselenophene units. Replacement of four thiophenes in 38π octathiaisophlorin **III.12** with furan lead to the formation of isoelectronic species with large structural variation **III.14A, III.14B** and interestingly, in case of **III.14A**, only one bithiophene adopted inverted ring structure. Anticipating another isoelectronic analog of 38π aromatic isophlorin, dithienyl dicarbinol was condensed with biselenophene (scheme-III.4) under similar reaction conditions (scheme-III.1). The formation of macrocycle was confirmed by MALDI-TOF/TOF mass spectrometry of the reaction mixture. The anticipated macrocycle was purified from the reaction mixture as a blue colored band in 15 % yield through column chromatography. Due to an intense color, the macrocycle was found to absorbs at 580 nm ($\varepsilon=105000$) when recorded in dichloromethane (figure-III.20)
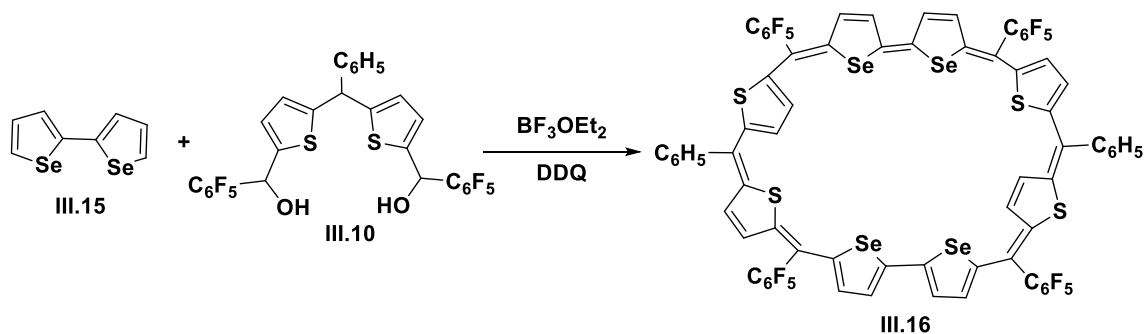
Scheme-III.4: Synthesis of 38 π aromatic isophlorin **III.16**.
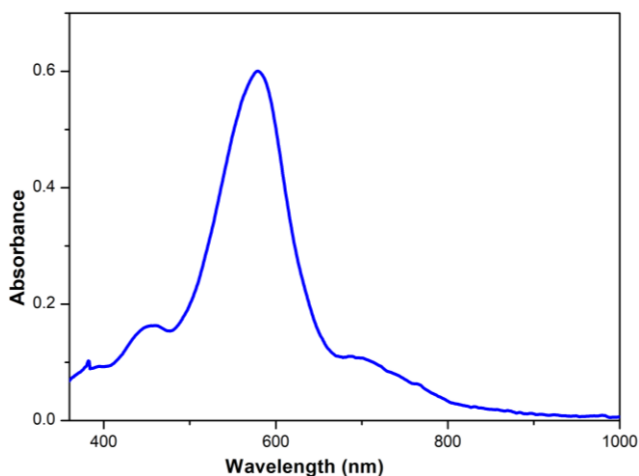
Figure-III.20: UV-Vis Absorption spectrum of [10^{-6}]. **III.16** in dichloromethane.

94

NMR studies:

The ^{1}H NMR spectrum of **III.16** displayed only two signals around δ 7.0 ppm at room temperature. This spectrum was found to exhibit a pattern similar to the room temperature spectrum of **III.12**. As the octathiophene, was found to be fluxional in nature, the same feature was prejudiced for **III.16** too. Therefore **III.16** was subjected to variable temperature ^{1}H NMR spectroscopy (figure-III.21). Upon decreasing the temperature to 233K, it displayed a well-resolved spectrum (figure-III.22), and the signals were observed between δ 8.5 to 5.5 ppm. These signals appeared similar to the β-protons of non-inverted thiophene rings in **III.12**. As signals resonated both in up field and down field region, it displayed a significant amount diatropic ring current effects. Signals at δ 8.32, 7.50, 7.38, 7.26 ppm corresponding to two protons each were identified for β-protons of non-inverted thiophene rings. A broad signal corresponding to four protons was observed at δ 7.02 ppm for the inverted rings. Two other signals corresponding to two protons each were observed at δ 5.69 and 5.58 ppm and the phenyl protons resonated at δ 6.62 to 7.58 ppm.
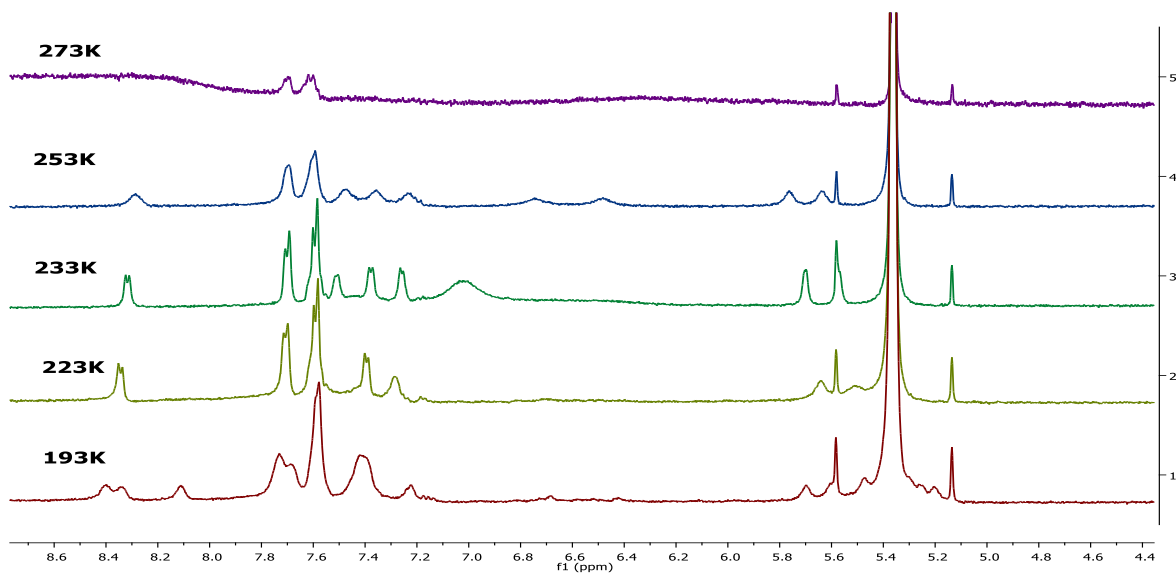
Figure-III.21: Variable temperature ^{1}H NMR of **III.16** in CD_2Cl_2.
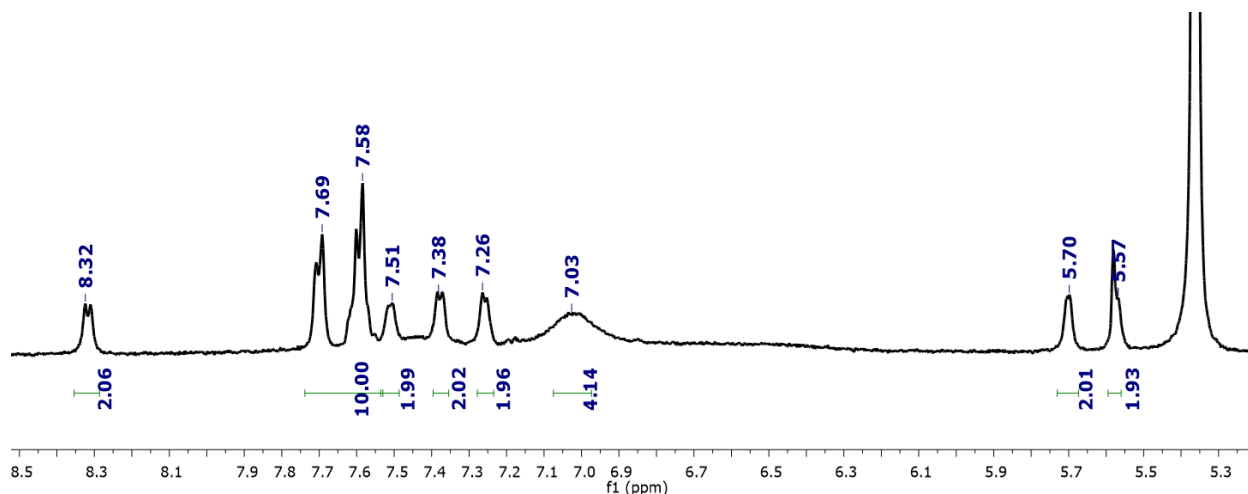
Figure-III.22: ^{1}H NMR of **III.16** in CD$_2$Cl$_2$ at 233K
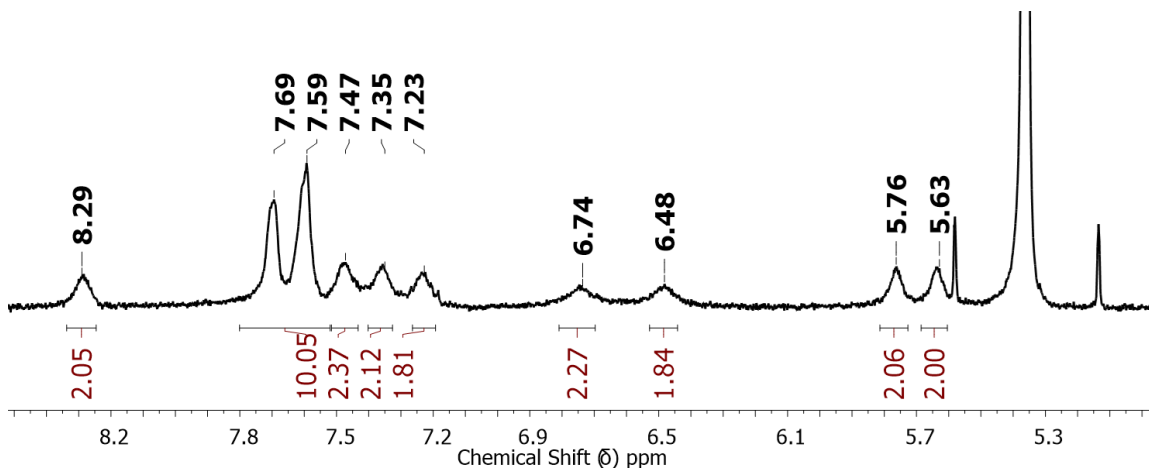
Figure-III.23: ^{1}H NMR of **III.16** in CD$_2$Cl$_2$ at 253K

Specifically, the broad singlet observed for four protons at δ 7.02 ppm at 233K for the β-protons shifted and split into two signals corresponding to two protons each at 253K. Unfortunately, at this temperature the other signals broadened and resulted in reduced resolution of the signal. Hence, ^{1}H-^{1}H COSY was recorded at 233K (figure-III.24), which showed correlations both in up field and down field regions. The correlations observed for the signals (i) 8.29 and 7.39, (ii) 7.50 and 7.30 for down field shifted proton and (iii) upfield shifted signals at 5.68, and 5.56 ppm was in support for the protons for inverted heterocyclic rings.
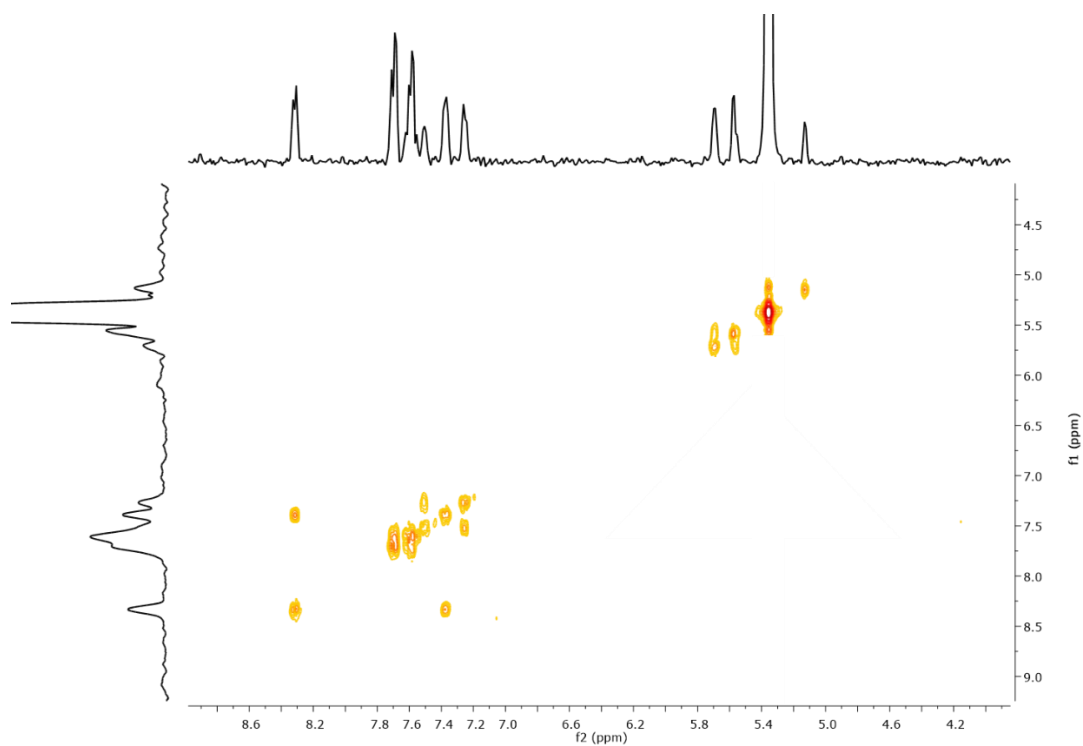
Figure-III.24: partial ^{1}H-^{1}H COSY spectrum of **III.16** at 233K in Dichloromethane-d_2

Single crystal X-ray diffraction analysis:

Molecular structure of **III.16** was determined by single-crystal x-ray diffraction analysis (figure-III.25). Good quality crystals were grown from benzene by slow evaporation method for **III.16**. It crystalized in triclinic system with P-1 space group, revealed highly planar geometry with zero deviation from the mean plane. This structure varied significantly from the other two 38π octaphyrins **III.12** and **III.14A** and **III.14B** described above. Surprisingly, both the biselenophene rings did not show an inverted ring structure; rather, two of the diametrically opposite thiophene rings from dicarbinol showed ring inversion. In the crystal lattice, it displayed π-π interaction with an inter-planar distance of 3.69Å (Figure-III.26). All the phenyl rings were found orthogonal to the mean plane defined by the meso four carbons of the macrocycle. The estimated NICS of -14.68 endorsed the experimental data of aromatic characteristics.
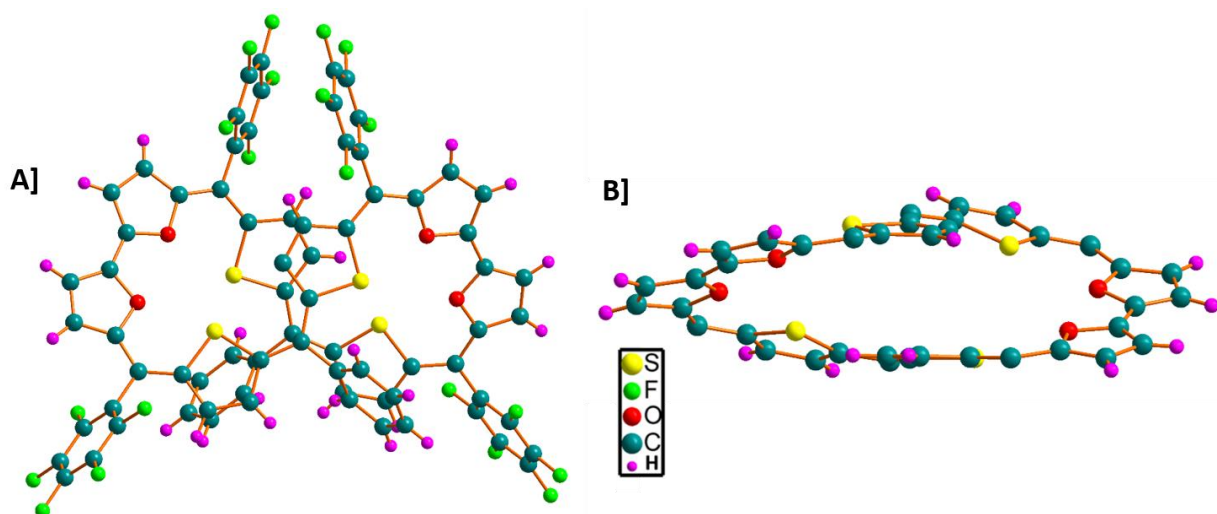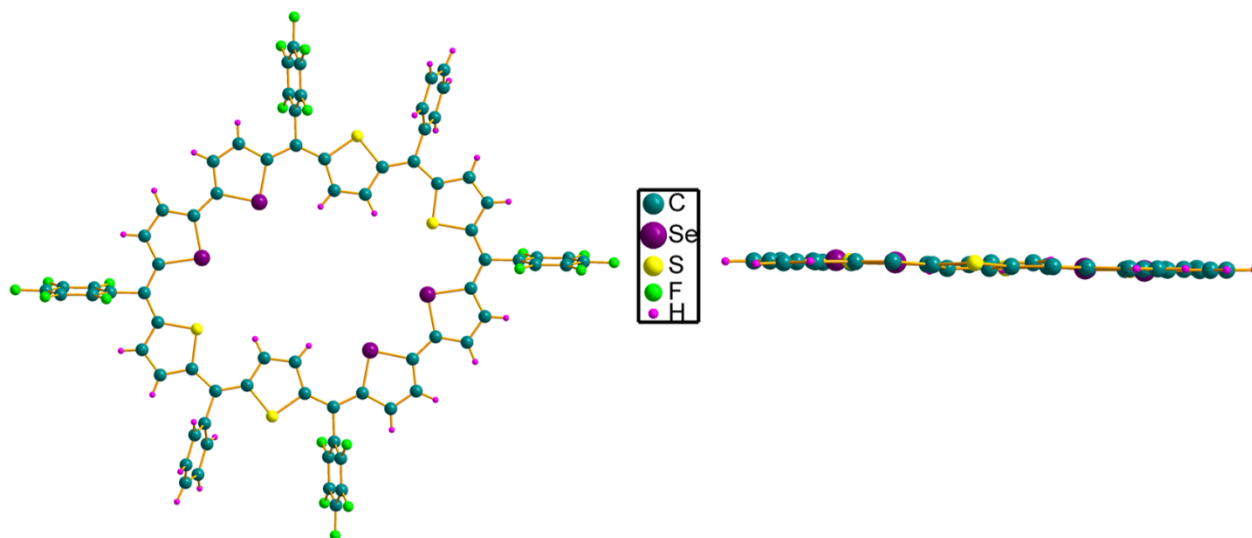
Figure-III.25: Top view (left) and side view (right) of molecular structure of. **III.16** (Meso-substituents from side view are omitted for clarity).
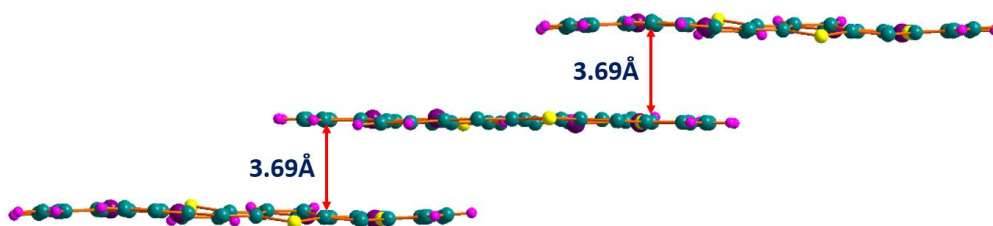
Figure-III.26: π-stacking of **III.16** phenyl groups and solvents are omitted for clarity.

All the four macrocycles, **III.12**, **III.14A, III.14B** and **III.16** represent isoelectronic 38π expanded isophlorins. However, they adopt different shapes depending on the nature of heterocyclic composition in the macrocycle. Accordingly, the strength of their aromatic character as estimated from NICS calculations was found to vary despite bearing the same number of π electron along the conjugated pathway. Hence, they form a unique of set of aromatic macrocycles to be explored for non-covalent interactions induced by electronic effects arising from π conjugation.

Part B

Additive Induced Conformational Polymorphism and Diradical Chemistry in Expanded Isophlorins

III.B.1. Additive induced conformational polymorphism in 38π Expanded Isophlorin

III.B.1. (a) Introduction

A 1:1 molecular complex between benzene and hexaflurobenzene was conceived in 1960, [61] by the electrostatic interaction between the two aromatic species. Molecular complex was established by neutron diffraction study, which showed π-π stacked interaction between alternate hexaflurobenzene and benzene (figure-III.27). The formation of such a molecular complex was explained based on the electronic environment of two aromatic rings. [61] The polarity of these aryl units complemented each other due to the strong electron withdrawing fluorines on the benzene ring. Hexaflurobenzene having six electrons withdrawing fluorines and having large positive quadruple moment $(31.7 \times 10^{-40} Cm^2)$ is in contrast to a benzene having large negative quadruple moment of $(-29.0 \times 10^{-40} Cm^2)$. The cooling curve of a mixture of two compounds displayed 1:1 complex formation that was attributed to charge transfer interaction between hexaflurobenzene and benzene. [62]
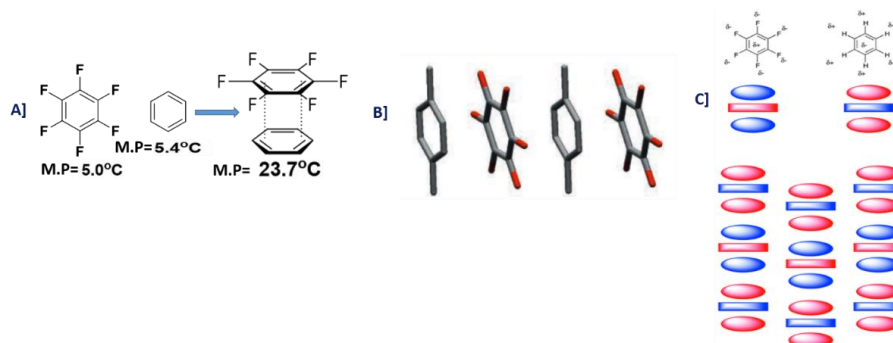
Figure-III.27: A] Molecular complex between benzene and hexaflurobenzene, B] molecular complex between hexaflurobenzene and methylated benzene, C] Schematic representation for quadrupole of benzene and hexaflurobenzene

Similarly, π-π stacked molecular complex between various other methylated derivatives of benzene and hexaflurobenzene [62] was determined by X-ray diffraction analysis. It is known that (4n+2)π systems are strongly stabilized by conjugation, resulting in bond equalization in the conjugation path. In contrast to that, Breslow coined antiaromatic destabilization energy for 4nπ systems resulting in bond alteration. In a previous study, it was established that the NICS value of several 4nπ antiaromatic macrocycles **III.17**, **III.18**, was almost opposite to octahthiaisophlorin **III.12**. Analogous to benzene/perflorobenzene combination, it can be speculated that formation of π-π stacked molecular complex can be realized between antiaromatic and aromatic macrocycles.

III.B.1 (b) Co-cyclization to study aromatic-antiaromatic interaction

With this hypothesis, an attempt was made to co-crystallize 1:1 mixture of octatiaisophlorin **III.12** with core modified hexaphyrin **III.17** in chloroform/methanol by solvent diffusion method. The charge transfer band expected for the molecular complex was not observed from UV-Vis spectroscopy. Upon crystallization, the morphology of crystals changed from a prismatic to needle shape suggesting the formation of 1:1 molecular complex. Single crystal X-ray diffraction analysis of the newly formed needle-shaped crystal revealed a serendipitous change in the conformation of **III.12**, from rectangular to almost square shape, **III.19,** with three thiophene ring inverting into the macrocyclic core. (scheme-III.5)
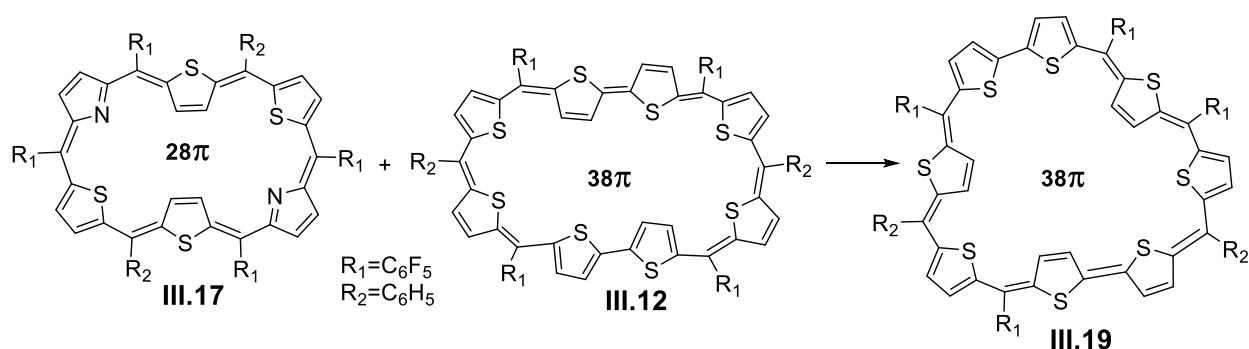
Scheme-**III.5**: Additive induced conformational change of **III.12** to **III.19.**

Estimated NICS value of -8.7 ppm, and clockwise orientation of arrows in AICD plot vindicated the retention aromaticity by **III.19**. Attempts to characterize this new polymorph in solution state went futile as this metastable state reverted back to **III.12** in solution state.

Single Crystal X-ray diffraction analysis of III.19:

Single crystal X-ray diffraction analysis of newly formed needle-shaped crystal for **III.19** revealed that molecule crystallized in a triclinic system with a P-1 space group. In this case, three thiophene rings preferred inverted ring structure into the macrocyclic core, and one of the inverted thiophenes slightly tilted from the mean plane (figure-III.28). This induced the macrocycle to adopt two different types of alternate π-π stacking interactions with a π-π inter planar stacking distance of 3.46Å and 3.75Å (figure-III.29).
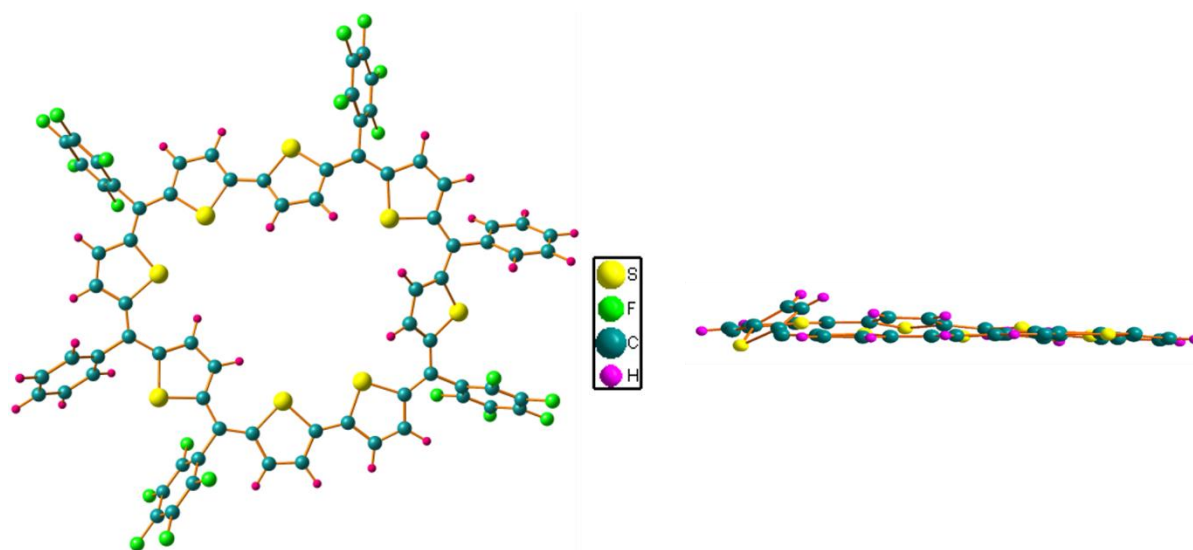
Figure-III.28: A] Molecular structure of. **III.19** lateral view B] side view.
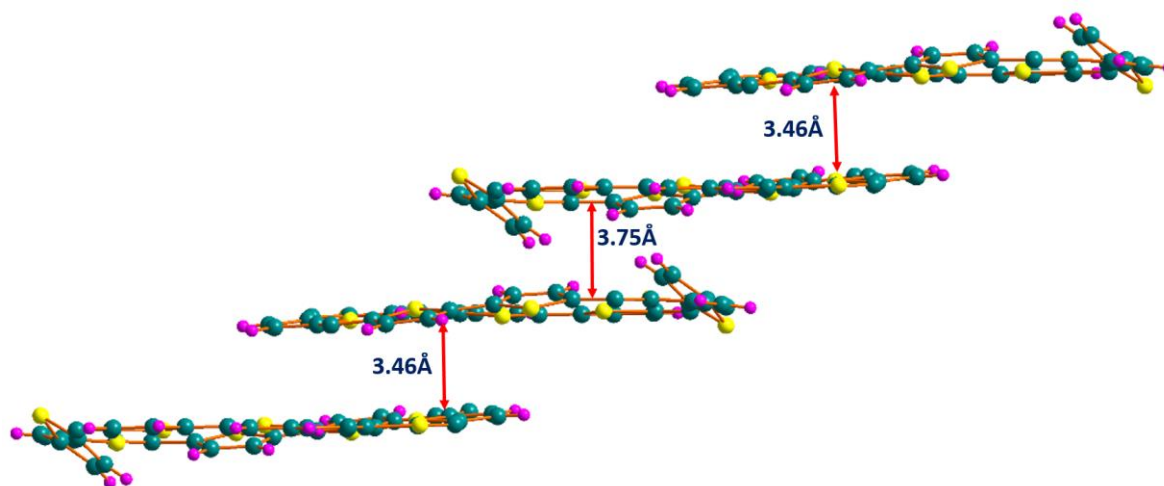
Figure-III.29: π-stacking of **III.16** phenyl groups and solvents are omitted for clarity.

III.B.1. (c) Co-cyclization to study aromatic-antiaromatic interaction with other macrocycles

Despite this unexpected result, further attempts were made to co-crystallize **III.12** with different anti-aromatic species. Therefore **III.12** was co-crystallized as a 1:1 mixture with ethylene bridged 32π antiaromatic isophlorin **III.18**, expecting the formation of molecular complex due to aromatic-antiaromatic interactions (scheme-III.6). However, neither conformational change similar to the previous case nor molecular complex was observed from the formed crystals. Rather both the macrocycles crystalized individually as their original conformers.
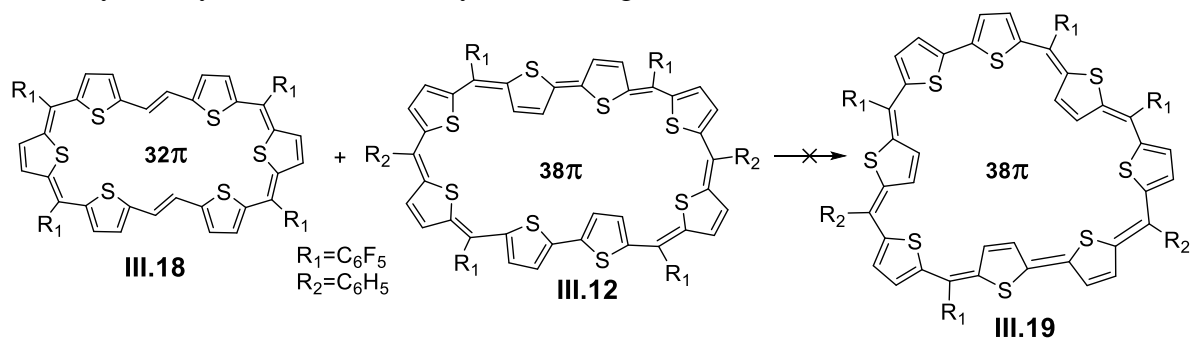
Scheme-III.6: Additive induced conformational change of **III.12** not observed with anti-aromatic **III.18.**

Even though earlier study implied that aromatic-antiaromatic interaction may be an important aspect for obtaining new polymorph, the inability of **III.18**, to induce any conformational change for **III.12** disproved the role of electronic effects in the crystallization process. Analogous to polymorphism of **III.12**, co-crystallization of 1:1 mixture of other 38π aromatic octaphyrin **III.14** and **III.16** was attempted with 28π hexaphyrin **III.17**. Yet, neither molecular complex nor conformational polymorph was observed between in the crystallized products. This observation further evinced that aromatic-antiaromatic interaction is not the only reason for the conformational polymorphism of **III.12** by using **III.17**. Structurally, both antiaromatic 28π core modified hexaphyrin **III.17** and the aromatic 38π octathiophene **III.12** adopt similar rectangular geometry. Such structural similarity in additives is known to induce changes to the parent molecule. This phenomenon is called as additive induced polymorphism, which was reported for a small group of organic molecule. [63] Desiraju and co-workers observed (figure-III.30) the change in space group of TNT from orthorhombic Pbca (centrosymmetric) to orthorhombic Pca2$_1$ (non-centrosymmetric) in the presence of structurally similar additive trisilane (TI).[40] Several other packing polymorphs

for ortho aminobenzoic acid in the presence of structurally similar benzoic acid has been explored.[41]
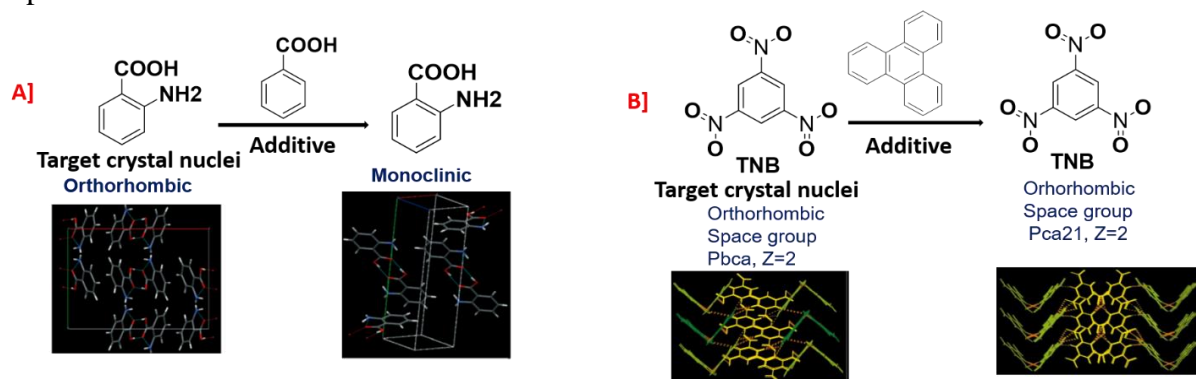
Figure-III.30: A] additive induced polymorphism of Ortho-amino benzoic acid, and B] additive induced polymorphism of trinitrobenzene (TNB).

III.B.1 (d) Co-crystallization with isostructural additives

To further study and correlate this interesting phenomenon of additive induced polymorphism, core-modified 30π hexaphyrins **III.20** and **III.21** were synthesized using a reported procedure. [51] These two molecules have structural similarities to the previously employed additive 28π hexaphyrin **III.16**. Therefore **III.12** was co-crystallized with 30π isophlorin **III.20** under similar conditions (scheme-III.7). A similar morphological change in the crystal shape was observed from diamond to needle shape in the product crystals. Singe crystal X-ray diffraction analysis of these needle revealed the earlier identifeid polymorphic form **III.19**. Encouraged by this observation, similar co-crystallization of **III.12** with nitrogen-containing core modified hexaphyrin **III.21** again lead to the formation of **III.19**. The observed results clearly demonstrated the role of additives in the induced conformational polymorphism for expanded isophlorins
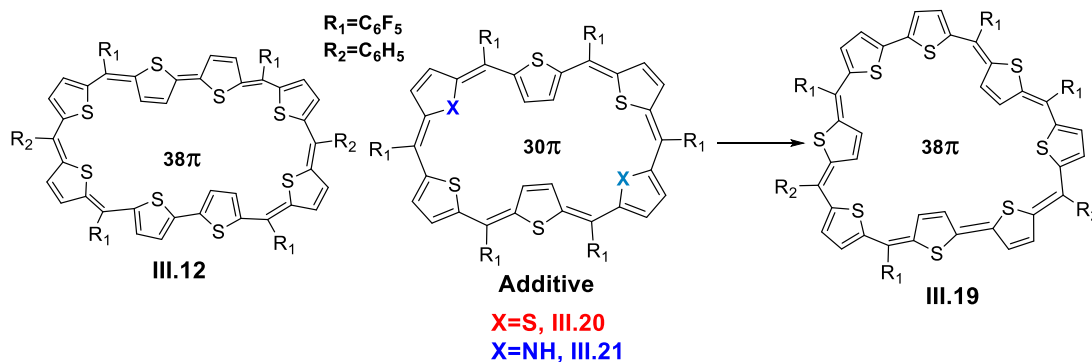
Scheme-III.7: additive induced a conformational change of **III.12** observed with aromatic core-modified hexaphyrin **III.20 and III.21** as an additive

To the best of knowledge, such type of conformational change due to external additive has not been reported for any porphyrinoid till date. Later, co-crystallization of **III.12** was attempted by varying the ratio of additive **III.20** from 1:1 to 1:0.25, it was noticed that 1: 0.25 ratio of target macrocycle to additive also induced conformational change to the parent **III.12**.

Quantum mechanical calculations: The aromatic character of 38π expanded isophlorins was further confirmed by Nucleus Independent Chemical Shift (NICS) calculations at global ring centers. All the macrocycles displayed negative NICS values ranging between - 8 to -19 ppm. The computed molecular orbital energy levels indicated relative stabilization of HOMO and LUMO in all the molecules due to aromatization (Table-III.1).

Macrocycle	NICS value in ppm	AICD	Aromaticity	HOMO-LUMO
III.12	-15.19	Clockwise	Aromatic	0.34
III.14	-18.23	Clockwise	Aromatic	0.57
III.16	-14.68	Clockwise	Aromatic	0.50
III.19	-8.80	Clockwise	Aromatic	0.55

(**Table-III.1**). Estimated NICS and HOMO-MUMO energy difference for 38πexpanded isophlorins.

III.B.2] 38π aromatic expanded isophlorins at the crossroads of diradical chemistry

III.B.2 (a) Introduction

As discussed in the first chapter, expanded porphyrins with an effective cyclic π conjugation pathway could be a good platform to obtain stable organic radical species. Due to the inherent low aromaticity, thiophene could be employed as an excellent platform for generating π conjugated systems.[44] Quinoidal polythiophenes are known to exist in aromatic diradical states. The first reference for the existence of Kekule diradical on thienoquinoid was reported by Huguchi et al. from their studies on tetracyano quinoidal tetra thiophenes with different substituents.[64] Takimiya et al. synthesized tetracycnoquinodimethane quinoidal oligothiophene ranging from monomer to hexamer (Scheme-III.8).[65] The existence of magnetically active centers was proven through ESR spectroscopy. Jishan Wu and co-corkers explored the diradical character of thiophene based expanded porphycene.[43] The main driving force for the appearance of diradical character was attributed to the presence of a quinoidal bithiophene. It regains its aromaticity and attains a benzenoid form, which ultimately leads to the formation of stable diradical species.

III.22A   **III.22B**
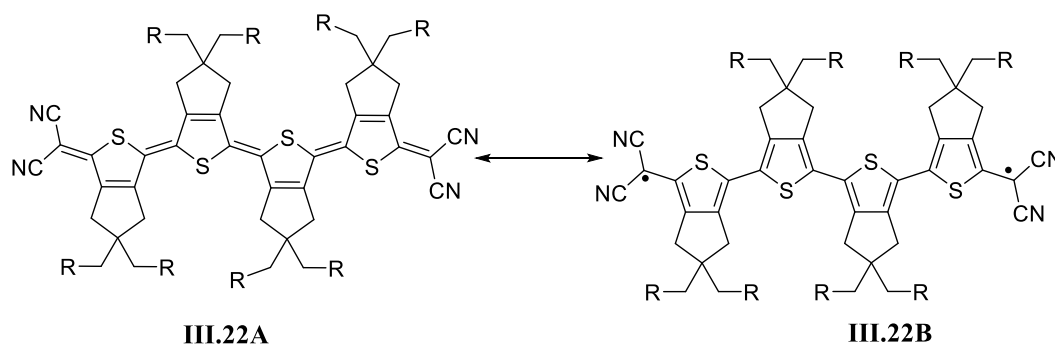
Scheme-III.8: Illustrative example chemical structure for teracyano-substituted quinoidal oligothiophene

III.B.2 (b) Experimental diradical studies for III.12

Earlier part of this chapter, described the conformational dynamics and additive induced conformation polymorphism of 38π aromatic expanded isophlorins. ^{1}H NMR spectral analysis of **III.12** at room temperature did not display signals for macrocyclic protons.

The presence of quinoidal bithiophene into the macrocyclic core inspired to investigate the diradical properties of **III.12**. At room temperature, this quinoidal bithiophene could be favored to convert into benzenoid form by the recovery of its aromaticity, which might have contributed to the generation of NMR inactive diradical species. This diradical was further unambiguously confirmed with ESR studies. **III.12** displayed a featureless broad ESR signal in support of paramagnetic species. This can be attributed to a resonance structure in which the thiophenes adopt a benzenoid form (scheme-III.9) leading to the formation of diradical species. Due to the cyclic conjugation, the generated unpaired electrons will be delocalized through the π bonds of octathiophene **III.12**
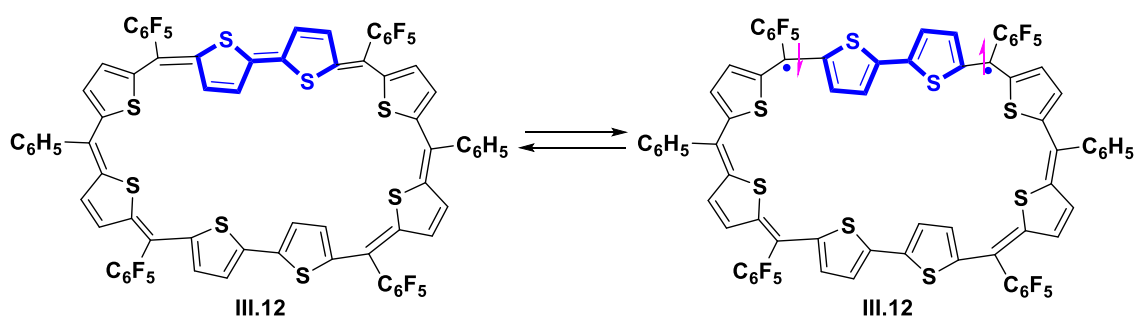
Scheme-III.9: Illustrative representation for diradical generation of **III.12**.

A *g* value observed at 2.006 for **III.12** corresponds to an organic free radical at room temperature in a solid state (figure-III.31A). The intensity of this ESR signal was found to decrease with lowering in temperature in support of open-shell singlet diradical nature for **III.12**. Superconducting quantum interface device (SQUID) measurement of the solid sample showed that the product of molar magnetic susceptibility ($\chi_M.T$) and temperature (T) of **III.12** gradually increased with increasing temperature (figure-III.31B) confirming the anti-ferromagnetic coupling of the two unpaired electrons.
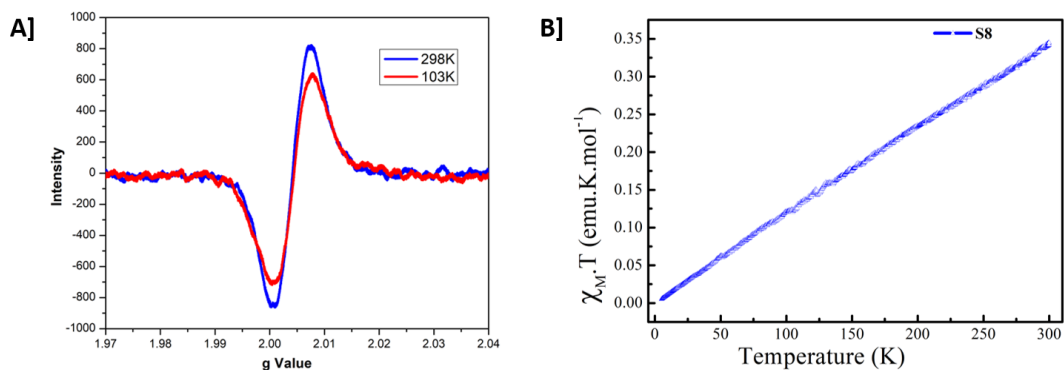
Figure-III.31: A] Variable temperature ESR spectra for **III.12** Blue line (298K), red line (103K) in solid-state **B]** SQUID measurement for **III.12** (product of molar magnetic susceptibility Vs. temperature).

The diradical character of **III.12** was supported by density functional theory (DFT) using a broken symmetry approach. Singlet-triplet energy gap for **III.12** was calculated using unrestricted UCAM B3LYP/631G (d), which was found to be -4.59 kcal/mol and the percentage diradical character value of 41.84% was estimated using natural orbital occupation number (NOON).[66] Spin density calculation suggested delocalized electron spin density distribution over the entire molecule.
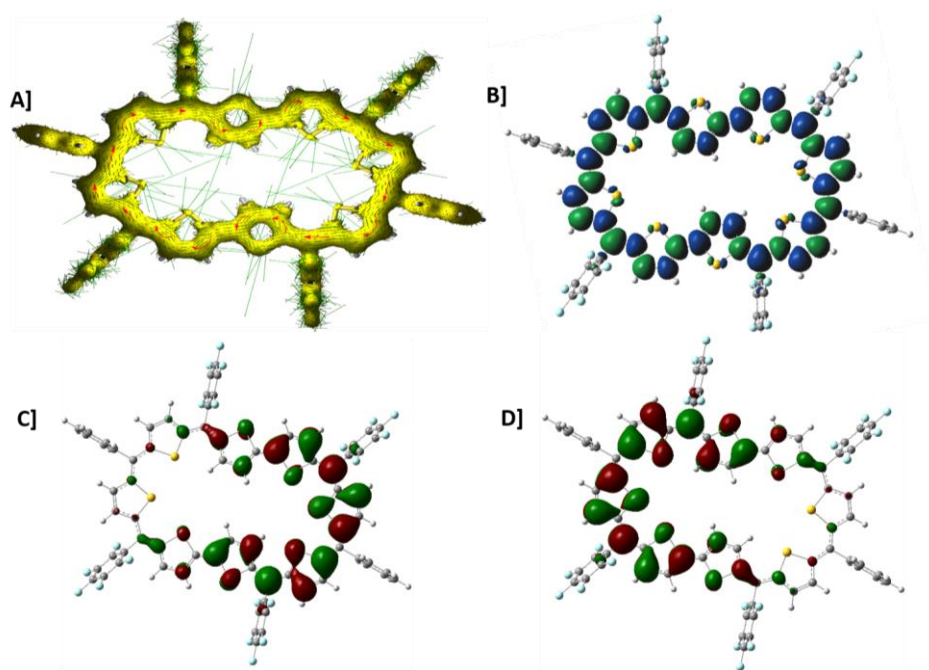
Figure-III.32: Calculated UCAM-B3LYP/631G (d) **A]** ACID plot **III.12** at iso value 0.005, the external magnetic field applied orthogonal to the plane of the macrocycle. **B]** Spin density distribution diagram C] and D] frontier molecular orbital for α and β electrons. Frontier molecular orbital profile revealed both α and β electrons occupied different parts of space over the macrocycle (figure-III.32).

III.B.2 (c) Diradical studies for III.14 and III.16

The unexpected finding of the diradical behavior for **III.12** was extended to understand the effect of introducing selenophene and furan rings on the percentage of diradical character in the isoelectronic 38π octaphyrins. Variable temperature EPR spectrum for **III.14** and **III.16** was recorded in the solid state; in both cases, it displayed EPR signal at g = 2.006, and the intensity of this signal decreased with a decrease in temperature. Observed EPR spectra are inconsistent with variable temperature ^{1}H NMR spectra. Diradical character was further supported from DFT broken symmetry approach UCAM B3LYP/631G (d). The estimated singlet-triplet energy gap for **III.14** and **III.16** was found to be -5.3 kcal/mol and -5.5kcal/mol, respectively. The percentage diradical character for selenophene derivative **III.14** was 30.55% with delocalized spin density distributed over the entire macrocycle. A clockwise orientation of arrows in the ACID plot further reiterated the aromatic characteristic of this macrocycle (figure-III.33). Whereas, the furan derivative **III.16** displayed 24% diradical character with global spin density distribution along with the clockwise orientation of arrows in the ACID plot (figure-III.34).
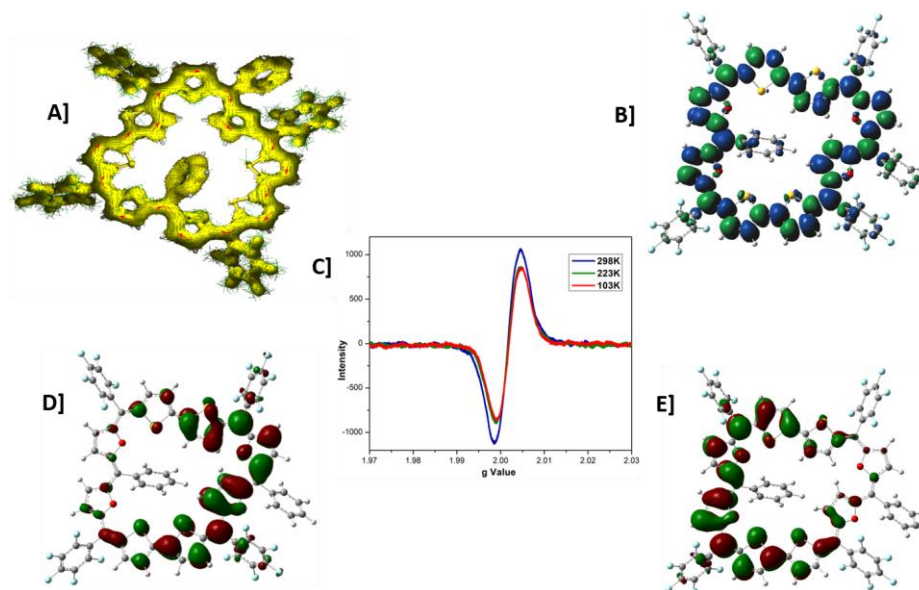
Figure-III.33: Calculated UCAM-B3LYP/631G (d) **A]** ACID plot **III.14** at iso value 0.005, the external magnetic field applied orthogonal to the plane of the macrocycle. **B]** Spin density distribution diagram **C]** frontier molecular orbital profiles for α and β electrons **C]** SOMO-α, **D]** SOMO-β for **III.14**, E] VT-EPR spectra for **III.14.**
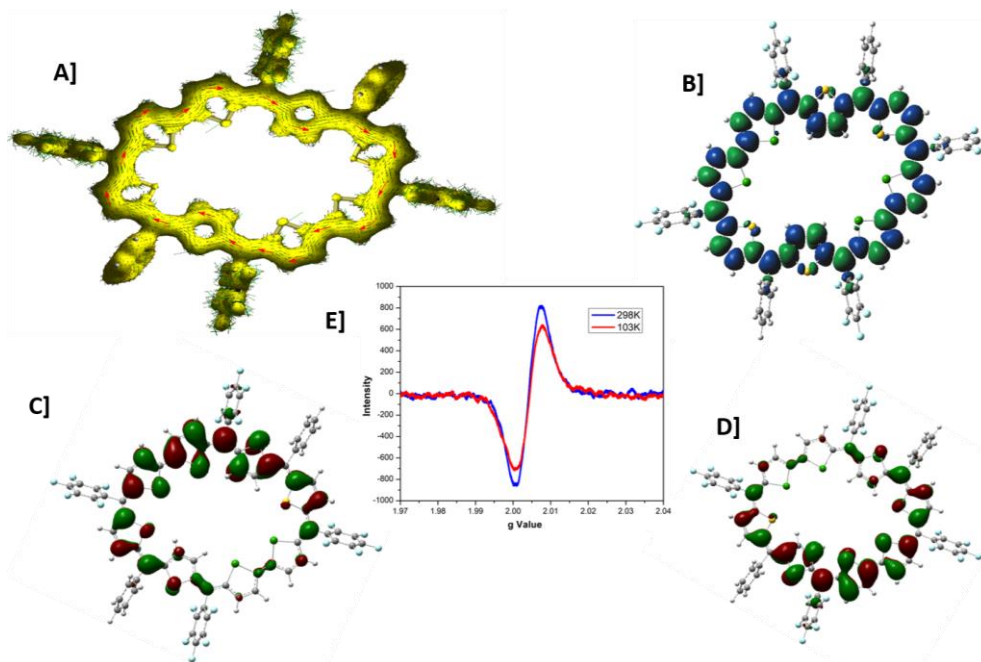
Figure-III.34: Calculated UCAM-B3LYP/631G (d) **A]** ACID plot **III.16** at iso value 0.005, the external magnetic field applied orthogonal to the plane of the macrocycle. **B]** Spin density distribution diagram **C]** frontier molecular orbital profiles for α and β electrons **D]** SOMO-α, **E]** SOMO-β for **III.16**, **C]** VT-EPR spectra for **III.16**

Conclusions:

In summary, this chapter describes three different structurally variants of 38π expanded isophlorins, which shows heterocyclic ring inversions to achieve planarity to the macrocycles. The number of ring inversions vary with the nature of heterocycle used. Also, we have discovered first example of additive induced polymorphism for porphyrinoids. Even though expanded porphyrinoids are known to alter their geometry between planar and non-planar topologies, this is the first example of inter-conversion between two different planar structures for the same macrocycle. Such structural modifications are perhaps impossible through a rational synthetic design. However, polymorphism offers a plausible route for such post-synthetic structural engineering and can unlock many unexpected molecular structures of these fascinating π-conjugated macrocycles. Due to the presence of quinoidal oligothiophene and oligoselenophene these macrocycles are identified as open shell singlet diradicals at room temperature.

Experimental Section:

General synthesis Procedures:

III.12:A flame-dried 250-mL two neck round-bottomed flask was charged with bithiophene **III.11**and(128mg,0.77mmol),and((phenylmethylene)bis(thiophene5,2diyl))bis((perfluorophenyl) methanol **III.10** (500mg, 0.77mmol) in 200 ml of freshly distilled anhydrous dichloromethane under an nitrogen atmosphere and degassed with nitrogen for further ten minutes. BF3.OEt2 (109.42 ml, 0.77mmol) was added under dark using a syringe, and the resulting solution was stirred for one hour under an inert atmosphere. After adding DDQ (700 mg, 3.085mmol), the solution was opened to air and stirred for one more hour. Few drops of Triethylamine were added, and the reaction mixture was concentrated under reduced pressure. Purification through basic alumina column chromatography by using CH_2Cl_2/hexane as eluent gave desired macrocycle **III.12** as purple-colored band in 28% yield.

HR-MS (ESI-TOF): m/z =1549.9462 (found), 1549.9481(calcd. For $C_{74}H_{26}F_{20}S_8$).

UV-Vis (CH_2Cl_2): λ_{max} (ε) L mol-1 cm^{-1} = 442nm (40000), 579(130000), 709 (20000), 759 (20000). **NMR Data:** ^{1}H NMR: (400 MHz, CDCl$_3$, 253K) δ 8.34 (d, J=4.8 Hz, 2H), 7.76 (m, 4H), 7.65 (m, 6H), 7.57 (d, J=6.4 Hz, 2H), 7.39 (d, J=4.4 Hz 2H), 7.36 (d, J=5.6 Hz 2H), 6.53 (br singlet, 2H), 6.20 (br singlet, 2H), 5.08 (br singlet, 4H).

Crystal data: $C_{74} H_{26} F_{20} S_8$, (C H Cl$_3$) (Mr 1790.16), triclinic, space group *P -1, a =*

10.027(2), *b* = 11.878(3), *c* = 15.510(4) Å, α=82.520(5) , β=89.893(6), γ=73.429(5).

V = 1754.1(7) Å3, *Z* = 1, *T* =100(2) K, D$_{calcd}$ = 1.695cm^{-3}, R$_1$ = 0.0518 (5512), *R*$_w$ (all data) = 0.1530(7367), GOF = 1.063.

III.14A: Bithiophene **III.11** ((150mg, 0.90mmol)) and difuryl diol **III.13** ((556mg, 0.90 mmol)) were reacted in presence of BF$_3$.OEt$_3$ as described above to yield **III.14** in ％16 yield.

HR-MS (ESI-TOF): *m/z*=1486.0381 (found), Calculated for ($C_{74}H_{26}F_{20}O_4S_4$); (1486.0395)

UV-Vis (CH_2Cl_2): λ_{max} nm (ε, Lmol^{-1}cm^{-1}): 593 (130000). 551 (80000).

^{1}**H NMR** (400 MHz, Acetone-d_6, 193K) δ: 9.45 (d, J=5.2 Hz, 1H), 9.34 (d, J=5.6 Hz, 1H), 9.24 (d, J=5.2, 1H), 9.06 (d, J=3.6, 1H), 8.61 (d, J=3.6 Hz, 1H), 8.49 (d, J=4.8 Hz, 1H), 8.41 (d, J=4.4

Hz, 1H), 8.25 (d, *br singlet*, 2H).), 8.19 (d, *J*=5.2 Hz, 1H),), 8.13 (d, *J*=2.8 Hz, 1H),), 7.98 (br singlet, , 2H),), 7.69 (br singlet, 3H),), 5.34 (m, 2H),), 5.03 (m, 3H),), 4.34 (br singlet, , 1H), 4.15 (br singlet, 1H),), 3.87 (br singlet, 1H),), 3.37 (br singlet,1H).

Crystal data $C_{74}H_{26}F_{20}O_4S_4$, 3(CHCl3), (*1845.29*), Triclinic, space group *P-1*, *a=13.895(6 b=15.646(7)*, *c=17.908(8)* Å, α = 106.334(10), *β = 94.553(10)*, γ = 100.806(11); *V* = 3634(3)Å3, *Z* = 2, *T* = 100(2) K , D_{calcd} = 1.686g cm^{-3}, R_1 = 0.1099(6543) , R_w (all data) = .3064(18136), GOF = 1.142.

III.14B: dithionyl dicarbinol **III.11** ((0.5g, 0.90mmol)**)** and bifuran **III.11b** ((0.100g, 0.90 mmol)) were reacted in presence of BF$_3$.OEt$_3$ as described above to yield **III.14B** in %2 yield.

HR-MS (ESI-TOF): *m/z*=1486.0381 (found), Calculated for ($C_{74}H_{26}F_{20}O_4S_4$); (1486.0395).

UV-Vis (CH$_2$Cl$_2$): λ$_{max}$ nm (ε, Lmol^{-1}cm^{-1}): 737 (84000), 508 (3600), 371(5100).

^{1}H NMR (400 MHz, Acetone-*d₆*, 233K) *δ*: 7.72 (d, *J*=4.4 Hz, 2H), 7.70 (d, *J*=4.4 Hz, 2H), 7.5-7.4 (br signal, 6H), 7.31 (d, J=5.2, 2H), 7.20 (d, *J*=4.8 Hz, 2H), 6.82 (br signal, 4H), 6.81 (d, *J*=4.4 Hz, 2H), 6.47 (d, *J*=5.2 Hz, 2H), 5.84 (d, *J*=5.2 Hz, 2H), (d, *J*=5.5 Hz, 2H).

Crystal data $C_{74}H_{26}F_{20}O_4S_4$, 3(CHCl3), (*1467.19*), Monoclinic, space group *C 2/c*, *a=25.991(3) b=28.344(4)*, *c=11.977(15)* Å, α = 90, *β = 113.851(3)*, γ = 90; *V* = 8051.2(18)Å3, *Z* = 4, *T* = 100(2) K , D_{calcd} = 1.224g cm^{-3}, R_1 = 0.0734(3703) , R_w (all data) = 0.1906(10149), GOF = 1.009.

III.16: Biselenophene **III.15** ((150mg, 0.57mmol)**)** and bithionyl diole **III.10** (374.07mg, 0.57 mmol) were reacted in presence of BF$_3$.OEt$_3$ as described above to yield **III.10** in 15% yield.

UV-Vis: (CH$_2$Cl$_2$): λ$_{max}$ nm (ε, Lmol^{-1}cm^{-1}): 451nm (2800). 579 (105000), 689(19000).
^{1}H NMR ^{1}H NMR (400 MHz, CD$_2$Cl$_2$-*d₆*, 253K) *δ*: 8.32 (d, *J*=5.2 Hz, 2H), 7.62-7.58 (m, 10H), 7.50 (d, J=2.8, 2H), 7.38 (d, J=5.2, 2H), 7.26 (d, *J*=4.4 Hz, 2H), 7.02 (br singlet, *J*=4.8 Hz, 4H), 5.69 (br singlet, 2H),), 5.58(br singlet, 2H).

Crystal Data: $C_{74} H_{26} F_{20} S_4 Se_4$, 3(C$_6H_6$), , Triclinic, space group *P-1*, *a=10.414(4 b=12.018(4)*, *c=19.688(7)* Å, α = 100.211(10), *β = 103.059(8)*, γ = 106.497(7); *V = 2223.3(14)*Å3, *Z* = 1, *T* = 100(2) K , D_{calcd} = 1.532g cm^{-3}, R_1 = 0.0959(6766) , R_w (all data) = 0.2895(10968), GOF = 1.65.

Crystal Data for III.19: Crystal data: $C_{74}H_{26}F_{20}S_8$, $3(C\ H\ Cl_3)$ (*M*r 1944.98), triclinic, space group *P -1, a =* 13.811(5), *b=17.187(6), c = 19.032(6),* α = 63.255(5), β = 79.509(6), γ = 79.031(6). *V* = 3937(2) Å3, *Z* = 2, *T* =100(2) K, Dcalcd = 1.641cm^{-3}, R$_1$ = 0.1142(6894), *R*w (all data) = 0.3159(19579), GOF = S = 1.167.

Chapter 4

Synthesis and redox chemistry of benzene Appended Isophlorins

Part A

IV.A Synthesis and redox chemistry of benzene and biphenyl appended isophlorins

IV.A.1: Introduction:

After the discovery of N-confused porphyrins[2], a variety of carbaporphyrinoid systems have been synthesized and investigated. By replacing a pyrrole unit within the porphyrin framework with cyclopentadiene, indene, cycloheptatriene, benzene, or azulene produced a new class of porphyrin like macrocycles having a carbon atom inside the macrocyclic core.[67] This kind of porphyrins are also called as Carbaporphyrins.[67] The presence of benzene or azulene alters the aromaticity of π conjugated macrocycles and prefer to adopt localized electron density. For example, cycloparaphenylenes (figure IV.A.1) have [4n] π-electrons in their circumferential conjugation path, yet are non-aromatic in their electronically neutral ground states.[68] Two electron oxidation of cycloparaphenylene yielded a dication that exhibited global aromaticity corresponding to $(4n+2)\pi$ electrons.[68] Incorporation of more than one benzene units into 30π expanded isophlorin has been studied earlier.[79] This macrocycle could achieve global aromaticity only when one of the phenylenes rings compromises with its aromaticity and adopt the quinoidal form.[69] Similarly, a very recent report on macrocycle containing alternate paraquinodimethane and triphenylamine units displayed annulene like anti-aromaticity at low temperature due to structural rigidity and participation of bridging nitrogen electrons. Its dication displayed global aromaticity for 30π electrons, with open-shell singlet diradical nature.[70]
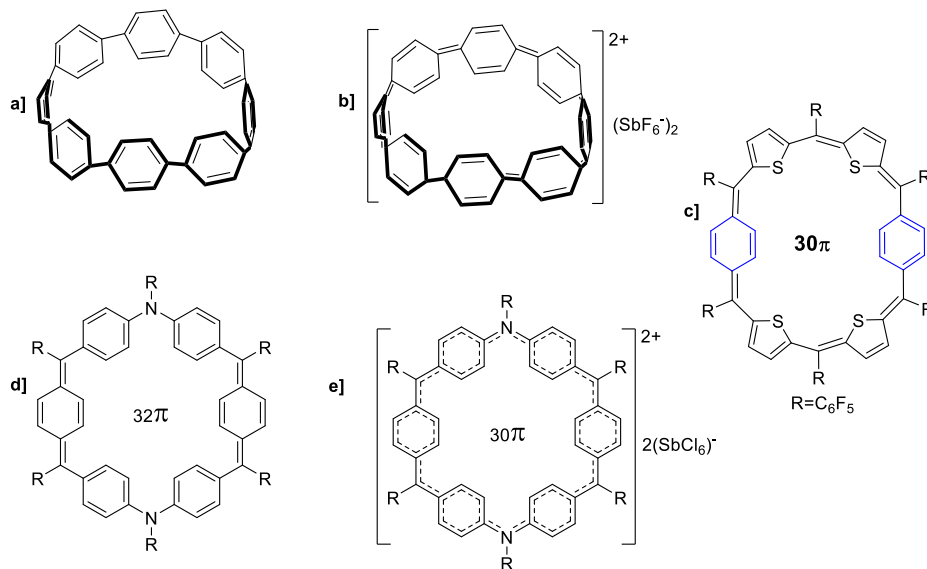
Figure-IV.A.1: Illustrative example for local and global aromatic macrocycles

Incorporation of the pro-aromatic unit such as *p*-quinodimethane (p-QDM) into expanded porphyrin/isophlorin framework may lead to the formation of the stable compound with distinctive diradical character (Scheme-IV.A.1). [44] Therefore, it was decided to introduce this pro-aromatic spacer into thiophene containing macrocycles.
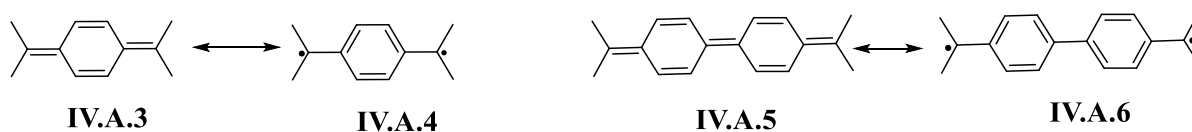
Scheme-IV.A.1: Schematic representation for the generation of diradical by regaining of aromaticity.

IV.A.2: Synthesis and characterization of benzo-Isophlorin IV.A.8

A simple and straightforward methodology of oxidative coupling was employed for the synthesis of benzo-isophlorin. A stoichiometric excess of anhydrous FeCl$_3$ was added to the solution of benzotrithiophene under dark and the reaction mixture was stirred for 1hr (scheme-IV.A.2). The formation of the expected macrocycle was confirmed from MALDI-TOF/TOF mass spectrometric analysis of the reaction mixture. The desired macrocycle was purified from the reaction mixture

through basic alumina column chromatography to give the benzoisophlorin **IV.A.8** as an orange-colored band in 6% yields.
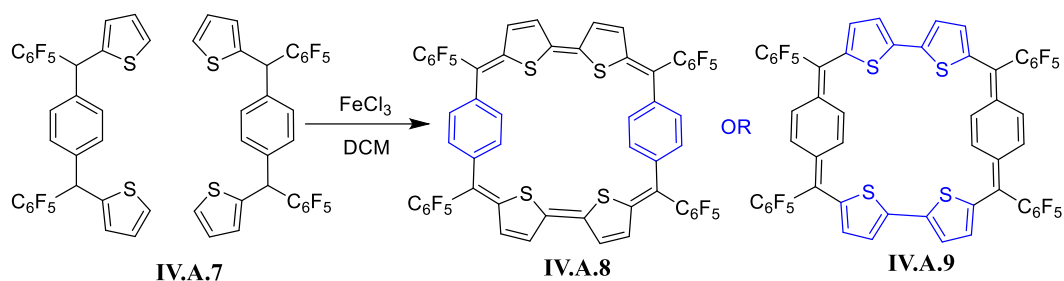
Scheme-IV.A.2: Synthesis of benzoisophlorin

There are two resonance structures to represent the chemical structure for benzoisophlorin. In the first case, **IV.A.8**, both the benzene rings retain their aromaticity, and all four thiophene lose their aromaticity upon converting to quinoidal form. In contrast, in another case, **IV.A.9**, benzene ring exists in quinoidal form, and all four thiophenes retain its aromaticity. The aromaticity of benzene is relatively higher in comparison to thiophene; therefore, structure **IV.8** is expected to be energetically more favorable.

IV.A.3 HRMS and Electronic absorption studies for IV.A.8:
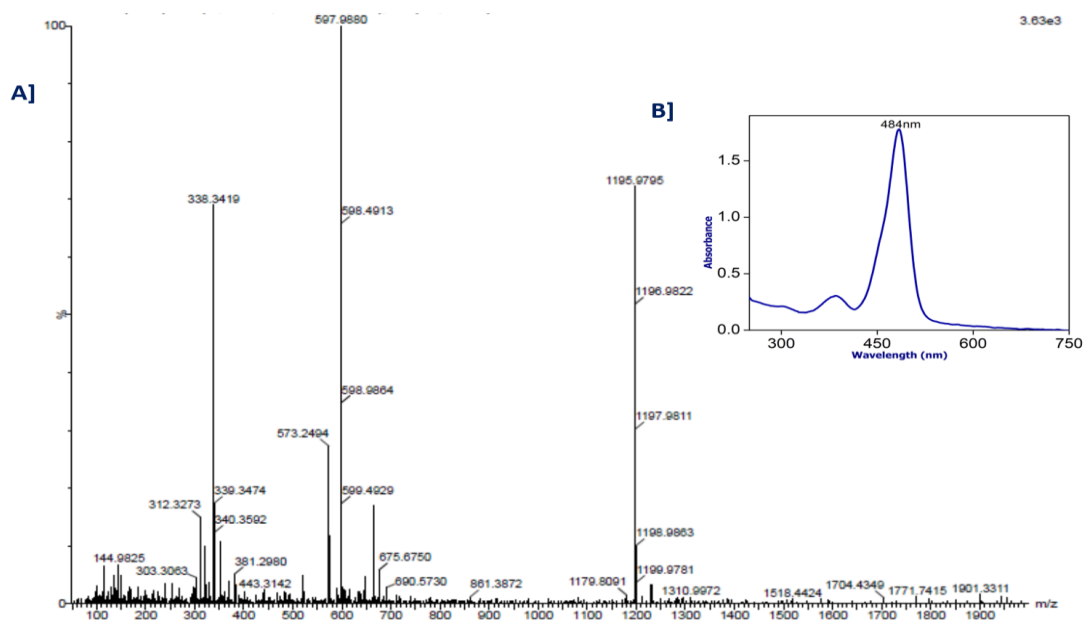
Figure IV.A.2: A] HRMS spectrum of **IV.A.8**, B] UV -Vis absorption spectrum of [10^{-6}M] **IV.A.8** in CH$_2$Cl$_2$.

115

High resolution mass spectrometric analysis displayed m/z at 1195.9795 corresponding to the exact mass of **IV.A.8**. Due to its conjugation it displayed absorption maxima at 484 nm in its UV-Vis absorption spectrum (figure-IV.A.2).

IV.A.4: ^{1}H NMR studies IV.A.8:

^{1}H NMR spectrum (figure-IV.A.3) of **IV.A.8** recorded in THF-*d8* at 298K displayed two well-resolved doublets for the β-protons of thiophene at δ 6.97 and 6.29 ppm. A singlet corresponding to four protons for benzene ring was observed at δ 7.88 ppm. The absence of a paratropic shift in the observed ^{1}H NMR spectrum suggested the resonance structure **IV.A.8,** where both the benzene rings retain their aromaticity and neglect possibility for the chemical structure of **IV.A.9**. ^{1}H-^{1}H COSY spectrum (figure-IV.A.4) recorded at 298K showed one correlation between protons for thiophene at (i) 6.97 and 9.29 ppm.
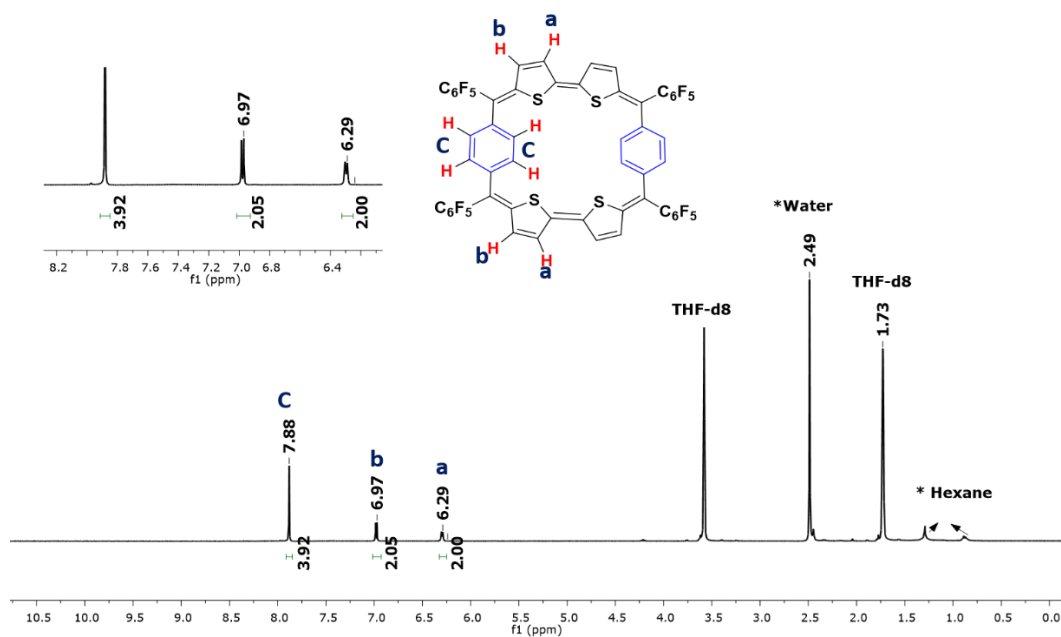
Figure-IV.A.3: ^{1}H-NMR spectrum of **IV.A.8** at 298K in THF-*d8.*

116
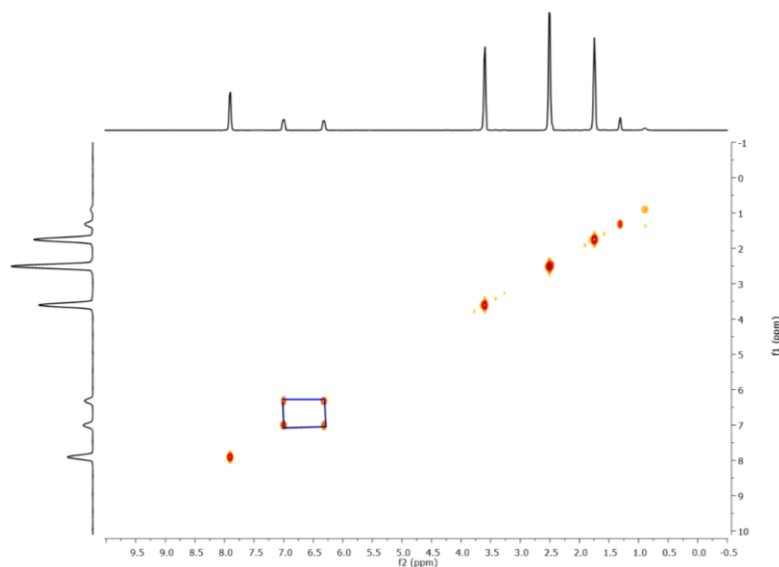
Figure-IV.A.4: ^{1}H-^{1}H COSY spectrum of **IV.A.8** at 298K inTHF-d_8

IV.A.5: Single Crystal X-ray diffraction analysis of IV.A.8:

Further, structural confirmation for **IV.A.8** was obtained by single-crystal X-ray diffraction analysis. Good quality single crystals were grown by diffusion of vapors of methanol into a solution of **IV.A.8** in tetrahydrofuran (THF). The obtained molecular structure revealed a near planar conformation (figure-IV.A.5) for **IV.A.8** with both the phenylene rings tilted away from mean macrocyclic plane by 45°.79. This structure is found to be in support of ^{1}H NMR spectrum for benzenoid nature of phenylene rings. Further, in the crystal packing of **IV.A.8**, strong C-F non-covalent interactions with a distance of 3.07 Å was observed, which is responsible for weak π-π stacked supramolecular architecture of **IV.A.8**. The estimated NICS value of 0.07ppm confirmed the non-antiaromatic characteristics for **IV.A.8** in addtional support fort the observed ^{1}H NMR spectrum.
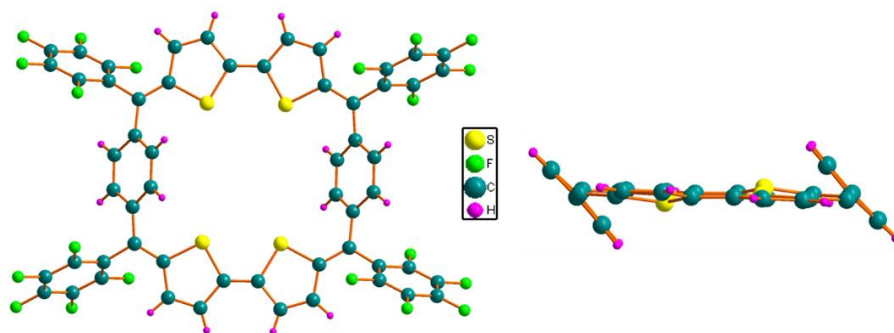
Figure-IV.A.5: Top view (left) and side view (right) of molecular structure for **IV.A.8**.

IV.A.6: Redox chemistry of IV.A.8:

Cyclic Voltamogram of **IV.A.8** (figure-IV.A.6) recorded in dichloromethane displayed two reduction waves at -1.67 and -0.76 V. It also displayed two oxidation waves centered at 0.91 and 1.77 V. Observation of two oxidation waves implied an opportunity to investigate the two-electron oxidation of $[4n]\pi$ macrocycle to its corresponding dication. Meerwein salt is known to be a very efficient one-electron oxidizing agent (scheme-IV.A.3) for π conjugated organic molecule. [52]

IV.A.10 **IV.A.11**
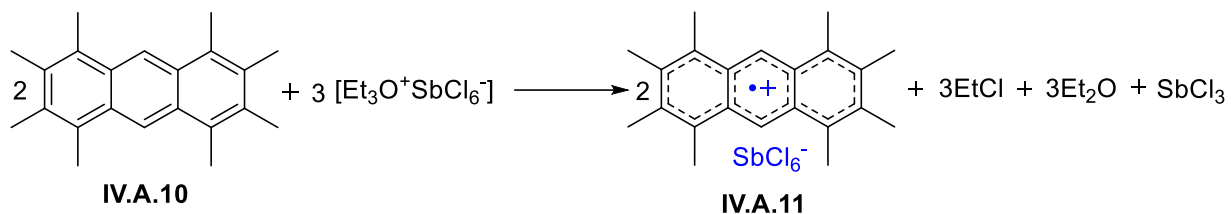
Scheme -IV.A.3: Illustrative example of oxidation with Meerwein salt
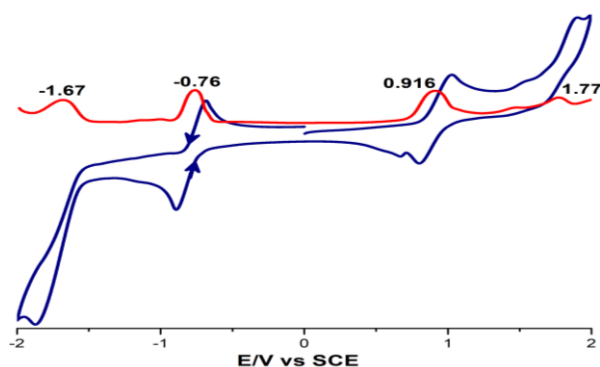
Figure -IV.A.6: Synthesis of benzoisophlorin**:** Cyclic (Blue) and Differential pulse (red) voltammograms of **IV.A.8** in dichloromethane containing 0.1M tetrabutylammonium perchlorate as the supporting electrolyte recorded at 50 mVs^{-1}.

118

IV.A.7: Synthesis and Electronic absorption studies of IV.A.12:
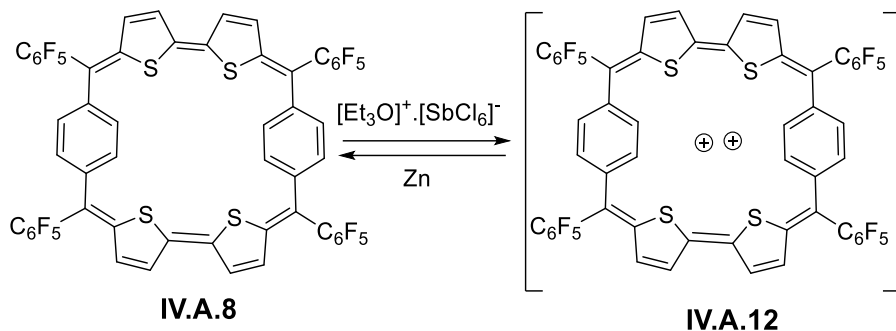
Scheme -IV.A.4: Two-electron oxidation of benzoisophlorin by Meerwein salt

Addition of Meerwein salt to **IV.A.8** in dry dichloromethane resulted in a vivid color change from orange to dark pink. UV-Vis absorption spectrum (figure-IV.A.7) showed a red-shifted absorption band of **IV.A.8** from 484 nm to a more intense absorption at 580 nm. An additional red-shifted broad absorption band was observed at 986 nm. Such huge redshift in absorption is generally expected for the formation of radical species.
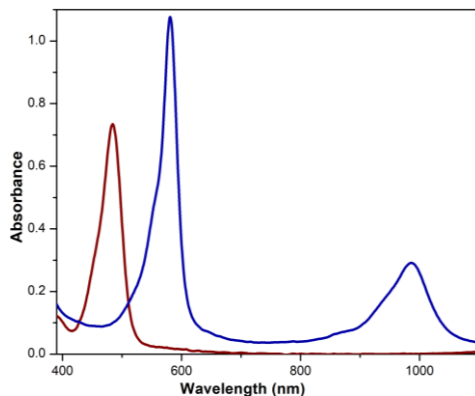
Figure-IV.A.7: Absorption changes observed to the solution of **IV.A.8** (wine red) upon addition of Meerwein salt to **IV.A.12** (blue).

IV.A.8: HRMS and NMR studies of IV.A.12

High resolution mass spectrometric (HRMS) analysis of **IV.A.12** displayed m/z at 597.9948, which exactly matches the m/2 mass of **IV.A.8**, to confirm the formation of dicationic species. ^{1}H NMR spectrum recorded in acetonitrile at room temperature did not show any signals corresponding to macrocycle. The absence of signals in its ^{1}H NMR spectrum could be due to the presence of open-shell singlet diradical as a ground electronic state for **IV.A.12**. As described

119

earlier, one of the benzene rings from **IV.A.8** would prefer to regain its aromaticity and generate a diradical of dicationic species (scheme-IV.A.5).
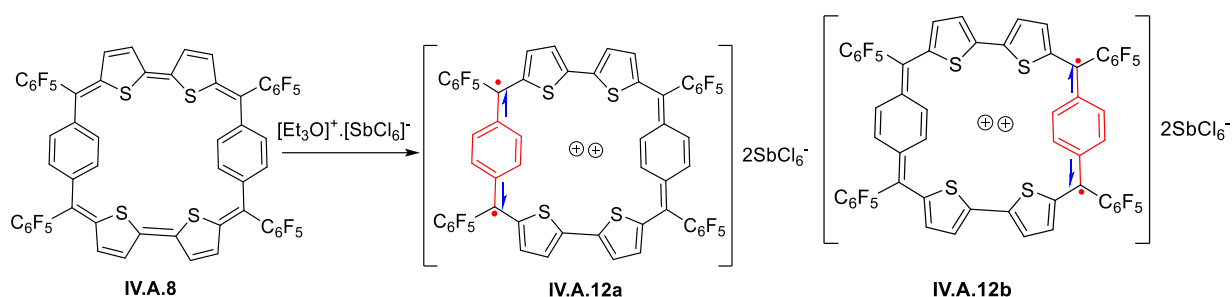
Scheme-IV.A.5: Possible resonance structures for diradical dication of **IV.12**.

A diradical can exist either in singlet or triplet state depending on the spin orientation of the two unpaired electrons (figure-IV.A.8). If the spin of two electrons is parallel, it accounts for a triplet diradical. On the other hand, if two unpaired electrons are located in two different orbitals with opposite orientation it accounts for a spin multiplicity of one called as singlet diradical. Upon lowering the temperature two unpaired electrons from singlet diradical get paired up to yield a diamagnetic species. Variable temperature ^{1}H NMR spectra of **IV.A.12** recorded in acetonitrile displayed broad signals for all protons corresponding to macrocycle were identified at 238K (figure-IV.A.9).
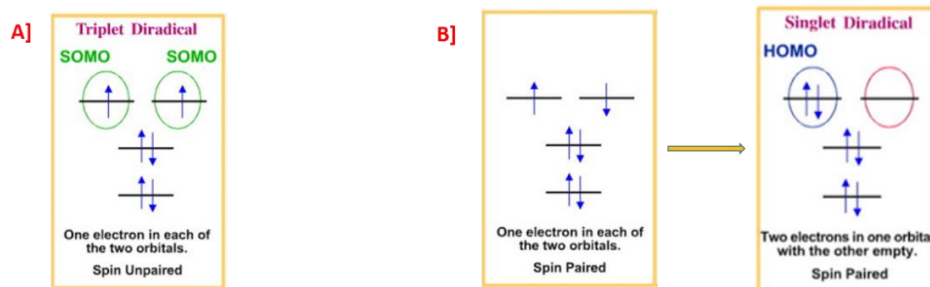
Figure -IV.A.8: A] representation of triplet diradical B] spin pairing of singlet diradical with lowering in temperature.
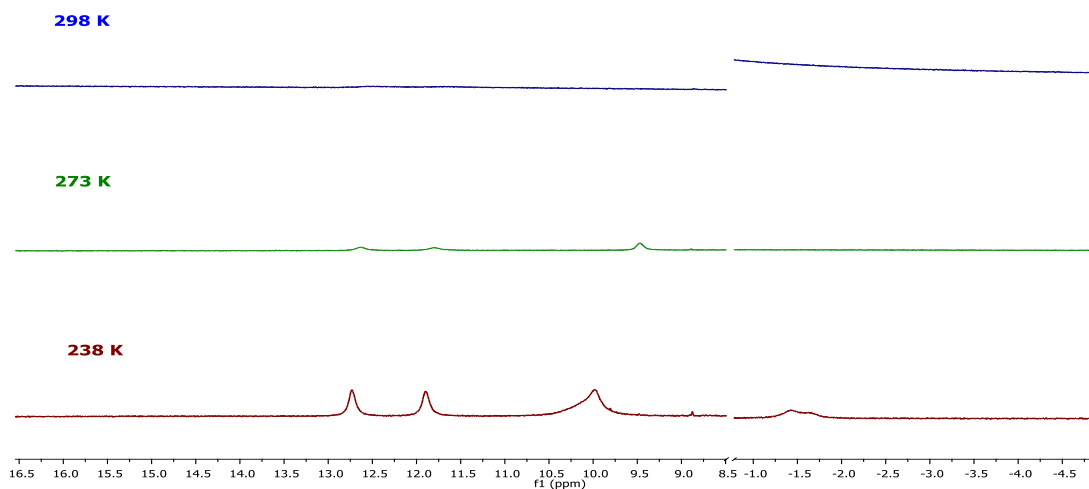
Figure -IV.A.9: Variable temperature ^{1}H NMR spectra of **IV.A.12** in acetonitrile-d_3
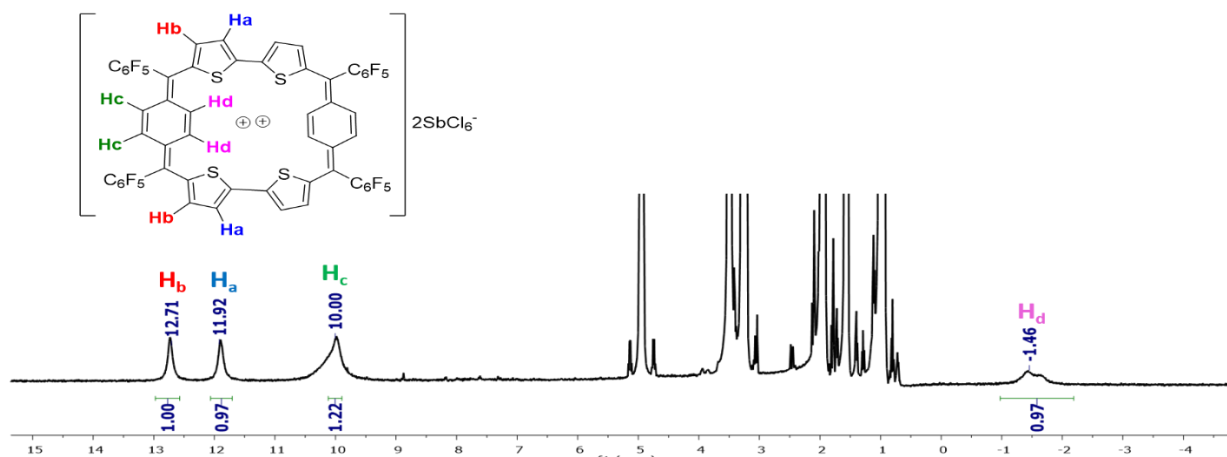
Figure -IV.A.10: ^{1}H NMR spectrum of **IV.A.12** at 238K in Acetonitrile-$d3$. (Signals from δ 1 to 5.5 ppm corresponds to the ethyl of ethyl chloride and diethyl ether from Meerwein salt)

The observed chemical shifts in the ^{1}H NMR spectrum suggested the presence of diatropic ring current effect for 26π electrons in **IV.A.12**. Two broad singlets corresponding to four protons each were identified for β-protons of thiophene at δ 12.71 and 11.92 ppm. Two broad singlets, one each in the downfield and up field corresponding to four protons each, were observed for benzene protons at δ10.00 and -1.46 ppm respectively. The obtained ^{1}H NMR spectrum could be inferred as a quinoidal deformation of both benzene rings. The estimated NICS value of -1.06 ppm further

121

supported weak aromatic characteristics for **IV.A.12**. Absence of signals in ^{1}H NMR spectrum at room temperature and appearance of signals at low temperature validated the singlet diradical character for **IV.A.12**. Temperature-dependent dynamic equilibria between benzenoid and quinoidal form could be possible for **IV.A.12**.
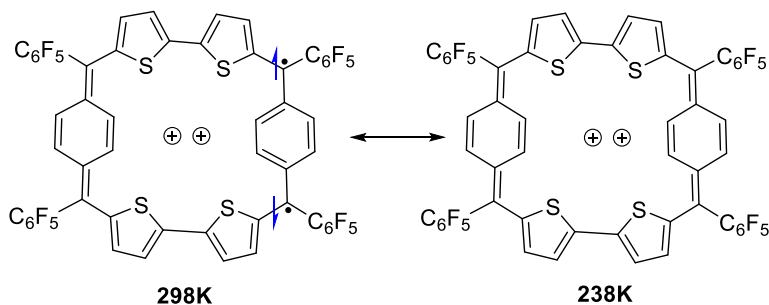
Scheme-IV.A.6: benzenoid to quinoidal changes with the temperature of **IV.A.12.**

IV.A.9: Magnetic studies for IV.A.12:

The singlet diradical character of **IV.A.12** was further studied using electron paramagnetic resonance (EPR) spectroscopic studies (figure-IV.A.11A). EPR measurement of **IV.A.12** in solid-state gave a featureless broad signal with $g_e = 2.004$ at room temperature (298K) characteristic for organic radical, intensity of which decreases with lowering in temperature. This gave clear evidence for the presence of singlet diradical character for **IV.A.12.** The magnetic properties of **IV.A.12** was investigated by measuring variable temperature magnetic susceptibility under 0.1 T applied field in the range of temperature 2-300 K by using a SQUID VSM magnetometer (figure-IV.A.11B). The measured moments and derived molar magnetic susceptibility of the sample were corrected by sample holder and diamagnetic corrections (estimated from Pascal's table)[71], respectively. At 300K the molar magnetic susceptibility ($\chi_M T$) of compound **IV.A.12** is 0.759 cm^3 mol^{-1} K (Figure IV.A.11B) which is very close to the theoretical value for two unpaired electrons (0.75 cm^3 mol^{-1} K for S = 1), and it decreases upon cooling reflecting antiferromagnetic exchange interactions between the spins. The plot of $1/\chi_M$ *vs.* T (Figure-IV.A.11B) at higher temperatures (above 50 K) was found to follow the Curie-Weiss behavior with C = 0.765 cm^3 mol^{-1} K and θ = -9.5 K, which further supports the presence of strong antiferromagnetic exchange interactions. Besides, to quantify the energy difference between singlet and triplet state the obtained experimental data was modeled using Bleaney- Bowers equation.[72] Although the data could not fit the lower temperature region, whereas a good fit of the higher temperature region gave ΔE_{ST} =

-0.1 KCal mol^{-1}. Therefore, the SQUID measurements indicate that the singlet ground state is more stable than the triplet ground state with a small energy gap.
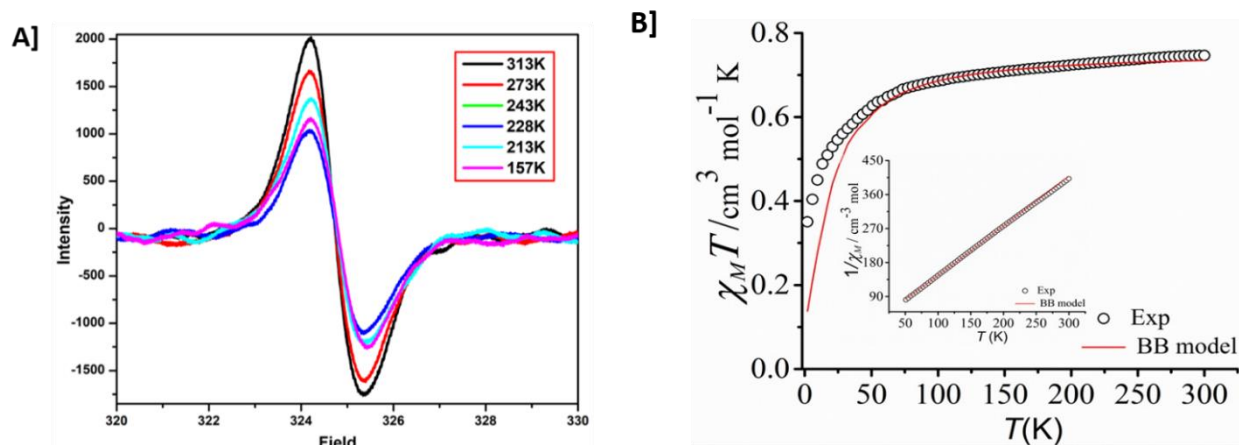
Figure -IV.A.11: A] EPR spectra of **IV.A.12** at 298K (red) and 103K (Blue), B] $\chi_{.M}$T-T curve in SQUID measurement for **IV.A.12.**

IV.A.10: Quantum mechanical calculation:

The diradical character of **IV.A.12** was further calculated by using unrestricted spin DFT (UCAM B3LYP/631G (d)) studies on energy optimized geometry. It showed singlet to triplet energy gap of ΔE S−T = -6.2 kcal mol$^{-1,}$ and the spin density distribution shows delocalization of electron density throughout the macrocycle, which was further supported by NICS values of -1.6 ppm, Percentage of diradical character for **IV.A.12** was estimated by NOON (natural orbital occupation number) [66] using CASSCF (complete active space self-consistent field) which was found to be 32%. The bond length alteration parameter is often used to measure the extent of quinoidal deformation of the benzene ring. The large BLA values for dication displayed a greater extent of quinoidal deformation of the p-phenylene moiety.

On the other hand, the BLA values (figure-IV.A.12) [73] of the central six-membered ring in a neutral molecule exhibited a negligible change. This observation indicated that the generated spins delocalized over the entire p-phenylene moiety in dication. The obtained highest occupied molecular orbital (HOMO) and lowest unoccupied molecular orbital (LUMO) for closed-shell neutral molecule showed localized electron density over the bithiophene unit whereas, HOMO and LUMO of closed-shell dication displayed delocalized electron density over entire macrocycle, which is again in agreement with experimental findings (figure-IV.A.13).

Bond length alternation for ring A and Ring B

	Neutral	Dication CS (closed shell)	Dication OS (open shell)
Ring A	0.0157	0.0424	0.0405
Ring B	0.0168		

Neutral

Dication-open shell
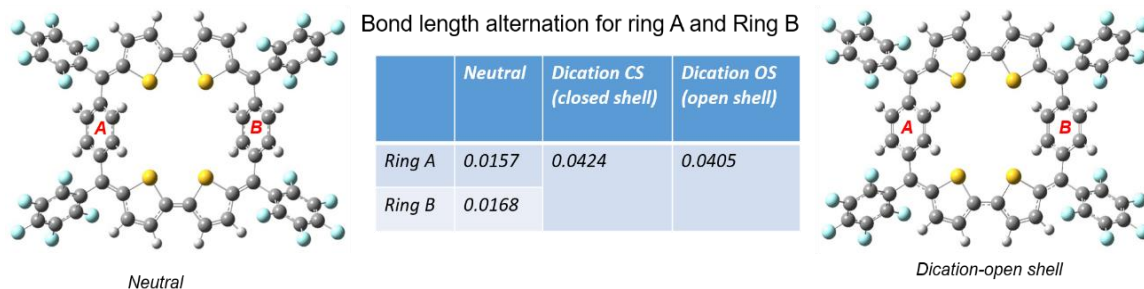
Figure -IV.A.12: Bond length alternation study for **IV.A.12**

LUMO = - 5.51

LUMO = - 6.80

HOMO = - 6.63

HOMO = - 6.30
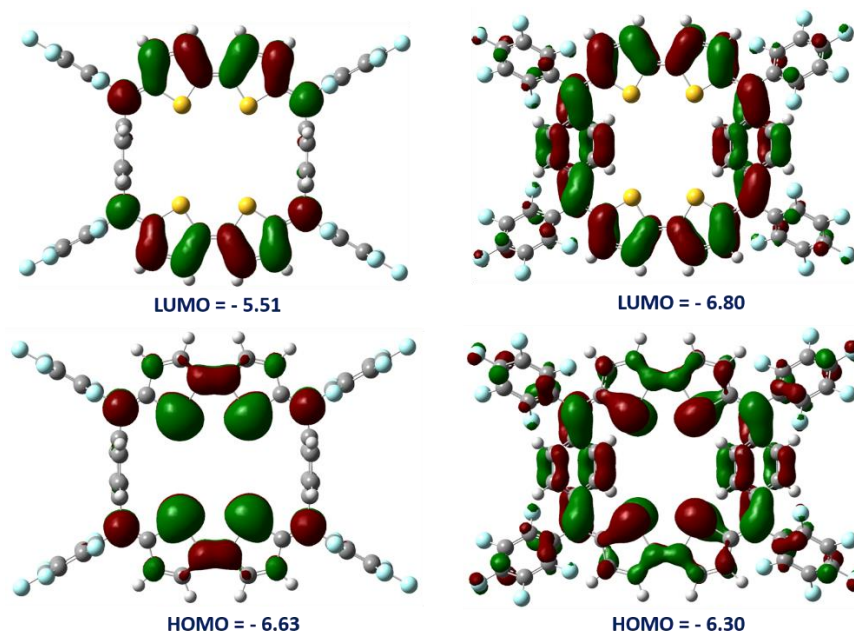
Figure -IV.A.13: Selected frontier MOs of **IV.A.8** (left) and **IV.A.12** (right) calculated at the B3LYP/6-31G (d, p) level.

IV.A.11: Biphenyl appended isophlorin IV.A.14:

Anticipating expanded derivative of benzoisophlorin with higher diradical character, it was decided to substitute phenylene with biphenyl in **IV.A.12.** In the case of dibenziisophlorin **IV.8**, two benzene rings existed in the aromatic state. Whereas, in dication **IV.10,** quinoidal deformation of both the benzene rings was observed, along with the existence of open-shell singlet diradical as a ground electronic state. Quinoidal deformation of four thiophenes was expected to achieve a global conjugation network for $(4n+2)\pi$ electrons.

IV.A.12: Synthesis and characterization of IV.A.14:

Synthesis of **IV.A.14** was achieved by FeCl₃ assisted oxidative coupling (scheme-IV.A.7) biphenyl appended trithiophene **IV.A.13**. The product was isolated from the reaction mixture through silica-gel chromatography in 3% yields as a dark orange-colored band with dichloromethane/hexane as eluent.
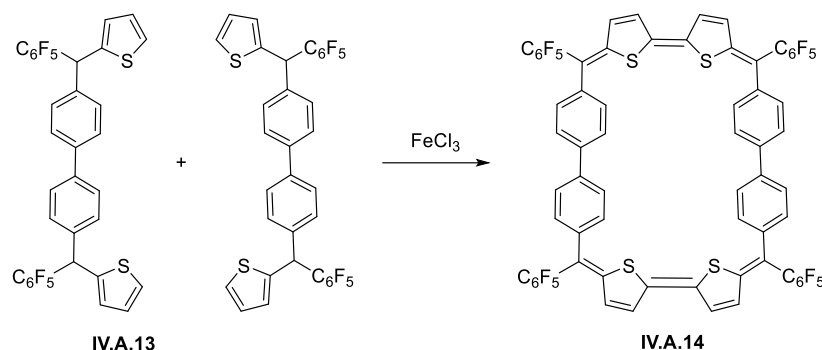
Scheme-IV.A.7: Synthesis of biphenyl appended expanded isophlorin **IV.A.14**.

IV.A.13: MALDI-TOF/TOF Mass Spectrometric Analysis and Electronic absorption studies for IV.A.14:

MALDI-TOF/TOF mass spectrometric analysis displayed a peak at 1348.8290, corresponding to the expected mass of macrocycle **IV.14**. UV-vis absorption spectrum of **IV.A.14** recorded in dry dichloromethane, displayed an absorption maxima at 498nm (21000) (figure-IV.A.14).
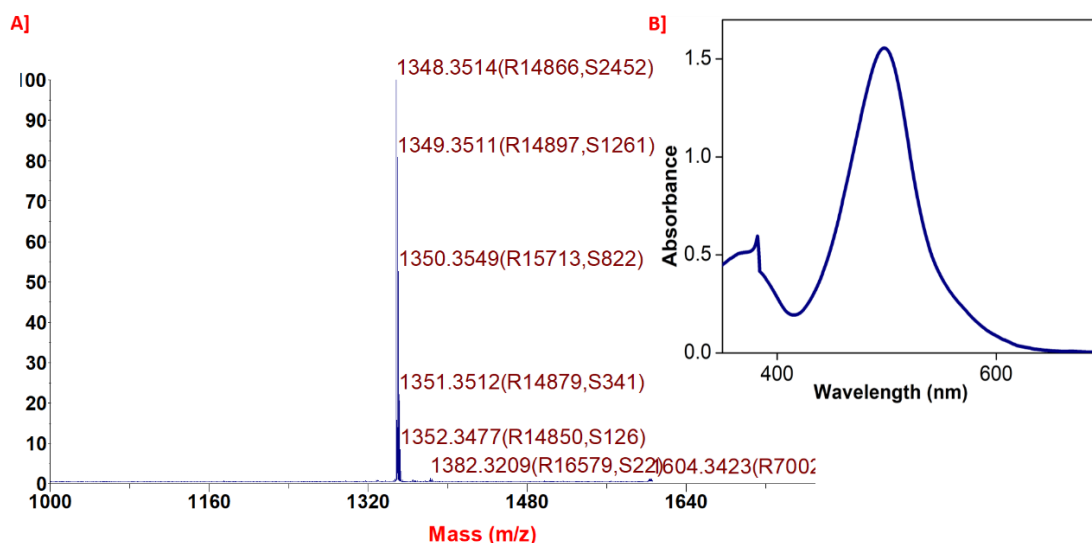
Figure -IV.A.14: UV-Vis absorption spectrum of **IV.A.14.**

IV.A.14: ^{1}H NMR studies for IV.A.14

^{1}H NMR spectrum recorded in chloroform-*d* at 298K, displayed two doublets at δ 7.10 and 6.45 ppm corresponding to four protons each for the β-protons of four thiophene rings (figure-IV.A.15). Whereas, two more doublets resonated at δ 7.71 and 7.52 ppm corresponding to four phenylene rings each. The observed ^{1}H NMR spectrum did not project any significant ring current effect and hence it was suspected that all the four phenylene rings are present in their benzenoid form. This was further supported by ^{1}H-^{1}H COSY spectrum recorded at 298K. Unfortunately, all the attempts to obtain good quality crystal for **IV.A.14** went futile. Therefore quantum chemical calculations were employed to obtain the energy-optimized geometry for this macrocycle (figure-IV.A.16). It displayed a structure similar to **IV.A.12**, wherein the biphenyl units were found to be orthogonal to the plane of the macrocycle. Such orientation as found to be in support with the observed ^{1}H NMR spectrum. Non-aromatic nature for **IV.A.14** supported by the estimated NICS value of -0.57 ppm.
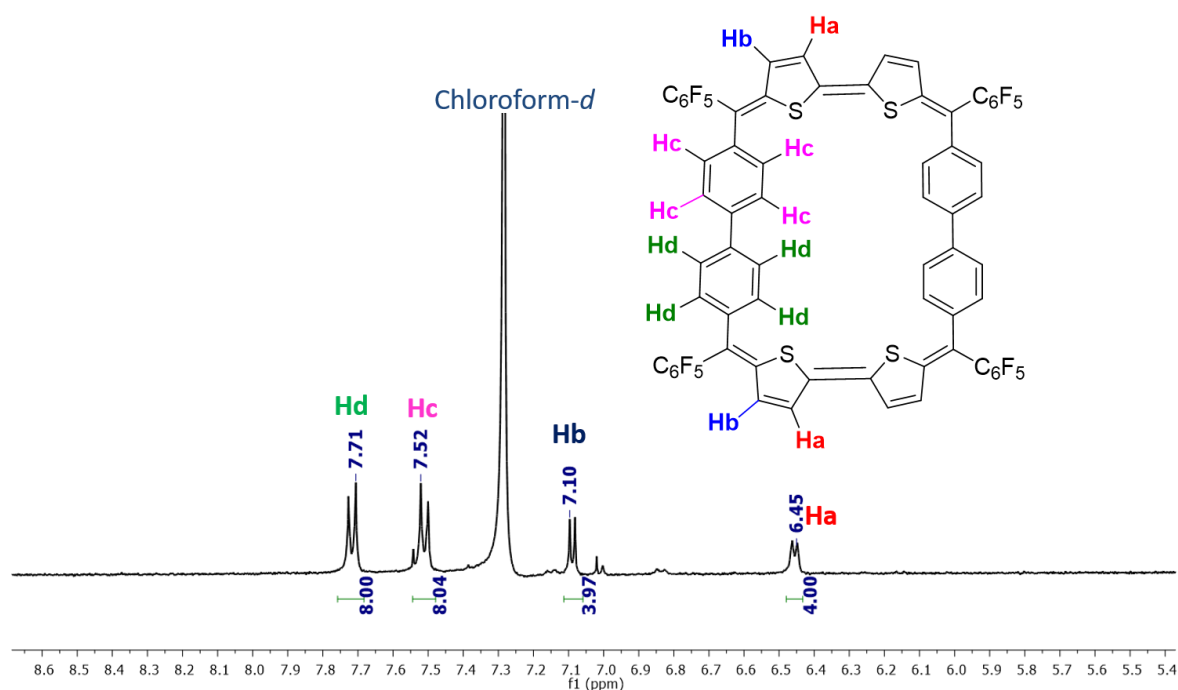
Figure -IV.A.15: ^{1}H NMR spectrum of **IV.A.14** at 298K in Chloroform-*d*.
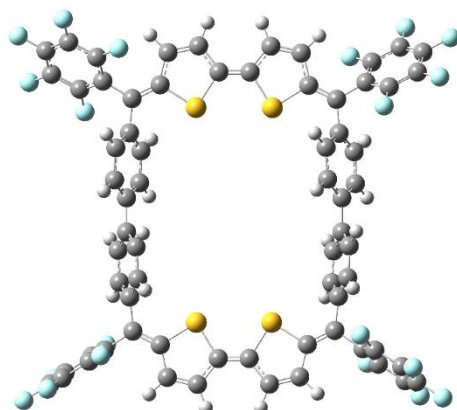
Figure-IV.A.16: Energy minimized geometry for **IV.A.14** obtained at B3LYP/631G (d, p) level of theory.

IV.A.15: Synthesis of IV.A.15
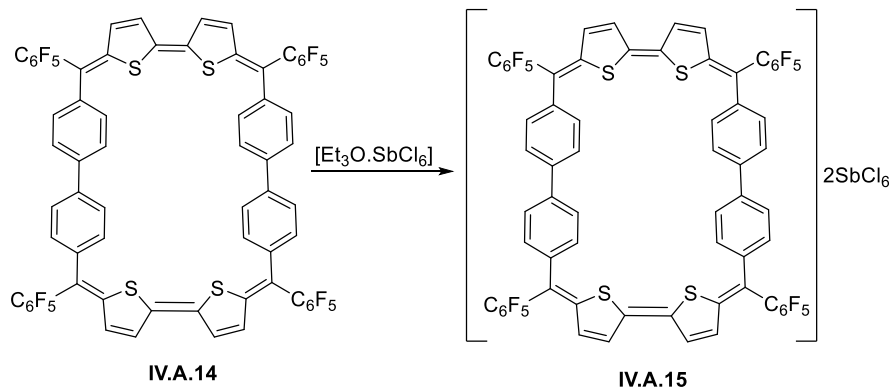
Scheme-IV.A.8: Two-electron oxidation of **IV.A.14** with Meerwein salt.

Interesting redox chemistry of dibenzi-isophlorin has been discussed in the previous part **IV.8**, where conversion of local to global aromaticity for benzene has been studied upon addition of oxidizing agent. Anticipating similar conversion for bisbiphenyl appended isophlorin, **IV.14**, cyclic voltammetric studies (figure-IV.A.17A) were conducted in dry dichloromethane, which displayed two reduction waves at -1.17V and -0.84V along with two oxidation waves at 1.06V and 1.54V. Therefore, **IV.A.14** was reacted with a stoichiometric excess of Meerwein salt and the progress of the reaction monitored by using UV-Vis spectroscopy (figure-IV.17.B). The color of the solution changed from orange to blue with a bathochromic shift in the absorption maxima from 498 nm to 700 nm.
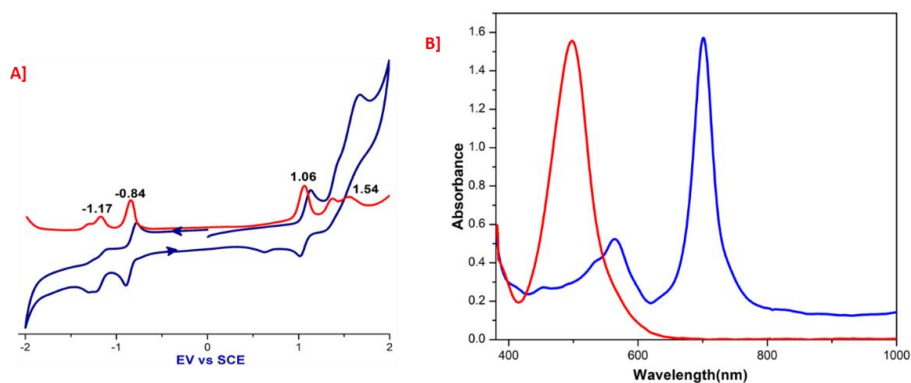
Figure -IV.A.17: A] Cyclic (Blue) and Differential pulse (red) voltammograms of **IV.A.14** in dichloromethane containing 0.1M tetrabutylammonium perchlorate as the supporting electrolyte recorded at 50 mVs^{-1}. B] Absorption changes observed to the solution of **IV.A.14** (red line) to (Blue line) **IV.A.15.**

IV.A.16: ^{1}H NMR and EPR studies:

As huge redshift in by 200 nm implied the possibility of formation of diradical dication similar to its **IV.A.8.** Variable temperature ^{1}H NMR spectra were recorded in acetonitrile-d$_3$, which showed very broad signals (figure-IV.A.18). However, based on the obtained ^{1}H NMR spectrum, it was not possible to arrive at any definite structure for **IV.15** in the solution state. Such broad NMR signals are generally expected for radical species. However, the estimated NICS value of -4.47 ppm and global delocalization of HOMO and LUMO supported the moderated aromatic characteristics for **IV.B.15**
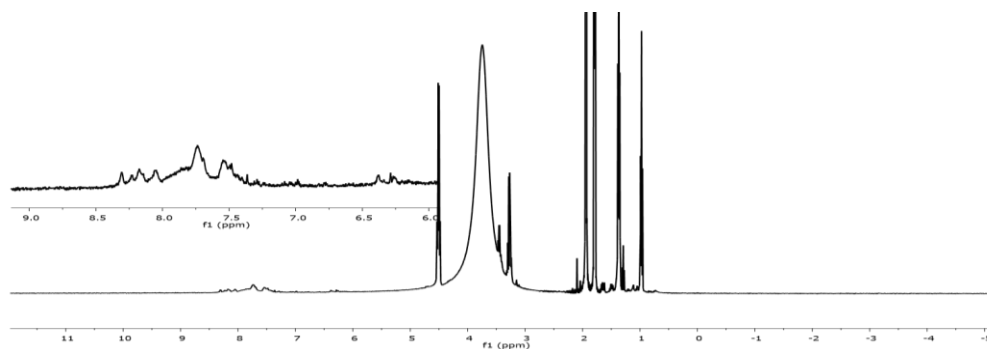
Figure -IV.A.18: ^{1}H NMR spectrum of **IV.A.15** at 238K in acetonitrile-d_3

The singlet diradical character of **IV.A.15** was further studied using electron paramagnetic resonance (EPR) spectroscopic. EPR measurement of **IV.A.15** in the solid-state (figure-IV.A.19) gave a characteristic signal for organic radical with field value 3378 (g$_e$=2.006) at room

temperature (298K). The intensity of EPR signals was found to decrease upon lowering the temperature to 103K. Observed EPR spectra was in agreement with the obtained NMR results.
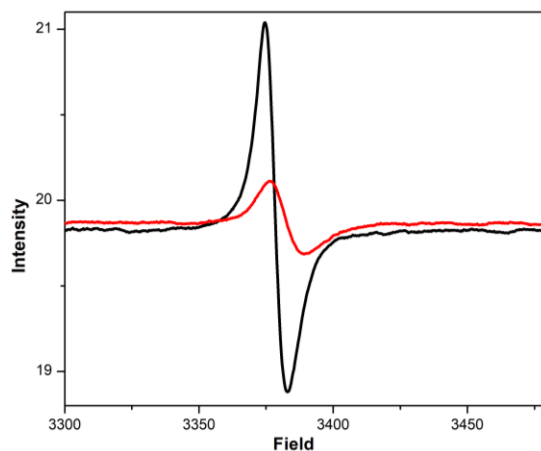
Figure –IV.A.19: EPR spectra of **IV.A.15** at 298K (Black) and at 103K (Red)

IV.A.17: Conclusions:

In conclusion, we have described synthesis and characterization of benzene appended isophlorin **IV.A.8**. Aromaticity of both the benzene ring in the **IV.A.8** remain intact in the neutral state. But, its two electron oxidation to the dication **IV.A.12** shows localized ring current effect for aromaticity, as confirmed by spectroscopic technique as well as though computationally. Dication of dibenzi-isophlorin was identified as an open shell singlet diradical with significant diradical character and a lower singlet-triplet energy gap. This diradical was found to be stable at room temperature in solid state, because of global delocalization of electrons. Similar attempt were made by two incorporating biphenyl rings in to isophlorin framework **IV.A.14**. It also showed localized electron density in the neutral state, and dication shows global aromaticity which was confirmed by NICS calculations.

Part B

Synthesis and Characterization of Phenylene Bridged Isophlorin Dimer

IV.B.1: Introduction:

The chemistry of antiaromatic systems is severely hindered by a very small number of anti-aromatic molecules due to a lack of sufficient synthetic strategies and their high reactivity. Even the simplest anti-aromatic system such as cyclobutene or cyclooctatetraene are known to undergo dimerization; due to inherent instability of $[4n]\pi$ system.[12] It still remains a challenge to explore the properties of these systems. Isophlorins are an anti-aromatic structural analogs of porphyrin, which are often known to stabilize anti-aromaticity upon modifications to a porphyrin framework.[46] Divalent chalcogen, such as furan and thiophene, are generally employed to achieve stable 20 π isophlorin. [4] The interlinked 20π isophlorin dimer **IV.B.2** is another class of 4nπ macrocycle which possesses meso-meso directly linked two isophlorin subunits. [74] The presence of a single bond between two isophlorin units adds flexibility to the dimeric structure **IV.B.2**. Therefore, the paratropic ring current effect for macrocycle can be observed for a globally conjugated 4nπ system. Anticipating local ring current effects for individual isophlorin units, it was decided to introduce benzene as a rigid and highly aromatic spacer between two isophlorin subunits.
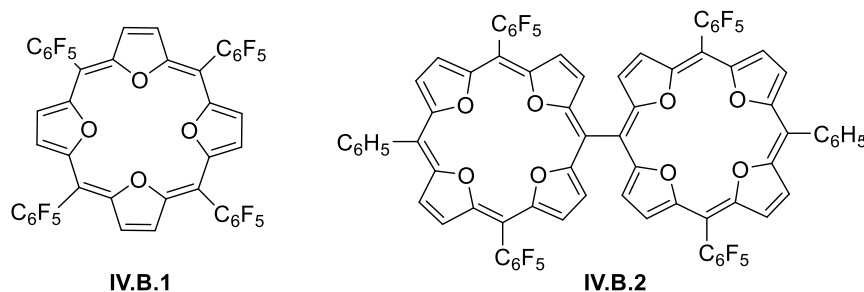
Figure -IV.B.1: Tetraoxaisophlorin and tetraoxaisophlorin dimer.

IV.B.2: Synthesis and structural characterization of IV.B.6:

The synthesis of benzene bridged tetroxaoxa isophlorin dimer **IV.B.5** was attempted by employing MacDonald type condensation between tetra furyl benzene **IV.B.4** and bisfuromethyl diole **IV.B.3** followed by oxidation with DDQ (scheme-IV.B.1). MALDI-TOF/TOF mass spectrometric analysis of reaction mixture revealed the formation of an expected mass of dimer along with a small amount of the mono condensed product. Purification through basic alumina column gave phenylene bridged isophlorin dimer **IV.B.5** as a red-colored band in a 6% yields. Depending upon the orientation of tetra furan, this reaction can also work in another way, which leads to the formation of **IV.B.6** as a bicyclic product.
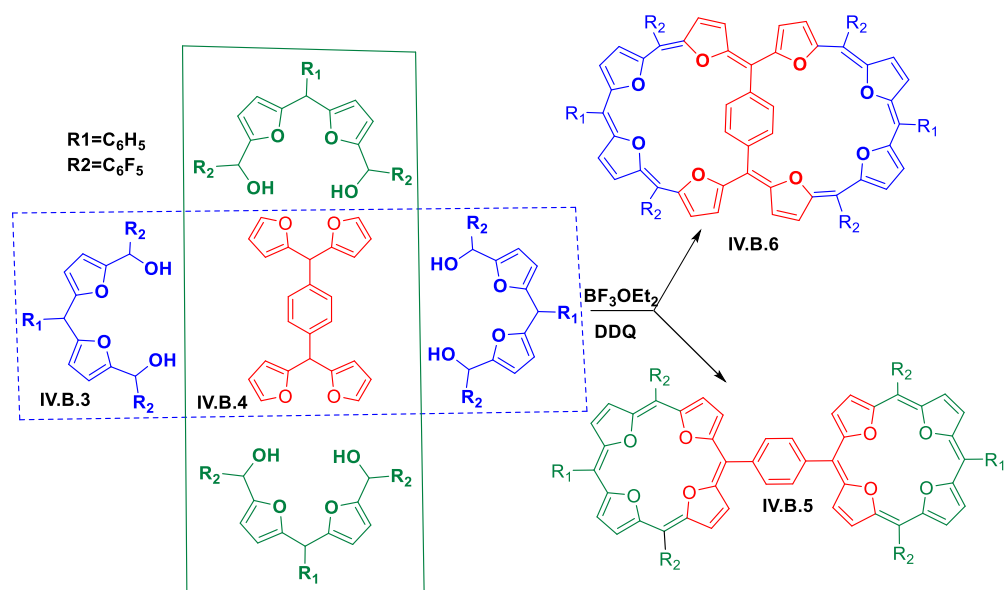
Scheme-IV.B.1: Synthesis of phenylene bridged isophlorin dimer.

IV.B.3: HRMS Studies for IV.B.6:

High resolution mass spectrometric analysis (figure-IV.B.2) of pure sample displayed a m/z at 1522.1584, which was found to be very close to the calculated mass of 1522.1661 for **IV.B.5.** In addition to the molecular ion peak, m/2 mass of exact mass was also observed suggesting two-electron oxidation of **IV.B.5**, to its dication.
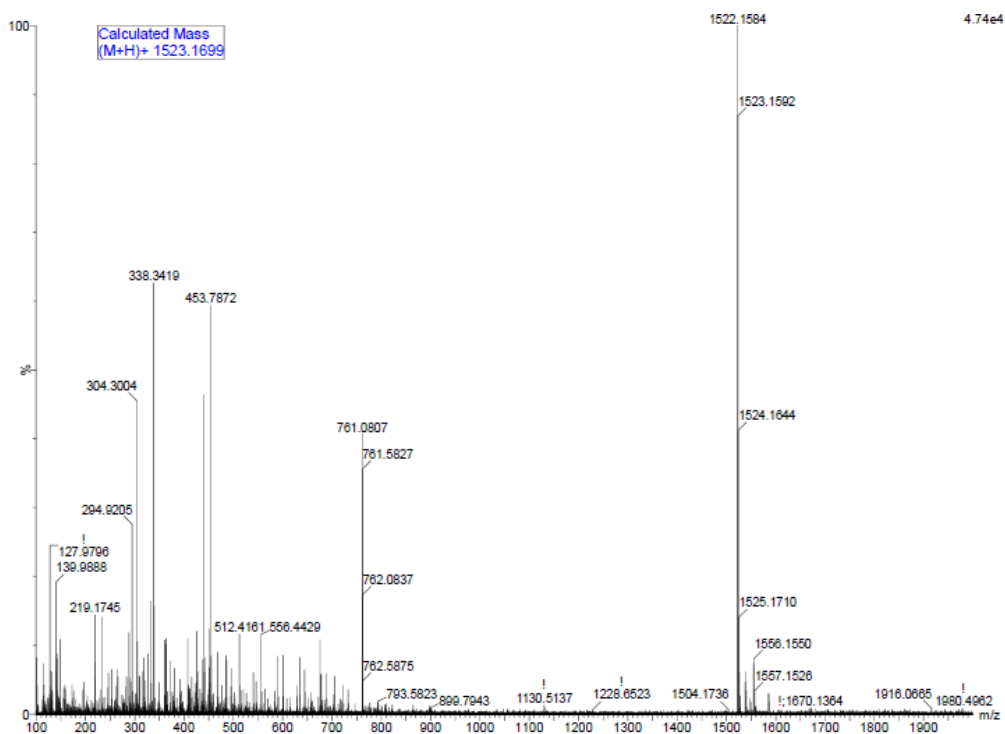
Figure -IV.B.2: HRMS of **IV.B.6.**

IV.B.4: Absorption studies:

The synthesized isophlorin dimer **IV.B.5** forms a reddish colored solution when dissolved in common organic solvents. The color of the solution can be attributed to the conjugated network of the macrocycle. **IV.B.5** displayed broad absorption at 513(56400) nm along with a high energy shoulder band at 410 nm.
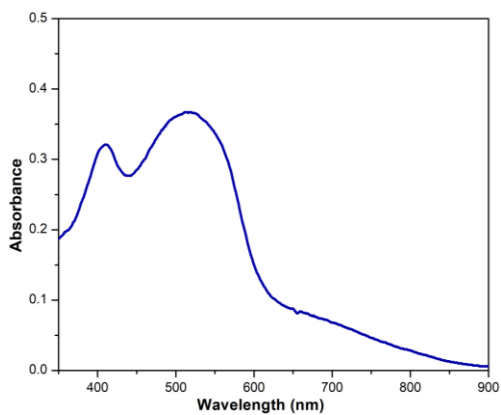
Figure -IV.B.3: UV-Vis Absorption spectrum of [10^{-6}M.] **IV.B.6** in CH_2Cl_2.

IV.B.5: ^{1}H NMR studies for IV.B.6:

^{1}H NMR spectrum of macrocycle recorded in toluene-d_8, displayed very broad signals at room temperature (figure-IV.B.4). Even though the monomer displayed well-resolved signals at room temperature, observation of broad signals could be attributed to the rotation of the macrocycles through the phenyl bridge. However, a well-resolved spectrum was observed at 213K (figure-IV.B.5), but it did not display the expected strong paratropic shift for 4nπ anti-aromatic macrocycle. Overall, eight doublets were observed in the region between δ 9.0 to 4.0 ppm for sixteen β-protons for macrocycle. Observed ^{1}H NMR pattern did not project any similarities with the reported meso-meso linked isophlorin dimer **IV.B.2**. As **IV.B.2,** is known to possesses C_{2V} symmetry and displayed four up field shifted doublets between δ 4.28 to 1.94 ppm, the observed ^{1}H NMR pattern could be considered for an alternative structure, wherein all four furans from tetra furan undergoes ring flipping to form a bicyclic structure **IV.B.6**.
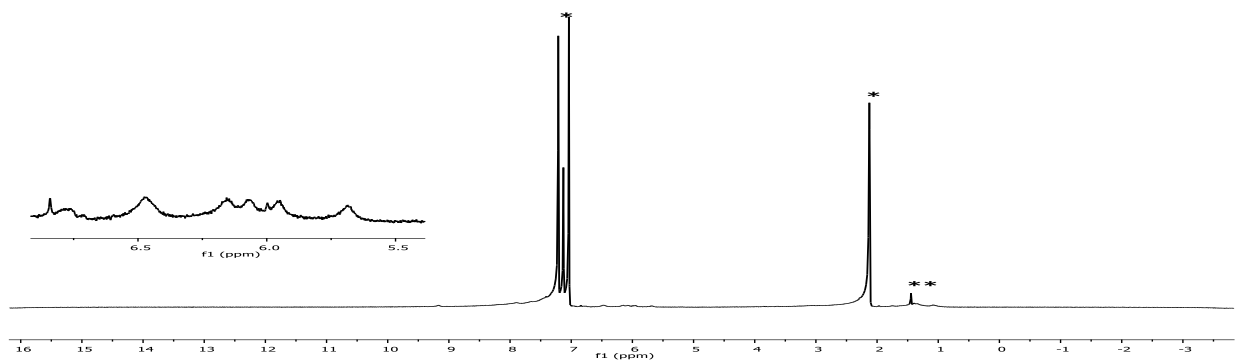
Figure -IV.B.4: ^{1}H NMR Spectrum of **IV.B.6** at 298K in Toluene-d_8.
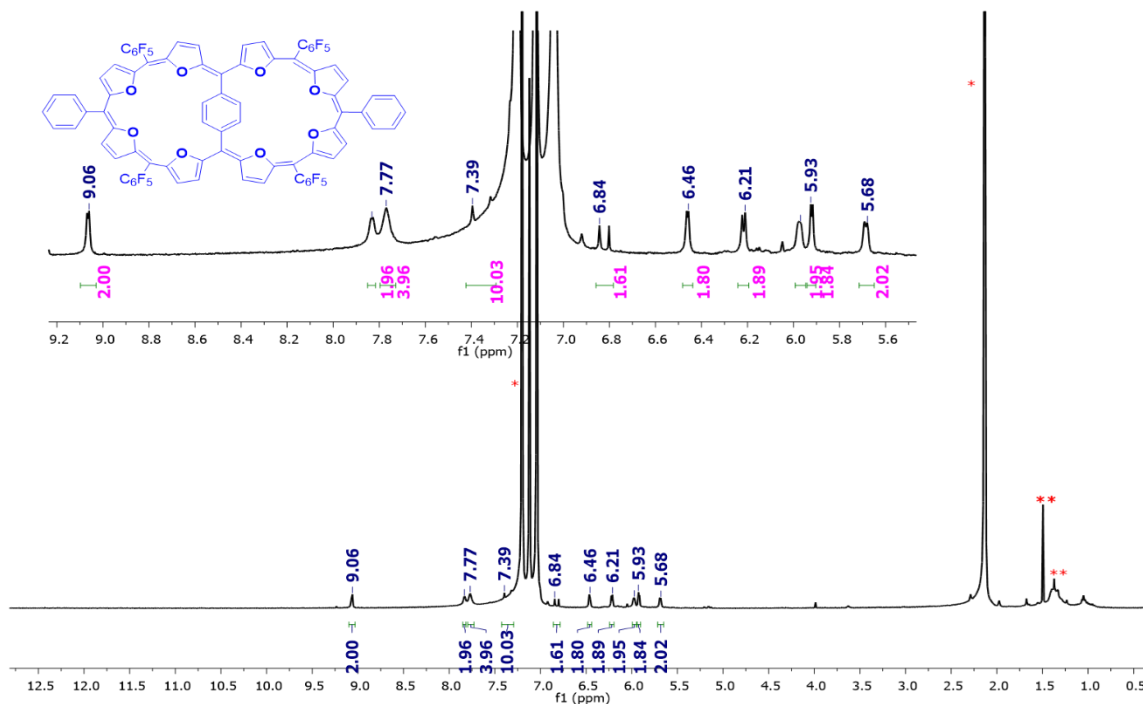
Figure -IV.B.5: ^{1}H NMR Spectrum of **IV.B.6** at 213K Toluene-d_8.

^{1}H NMR spectrum also displayed a singlet corresponding to four protons which could be accounted for bridging phenylene ring. Consideration of this structure signified that the phenylene ring preferred to retain its aromaticity in the benzenoid form. Weak signals corresponding to ten protons for the two phenyl rings were identified at δ 7.3 ppm. The signals of meso phenyl were merged with toluene-d_8 signals. Further, the observed ^{1}H NMR pattern was strongly supported by ^{1}H-^{1}H COSY spectrum (figure-IV.B.6) recorded at 213K. It displayed four strong correlations for the protons of the macrocycle **IV.B.6** at (i) 9.06 and 6.83 (ii) 6.89 and 5.93, (iii) 6.46 and 5.93, (iv) 6.21 and 5.68 ppm. The observed weak antiaromatic nature of macrocycle was further supported by the estimated NICS (0) value of +1.21 ppm for the energy minimized geometry. The NICS (0) value at benzene ring was found to be -6.95 ppm in support of a benzenoidal nature of embedded benzene ring.
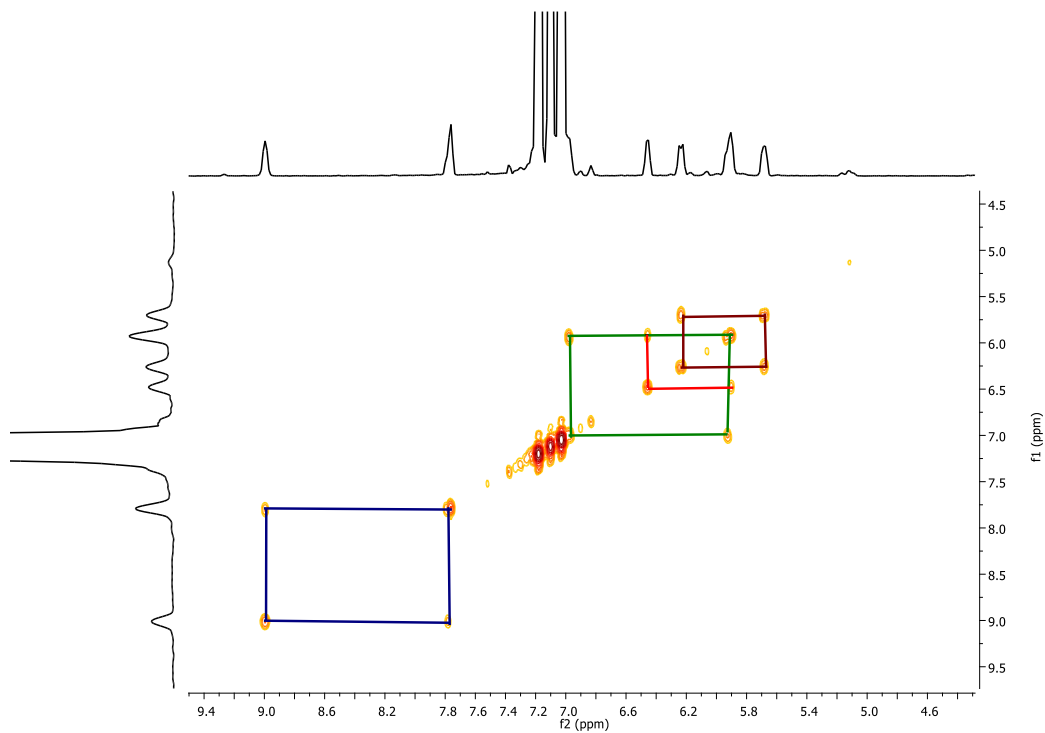
Figure -IV.B.6: Partial ^{1}H-^{1}H COSY spectrum of **IV.B.6** at 213K in Toluene-*d*.

IV.B.6: Synthesis and absorption studies of IV.B.7:

HRMS analysis of benzene appended isophlorin **IV.B.6** displayed an m/2 peak, signifying two electrons oxidation it to its dication. Therefore **IV.B.6** was reacted with Meerwein salt (scheme-IV.B. 2) to obtain its dicationic species.
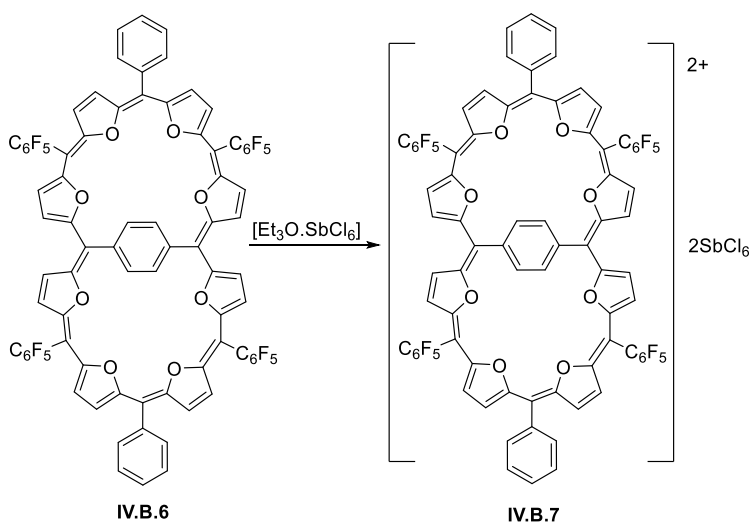
Scheme-IV.B.2: Two-electron Oxidation of **IV.B.6** using Meerwein salt.

135

The color of the solution displayed a subtle change from red to dark green with a huge red shift in the absorption from 519 nm to a more intense high energy absorption at 739 nm (figure-IV.B.7). It also displayed two low energy absorptions in the near IR region at 1053 nm, 1163 nm and 1226 nm which is characteristics for porphyrinoid type macrocycle. The periphery of bicyclic macrocycle **IV.B.6** accounts for $4n\pi$ electron, and its two-electron oxidation products gave 38π $(4n+2)\pi$ aromatic system **IV.B.7.**
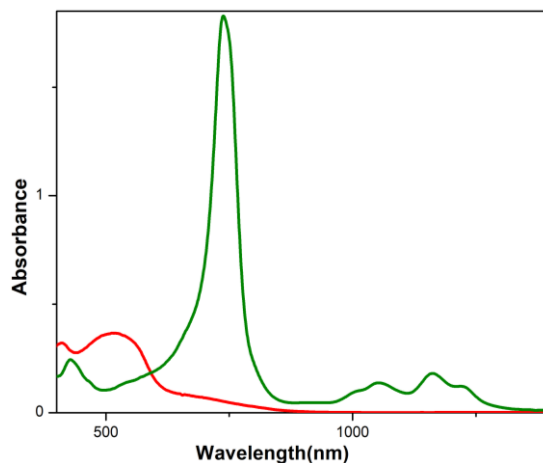
Figure -IV.B.7: Absorption changes observed in the [10^{-6}M] solution of **IV.B.6** (red) to **IV.B.7** (green) upon addition of Meerwein salt in DCM.

IV.B.7: ^{1}H NMR Studies for IV.B.7:

^{1}H NMR spectrum of **IV.B.7** recorded in acetonitrile-d$_3$ at 233K displayed signal for two sets of magnetically distinct protons (figure-IV.B.8). Eight downfield shifted signals corresponding to sixteen protons were found for β protons of furan between 11.10 to 8.94 ppm. In contrast, two up filed shifted signals corresponded to two protons. They resonated at δ -3.45 and -4.54 ppm for the internal phenylene ring. Protons of phenylene ring were influenced by diatropic ring current effect as expected for 38π aromatic macrocycle. The observed ^{1}H NMR pattern further gave direct evidence for the presence of a bicyclic structure for **IV.B.7,** neglecting the possibility for the formation of the expected dimeric structure. The observed high up field and down field shift in the NMR spectrum was further supported by NICS value of -7.77 ppm and -14.29 ppm for the embedded phenyl ring (figure-IV.B.9).
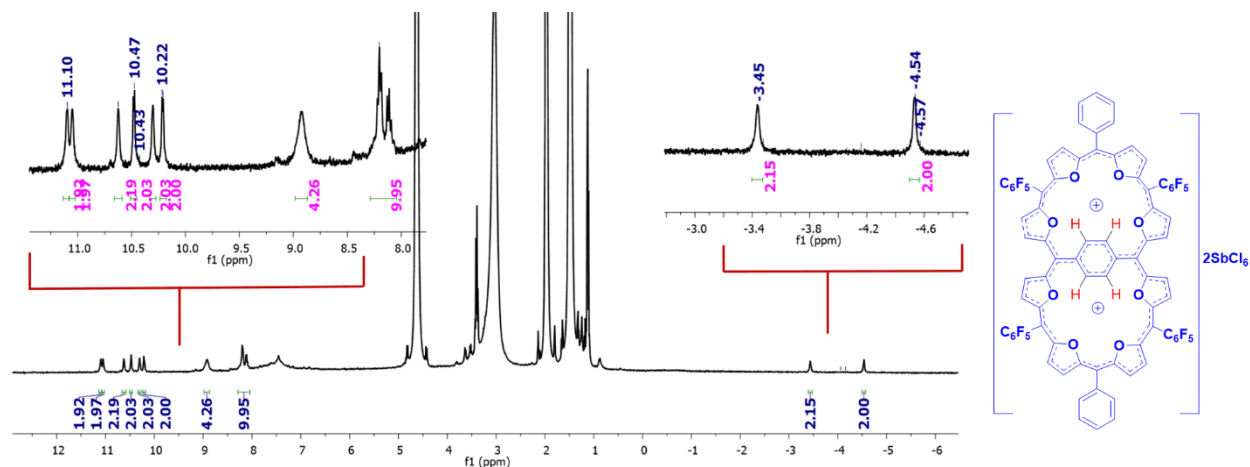
Figure -IV.B.8: ^{1}H NMR spectrum **IV.B.7** in acetonitrile-d$_3$ at 233K.
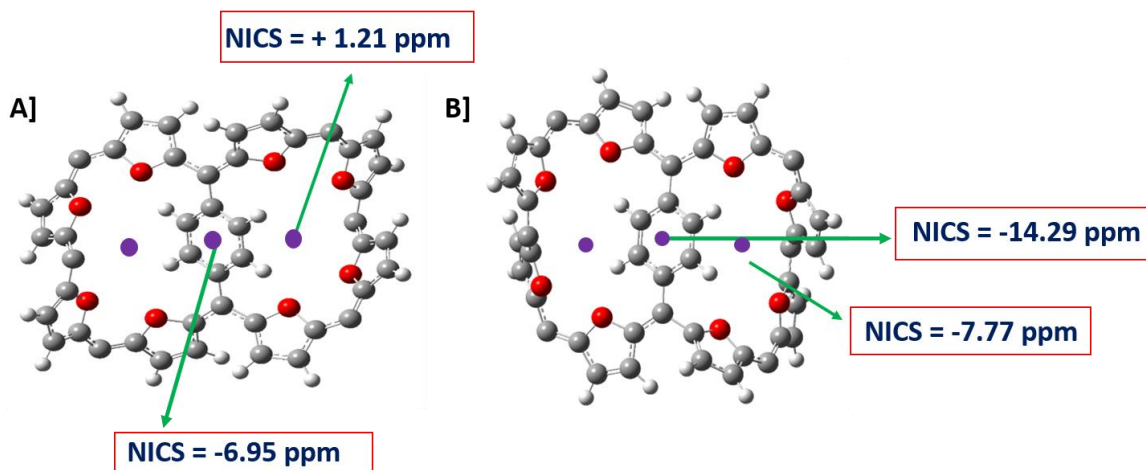
Figure-IV.B.9: Estimated A] NICS(0) for **IV.B.6** B] NICS(0) for **IV.B.7**

IV.B.8: Conclusions:

In an attempt to obtain isophlorin dimer, a 40π bicyclic structure **IV.B.6** with weak antiaromatic characteristics was observed. The weak antiaromatic nature of **IV.B.6** was reflected in the NMR data which was further supported by NICS calculation. Two electron oxidation of **IV.B.6** generated more aromatic dication **IV.B.7.** The up filed shift of protons for the embedded phenyl rings and down field shift of periphery protons confirmed enhancement of aromaticity in the dication. The estimated NICS values are in complete agreement with the experimental findings.

Experimental section:

Synthetic procedure for IV.A.8

Anhydrous FeCl$_3$ (538mg, 3.32mmol) added to the solution of benzotrithiophene (0.250 mg, 0.414mmol) in dry dichloromethane, stir the reaction mixture under dark for 1hr. Quench the reaction by adding a drop of triethylamine; then, the crude was passed through a short pad of basic alumina. The compound purified by using basic alumina column chromatography using Hexane/DCM system as eluent. The obtained orange color band identified as benzoisphlorin **IV.A.8**

HR-MS (ESI-TOF): *m/z*=1195.9795 (found), Calculated for (C$_{56}$H$_{16}$F$_{20}$S$_4$); (1195.9815).

UV-Vis (CH$_2$Cl$_2$): λ$_{max}$ nm (ε, Lmol^{-1}cm^{-1}): 484 (87000).

^{1}H NMR (400 MHz, CDCl$_3$, 298K) *δ*: 6.71 (d, *J*=5.6 Hz, 4H), 6.12 (d, *J*=5.6 Hz, 4H), 7.78 (s, 8H).

Selected Crystal data: C$_{56}$ H$_{16}$ F$_{20}$ S$_4$ (+ solvent) (*M*$_r$ = 1396.24), triclinic, space group *P -1*, *a* = 6.0778(13), *b* =12.795(3), *c* =19.877(4) Å, α = 76.466(5), β = 82.741(5), γ = 78.165(6), *V* = 1466.3(6) Å, Z = 1, *T* =100(2) K, D$_{calcd}$ = 1.582cm^{-3}, R$_1$ = 0.0657 (I>2sigma (I)), *R*$_w$ (all data) = 0.2126(7294), GOF = 1.33

Redox: E$_1$red = -1.67mV, E$_2$red = -0.76 E$_1$ox = 0.91mV, E$_2$ox = 1.77mV.

Synthetic procedure for IV.A.12: The dication **IV.A.12**, was synthesized by the addition of triethyl oxonium hexafluoroantimonate (10 mg) to a solution of **IV.A.8** (2.5 mg) in dry dichloromethane at -20°C and the resulting solution was stirred for ten minutes under nitrogen atmosphere. Allow the reaction mixture to room temperature for one hr. Evaporation of the solution gave a golden-colored compound. Wash the obtained compound several times with hexane to remove ethyl chloride.

HR-MS (ESI-TOF): *m/z*=597.9895 (found), Calculated for (C$_{56}$H$_{16}$F$_{20}$S$_4$)$^+$; (597.9907).

UV-Vis (CH$_2$Cl$_2$): λ$_{max}$ nm (ε, Lmol^{-1}cm^{-1}): 581 (200000), 986(5400).

^{1}H NMR (400 MHz, Acetonitrile-*d$_3$*, 238K) *δ*: 12.73 (br s, 4H), 11.89 (br s, 4H), 9.98 (br s, 4H), -1.43 (br s, 4H).

Synthetic procedure for IV.A.14:

Anhydrous $FeCl_3$ (478mg, 2.95mmol) was added to the solution of benzotrithiophene **IV.A.13** (0.250 mg, 0.36mmol) in dry dichloromethane, stir the reaction mixture under dark for 1hr. Quench the reaction by adding a drop of triethylamine. Then the crude was passed through a short pad of basic alumina. The compound was purified by using basic alumina column chromatography using Hexane/DCM system as eluent. The obtained orange reddish-orange color band was identified as biphenyl appended isophlorin **IV.A.14**

UV-Vis (CH_2Cl_2): λ_{max} nm (ε, $Lmol^{-1}cm^{-1}$): 581 (21,000).

^{1}H NMR (400 MHz, $CDCl_3$, 298K) δ: 7.72 (d, J=8.4 Hz, 8H), 7.52 (d, J=8.4 Hz, 8H), 7.09 (d, J=5.6 Hz, 4H), 6.46 (d, J=6.0 Hz, 4H).

Redox: E_1red = -1.17mV, E_2red = -0.84 E_1ox = 1.06mV, E_2ox = 1.54mV.

Synthetic procedure for IV.13:

The dication **IV.A.15** was synthesized by the addition of triethyl oxonium hexafluoroantimonate (15 mg) to a solution of **IV.A.14** (1.5 mg) in dry dichloromethane at -20°C and the resulting solution was stirred for ten minutes under nitrogen atmosphere. Allow the reaction mixture to room temperature for one hr. Evaporation of the solution gave golden-colored compounds. Wash the obtained compound several times with hexane to remove ethyl chloride.

UV-Vis (CH_2Cl_2): λ_{max} nm (ε, $Lmol^{-1}cm^{-1}$): 7.1 (31,500).

^{1}H NMR (400 MHz, Acetonitrile-d_3, 298K) broad signals observed even at 238K.

Synthetic procedure for IV.B.6:

The mixture of benzotetrafuran **IV.16** (0.50mg. 0.13mmol) and difuryl dicarbinol **IV.15** (166.42mg, 0.26 mmol) was stirred in 250 ml dry dichloromethane in 500 ml round bottom flask. The solution was bubbled with argon for 10 min. BF_3OEt_2 (16.66 mmol, 0.13mmol) was added under dark. The resulting solution was stirred for 2.5hr, add few drops of triethylamine followed by the addition of DDQ (137 mg, 0.6 mmol). Stir the reaction for an additional 2hr. The reaction mixture was passed through a short basic alumina column. This mixture was purified on basic alumina column chromatography. A reddish solid was identified as **IV.17** in a 5% yield.

HR-MS (ESI-TOF): $m/z=1522.1584$ (found), Calculated for ($C_{82}H_{30}F_{20}O_8$); (1522.1621).

UV-Vis (CH_2Cl_2): λ_{max} nm (ε, Lmol^{-1}cm^{-1}): 521 (56400).

^{1}H NMR (400 MHz, Toluene-d_8, 213K) δ: 9.06 (d, $J=3.6$ Hz, 2H), 7.83 (d, $J=3.6$ Hz, 2H), 7.77 (br s, 4H), 7.79 to 7.31 (br m, 10H), 6.84 (br d, 2H), 6.46 (d, $J=3.2$ Hz, 2H), 6.24(d, $J=5.6$ Hz, 2H), 5.98 (d, $J=4$ Hz, 2H), 5.92 (d, $J=3.6$ Hz, 2H), 5.69(d, $J=4.4$ Hz, 2H).

Synthetic procedure for.4.B.7:

The dication **IV.B.7** was synthesized by the addition of stoichiometric excess of triethyl oxonium hexachloridoantimonate to a solution of **IV.B.6** (2 mg) in dry dichloromethane at -20°C. The resulting solution was stirred for ten minutes under a nitrogen atmosphere. Allow the reaction mixture to cool at room temperature for one hr. Evaporation of the solution gave a green colored compound.

HR-MS (ESI-TOF): $m/z=761.0907$ (found), Calculated for ($C_{82}H_{30}F_{20}O_8$)$^{2+}$; (761.0792).

UV-Vis (CH_2Cl_2): λ_{max} nm (ε, Lmol^{-1}cm^{-1}):) 738(27800) 1052(2100), 1161(2700), 1226(1800).

^{1}H NMR (400 MHz, Acetonitrile-d_3, 238K) δ: 11.10 (d, $J=4$ Hz, 2H), 11.05 (d, $J=3.2$ Hz, 2H), 10.62 (br s, 2H), 10.48 (d, $J=4.4$ Hz, 2H), 10.30 (d, $J=3.2$ Hz, 2H), 10.21 (d, $J=4.4$ Hz, 2H), 8.92(br s, 4H), 8.2 to 8.0 (m, 10H), -3.43 (br s, 2H), -4.53(br s, 2H).

Synthetic procedure for IV.11

IV.B.13.a) synthesis of biphenyl dialdehyde

n-BuLi (14.10ml, 35.26mmol) 2.5M solution in hexane was added to a stirred solution of 4,4'-dibromo-1,1'-biphenyl (5gm, 16.03mmol) in dry THF under nitrogen at -78°C. The reaction was stirred for 2hr. Allow the reaction mixture to cool at room 0°C followed by dropwise addition of DMF (4.94ml, 64.10 mmol), stir the reaction mixture at 0°C for 15min, and then warmed to room temperature and stir for three more hr. An ice-cold solution of NH_4Cl was added, and the reaction mixture was extracted with ethyl acetate, the organic fraction was dried over anhydrous sodium sulfate, and evaporated under reduced pressure. Silica gel column chromatography gave IV.11 as a colorless solid in 50%yiled.

¹H NMR (400 MHz, CDCl₃, 298K) δ: 10.09 (s, 2H), 8.03 (d, J=8.4 Hz, 4H), 8.01, 7.84 (d, J=8.4 Hz, 4H).
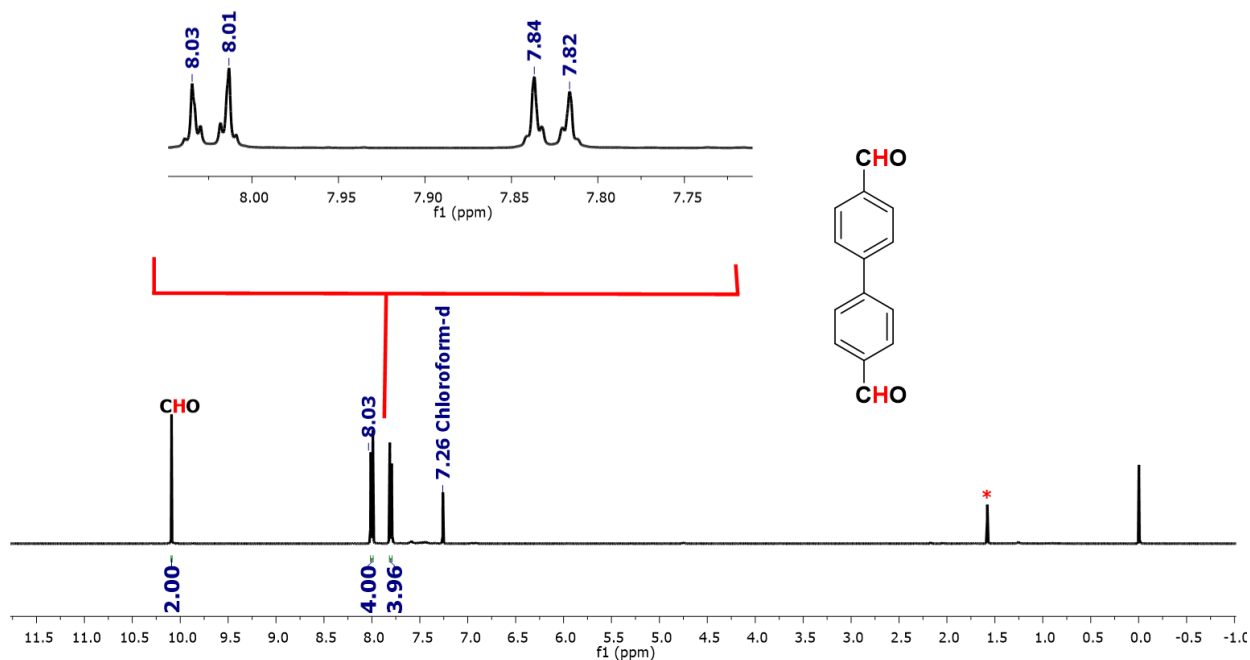
Figure -IV.A.20 ¹H NMR spectrum of biphenyl dialdehyde **IV.B.13.a**

IV.B.13.b) synthesis of biphenyl 4, 4-dicarbinol

To the solution of bithiophene carboxaldehyde (2.5 gm, 11.89 mmol) under an argon atmosphere at 0°C freshly prepared Grignard Reagent (C₆F₅MgBr2.5 mmol) was added. Stirring was allowed for 2 hr to attain room temperature, and the reaction mixture was quenched with aqueous NH₄Cl solution. The organic layer was extracted with ether, and the combined organic layer was washed with water and brine solution. After drying over anhydrous Na₂SO₄, the solvent was removed under reduced pressure, and purification through silica gel (100-200 mesh) column chromatography gave the pure compound as colorless solid in 70% yield.

¹H NMR (400 MHz, CDCl₃, 298K) δ: 7.61 (d, J=8.4 Hz, 4H), 7.50 (d, J=8.4 Hz, 4H), 6.30 (br s, 2H, exchangeable with D₂O), 2.68 (br s, 2H, exchangeable with D₂O).
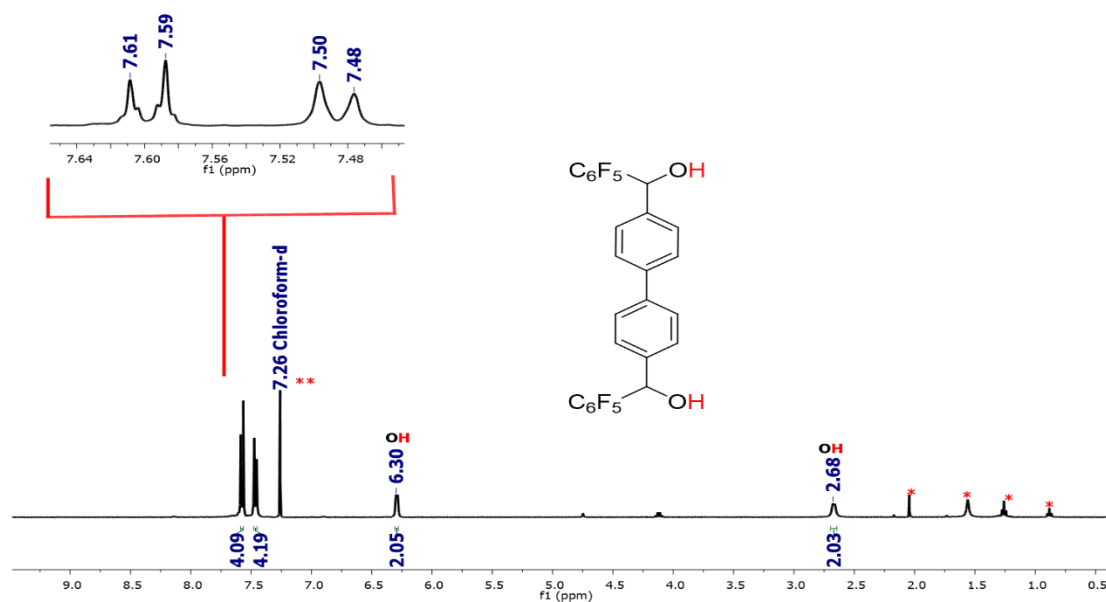
Figure -IV.A.21 ^{1}H NMR spectrum of biphenyl dialcohol **IV.B.13.b**

IV.B.13.c) Synthesis of biphenyl appended trithiophene

4, 4-biphenyl dicarbinol (1.5 gm, 2.75 mmol) was dissolved distilled thiophene (22.00ml, 274.54 mmol. The reaction mixture was bubbled with nitrogen for 5 min, then BF$_3$OEt$_3$ (0.5 ml, 4.12 mmol) was added dropwise under dark. Stir the reaction mixture for 12hr. quench the reaction with 0.1N NaOH solution. Extract the organic phase with dichloromethane; the solvent was evaporated under reduced pressure, purification through silica gel column chromatography gave biphenyl appended trithiophene **IV.B.13c**.

^{1}H NMR (400 MHz, CDCl$_3$, 298K) δ: 7.54 (d, J=8.4 Hz, 4H), 7.35 (d, J=8.4 Hz, 4H), 7.28 (d, J=1.2 Hz, 2H), 7.26 (d, J=1.2 Hz, 2H), 6.98(dd, 4H), 6.07 (s, 2H).
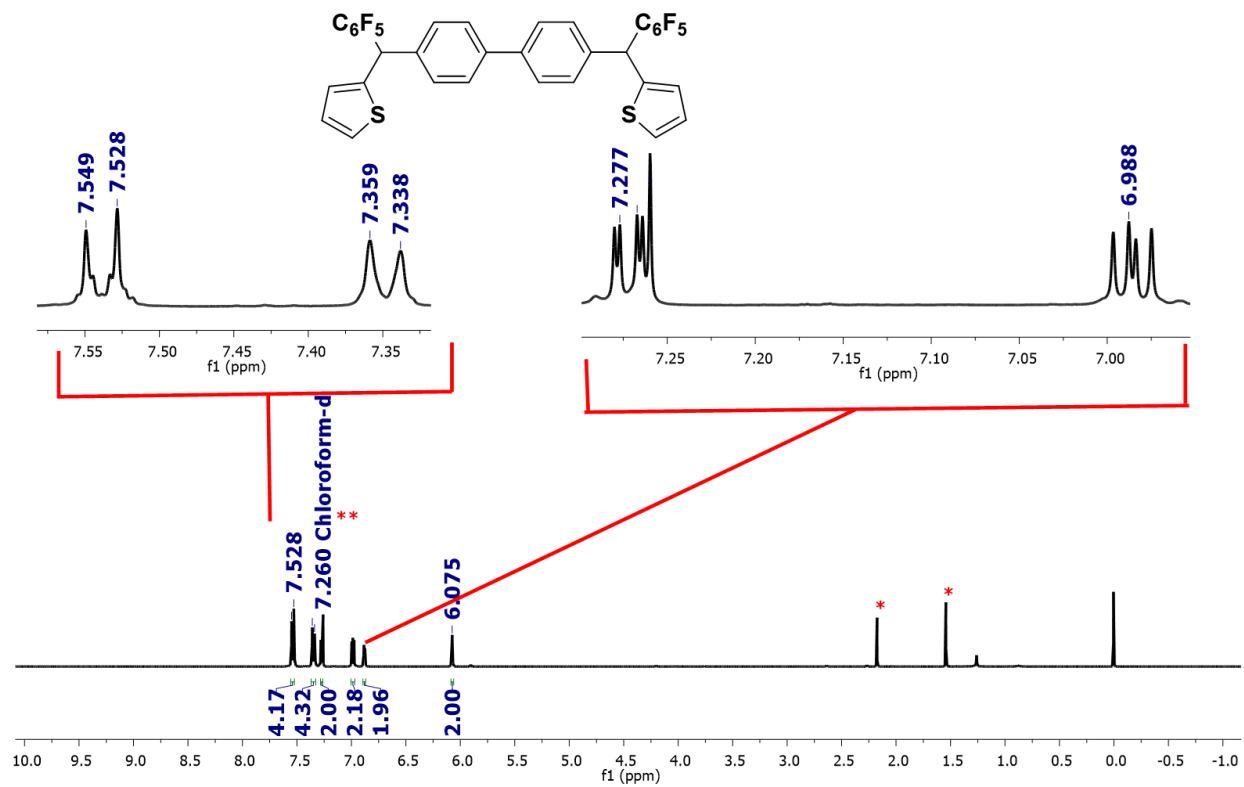
Figure -IV.A.22: ^{1}H NMR spectrum of **IV.B.13c** in CDCl$_3$

Summary of this thesis

This thesis describes Synthesis, Characterization and redox chemistry of novel expanded porphyrinoids derived from pyrrole, furan, thiophene and selenophene heterocycles. After detailed analysis and spectroscopic characterization of isolated macrocycles, interesting electronic and structural features of these macrocycles was studies. The most interesting achievement of this thesis is the development simple and straight forward methodology to access highly reduced states of pyrrole containing expanded porphyrinoids. We have successfully isolated three stable redox states for core modifies hexaphyrin between 26π, 28π, and 30π, electrons and four redox states for octaphyrin i.e. 34π, 36π, 38π, 40π. All these redox states are interconvertible between each other with appropriate reagent. Reversible six electron redox between 34π and 40π attracted wide attention. To the best of our knowledge, such reversible six electron redox is not known for any porphyrinoid till date. These isolated redox states displayed huge structural diversity between each state. Reduction of macrocycles using metallic zinc signifies their pro-metallic character. Given the fact that these macrocycles undergo multiple redox switching, they appear to possess potential characteristics expected of cathode material for organic rechargeable batteries.

The properties of aromatic expanded isophlorins with 38π electrons exhibited significant change with increase in the length of their conjugation. Extended π conjugation alters the electronic properties as well as structural features with respect to 30π aromatic expanded isophlorins. All the 38π expanded isophlorin with different heterocycle displayed planar topology in distinct fashion. These 38π expanded isophlorins are counted as a rare examples for aromatic isophlorins with eight heterocycles. Aromaticity of these 38π expanded isophlorins was supported with NICS and ACID Calculations. In an attempt to obtain π-π stacked molecular complex between antiaromatic and aromatic macrocycles, we have serendipitously discovered additive induced conformational polymorphism in the 38π expanded isophlorin with eight thiophene rings. Different isostructural additives are tested to prove these findings. Even though expanded porphyrinoids are known to alter their geometry between planar and non-planar topologies, this is the first example of inter-conversion between two different planar structures for the same macrocycle. This post synthetic modification can be utilize to unlock different conformers for the expanded porphyrinoids. These isolated 38π aromatic isophlorins are identified to exist as open shell singlet diradical, as their electronic ground state. The diradical character of these macrocycles was studies using variable

temperature NMR and Variable temperature EPR as well as through SQUID measurement. The recovery of aromaticity of quinoidal bithiophene is responsible for the diradical nature of these macrocycles. This diradical properties was further supported by computational studies. The octathiaisophlorin exhibits 42% of diradical character, whereas after replacing four thiophene with selenophene the diradical character was decrease to 31%, and by substituting four furan with four thiophene of octathiaisophlorin, further reduced the diradical character to 24 %. This diradical studies were performed by NOON calculations.

This existence of diradical character due to recovery of aromaticity of thiophene rings from bithiophene, in the expanded isophlorin framework, inspired us to further extend this work. We have synthesized 28π isophlorin molecule which contain two bithiophene and two phenylene rings. As the benzene is more aromatic than thiophene, therefore, we expected diradical of 28π isophlorin due to quinoidal deformation of bithiophene. In the neutral state, this 28π dibenzi isophlorin exist as close shell ground electronic state. But, after two electron oxidation with meerwein salt, the formed dication was identified as singlet diradical. The conversion of localized ring current in the neutral state gets globalized in the dication. The diradical properties of this dication was studied using variable temperature EPR and variable temperature NMR, and SQUID measurement. The plot of $1/\chi_M$ *vs.* T at higher temperatures (above 50 K) was found to follow the Curie-Weiss behavior with C = 0.765 cm^3 mol^{-1} K and θ = -9.5 K, which further supports the presence of strong antiferromagnetic exchange interactions. The experimental results were further supported with computational studies. Further, bis biphenyl derivative of expanded isophlorin was synthesized, similar to dibenzi isophlorin, this also displayed local to global aromaticity conversion from the neutral to dicationic states with distinctive diradical character as identified experimentally. Such conversion of local to global ring current upon oxidation with meerwein salt could be useful for inducing aromaticity to the other cyclic non-aromatic molecules containing paraphenylene.

In an attempt to obtain benzene bridged isophlorin dimer, the 40π bicyclic structure isophlorin with weak antiaromatic characteristics was observed. The weak antiaromatic nature was reflected in its proton NMR spectrum. Which was further endorsed by NICS of +1.21ppm. Two electron oxidation of formed 40π isophlorin resulted into the aromatic dication. The up filed shift of protons for the embedded phenyl rings and down field shift of periphery protons confirmed enhancement of aromaticity in the dication. The estimated NICS for dication was -6.95ppm, this signifies

145

conversion from weak antiaromatic to more aromatic states for isolated macrocycle which was completely in agreement with the NMR findings.

In conclusion, this thesis reveals the unexplored properties of expanded porphyrinoid, which can be extrapolated many expanded porphyrinoids in general. The use of Zn+NH$_4$Cl can be used to achieve highly reduced states for the porphyrinoids with more than eight heterocycles. Additive induced conformational polymorphism is a very important aspect of this thesis for obtaining new conformers for expanded porphyrinoids without any chemical modification. The development diradical chemistry into expanded isophlorins can find potential application of these materials in the organic electronics.

References

[1] D. Dolphin, *The Porphyrins*, Academic press, **1978**.

[2] a) H. Furuta, T. Asano, T. Ogawa. *J. Am. Chem. Soc.* **1994**, 116, 767–768, b) P. J. Chmielewski, L. Latos-Grazynski, K. Rachlewicz, T. Glowiak, *Angew. Chem., Int. Ed. Engl.* **1994**, 33, 779–781

[3] (a) R. B. Woodward. *Angew. Chem*. **1960**, 72, 651–662, (b) Y. Yamamoto , Y. Hirata , M. Kodama , T. Yamaguchi , S. Matsukawa , K.-Y. Akiba , D. Hashizume , F. Iwasaki , A. Muranaka , M. Uchiyama , P. Chen , K. M. Kadish and N. Kobayashi , *J. Am. Chem. Soc.*, **2010**, 132 , 12627 —12638

[4] a) E. Vogel, W. Haas, B. Knipp, J. Lex, H. Schmickler, *Angew. Chem. Int. Ed.* **1988**, *27*, 406;   b) H. Wilhelm, K. Bernd, S. Martin, L. Johann, V. Emanuel, *Angew. Chem., Int. Ed.* **1988**, *27*;c) E. Vogel, P. Rohrig, M. Sicken, B. Knipp, A. Herrmann, M. Pohl, H. Schmickler, J. Lex, *Angew.   Chem., Int. Ed.* **1989**, *28*, 1651 d) M. Pohl, H. Schmickler, J. Lex, E. Vogel, *Angew. Chem., Int. Ed.* **1991**, *30*, 1693 e) R. Bachmann, F. Gerson, G. Gescheidt, E. Vogel, *J. Am. Chem. Soc.* **1992**, *114*, 10855; f) E. Vogel, M. Pohl, A. Herrmann, T. Wiss, C. König, J. Lex, M. Gross, J. P. Gisselbrecht, *Angew. Chem. Int. Ed.* **1996**, *35*, 1520.

[5] J. L Sessler, S. J. Geghorn, Pergamon Press: New York, **1997**.

[6] J. L. Sessler, D. Seidel. *Angew. Chem., Int. Ed.* **2003**, 42, 5134–5175.

[7] T. K. Chandrashekar, S. Venkatraman. *Acc. Chem. Res.* **2003**, 36, 676–691.

[8] S. Saito, A. Osuka. *Angew.Chem., Int. Ed*. **2011**, 50, 4342–4373.

[9] M. Stępien, N. Sprutta, L. Latos-Grazynski. *Angew. Chem., Int. Ed.* **2011**, 50, 4288–4340.

[10] J. Y. Shin, K. S. Kim, M. C. Yoon, J. M. Lim, Z. S. Yoon, A. Osuka, D. Kim. *Chem. Soc. Rev.* **2010**, 39, 2751–2767.

[11] P. J. Garratt, *Aromaticity*, Wiley:, New York, **1986**.

[12] R. Breslow, *Chem. Eng. News* **1965**, *43*, 90; b) F. Sondheim. *Acc. Chem. Res.* **1972**, *5*, 81.

[13] V. J. Bauer, D. L. J. Clive, D.Dolphin, J. B. Paine, F. L. Harris, M. M. King, J. Loder, S.-W. C Wang, R. B. Woodward, *J. Am. Chem. Soc*. **1983**, 105,6429–6436.

[14] J. L Sessler, M. J, Cyr, V Lynch, E. McGhee, J. A Ibers *J. Am. Chem. Soc.* **1990**, 112, 2810–2813

[15] S. W Young, F. Qing, A. Harriman, J. L Sessler, W. C Dow, T. D Mody, G. W Hemmi, Y. Hao, R. A Miller, *Proc. Natl. Acad. Sci. U. S. A*. **1996**, 93, 6610–6615.

[16] J. L Sessler, N. A Tvermoes, D. M. Guldi, T. D. Mody, W. E. Allen*, J. Phys. Chem. A* **1999**, 103, 787–794.

[17] J. L Sessler, R. A. Miller*, Biochem.Pharmacol*. **2000**, 59, 733–739.

[18] J. L. Sessler, S. J. Weghorn, V. Lynch, M. R. Johnson, *Angew. Chem.* **1994**, *106*, 1572-1575; *Angew. Chem. Int. Ed.* **1994**, 33, 1509-1512.

[19] J. L Sessler, D. Seidel,. *Angew. Chem., Int. Ed.* **2003**, 42, 5134–5175.

[20] J. Y. Shin, H. Furuta, K. Yoza, S. Igarashi, A Osuka*, J. Am. Chem. Soc*. **2001**, 123, 7190–7191.

[21] A. Osuka. *Chem. Rev*. **2015**, 15, 143–159.

[22] S. Shimizu, A. Osuka J. Porphyrins Phthalocyanines. **2004**, 08, 175–181.

[23] a) E. Vogel, M. Broring, J. Fink, D. Rosen, H. Schmickler, J. Lex, K. W. K. Chan, Y.-D. Wu, D. A. Plattner, M. Nendel, K. N. Houk, *Angew. Chem.* **1995**, *107*, 2705-2709; *Angew. Chem., Int. Ed.* **1995**, *34*, 2511-2514; b) M. Broring, J. Jendrny, L. Zander, H. Schmickler, J. Lex, Y.-D. Wu, M. Nendel, J. Chen, D. A. Plattner, K. N. Houk, E. Vogel, *Angew. Chem.* **1995**, *107*, 2709-2711; *Angew. Chem. Int. Ed.* **1995**, *34*, 2515-2517.

24] H. Kido, J. Y. Shin, H. Shinokubo, *Angew. Chem.* **2013**, *125*, 13972-13975; *Angew. Chem. Int. Ed.* **2013**, *52*, 13727-13730.

[25] T. Ito, Y. Hayashi, S. Shimizu, J. Y. Shin, N. Kobayashi, H. Shinokubo, *Angew. Chem.* **2012**, *124*, 8670- 8673; *Angew. Chem. Int. Ed.* **2012**, *51*, 8542- 8545.

[26] H. Rath, J. Sankar, V. PrabhuRaja, T. K. Chandrashekar, B. S. Joshi, R. Roy, *Chem. Commun.* **2005**, 3343-3345

[27]N. Sprutta, L. Latos-Grazynski, *Chem. Eur. J.* **2001**, *7*, 5099-5112.

[28] P. Gupta, V.G. Anand *J. Chem. Sci.* **2016,** Vol. 128, No. 11, November, 1703–1707

[29]   V. G. Anand, S. K. Pushpan, S. Venkatraman, A. Dey, T. K. Chandrashekar, B. S. Joshi, R. Roy, W. Teng, K. R. Senge, *J. Am. Chem. Soc.* **2001**, *123*, 8620-8621.

[30] V. G. Anand, S. Venkatraman, H. Rath, T. K. Chandrashekar, W. Teng, K. Ruhlandt-Senge, *Chem. Eur. J.* **2003**, *9*, 2282-2290.

(31) J. S. Reddy, S. Mandal, V. G. Anand. *Org. Lett*. **2006**, 8, 5541–5543

32) W.-Y Cha, T.Soya, T.Tanaka, H. Mori, Y. Hong, S. Lee, K. H Park, A. Osuka, D. Kim *Chem. Commun*. **2016,** 52, 6076–6078

[33] G. Karthik, J. M. Lim, A. Srinivasan, C. H. Suresh, D. Kim, T. K. Chandrashekar, *Chem. Eur. J.* **2013**, *19*, 17011-17020

[34] R. Mysliborski, K. Hurej, M. Pawlicki, and L.Latos-Grazynski *Angew. Chem. Int. Ed.* **2018***, 57, 16866–16870.

[35] 40 M. Ishida, S. J. Kim, C. Preihs, K. Ohkubo, J. M. Lim, B. S. Lee, J. S. Park, V. M. Lynch, V. V. Roznyatovskiy, T. Sarma, P. K. Panda, C. H. Lee, S. Fukuzumi, D. Kim, J. L. Sessler, *Nat Chem.* **2013**, *5*, 15.

[36] T. Sarma, G. Kim, S. Sen, W -Y Cha, Z. Duan, M. D. Moore, V. M. Lynch, Z. Zhang, D. Kim, and J. L. Sessler *J. Am. Chem. Soc.* **2018**, 140, 12111–12119.

[37] T. Tanaka, N. Aratani, A. Osuka, *Chem-Asian J.* **2012**, *7*, 889-893.

[38] J. Sankar, S. Mori, S. Saito, H. Rath, M. Suzuki, Y. Inokuma, H. Shinokubo, K. Suk Kim, Z. S. Yoon, J.-Y. Shin, J. M. Lim, Y. Matsuzaki, O. Matsushita, A. Muranaka, N. Kobayashi, D. Kim, A. Osuka, *J. Am. Chem. Soc.* **2008**, *130*, 13568.

[39] 44 M. Stepien, B. Szyszko, L. Latos-Grażynski, *J. Am. Chem. Soc.* **2010**, *132*, 3140.

[40] P. K. Thallapally, R. K. R. Jetti, A. K. Katz, H. L. Carrell, K. Singh, K. Lahiri, S. Kotha, R. Boese, and G. R. Desiraju *Angew. Chem. Int. Ed*. **2004**, 43, 1149 –1149

[41] 46 E. Simone, G. Steele and Z. K. Nagy *CrystEngComm*. **2015**, 17, 9370–9379

[42] D. Shimizu and A. Osuka *Chem. Sci.* **2018**, 9, 1408–1423.

[43] A. Rana, Y. Hong, T. Y. Gopalakrishna H. P Herng, T. Seng, P. Yadav, J. Ding, D. Kim, and J. Wu. *Angew. Chem. Int. Ed*. **2018**, *57*, 12534 –12537

[44] a) Z. Zeng, X. Shi, C. Chi, J. T. L. Navarrete, J. Casado and J. Wu *Chem. Soc. Rev.,* **2015**, 44, 6578-6596 b) M. Abe, *Chem. Rev.* **2013**, 113, 7011–7088

[45] V. G. Anand, S. Saito, S. Shimizu, A. Osuka, *Angew. Chem.* **2005**, *117*, 7410-7414; *Angew. Chem. Int. Ed.* **2005**, *44*, 7244 –7248.

[46] a) C. Liu, D.-M Shen, & Q.-Y Chen. *J. Am. Chem. Soc.* **2007**, 129, 5814-5815. b) W. Suzuki, H. Kotani, T. Ishizuka, Y. Shiota, K. Yoshizawa and T. Kojima. *Angew. Chem. Int. Ed.* 57, **2018**, 1973-1977.

[47] Y. Yamamato, Y.Hirata, M.Kodama, T. Yamaguchi, S. Matsukawa, K-Y Akiba, D.Hashizume, F.Iwasaki, A. Muranaka, M. Uchiyama, P.Chen, K.M. Kadish and N. Kobayashi. *J. Am. Chem. Soc.* **2010**. 132, 12627-12638.

[48]M.G. P. M. S. Neves, R. M. Martins, A. C. Tome, A. J. D. Silvestre, A.M. S. Silva,V. Felix, M. G. B. Drewb and J. A. S. Cavaleiro. C*hem. Comm.* **1999** 385-386.

[49] M. Suzuki, A.Osuka. *Chem. Commun. 2***005,** 29, 3685-3687.

(50) T. Higashino, A. Osuka. Chem. Sci. **2013,** 4, 1087−1091.

[51] J. S Reddy, V.G. Anand. *J. Am. Chem.Soc***, 2009**, 131, 15433−15439.

[52] R Rathore, A. S. Kumar, S.V. Lindeman, J. K. Kochi. *J. Org. Chem.* **1998,** 6*3*, 5847-5856.

[53]T. Y. Gopalakrishna, & V. G. Anand. A*ngew. Chem. Int. Ed.* **2014***,* 53**,** 6678-6682.

[54]S. P Panchal, S.C. Gadekar, & V. G. Anand. A*ngew. Chem. Int. Ed.* 5**5,** 7797-7800 (2016).

[55]   P. v. R Schleyer, C. Maerker, A. Dransfeld, H. Jiao. & N. J. R.van Eikema Hommes. J*. Am. Chem. Soc***.1996** 1**18,** 6317-6318.

[56]   D. Geuenich, K. Hess, F. Kohler, R. Herges, *Chem. Rev*. **2005**, *105*, 3758–3772.

[57]   N. Shivran, S. C. Gadekar, V. G Anand, *Chem. -Asian J.* **2017,** 1*2* (1), 6-20.

[68] [47] Gaussian 09, Revision D.01, M. J. Frisch, G. W. Trucks, H. B. Schlegel, G. E. Scuseria, M. A. Robb, J. R. Cheeseman, G. Scalmani, V. Barone, B. Mennucci, G. A. Petersson, H. Nakatsuji, M. Caricato, X. Li, H. P. Hratchian, A. F. Izmaylov, J. Bloino, G. Zheng, J. L. Sonnenberg, M. Hada, M. Ehara, K. Toyota, R. Fukuda, J. Hasegawa, M. Ishida, T. Nakajima, Y. Honda, O. Kitao, H. Nakai, T. Vreven, J. A. Montgomery, Jr., J. E. Peralta, F. Ogliaro, M. Bearpark, J. J. Heyd, E. Brothers, K. N. Kudin, V. N. Staroverov, R.

Kobayashi, J. Normand, K. Raghavachari, A. Rendell, J. C. Burant, S. S. Iyengar, J. Tomasi, M. Cossi, N. Rega, J. M. Millam, M. Klene, J. E. Knox, J. B. Cross, V. Bakken, C. Adamo, J. Jaramillo, R. Gomperts, R. E. Stratmann, O. Yazyev, A. J. Austin, R. Cammi, C. Pomelli, J. W. Ochterski, R. L. Martin, K. Morokuma, V. G. Zakrzewski, G. A. Voth, P. Salvador, J. J. Dannenberg, S. 113 Dapprich, A. D. Daniels, Ö. Farkas, J. B. Foresman, J. V. Ortiz, J. Cioslowski, and D. J. Fox, Gaussian, Inc., Wallingford CT, 2009.

[59] a) R. Gleiter, G. Haberhauer, Wiley-VCH, **2012**; b) T. M. Krygowski, M. K. Cyrañski, Z. Czarnocki, G. Häfelinger, A. R. Katritzky, *Tetrahedron.* **2000**, *56*, 1783–1796. c) H. J. J. Dauben, J. D. Wilson, J. L. Laity, *J. Am. Chem. Soc.* **1969**, *91*, 1991–1998; d) J. A. N. F. Gomes, R. B. Mallion, *Chem. Rev.* **2001**, *101*, 1349–1383; e) P. Lazzeretti, *Prog. Nucl. Magn. Reson. Spectrosc.* **2000**, *36*, 1–88

 (60) J. S. Reddy, V. G. Anand, *J. Am. Chem. Soc*. **2008,** 130, 3718–3719.

 [61] C. R. Patrick and G. S. Prosser, *Nature.* **1960,** 1021.

[62] C. A. Hunter, K. R. Lawson, J. Perkins and C. J. Urch**.** *J. Chem. Soc., Perkin Trans. 2*, **2001**, 651–669

[63] a) A. J. Cruz-Cabeza and J. Bernstein, *Chem. Rev*. **2014**, *114*, 2110-2191; b) J. Liebig, F. Wohler, *Ann. Pharm. III* **1832**, *249*, 514; c) W. I. F David, K. Shankland, C. R Pulham, N. Blagden, R. J. Davey, M. Song, *Angew. Chem. Int. Ed.* **2005**, *44*, 7032-7035; d) J. Bernstein, G. Desiraju Ed. Elsevier. **1987**, pp 471–518

[64] (a) H. Higuchi, T. Nakayama, H. Koyama, J. Ojima, T. Wada and H. Sasabe, *Bull. Chem. Soc. Jpn.* **1995**, 68, 2363; (b) J. Casado, L. L. Miller, K. R. Mann, T. M. Pappenfus, H. Higuchi, E. Orti, B. Milian, R. P-Amerigo, V. Hernandez and J. T. L. Navarrete, *J. Am. Chem. Soc*. **2002**, 124, 12380

[65] T. Takahashi, K. Matsuoka, K. Takimiya, T. Otsubo and Y. Aso*, J. Am. Chem. Soc*. **2005**, 127, 8928.

[66] D. Dohnert, and J. Koutecky. *J. Am. Chem. Soc.* **1980**, *102*, 1789-1796.

 [67] a) T. D. Lash, *Acc. Chem. Res*. **2016**, 49, 471-482, b) T. D. Lash, Chem. Rev. **2017,** 117, 2313–2446.

[68] N. Toriumi, A. Muranaka, E. Kayahara, S. Yamago, M. Uchiyama, *J. Am. Chem. Soc.* **2015**, *137*, 82–85.

[69] J. S. Reddy and V. G. Anand, *Chem. Commun*. **2008**, 1326–1328.

[70] S. Dong, T. Y. Gopalakrishna, Y. Han, and C. Chi, *Angew. Chem. Int. Ed.* **2019**, 131, 11868 –11872

[71]. O. Kahn, VCH Publishers Inc. **1991**.

[72] C. Shu, H. Zhang, A. Olankitwanit S. Rajca, A. Rajca. *J. Am. Chem. Soc.* **2019,** *141*, 17287-17294.

[73] R. Kurata, D. Sakamaki, and A. Ito, *Org. Lett*. **2017**, 19, 3115–3118

[74] B. K. Reddy, S. C. Gadekar and V. G. Anand, *Chem. Commun.* **2016**, 52, 3007—3009.